Universidad del País Vasco/ Euskal Herriko Unibertsitatea

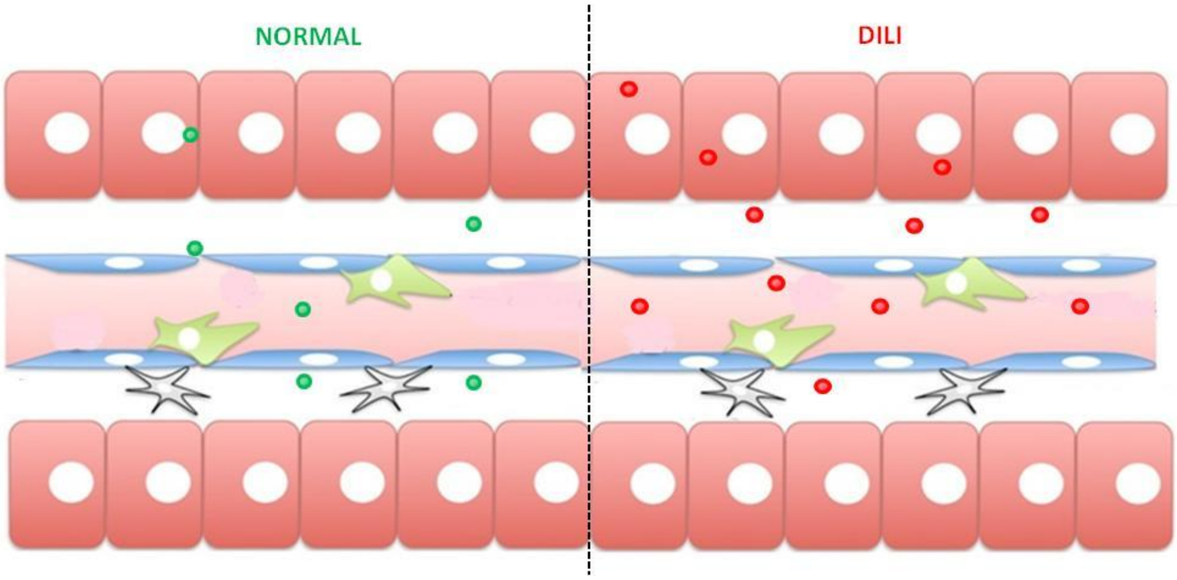

Metabolic implications and characterization of hepatic extracellular vesicles in drug-induced liver injury

Tesis doctoral para optar al grado de Doctora, presentada por:

Laura Palomo Díaz
2015

Director de Tesis:
Dr. Juan Manuel Falcón Pérez

(c)2015 LAURA PALOMO DIAZ

Esta tesis doctoral ha sido realizada gracias a una beca predoctoral de CIC-bioGUNE durante el periodo 2010-2014.

El trabajo ha sido financiado por los proyectos PI060621, PS09/00526 y PI12_01604, cofinanciados por el ISCIII-Subdirección General de Evaluación y Fondo Europeo de Desarrollo Regional (FEDER), el Departamento de Educación, Política Lingüística y Cultura del Gobierno Vasco (PI2012-45), el Departamento de Sanidad del Gobierno Vasco (2012-2015), Subprograma Ramón y Cajal RYC-2007- 00228 y la Fundación IKERBASQUE. Becas de movilidad financiadas por COST European Actions BM0901 y BM1202.

AGRADECIMIENTOS

En primer lugar y ante todo a mi director de tesis, por brindarme la oportunidad de formar parte de su pequeño, pero a la vez, gran grupo de investigación y adentrarme en el mundo de esas pequeñas vesículas que tantos quebraderos de cabeza nos han traído. La verdad que nunca hubiese imaginado que algo tan pequeño podría llegar a convertirse en algo tan grande durante estos cuatro años. Darle las gracias por ser un jefe ejemplar, por creer en mí y apoyarme en todo momento. Darle las gracias también por guiarme siempre en este duro recorrido y hacerme ver que todo esfuerzo tiene su recompensa. Y por último darle las gracias por ser un gran jefe pero mejor persona.

A José María Mato, el director de nuestro centro de investigación, por encargarse siempre de dejar el listón bien alto.

A Ana Zubiaga, mi tutora de tesis, por la atención y amabilidad prestada en todo momento.

A Espe, por ayudarme, por tratar de enseñarme a ser paciente (aún estoy en ello), por sus buenos consejos, por estar ahí en los momentos difíciles, por su gran apoyo tanto a nivel profesional como personal y, sobre todo, gracias por darnos a todos una gran lección de valentía.

A Félix, por poner ese toque de humor que le caracteriza, por darme siempre una solución alternativa, por encargarse de todas las perfusiones y por esos ratos en cultivos escuchando "Máxima fm".

A Justyna, por traer un aire fresco al grupo, por sus ganas de aprender y sobre todo por contagiarme esa energía que tanto me ha hecho falta en esos últimos meses.

A Dixon, por ser un trabajador nato, por su dedicación, por el excelente trabajo realizado, por su gran espíritu de sacrificio, por sacarme de más de un apurillo, por todos esos buenos momentos que hemos compartido. No me cabe la menor duda de que llegarás a ser un gran enfermero.

A Javi, por aguantarme a mi llegada al labo con mi interminable lista de preguntas en la recta final de su tesis. Yo no lo hubiera hecho igual de bien.

A Kika, por haberme enseñado tanto en esta carrera de fondo que ya va viendo la luz. Por aguantar mis chapas y por estar siempre dispuesta a ayudarme con todo.

A Diana, por esa disposición para echar una mano en cualquier momento, por tener siempre una sonrisa para mí, por haber estado a pie de cañón en estos últimos meses y por todos esos *kit-kat* de la planta 0 que tanto me han ayudado.

A Sebastiaan, por brindarme su ayuda y enseñarme las bases de la metabolómica.

A Malu y a todas las personas que forman su gran grupo de investigación. Por todos los momentos que hemos vivido juntos y porque cada uno de ellos me ha aportado una cosa diferente que me ha hecho crecer durante estos 4 años.

A Marta txiki, por todos los momentos que hemos vivido juntas durante todo este tiempo. Por preocuparse y aconsejarme, y sobre todo por aguantar mis chapas en estos últimos meses. Más que a una compañera, me llevo a una gran amiga.

A Marta Palomo, en este poco tiempo que nos conocemos me ha demostrado que es una gran persona. Dada su perseverancia y sus ganas de aprender, no me cabe la menor duda de que llegará lejos.

A Gotxi, por contagiarme esa alegría que la caracteriza y por preocuparse y ayudarme siempre.

A Lucia, mi compi de pasillo o de *bench* o como lo queráis llamar, por tener la habilidad de sacarme una sonrisa siempre.

A Vir, que decir de la gran Vir, la salvadora de todos y cada uno de nosotros. Gracias por poner siempre un toque de humor a todo.

A Sara, que aunque ya no está en el labo la seguimos recordando. Una trabajadora nata sin duda.

A Nieves, por sus consejos y por animarme cuando lo he necesitado.

A David y Sandra del servicio de microscopia electrónica, por su colaboración.

A todos los chicos de administración. Pero sobre todo a Bego, Mada y Loli por ayudarme con todos los trámites y papeleos. Perdón por volveros un poco locas en alguna ocasión.

A Urra y Ana por darme más de una lección en cuestiones de limpieza, por preocuparse y por hacerme compañía cuando no quedaba nadie más en el labo.

A Nuria, nuestra chica del autoclave, por esos favorcillos cuando no he llegado a tiempo y por los ánimos y apoyo recibido.

A todos mis amigos, por estar ahí siempre, apoyándome y dándome fuerzas en los momentos más difíciles.

A mi hermana, por lo bien que me ha cuidado siempre y por haber estado a mi lado en todo momento.

A mis padres, por creer en mí y darme fuerzas para seguir adelante. Por esforzarse cada día para ofrecerme lo mejor. Por enseñarme todo lo que hoy soy y hacerme crecer como persona. Sin vosotros nada de esto hubiese sido posible.

A todos, gracias.

INDEX

1. ABBREVIATIONS....28
2. RESUMEN/SUMMARY....33
3. INTRODUCTION....36
    - 3.1. LIVER AND DRUG INDUCED LIVER INJURY....36
    - 3.2. EXTRACELLULAR VESICLES (EVs)....38
    - 3.4. HEPATIC EVs IN DRUG INDUCED LIVER INJURY....45
        - 3.4.1. CARBOXYLESTERASE (CES*)*....46
        - 3.4.2. METHIONINE ADENOSYL-TRANSFERASE (MAT)....47
        - 3.4.3. CATECHOL-*O*-METHYL TRANSFERASE (COMT)....48
        - 3.4.4. METABOLOMIC PROFILING OF HEPATIC EVS....51
4. HYPOTHESIS AND OBJECTIVES....54
5. EXPERIMENTAL PROCEDURES....56
    - 5.1. REAGENTS AND CELL CULTURE....56
    - 5.2. ANIMAL EXPERIMENTATION....56
    - 5.3. CELL VIABILITY ANALYSIS....57
    - 5.4. IMMUNOFLUORESCENCE STAINING....57
    - 5.5. WESTERN BLOT ANALYSIS....58
    - 5.6. CRYO- ELECTRON MICROSCOPY (Cryo-EM)....58
    - 5.7. RAMAN TWEEZERS MICROSPECTROSCOPY (RTM)....58
    - 5.8. RNA ISOLATION AND QUANTITATIVE REAL-TIME PCR (qPCR)..59
    - 5.9. RAT LIVER EXTRACT PREPARATION....61
    - 5.10. RAT MICROSOMES PREPARATION....61
    - 5.11. PRODUCTION AND ISOLATION OF EVs SECRETED BY PRIMARY HEPATOCYTES....61
    - 5.12. PRODUCTION AND ISOLATION OF EVs SECRETED BY MLP-29 MURINE CELL LINE....63
    - 5.13. FRACTIONATION OF EVs ONA CONTINUOUS SUCROSE DENSITY GRADIENT....63
    - 5.14. NANOPARTICLES TRACKING ANALYSIS (NTA)....64
    - 5.15. DETERMINATION OF CES ACTIVITY BY USING A FLUOROMETRIC ASSAY....64
    - 5.16. MEASUREMENTS OF MAT AND COMT ACTIVITIES BY UPLC-MS64

5.16.1. INCUBATION CONDITIONS....64
5.16.2. SOLID-PHASE EXTRACTION (SPE)....66
5.16.3. CALIBRATION CURVE AND QUALITY CONTROLS....68
5.16.4. LIQUID CHROMATOGRAPHY AND MASS SPECTROMETRY (UPLC- MS) CONDITIONS....69
5.16.5. ANALYTICAL METHOD....70
5.16.6. DATA ANALYSIS OF UPLC-MS RESULTS PROVIDED BY MAT AND COMT ACTIVITY ASSAYS....71
5.17. METABOLIC PROFILING OF HEPATIC EVs BY UPLC-MS METABOLOMICS....72
5.17.1. SELECTION OF METABOLITES EXTRACTION METHOD....72
5.17.2. BIPHASIC METABOLIC EXTRACTION OF CELLS AND EVs....72
5.17.3. ULTRA PERFORMANCE LIQUID CHROMATOGRAPHY – MASS SPECTROMETRY CONDITIONS....73
5.17.4. DATA PROCESSING, MULTIVARIATE ANALYSIS AND METABOLITE IDENTIFICATION....74
6. RESULTS AND DISCUSSION....76
6.1.1. CELL VIABILITY....76
6.1.2. CELL MORPHOLOGY....77
6.1.3. WESTERN BLOT ANALYSIS....81
6.2. EVs SECRETED BY PRIMARY RAT HEPATOCYTES IN MODELS OF DILI....83
6.2.1. EVs SIZE, MORPHOLOGY AND CONCENTRATION ANALYSIS 83
6.2.2. WESTERN BLOT ANALYSIS....86
6.2.3. EVs OVERALL COMPOSITION ANALYSIS....86
6.2.4. EVs RNA CONTENT ANALYSIS....90
6.2.5. CES ACTIVITY ANALYSIS....91
6.2.5.1. Esterase Activity analysis....92
6.2.5.2. Continuous density gradient analysis....92
6.2.6. MAT ACTIVITY ANALYSIS....94
6.2.6.1. Analytical method development....94
6.2.6.1.1. Optimization of the incubation condition for the enzymatic reaction to assay MAT activity....94
6.2.6.1.2. Ultra performance Liquid Chromatography-Mass Spectrometry optimization....98

6.2.6.1.3. Solid-Phase Extraction (SPE) method development................100
6.2.6.2. Analytical method optimization 104
6.2.6.2.1. Specificity of the enzymatic assay..104
6.2.6.2.2. Linearity of Calibration Curves and Lower Limits of Quantification (LLOQ)..104
6.2.6.2.3. Precision and Accuracy of the enzymatic assay 105
6.2.7. COMT ACTIVITY ANALYTICAL METHOD..................................105
6.2.7.1. Analytical method development..105
6.2.7.1.1. Optimization of the incubation condition for the enzymatic reaction to assay COMT activity..105
6.2.7.1.2. Ultra Performance Liquid Chromatography-Mass Spectrometry optimization...106
6.2.7.1.3. Solid-Phase Extraction (SPE) Method development 108
6.2.7.2. Analytical Method optimization..109
6.2.7.2.1. Specificity of the enzymatic assay...109
6.2.7.2.2. Linearity of Calibration Curves and Lower Limits of Quantification (LLOQ)..111
6.2.7.2.3. Precision and Accuracy of the enzymatic assay 111
6.2.8. MAT ENZYMATIC ACTIVITY ANALYSIS IN HEPATIC EVs......113
6.2.9. COMT ENZYMATIC ACTIVITY ANALYSIS IN HEPATIC EVs ...118
6.3. METABOLIC PROFILING OF HEPATIC EVs 124
6.3.1. METABOLITES EXTRACTION METHOD SELECTION................124
6.3.2. ULTRA PERFORMANCE LIQUID CHROMATOGRAPHY – MASS SPECTROMETRY ANALYSIS...127
6.3.3. DATA PROCESSING 128
6.3.4. MULTIVARIATE DATA ANALYSIS: PRINCIPAL COMPONENT ANALYSIS (PCA)..129
6.3.5. EVs METABOLIC PROFILING, METABOLIC SIGNAL SELECTION AND METABOLITE IDENTIFICATION..131
7. GENERAL DISCUSSION...143
8. CONCLUSIONS 150
9. BIBLIOGRAPHY 152
10. SUPPORT..170

LIST OF FIGURES AND TABLES

FIGURES

Figure 1. Schematic representation of different type of extracellular vesicle (EVs)…………………………………………………………….... 39

Figure 2. Biogenesis of EVs………………………………………………………. 40

Figure 3. Overall composition of EVs…………………………………………. 42

Figure 4. Schematic view of Methionine cycle metabolism…………………… 48

Figure 5. The basic function of Catechol- O-Methyltransferase……………..... 49

.

Figure 6. Cathechol-O-Methyltransferase catalyses methylation of Dopamine and Norepinephrine... 51

Figure 7. Experimental design to perform the study of the enzymatic activities... 65

Figure 8. Preparation of standard and test samples for evaluation of solid phase extraction method recovery…………………………………… 68

Figure 9. Cellular viability analysis of rat hepatocytes exposed to liver-damaging drugs……………………………………………………… 76

Figure 10. Reproducibility analysis of cellular viability in independent rat hepatocytes preparations ………………………………………... 77

Figure 11. Confocal analysis of primary rat hepatocytes in DILI conditions…. 78

Figure 12. Western-blot analysis of primary rat hepatocytes and their corresponding secreted EVs ……………………………………..... 82

Figure 13. Ultrastructural characterization of EVs in DILI models………….... 84

Figure 14. Total number of particles secreted in DILI models………………..... 85

Figure 15. Total protein amount of EVs secreted in DILI models…………….. 85

Figure 16. Raman tweezers microspectroscopy technique applied to study EVs global composition in DILI models... 87

Figure 17. Average Raman spectra interpretation for rat hepatocytes derived EVs……………………………………………………………… 88

Figure 18. Analysis of overall composition of hepatocytes-secreted EVs in DILI models... 89

Figure 19. RNA cargo of hepatic EVs in DILI models……………………….. 91

Figure 20. Carboxylesterase activity in EVs from DILI models…..................... 92

Figure 21. Density fractionation and CES activity analysis of hepatic EVs in DILI models.. 93

Figure 22. Optimization of pH for MAT enzymatic activity.............................. 95

Figure 23. Optimization of temperature reaction for MAT activity................... 96

Figure 24. Optimization of divalent (Mg^{2+}) and monovalent (K^{+}) cations content in the reaction.. 96

Figure 25. Optimization of L-methionine concentration for MAT activity....... 97

Figure 26. Optimization of ATP concentration for MAT activity..................... 97

Figure 27. Optimization of incubation reaction time for MAT activity............. 98

Figure 28. Representatives chromatograms and mass spectra obtained from rat liver extract spiked with SAMe and SAH……………………….… 100

Figure 29. Phenilboric acid (PBA) based solid phase extraction mechanism…. 101

Figure 30. UPLC-MS analysis of matrix effect for SAMe, SAH and MTA…... 102

Figure 31. SPE process efficiency for SAMe, SAH and MTA…...................... 103

Figure 32. Recovery analysis for SAMe, SAH and MTA in the PBA-SPE method…………………………………………………………... 104

Figure 33. Representative chromatograms and mass spectra obtained from rat liver extract spiked with Dopamine and 3-Methoxytyramine…………………………………………………... 107

Figure 34. Representative chromatograms and mass spectra obtained from rat liver extract spiked with Norepinephrine and Normetanephrine………………………………………………… 107

Figure 35. Oasis WCX retention mechanism for strong bases………………… 108

Figure 36. Chromatograms obtained for 3-Methoxytyramine (*m/z* 151.075, t_r 1.15)……………………………………………………………... 110

Figure 37. Superimposed chromatogram obtained for Normetanephrine (*m/z* 166.086, t_r 1.30)………………………………………………..... 110

Figure 38. Western-blot analysis of samples employed for measuring MAT and COMT enzymatic activity……………………………………... 112

Figure 39. Chromatograms of SAMe and SAH generated by MAT enzymatic activity in liver extract………………………………………………… 114

Figure 40. MAT activity in microsomes prepared from untreated and drug-treated primary hepatocytes……………………………………... 115

Figure 41. MAT activity in EVs secreted by primary hepatocytes…………….. 116

Figure 42. Chromatograms of the products NMN or 3-MT of COMT activity in liver extract……………………………………………………....... 119

Figure 43. COMT enzymatic activity in microsomes from untreated and DCF-treated hepatocytes…………………………………………….... 120

Figure 44. COMT enzymatic activity in hepatic microsomes and EVs........... 121

Figure 45. COMT enzymatic activity in hepatic EVs……………….................. 122

Figure 46. COMT enzymatic activity in hepatic EVs incubating different amounts of protein…………………………………………….….. 123

Figure 47. Principal Component Analysis (PCA) of the metabolic profiles obtained using different extraction methods ……………………… 126

Figure 48. Representative base peak chromatograms of UPLC-MS analysis of MLP29 cells and corresponding secreted EVs................................ 129

Figure 49. Principal component analysis (PCA) of UPLC-MS data obtained from MLP29 cells and their corresponding secreted EVs………………………………………………………………….... 131

Figure 50. Metabolic background introduced by tissue culture media in EVs analysis…………………………………………………………….. 131

Figure 51. Scatter plots of polar and apolar dataset, run in ESI+ .and ESI-mode for MLP-29 cells and secreted EVs………………………… 138

Figure 52. Example of the identification of a metabolite enriched in EVs in the aqueous phase……………………………………………….….... 140

Figure 53. Example of the identification of a metabolite enriched in EVs in the organic phase………………………………………………………. 141

Figure 54. Overview of the main results obtained in this doctoral thesis……… 148

TABLES

Table 1. Main features of cell-derived EVs....................................... 41

Table 2. List of primers used for DNA amplification.. 60

Table 3. MAT activity derived metabolites structure and properties.................... 99

Table 4. COMT activity derived metabolites structure and properties.................. 106

Table 5. MAT activity in liver extract, microsomes and EVs from primary hepatocytes... 113

Table 6. COMT activity in liver extract, microsomes and EVs from primary hepatocytes... 118

Table 7. Number of metabolic signals in C18 and amide columns using different Metabolic extraction methods.. 127

Table 8. Metabolic signals detected by UPLC-MS in MLP29 cells and their Secreted EVs... 128

Table 9. The metabolome of EVs secreted by MLP-29 hepatic cell line…........... 133

Table 10. Hepatic EVs metabolome characterization…………………………..… 136

Table 11. Metabolites implied in different pathways are contained in hepatic EVs………………………………………………………………….. 137

Table 12. Metabolic signals enriched in hepatic EVs secreted by MLP-29 cell line…………………………………………………………............. 139

1. ABBREVIATIONS

ALT	Alanine transaminase
3-MT	3-methoxytyramine
ACN	Acetonitrile
AHCY	AdoHcy hydrolase
Alb	Albumin
ALF	Acute liver failure
AMP	Adenosin monophosphate
Asgr	Asialoglycoprotein receptor
ALT	Alanine Aminotransferase
APAP	Acetaminophen
AST	Aspartate Aminotransferase
BSA	Bovine serum albumin
Cd63	Cluster of Differentiation 63
Cd81	Cluster of Differentiation 81
cDNA	Copy Deoxyribonucleic acid
CES	Carboxylesterases
Ces1d	Carboxylesterase 1d
COMT	Cathecol-*O*-Methyl transferase
Cox IV	Citochrome c Oxidase IV
CPT-11	7-ethyl-10-[4-(1-piperidino)-1-piperidino]-carbonyloxy camptothecin
Cryo-EM	Cryo-Electron Microscopy
CV	Coefficient of variation
DA	Dopamine
DAPI	4',6-diamidino-2-phenylindole
DCF	Diclofenac
DHA	Docosahexanoic acid
DILI	Drug-induced liver injury

DMEM	Dulbecco’s modified eagle medium
DNA	Deoxyribonucleic acid
DPBS	Dulbecco’s modified phosphate-buffered saline
DTT	Dithiothreitol
EDC	Enhanced Duty Cycle
EMRT	Exact mass-retention time pair
ESI-	Electrospray ionization mode negative
ESI+	Electrospray ionization mode positive
EVs	Extracellular Vesicles
FABP	Fatty acid binding protein
FDA	Food and Drug Administration
GalN	Galactosamine
GGT	Gamma-glutamyl transferase
GNMT	Glycine N-Methyltranferase
GNBL1	Beta polypeptide 2-like 1
Grp 78	Glucose-regulated protein 78
GSH	Glutathione
GSSG	Glutathione Disulfide
GST	Glutathione S-transferase
HCC	Hepatocellular carcinoma
HCV	Hepatitis C virus
Hcy	Homocysteine
HIV-1	Human immunodeficiency virus-1
Hsp 70	Heat Shock Protein 70
Hsp 90	Heat Shock Protein 90
HEPES	4-(2-hydroxyethyl)-1-piperazineethanesulfonic acid
HILIC	Hydrophilic Interaction Chromatography
HMDB	Human Metabolome Database
HRP	Horse radish peroxidase
ILVs	Intraluminal vesicles

LC-MS/MS	Liquid chromatography-tandem mass spectrometry
We	Lysosomal integral membrane protein type 2
LIMP II	
LLOD	Lower Limit of Detection
LLOQ	Lower Limit of Quantification
L-NMMA	N^G-monomethyl-L-arginine
MAT	Methyl-AdenosylTransferase
MAT1A	Methyl-AdenosylTransferase 1A
MB-COMT	Membrane-bound Cathecol-*O*-Methyl transferase
MeOH	Methanol
METLIN	Metabolite Link
miRNA	Micro ribonucleic acid
MLP-29	Mouse Liver Progenitor -29
MP	Microparticles
mRNA	Messenger ribonucleic acid
MT	Methyltransferases
MTA	5´-methylthioadenosine
MV	Microvesicles
MVBs	Multivesicular bodies
NAPQI	N-acetylp-benzoquinoneimine
NE	Norepinephrine
NMN	Normetanephrine
NO	Nitric oxide
NSAID	Nonsteroidal Antiinflammatory Drug
NTA	Nanoparticles Tracking Analysis
P450	Cytochromes P450
PBA	Phenylboronic acid
PIP2	Phosphatidylinositol-(4,5)-bisphosphate
PC	Principal component
PCA	Principal components analysis

PE	Phosphatidylethanolamine
PPT	Protein precipitation
PUFA	Polyunsaturated fatty acid
PVDF	Polyvinylidene difluoride
QC	Quality Control
qPCR	Quantitative polymerase chain reaction
RBP4	Retinol binding protein 4
RNA	Ribonucleic acid
RP-LC/MS	Reversed-phase liquid chromatography-Mass spectrometry
RTM	Raman tweezers microspectroscopy
SAA	Salvianoic acid A
SAMe	S-adenosylmethionine
SAH	S-adenosylhomocysteine
S-COMT	Soluble Cathecol-*O*-Methyl transferase
SN-38	7-ethyl-10-hydroxycamptothecin
SPE	Solid-Phase Extraction
ToF	Time of Flight
UGT	UDP-glucuronosyltransferase
UPLC-MS	Ultra Performance Liquid Chromatography- Mass Spectrometry

2. RESUMEN/SUMMARY

RESUMEN

El daño hepático inducido por drogas (DILI) es un grave problema en las sociedades desarrolladas, siendo el responsable de más del 50% de los casos de fallo hepático agudo. Un área de gran interés, tanto en el diagnóstico clínico como en la industria farmacéutica, es la búsqueda de marcadores no invasivos, tanto para el diagnóstico de esta patología, como para dilucidar el mecanismo molecular que se encuentra tras ella. En este sentido, el descubrimiento de vesículas extracelulares (EVs) secretadas por células, ha proporcionado un nuevo componente celular con la posibilidad de ser un agente activo en diferentes procesos tanto fisiológicos como patológicos. Estas vesículas han sido detectadas tanto en muestras de sangre como de orina, proporcionando una nueva plataforma para la identificación de marcadores no invasivos de enfermedades de diversa índole. Estas vesículas son secretadas por la mayoría de tipos celulares, incluyendo el hepatocito. Sin embargo, a pesar de la intensa investigación llevada a cabo en estas vesículas, actualmente poco se conoce acerca de su papel fisiológico y de su implicación en el desarrollo de enfermedades.

Los hepatocitos secretan EVs que contienen enzimas implicadas en el metabolismo de drogas, sugiriendo una posible implicación de estas vesículas en el desarrollo de DILI. En este sentido, en esta tesis doctoral se ha caracterizado la secreción de EVs hepáticas en diferentes modelos de DILI *in vitro* mediante el uso de técnicas tanto bioquímicas como moleculares. Los resultados obtenidos muestran que el contenido de las EVs hepáticas es sensible a los diferentes modelos de DILI empleados, lo que podría ser de utilidad para fines diagnósticos. Además, las EVs hepáticas contienen diversas enzimas activas relacionadas con DILI incluyendo: la carboxylesterasa (CES), methionine adenosyl transferasa (MAT) y catechol *O*-methyltransferasa (COMT). En base a la caracterización mediante UPLC-MS del metaboloma asociado a EVs hepáticas, se han detectado diversas rutas celulares así como funciones susceptibles de ser modificadas mediante estas vesículas. Un ejemplo de ello son el ciclo de la metionina, el metabolismo energético, la síntesis de purinas y ADN o el control de la presión sanguínea local.

En conclusión, los resultados obtenidos apoyan que las EVs hepáticas podrían estar implicadas tanto en DILI como en la respuesta a otro tipo de daño hepático. Asimismo, también se presentan varias enzimas y moléculas como candidatos a marcadores de baja invasividad para la detección de DILI.

SUMMARY

Drug induced liver injury (DILI) is a serious worldwide health problem that accounts for more than 50% of acute liver failure. A great interest in clinical diagnosis and pharmaceutical industry is to find non-invasive markers for this pathology and also to elucidate the molecular mechanisms behind it. The discovery of cell-secreted extracellular vesicles (EVs) has provided a new cellular component with the ability to influence different biological and pathological processes. These EVs have been detected in blood and urine samples providing a new platform to identify non-invasive markers for different diseases. These vesicles are secreted by most cell types of the body including hepatocytes but despite the intense research on EVs, there is currently not too much knowledge neither on their physiological role or their implication in the development of diseases.

Hepatic EVs contain enzymes involved in drug metabolism, suggesting a possible role of these EVs in DILI. In this regard, in this doctoral thesis it has been characterized the secretion of hepatic EVs in different DILI *in vitro* models using molecular and biochemical approaches. The results showed that the molecular cargo of hepatic EVs is sensitive to DILI condition what could be useful for diagnosis purposes. In addition, hepatic EVs displayed several enzymatic activities that have been related with DILI including carboxylesterase (CES), methionine adenosyl transferase (MAT) and catechol *O*-methyltransferase (COMT). Furthermore, by using UPLC-MS based metabolomics to characterize the metabolome associated to hepatic EVs, a number of cellular pathways and functions susceptible to be modified by these vesicles were unravelled including methionine cycle metabolism, purine and DNA (Deoxyribonucleic acid) synthesis, energetic metabolism and local blood pressure.

In conclusion, our data support that hepatic EVs could play a role in DILI as well as in the response to other liver stresses, and also provide a number of molecules and activities as low-invasive candidate biomarkers for drug-induced liver injury.

3. INTRODUCTION

3.1. LIVER AND DRUG INDUCED LIVER INJURY

The liver is a multifunctional organ essential for the life. It is involved in an elevated number of metabolic pathways [1] such as glucose, proteins and fat metabolism. Particularly, the liver plays a prominent role in regulating blood glucose levels, storing the glucose as a glycogen reservoir or releasing it in the bloodstream as necessary under hormonal control [2]. As for protein metabolism, this organ not only synthesizes non-essential amino acid by means of transaminases, but also the most plasma proteins including albumin and coagulation factors. Conversely, it also breaks down proteins and removes the resulting toxic ammonium ion by converting it into urea [3]. In addition to this, the liver metabolizes fats or synthesizes triglycerides from excess carbohydrates and proteins and synthesizes cholesterol from fatty acids [4]. This organ also produces bile, which takes part in fat digestion along with the lipases to breakdown the ingested fat. Finally, the liver also acts as vitamin and mineral storage and is the main organ involved in xenobiotics metabolism [5].

To accomplish all these tasks, the liver employs not just hepatocytes, but also other non-parenchymal immune and non-immune cells. Liver tissue macrophages (Kupffer cells), natural killer cells, T cells and B cells are members of the hepatic immune system [6]. These cell populations regulate the immune system in liver and are important mediators in inflammation [7]. Among non-immune cells, the hepatic stellate cells, also known as Ito cells, are involved in angiogenesis and fibrosis processes [8]. However, the parenchyma of liver consists mostly of hepatocytes, which are the main cell type in the liver (~80%). Hepatocytes are polarized cells with multiple and complex functions. Among them, hepatocytes play an important role in detoxification, production and clearance of blood components.

The liver is prone to xenobiotic-induced injury because of its central role in xenobiotic metabolism, its portal location within the circulation, and its anatomic and physiologic structure [5][9]. In this regard, drug-induced liver injury (DILI) remains a major cause of worldwide mortality, according to the United States Acute Liver Failure Study Group [10]. DILI is a clinically important etiology of hepatic disease that, if not recognized, can lead to hepatic severe failure. Indeed, it accounts for more than 50% of acute liver failure. DILI can affect both parenchymal and nonparenchymal cells of the liver, leading to a wide variety of pathological conditions, including acute and chronic hepatocellular hepatitis, fibrosis/cirrhosis, cholestasis, steatosis, as well as sinusoidal and hepatic artery/vein damage [11]. Between these pathologies, the predominant forms of DILI include acute hepatitis (liver inflammation of abrupt onset), cholestasis (interruption in the excretion of bile), and a mixed pattern [12].

Although the exact mechanism of DILI remains unknown, it appears to involve 2 pathways; direct hepatotoxicity and adverse immune reactions (innate and adaptative immunity), being direct hepatotoxicity the most common pathway [13]. Direct hepatotoxicity is often caused by the direct action of a drug, or more often a reactive metabolite of the drug against different components of the hepatocytes causing a malfunctioning of them. In most instances, DILI is initiated by the bioactivation of drugs to chemically reactive metabolites, which have the ability to interact with cellular macromolecules such as proteins, lipids, and nucleic acids, leading to protein dysfunction, lipid peroxidation, DNA damage, and oxidative stress. These reactive metabolites may induce disruption of ionic gradients and intracellular calcium stores, resulting in mitochondrial dysfunction and loss of energy production. This impairment of cellular function can culminate in cell death and possible liver failure [13]. In adverse immune reactions, hepatocyte damage triggers the activation of other cells, which can initiate an innate and/or an adaptive immune response. The innate immune system provides an inflammatory reaction that is first line of defense against microbial infection, but it is not sufficient in eliminating all the components of infectious organisms. In this regard, cells of the innate immune system play an integral role in the initiation of adaptive immunity by presenting antigens and are crucial in determining the subsequent T cell or antibody-mediated immune response. Collectively, the innate and adaptive immune cells contribute to the unique immune responses of the liver, such as removal of pathogenic microorganisms or clearance of particles and soluble molecules from circulation [14].

The idiosyncratic nature and poor prognosis of DILI, makes it a major safety issue during drug development, as well as the most common cause for the withdrawal of drugs from the pharmaceutical market. Indeed, because of the significant patient morbidity and mortality associated with DILI [15], the U.S. Food and Drug Administration (FDA) has removed several drugs from the market, representing a serious clinical and financial problem [16]. The cost of introducing a new drug to the market (estimated at hundreds of millions of dollars) generates a high socio-economical pressure to understand the underlined mechanisms and to generate new tools and approaches for the identification of sensitive biomarkers for hepatotoxicity. In this regard, the clinical diagnosis and prediction of DILI remain a major challenge due to various confounding factors which include preexisting liver disease, multiple drug usage by patients, and most important, lack of reliable screening methods and diagnostic standards [13]. Currently, besides liver biopsy, the activity of a series of hepatic enzymes and proteins released into the blood by damaged liver cells are the most useful tools available in detecting liver damage in a non-invasive manner. Hepatic screening test measuring bilirubin (total and unconjugated), alkaline phosphatase, aspartate aminotransferase (AST), alanine aminotransferase (ALT), albumin, gamma-glutamyl transferase (GGT), prothrombin time and glutathione-S-transferase are routinely used in both preclinical and human clinical drug studies [17]. As a general rule, ALT levels greater than 3 times the upper limits of normal have been identified as a marker for liver injury. This observation is currently employed by the FDA in the evaluation of hepatotoxicity for newly developed drugs [15]. Nevertheless, none of them is sensitive or specific enough to be consider as specific marker for detecting DILI [17][18]. Therefore, the development of novel diagnostic biomarkers with greater sensitivity and specificity is needed for the development of improved preclinical screens and the design of more effective clinical trials to evaluate potential hepatotoxic effects of new drugs before its release into the pharmaceutical market.

Over 1000 drugs and herbal products have been implicated in the development of DILI and the list continue to grow [19]. In the present doctoral thesis, different liver injury models are studied in order to find new and specific biomarkers for DILI. Such models are based on galactosamine (GalN), acetaminophen (APAP) and diclofenac (DCF), three compounds that cause liver damage by different mechanisms. GalN is a well characterized hepatotoxin that causes acute liver injury similar to human viral hepatitis via depletion of uridine nucleotides, which subsequently diminishes synthesis of RNA (Ribonucleic acid) and proteins [20][21]. Although this compound also inhibits the energy metabolism of hepatocytes [22]. Model of GalN hepatotoxicity is frequently used in animal experiments *in vivo* [20]. Similarly, APAP is a classically used drug to study the mechanisms of hepatotoxicity [13]. This drug is an over-the-counter analgesic that is safe at therapeutic doses but at overdose can produce centrilobular hepatic necrosis, which may lead to acute liver failure. According to the United States Acute Liver Failure Study Group, hepatotoxicity caused by overdose of APAP accounts for 39% of acute liver failure. APAP is metabolized to its toxic metabolite, N-acetylp-benzoquinoneimine (NAPQI) [23], which during APAP overdose leads to the disruption of calcium homeostasis, mitochondrial dysfunction, oxidative stress and may eventually culminate in cellular damage and death [24][25]. Finally, the nonsteroidal antiinflammatory drug (NSAID) DCF is a model of idiosyncratic hepatotoxicity. It causes rare but significant cases of serious hepatotoxicity, typically with a delayed onset (1–3 months) [26]. Like other NSAIDs, DCF acts by inhibiting cellular cyclooxygenases (Cox-1 and Cox-2), which results in a decreased production of pro-inflammatory prostaglandin, prostacyclin and thromboxane products, important mediators of inflammation and pain. This drug is one of the most frequently used over-the-counter antiinflamatory worldwide. More than a hundred instances of clinically apparent liver injury due to DCF have been reported in the literature. Indeed, DCF ranks in the top 10 causes of drug induced liver injury. In overdose, it causes oxidative stress and mitochondrial injury with a pattern predominantly hepatocellular [27].

3.2. EXTRACELLULAR VESICLES (EVs)

A molecular biomarker is any biological molecule or pattern (proteins, metabolites, RNAs, gene expression profiles, etc.) that functions as a measurable indicator of the presence of a disease including its stage, progression and localization. As a consequence, a variety of strategies have been adopted for their discovery such as metabolomics, proteomics or transcriptional profiling. A key interest in clinical diagnosis and pharmaceutical industry is to have a repertoire of low-invasive biomarkers to be able to predict the degree of injury caused by a pathological condition or a drug. In this regard, the study of cell-secreted EVs as a platform to identify new disease biomarkers [28] has evolved rapidly in the recent years.

The discovery of EVs dates back to 1940, when preliminary studies were performed, addressing the “biological significance of the thromboplastic protein of blood” [29]. More than 20 years later, in 1967, this subcellular fraction was identified by electron microscopy and was shown to consist of small vesicles originating from platelets and termed “platelet dust” [30]. One decade later, fetal bovine serum was also shown to contain “numerous microvesicles” and they were presented as the breakdown products of normal cell components [31]. Meanwhile, within a completely different line of research, EVs were identified as being released from reticulocytes during their maturation into erythrocytes, whereby the transferrin receptor as a constituent component of those EVs becomes downregulated in the mature erythrocytes [32].

Since then, EVs are known to be released from most cell types including mast cells, dendritic cells, B lymphocyte cell lines, astrocytes, platelets, hepatocytes, neurons, endothelial cells, and epithelial cells [33]. Furthermore, EVs have been isolated from diverse body fluids, including semen [34][35], blood [36], urine [37], saliva [38], breast milk [39], amniotic fluid [40], ascites fluid [41], cerebrospinal fluid [42] and bile [43].

There is accumulating evidence that vesicles released from cells are heterogeneous in terms of biogenesis, secretion process and size [44]. In this regard, three main groups have been identified **(Figure 1)**: endosome-derived vesicles named exosomes, plasma membrane-shedding vesicles called ectosomes or microvesicles (MVs), and apoptotic bodies [1].

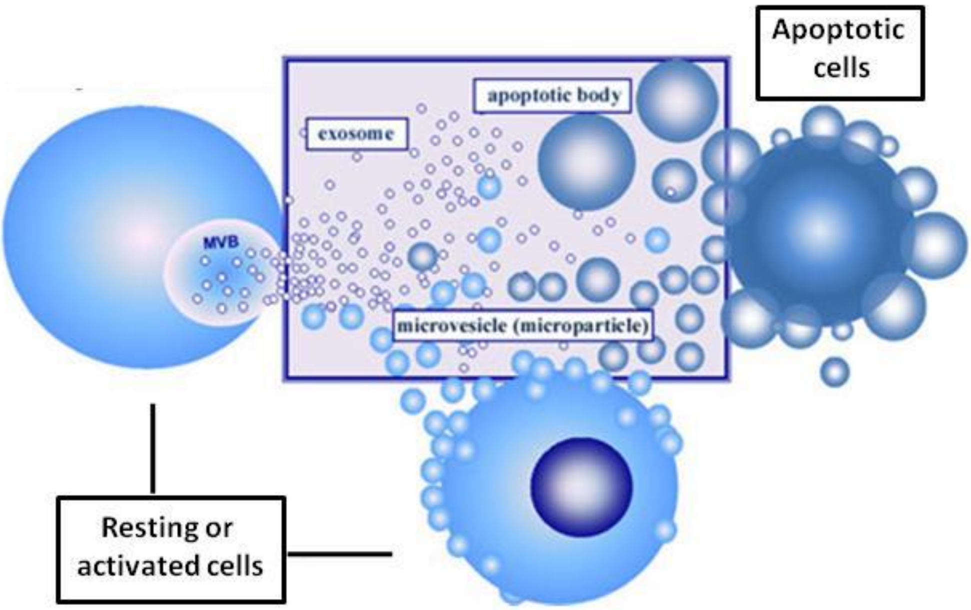

Figure 1. Schematic representation of the different type of extracellular vesicles (EVs). Major populations include exosomes, microvesicles and apoptotic bodies. Adapted from György *et al*. 2011[45].

Regarding cell-derived vesicles formation, at present, the detailed underlying mechanisms remain unclear [33]. However, there is enough evidence supporting the endocytic origin of some of these vesicles [46][47][48]. The release of this type of EVs is a process that appears to be conserved throughout evolution [49][50] suggesting essential functions of a dynamic EVs compartment. The endocytic pathway consists of highly dynamic membrane compartments involved in the internalization of extracellular ligands or cellular components, their recycling to the plasma membrane, and/or their degradation [51]. One of the compartments of the endocityc pathway are early endosomes, that matures into late endosomes [52] by changes in form, size, content and pH. During this process, late endosomes accumulate intraluminal vesicles (ILVs) that are formed by inward budding of the late endosome membrane, at the same time that some cytoplasmic molecules are engulfed. Because of the morphological features of late endosomes, they are generally referred to as multivesicular bodies (MVBs). The MVBs, have then two possible fates; fusion with lysosome (acidic compartment that contains lysosomal hydrolases), ensuring the degradation of their content, or fusion with the plasma membrane and consequent release of ILVs to the extracellular milieu, which are then called exosomes [53] **(Figure 2)**. Regarding MVs and apoptotic bodies, they are formed by regulated release of outward budding of the plasmatic membrane and as blebs containing cellular portions undergoing apoptosis respectively.

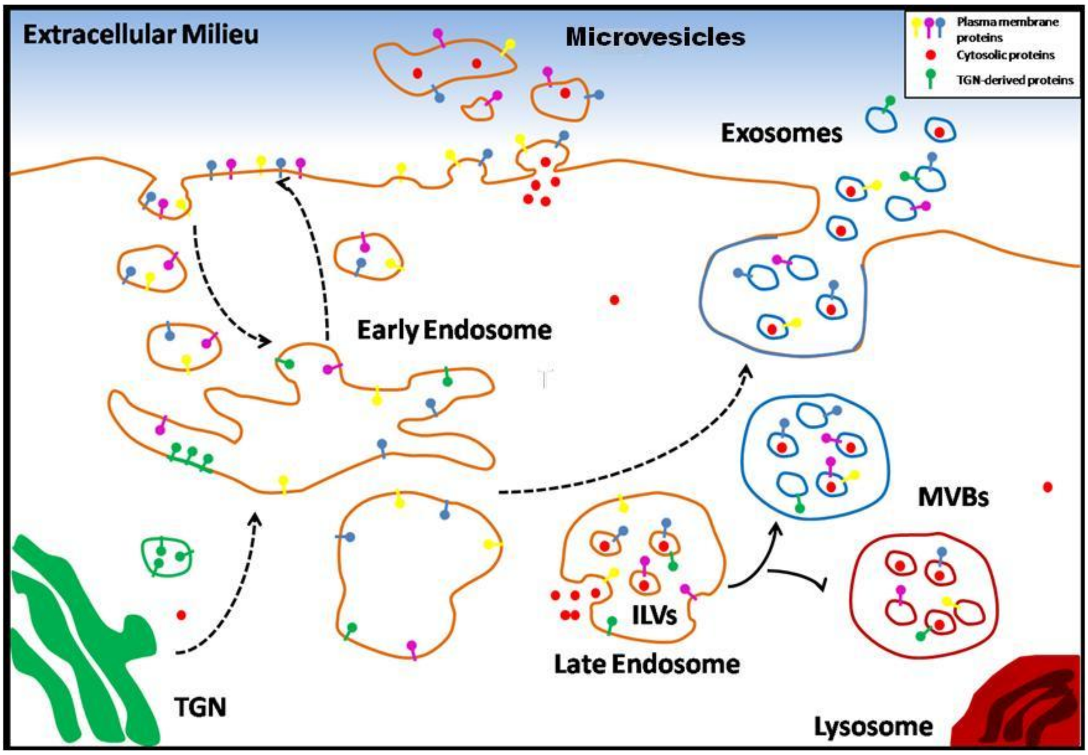

Figure 2. Biogenesis of EVs. Microvesicles bud directly from the plasma membrane. Exosomes are first termed ILVs when formed by inward budding into late endosomes (MVBs). Then, when ILVs are released by fusion of MVBs with the plasma membrane, are called exosomes. MVBs content can also go to degradation and therefore fuse with lysosomes. Plasma membrane proteins and lipids are represented in yellow, purple and blue. Cytosolic components in red and Trans Golgi network derived proteins in green. Arrows indicate proposed directions of protein and lipid transport between organelles and between MVBs and the plasma membrane for exosomes and MVs secretion.

All EVs present important differences but share some characteristics. As mentioned, exosomes have endocityc origin while MVs and apoptotic bodies are originated from plasma membrane. Moreover, the size is another of the main differences among the different types of EVs. Apoptotic bodies are the biggest vesicles, ranging from 1 to 5µm; then MVs, with a diameter size that ranges from 100 to 1000 nm and finally the exosomes, ranging between 50 and 150 nm. However, all EVs contain proteins, lipids and nucleic acids and also share some markers such as Annexin V, Cd81 or CD9 in the case of exosomes and MVs [45]. **Table 1** summarized the major key features of the different EVs.

Table 1. Main features of cell-derived EVs

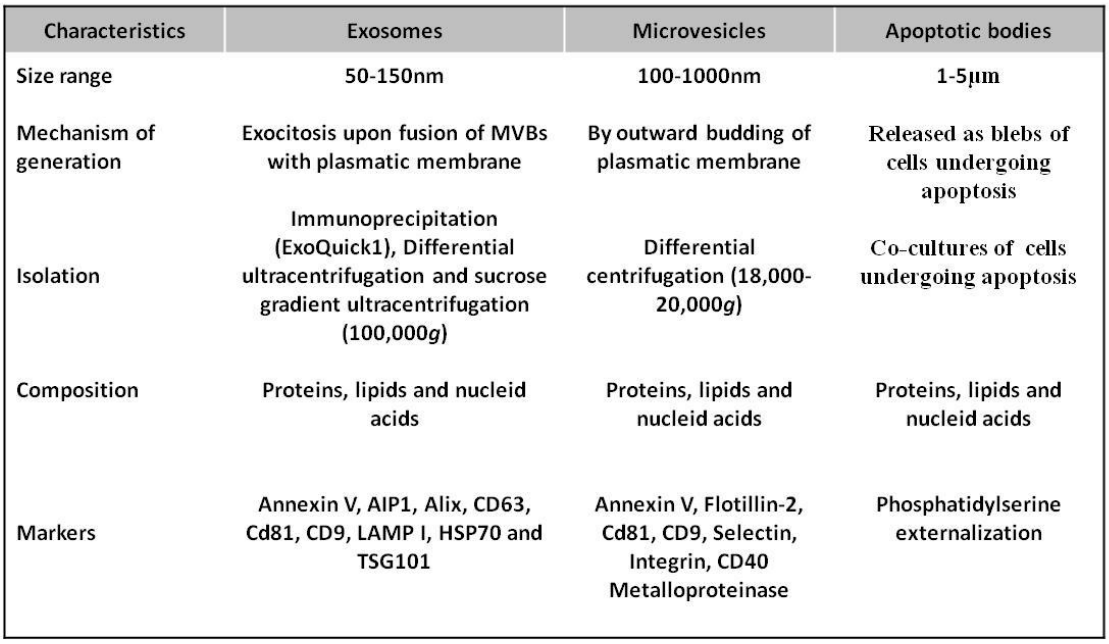

Characteristics	Exosomes	Microvesicles	Apoptotic bodies
Size range	50-150nm	100-1000nm	1-5µm
Mechanism of generation	Exocitosis upon fusion of MVBs with plasmatic membrane	By outward budding of plasmatic membrane	Released as blebs of cells undergoing apoptosis
Isolation	Immunoprecipitation (ExoQuick1), Differential ultracentrifugation and sucrose gradient ultracentrifugation (100,000*g*)	Differential centrifugation (18,000-20,000*g*)	Co-cultures of cells undergoing apoptosis
Composition	Proteins, lipids and nucleid acids	Proteins, lipids and nucleid acids	Proteins, lipids and nucleid acids
Markers	Annexin V, AIP1, Alix, CD63, Cd81, CD9, LAMP I, HSP70 and TSG101	Annexin V, Flotillin-2, Cd81, CD9, Selectin, Integrin, CD40 Metalloproteinase	Phosphatidylserine externalization

There are several isolation methods described for EVs. The conventional procedure to isolate exosomes and MVs involves mainly differential ultracentrifugation [60]. Briefly, the culture media is collected and filtered through 0.22 microns-pore filters, followed by subsequent ultracentrifugations at 10,000 x *g* (30 min) and 100,000 x *g* (60 min). The resulting pellet is enriched in EVs. An extra purification step involving a continuous density gradient has also been indicated to ensure obtaining exosomes-enriched preparations. The density at which exosomes float has been determined to range from 1.13 to 1.21 g/ml. In addition, in the last years, different commercial precipitating agents (e.g. Exoquick) have been developed in order to isolate EVs using methods more suitable for clinical practise. However, it is important to bear in mind that the EVs isolated using these precipitating methods are contaminated with non-vesicular material [54].

Most studies reported so far regarding biochemical composition of EVs, involve analysis of mixed populations of vesicles obtained by differential ultracentrifugation. Thus, the actual constitution of each subtype of EVs remains unknown. As a whole, EVs harbor a wide variety of proteins, phospholipids, lipids, mRNAs and microRNAs. **Figure 3** shows the overall composition of EVs. Nevertheless, their specific composition depends on the cell type of origin and the state of them, which is revealed by proteomic analysis in large scale of EVs from various cell types [33].

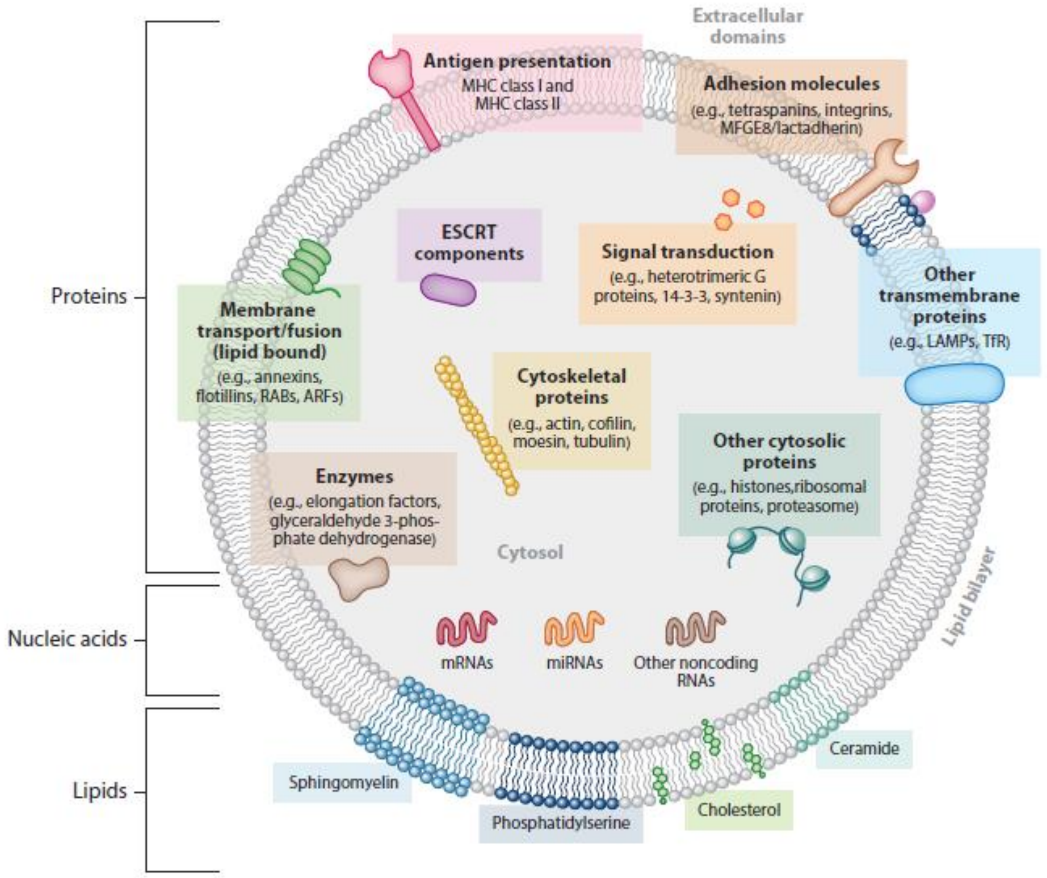
Extracellular domains
Antigen presentation
MHC class I and MHC class II
Adhesion molecules
(e.g., tetraspanins, integrins, MFGE8/lactadherin)
Proteins
ESCRT components
Signal transduction
(e.g., heterotrimeric G proteins, 14-3-3, syntenin)
Other transmembrane proteins
(e.g., LAMPs, TfR)
Membrane transport/fusion (lipid bound)
(e.g., annexins, flotillins, RABs, ARFs)
Cytoskeletal proteins
(e.g., actin, cofilin, moesin, tubulin)
Other cytosolic proteins
(e.g., histones,ribosomal proteins, proteasome)
Enzymes
(e.g., elongation factors, glyceraldehyde 3-phosphate dehydrogenase)
Cytosol
Lipid bilayer
Nucleic acids
mRNAs
miRNAs
Other noncoding RNAs
Lipids
Ceramide
Sphingomyelin
Cholesterol
Phosphatidylserine

Figure 3. Overall composition of EVs (Adapted from Colombo and Raposo. 2014) Schematic representation of the composition (families of proteins, lipids, and nucleic acids) and membrane orientation of EVs. Examples of tetraspanins commonly found in EVs include CD63, CD81, and CD9. Note that each listed component may in fact be present in some subtypes of EVs and not in others. For instance, histones and proteasome and ribosome components are probably secreted in large plasma membrane–derived EVs rather than exosomes. Abbreviations: ARF, ADP ribosylation factor; ESCRT, endosomal sorting complex required for transport; LAMP, lysosome-associated membrane protein; MHC, major histocompatibility complex; MFGE8, milk fat globule–epidermal growth factor-factor VIII; RAB, Ras-related proteins in brain; TfR, transferrin receptor.

Proteomic analysis shows a large overlap of protein expression between exosomes and MVs. As a consequence of their origin, EVs from different cell types contain endosome-associated proteins (e.g., Rab GTPase, SNAREs, Annexins and Flotillin), some of which are involved in MVB biogenesis (e.g., Alix and Tsg101 [55]). Membrane proteins that are known to cluster into microdomains at the plasma membrane or at endosomes often are also enriched on EVs. These include tetraspanins, a family of more than 30 proteins that are composed of four transmembrane domains [56]. Some of the tetraspanins contained in EVs are Cd63, Cd81, Cd82, Cd53, and Cd37. EVs are also enriched in proteins that associate with lipid rafts, including glycosylphosphatidylinositol- anchored proteins and Flotillin [49].

After the demonstration that EVs cargo included both mRNA and miRNA of various sizes and that EVs associated mRNAs could be translated into proteins by target cells [57][58], numerous groups have analyzed the presence of genetic material in EVs. Recently, it has been demonstrated that, in addition to mRNA and miRNA, EVs also contain a large variety of other small noncoding RNA species, including RNA transcripts overlapping with protein coding regions, repeat sequences, structural RNAs, tRNA fragments, vault RNA, Y RNA, and small interfering RNAs [59][60].

Fewer studies have analyzed the lipid and metabolites composition of EVs [61]. When comparing secreted vesicles with the total cell membranes, most of these studies observed enrichment of sphingomyelin, cholesterol, phosphatidylserine (PS), phosphatidylcholine, phosphatidylethanolamine and generally of saturated fatty acids [49]. These fatty acids together with the high concentration of cholesterol, may account for lateral segregation of these lipids into ILVs during their formation at MVBs. In this line, EVs are also enriched in proteins associated with lipid rafts, including glycosylphosphatidylinositol- anchored proteins and flotillin [62] [63].

The overall composition of EVs described above is representative of vesicles mixed populations. The databases ExoCarta [64], Vesiclepedia [65] and EVSpedia [66] catalog proteins, lipids, and RNA that have been identified in EVs from different sources.

Regarding EVs functions, they were first described to work as a cellular mechanism to remove unwanted plasma membrane proteins during the maturation process of reticulocytes. Ten years later, EVs were shown to bear MHC molecules and participate of immune reactions. Since then, several functions in cell-to-cell communication processes have been attributed to EVs such as a vehicle to exchange genetic material (mRNA and miRNA) between cells or as a shuttle for infectious agents (HIV, prions) to escape immune surveillance [57][67].

Many other functions have been assigned to EVs such as immune suppression, antigen-presenting, signaling molecules carriers, inflammation control, tumor growth (i.e. metastasis and angiogenesis), cell adhesion, coagulation, vascular repair, waste management and protection against stress among others [68].

3.3. HEPATIC EVs

Despite the increasing interest in EVs, at present there are few studies focusing on hepatic EVs. They were first described and characterized in 2008 by Conde-Vancell *et al* [69] in non-tumoral hepatocytes. In the study, it was reported a proteomic analysis of hepatic EVs where the vesicles content reflected the cell type of origin [69]. The proteomics analysis identified multiple proteins known to be involved in the endosomal pathway, such as annexins, small

GTP-binding proteins and several cytoskeletal (actin, tubulin), cytoskeletal binding-proteins (moesin, cofilin-1) and motor proteins (myosins). Another significant group consisted of secreted proteins, such as coagulation-related proteins, serum albumin and apolipoproteins that are released to the blood stream mainly by the liver. Conversely, numerous cytosolic proteins, presumably trapped during EVs biogenesis, were also identified. Besides these, many other proteins were also detected, such as cytochromes and UDP-glucuronosyltransferases that are involved in detoxification processes of both exogenous and endogenous compounds.

Regarding nucleic acid content, 1300 transcripts were detected associated to EVs released by rat hepatocytes [70]. From them, 223 transcripts were found associated mainly with hepatocyte functions. Remarkably, some of those RNAs are enriched in the EVs in comparison with the intracellular transcriptome suggesting that RNA cargo is selectively incorporated [26].

Several physiological roles for hepatic EVs have been suggested:

- **Intercellular communication:** Recently, the role of secreted EVs in the exchange of proteins, nucleic acids and lipids has awakened considerable interest in the field of intercellular signaling [6]. Indeed, several reports [71][72] have identified and characterized the role of EVs in intercellular communications. As mentioned before, EVs can transfer different types of molecules (e.g. proteins, lipids, mRNAs or even if viruses) to target cells, inducing a change in composition or behavior of target cells [70]. Remarkably, circulating liver-specific mRNA associated with EVs has been described in the bloodstream [73]. In general, the role of bloodstream mRNAs is still unclear. Since the first descriptions of mRNA associated to EVs, functional transfer of EV-associated RNA to the acceptor cells has been shown [57].
- **EV pathway for virus propagation:** Hepatitis C virus (HCV) is a major cause of chronic liver disease. HCV can entry into the cell and be delivered into early endosomes [74]. Indeed, in HCV-infected patients, viral RNA is associated with EVs in plasma [75].
- **EVs in regeneration and differentiation:** Liver is involved in detoxification of xenobiotics and noxious endobiotics, and therefore, continuously exposed to injuries. According to this, tissue regeneration is an important defensive mechanism maintaining the viability of this organ. Several studies support the possible role of hepatic EVs in liver regeneration [76][77][78].
- **EVs in bile duct proliferation:** Biliary EVs secreted by cholangiocytes take part in a pathway associated with the inhibition of cholangiocyte proliferation [79].
- **EVs in liver inflammation:** Non-alcoholic fatty liver disease is emerging as a major global liver disorder. It encompasses a spectrum of diseases from simple steatosis to hepatocellular carcinoma. But, the role of EVs in inflammation is ambiguous because EVs can elicit either inflammation [80] or immunosuppressive effects [81][82].
- **EVs´ miRNA and cancer:** Tumoral cells undergo deregulation of miRNA expression and are known to release miRNAs associated with EVs [83]. An exhaustive catalogue

of miRNAs present in EVs released by hepatic cancer cells has pointed towards TAK1 protein as one of the central targets of tumour-derived EV miRNA [84], which is an essential inhibitor of hepatocarcinogenesis.

To elucidate whether one or several of these possibilities are achieved by hepatic EVs, further investigation and better knowledge of the cargo and activities that are present in EVs is needed.

3.4. HEPATIC EVs IN DRUG INDUCED LIVER INJURY

Liver is the major body reservoir for enzymes involved in the metabolism of endogenous and xenobiotic compounds. In this regard, there are several works that have revealed the presence of different xenobiotic metabolizing enzymes in hepatic EVs [85][86]. Thus, several members of Cytochromes P450 (P450s), UDP-glucuronosyltransferases (UGTs), and Glutathione S-transferases (GSTs) proteins families [87], all of them important enzymes involved in xenobiotic metabolism, were detected in EVs secreted by hepatocytes.

Cytochromes P450s are monooxygenases that catalyze phase I reactions. They constitute the largest family of xenobiotic compound metabolizing enzymes. It metabolizes a wide variety of xenobiotics to pharmacologically inactive metabolites (approximately 75% of all clinically relevant drugs), and occasionally, to toxicologically active metabolites [35]. Impairment of cytochrome P450 activity, which may be either genetic or environmental, may lead to toxicity caused by the parent compound itself, affecting the susceptibility to hepatic injury. P450 enzymes may also convert the drug to a chemically reactive metabolite, which, if not detoxified, may lead to various forms of hepatic and extrahepatic toxicity, including cellular necrosis, hypersensitivity, teratogenicity, and carcinogenicity.

UGTs catalyze phase II glucuronidation reactions and metabolize a wide range of drugs as well as other xenobiotics, including environmental and dietary xenobiotics [88]. In addition, the other major contributor to drug metabolism, the GSTs family, also catalyzes Phase II reactions. The general action of GST enzymes is the addition of glutathione (GSH) to a wide variety of endogenous and exogenous substrates [89]. GSTs are commonly responsible for the metabolism of oxidation products such as epoxides derived from the metabolism of P450s on polycyclic aromatic hydrocarbons. The addition of GSH moieties to these metabolically reactive epoxides turns them up into inactive forms that are readily excretable from the body [90]. Interestingly, the mediated conjugation of GSH to xenobiotic compounds by GSTs has also been observed to yield metabolites that are cytotoxic and if not detoxified, may lead to various forms of hepatic and extrahepatic toxicity, including cellular necrosis, hypersensitivity, teratogenicity, and carcinogenicity [91].

These drug-metabolizing enzymes, apart from metabolizing drugs to their corresponding inactive forms, may also cause a toxicological effect provoking direct hepatotoxicity by reacting with different molecules and altering their normal functions. For instance, it is reported that P450 and UGT families are target proteins of autoantibodies in several hepatic and extrahepatic autoimmune diseases, causing immune-mediated liver injury [92]. All these data support a role of hepatic EVs in establishment and propagation of DILI.

EVs act as vectors since they transport and protect not only proteins but also phospholipids, microRNAs and messenger RNAs (mRNAs) as biological messages [33]. In particular, hepatocyte-derived EVs contain liver specific mRNAs that are found in the bloodstream [93]. Importantly, amplification and quantification of these nucleic acids in blood samples have proved to be more sensitive than traditional transaminase activity quantification for detecting liver damage [73]. In this regard, it has been reported the possible role of hepatic RNA-containing EVs as a suitable non-invasive biomarker for liver toxicity [94]. Using *in vitro* and *in vivo* liver disease models based on GalN, APAP and DFC it was found that the expression of various RNAs enriched in the corresponding EVs was altered.

By examining the levels of albumin and beta polypeptide 2-like 1 (Gnb21) transcripts it was possible to distinguish between the three treatments. Therefore, liver damaging drugs are able to modify RNA content of these vesicles. Overall, these results suggest that the RNAs contained in hepatic EVs are a suitable biological source for non-invasive biomarker discovery of liver toxicity and for discrimination between different liver injuries.

In addition, the comprehensive proteomic analysis performed in hepatocyte-derived EVs, revealed the presence of other relevant metabolic enzymes [69][95], such as Carboxylesterase 1d (Ces1d), Methyl-adenosyltransferase (MAT) and Cathecol-*O*-methyl transferase (COMT) that could also play a role in the development of DILI.

3.4.1. CARBOXYLESTERASE (CES*)*

There are different types of chemical reactions used to metabolize drugs, being the hydrolysis reactions the most common. In this sense, there is an immense variety of hydrolases, being CES one of the most significant related with xenobiotic metabolisms playing an important role in detoxification processes [87].

CES proteins belong to Phase I group of drug metabolizing enzymes. These enzymes efficiently catalyze the hydrolysis of a variety of ester- and amide-bonds containing chemicals and drugs to their respective free acids. They are involved in detoxification and metabolic activation of various drugs, environmental toxicants and carcinogens. CES also catalyze the hydrolysis of endogenous compounds such as short and long chain acyl-glycerols, long-chain acyl-carnitine and long-chain acyl-CoA esters [96].

CES comprise a multi-gene family whose gene products are localized in the endoplasmatic reticulum of many mammal tissues including liver, small intestine, lung, testis and macrophages [97]. Experimentally, microsomes purification from CES expressing cells is the best source of this type of enzymes [96].

Mammalian CES are members of an *α,β*-hydrolase-fold family and they can be classified into five major groups denominated CES1-CES5 according to the homology of the amino acid sequence. There are some differences between these groups in terms of substrate specificity, tissue distribution, immunological properties and gene regulation [96], [98].

CES1, CES2 and CES3 are the three major carboxylesterases detected in human liver [99]. *Ces1d* isoform, which is homologous to human CES1 [69], is the most abundant in EVs secreted by rat hepatocytes. In this regard, one of the objectives in this doctoral thesis is to demonstrate that this enzyme is active in hepatocytes-secreted EVs.

3.4.2. METHIONINE ADENOSYL-TRANSFERASE (MAT)

MAT is the only enzyme responsible for the biosynthesis of S-adenosylmethionine (SAMe), the principal biological methyl donor, precursor of polyamines and in the liver, precursor of glutathione [100], that has a relevant role in controlling oxidative stress.

The unique chemical structure of SAMe confers it the ability to participate in multiple biological reactions, being methylation, transsulfuration and aminopropylation the three major ones [101] **(Figure 4)**. In methylation reactions, the methyl group is transferred to a large variety of substrates, such as DNA, RNA, proteins, phosphatidylethanolamine (PE), glycine and guanidinoacetate. These transmethylation reactions are catalyzed by specific methyltransferases (MTs) and over 200 proteins in the human genome have been identified as known or putative SAMe-dependent MTs [102]. During transmethylation, the methyl group of SAMe is transferred to the acceptor substrates and S-adenosylhomocysteine (SAH) is generated. SAH is then hydrolyzed to homocysteine (Hcy) and adenosine in a reversible reaction. In transsulfuration reactions, the sulfur atom of SAMe undergoes a series of reactions and is converted to cysteine and GSH, one of the main anti-oxidant molecules in cells. SAMe can also take part in radical reactions via its adenosine group and generate the 5´-deoxyadenosyl radical, which is a powerful oxidizing agent **(Figure 4)**. On the other hand, aminopropylation is involved in the synthesis of polyamines, necessary for cell proliferation among other functions. Through this pathway, SAMe is decarboxylated and its aminopropyl group is transferred, first to putrescine to form spermidine and 5´-methylthioadenosine (MTA) and then to spermidine to form spermine and a second molecule of MTA. The two molecules of MTA generated during this process exert an inhibitory effect on polyamine synthesis and consequently, on methionine synthesis as well [103]. The MTA molecules are then eliminated in order to restore the methionine levels of the cell **(Figure 4)**.

An integrated view of SAMe metabolism combine methylation, transsulfuration and amynopropilation pathways. Importantly, these reactions can affect a wide spectrum of biological processes ranging from metal detoxification and catecholamine metabolism to membrane fluidity, gene expression, cell growth, differentiation, and apoptosis [104].

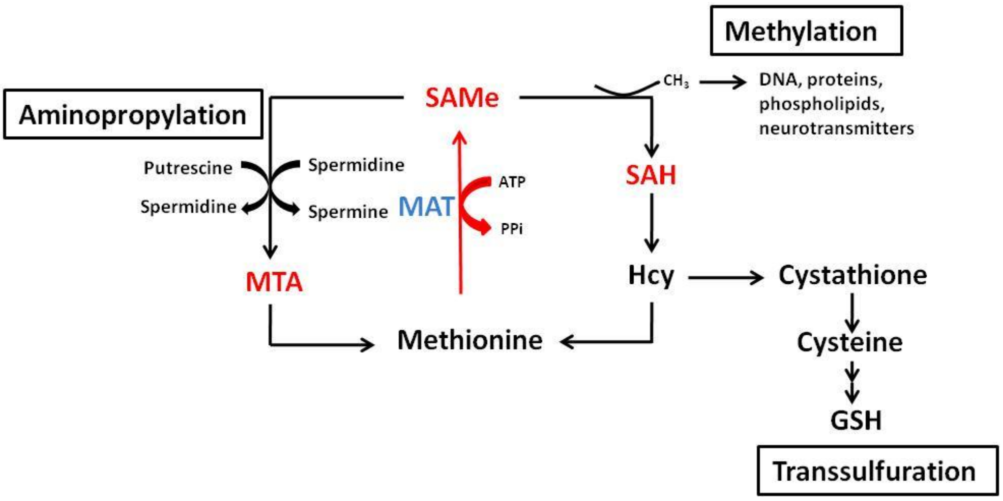

Figure 4. Schematic view of Methionine cycle metabolism. Methionine adenosyltransferase is involved in methionine cycle. SAMe participates in multiple biological processes, including methylation, transsulfuration and amynopropylation pathways. During methylation, MAT converts methionine to SAMe using ATP as co-substrate. When the methyl group of SAMe is transferred to the acceptor substrates, S-adenosylhomocysteine (SAH) is generated, which is then hydrolyzed to form homocysteine (Hcy). Moreover, when SAMe is decarboxylated to transfer its aminopropyl group for polyamines synthesis, 5´-methylthioadenosine (MTA) is generated as a by-product.

Although all mammalian cells synthesize SAMe, the liver is where the bulk of SAMe is generated, as it is the organ where about 50% of all dietary methionine is metabolized and where up to 85% of all transmethylation reactions take place [105][106]. Thus, SAMe regulation is very important for liver homeostasis. Abnormal MAT activity is linked to many diseases outside and inside the liver. Indeed a failure in SAMe regulation can lead to fatty liver disease, cirrhosis or hepatocellular carcinoma (HCC) among others [100].

3.4.3. CATECHOL-*O*-METHYL TRANSFERASE (COMT)

COMT is a enzyme that catalyzes the transfer of a methyl group from SAMe to one of the hydroxyl groups of a catecholamine **(Figure 5)** [107], [108]. By means of this reaction, the general function of COMT is the elimination of biologically active or toxic hydroxylated metabolites and catechols. In this line, COMT acts as an enzymatic detoxicating barrier between the blood and other tissues shielding against the detrimental effects of xenobiotics [109].

Catecholic compounds belong to a heterogenous group of reactive molecules that participate in chemical and biological reactions such as redox cycling, production of reactive oxygen species (ROS) or DNA and protein damage [110]. In mammals, catechols can occur as cathecol drugs (some dietary and medicinal products), metabolites in the degradation of cathecolestrogens or other endogenous compounds, such as cathecholamine neurotransmitters or regulators of endothelial permeability. So, catechol-metabolizing system has a potential pathophysiological and pathogenic significance in estrogen-induced hormonal cancers, in the development of degenerative brain disorders as Parkinson's disease or depression, as well as in the development of cardiovascular diseases [111].

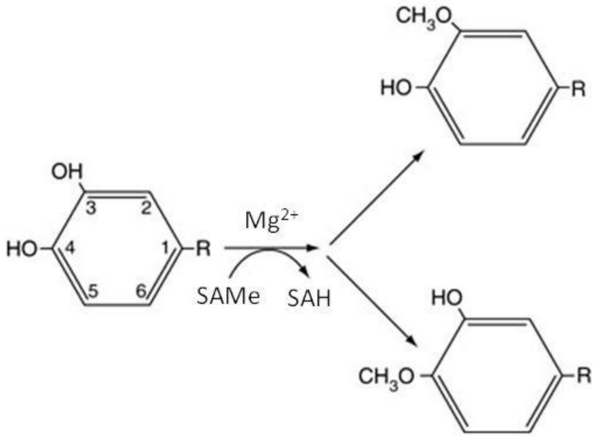

Figure 5. The basic function of Catechol-O-Methyltransferase. Enzymatic O-methylation of the catechol substrate to 3-Methoxy (major route) or 4-Methoxy (minor route) products in the presence of Mg^{2+} and SAMe [109].

Among cathecolestrogens, 17-beta estradiol and salvianolic acid A (SAA) are found. 17-beta estradiol [112] is an essential estrogen hormone for sexual and reproductive development, mainly in females, although it also has important effects in many other tissues including liver. In this regard, it can lead to cholestasis by inducing a reversible inhibition of bile flow. Therefore, 17-beta estradiol is a toxicologically active metabolite that requires to be removed by COMT [113]. Concerning SAA, COMT is also responsible for methylated transformation of this phenolic acid metabolically unstable. Interestingly, metabolites derived from O-methylation of SAA display high antioxidant potency against liver lipid peroxidation [114]. Moreover, considerable evidence has also demonstrated the potent protective effects of SAA against ischemia-induced injury [115][116].

Among cathecholamine neurotransmitters, dopamine (DA) and norepinephrine (NE), also called noradrenaline are found. DA and NE neurotransmitters play essential roles in controlling several forebrain functions. Consequently, perturbations of these neurotransmitters may contribute to the pathophysiology of neuropsychiatric disorders. [117]. According to this, the role of NE and DA neurotransmitters in the mechanism of action of antidepressant drugs as well as of drugs for Parkinson's disease prompted extensive studies.

In Parkinson's disease, dopaminergic neurons in the brain are gradually destroyed, leading to a DA deficiency and to the onset of symptoms of Parkinson's disease [118]. To overcome this, an option is to administrate DA precursors such as Levodopa (L-DOPA), the most effective medication in Parkinson's disease [119]. However, L-DOPA is removed by COMT. Thus, in the late 1980s, potent and selective COMT inhibitors were introduced [120]. In this way, when L-DOPA is administered together with COMT inhibitors, the peripheral metabolism of L-DOPA diminishes, increasing its bioavailability [121]. Tolcapone, for instance, is a selective COMT inhibitor that extends the duration of action of L-DOPA. But it has been observed to cause hepatotoxicity such as cholestatic injury which is reflected by an abnormal increased level of liver transaminases. Moreover, Tolcapone also caused hepatocellular injury since the mitochondrial ATP/ADP ratio is also decreased [122].

With reference to NE neurotransmitter, it produces wide-ranging effects on many areas of the body and is often referred to as a 'fight or flight' chemical, as it is responsible for the body's reaction to stressful situations. It triggers the release of glucose into the blood stream and increases blood pressure, heart rate, mental alertness and respiratory rate. Depression, anxiety, arterial hypotension, heart rate issues, and many other illnesses can be attributed, at least partially, to NE deregulation. In this regard, arterial hypotension occurs frequently in patients with acute liver failure (ALF). Treatment with NE and DA in patients with ALF is widely used as a vasopressor medication [123]. Moreover, NE concentrations in plasma are elevated in patients with cirrhosis [124].

Although COMT can be found in many tissues, the liver is the most important site for the metabolism of circulating catechols containing molecules [107]. Indeed, the liver exhibits clearly the highest COMT activity and protein levels followed by kidney, intestinal tract, heart and brain [125]. Consistent with this, COMT has been recently reported as a biomarker of liver injury. In the early stages, even before the current standard liver biomarker, alanine transaminase (ALT) and histopathology indicate liver injury, COMT levels change significantly in both liver tissue and plasma [126].

Given the importance of the processes in which COMT is involved, the interest in this enzyme has considerably increased. Thus, more reliable, sensitive and rapid analytical COMT assays are needed, for example, to test *in vitro* efficacy of new COMT inhibitor candidates, to the determination of the structure-activity relationship of COMT or to measure COMT activity in various human disorders including schizophrenia, kidney disease, hypertension, Parkinson´s disease, and estrogen-induced cancers [107], [127]. According to COMT inhibitors, their efficacy is commonly determined in clinical studies and therefore, good sensitivity analytical method is required. To do that, there is a great variation in analytical methods for COMT activity measurement. Yet, High Performance Liquid Chromatography (HPLC) methods and radiochemical assays are the most commonly used methods[108], [128]–[132].

In this doctoral thesis a novel method has been developed for the determination of COMT activity by UPLC-MS, using two different endogenous substrates (DA and NE) (**Figure 6**).

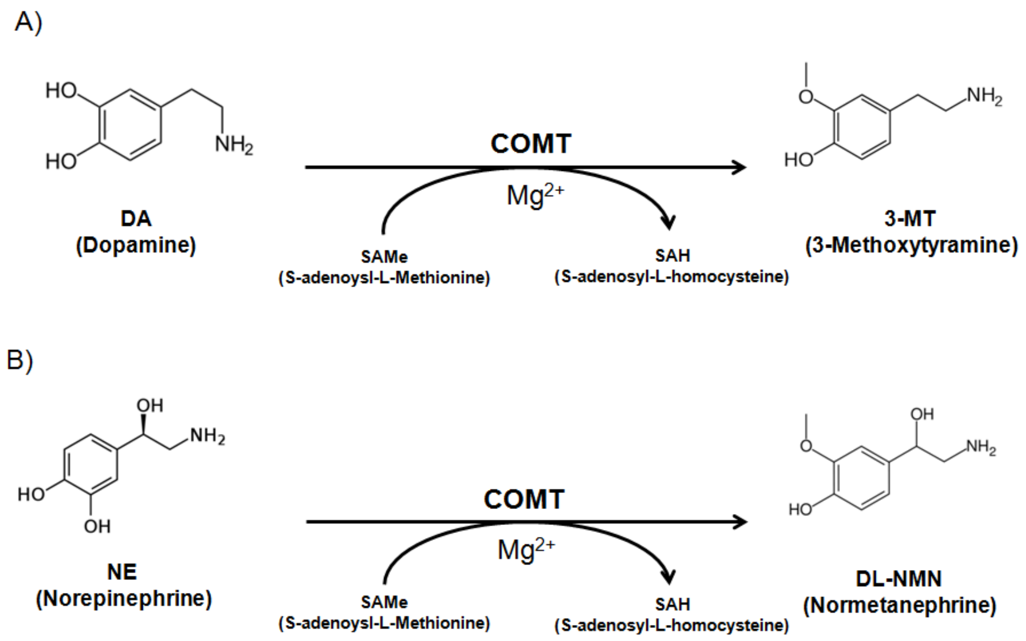
A)
HO
HO
NH2
DA
(Dopamine)
COMT
Mg2+
SAMe
(S-adenoysl-L-Methionine)
SAH
(S-adenosyl-L-homocysteine)
O
HO
NH2
3-MT
(3-Methoxytyramine)
B)
OH
NH2
HO
OH
NE
(Norepinephrine)
COMT
Mg2+
SAMe
(S-adenoysl-L-Methionine)
SAH
(S-adenosyl-L-homocysteine)
O
HO
OH
NH2
DL-NMN
(Normetanephrine)

Figure 6. Cathechol-O-Methyltransferase catalyses methylation of Dopamine and Norepinephrine. (A) The methyl group of SAMe is transferred to Dopamine forming 3-methoxytyramine **(B)** or to Norepinephrine forming Normetanephrine in a reaction catalyzed by COMT.

Overall, the alteration in protein expression of the studied enzymes [95] together with their presence in hepatic EVs, were the main reasons to study in detail their activity in diverse *in vitro* drug induce liver injury models.

3.4.4. METABOLOMIC PROFILING OF HEPATIC EVS

Over the last decades there has been an important revolution in biomedical science with the search for single genes, transcripts, proteins or metabolites being substituted by the coverage of the entire genome, transcriptome, proteome and metabolome. Genomics, trancriptomics and metabolomics are considered important tools for interpreting and understanding the complex biological processes given their capability to measure changes in multiple entities simultaneously, providing an overview of different physiological or pathological conditions [133].

From these “omics” technologies, metabolomics is the most recently developed and involves the measurement of hundreds to thousands of small molecules called metabolites (<2000 Da). These metabolites include molecules from different chemical nature, such as carbohydrates, vitamins, lipids and amino or fatty acids [134]. Metabolomics allows the qualitative and quantitative measurement of the metabolic response of a biological system to physiological or pathological stimuli.

Metabolomics can be divided into two different types, targeted (metabolic target analysis) and untargeted (metabolic profiling) [135][136]. The use of targeted approaches in research is quite old, and appeared long before the emergence of the “metabolomics” terminology [135]. This analysis includes the identification and quantification of a small set of metabolites using the most suitable analytical techniques for those compounds to avoid interferences [137]. The chemical identities of the metabolites to be assayed are known before data acquisition commences and this is a significant advantage with regards to metabolic profiling. In this regard, in this doctoral thesis, targeted metabolomics has been applied to the study of COMT and MAT enzymatic reactions.

In contrast, in metabolic profiling, the aim is to provide a holistic picture of the system. From the metabolite it is infered the protein involved in the regulation of that metabolite, and therefore the transcript and the gene. A large number of metabolites can be quantified [138] from cells, tissues or biofluids to generate metabolic profiles [139]. Then, the biological relevance of these metabolic profiles can be evaluated via pathway analysis. The combination of metabolomics and software specialized in visualizing cellular pathways, offer a tool to identify and integrate the different metabolic pathways that are affected by a determined stimuli [140]. Interestingly, comparisons of such profiles from different genotypes are being used to identify specific metabolic changes leading to the understanding of physiology, toxicology and disease progression. Overall, both, targeted and untargeted metabolomics, reveal the expected behavior of known metabolites, but only untargeted metabolomics allows also the detection of synergic effects between variables which cannot be observed at an individual level [141].

The metabolome is highly dynamic, so it reflects the actual biological state given the rapid metabolic response to microenvironment changes [142]. This is particularly important for the assessment of rapid and progressive diseases. In this regard, application of metabolomics is growing rapidly covering a wide range of applications [143][135] including: disease diagnosis, drug discovery and development, pharmacometabolomics and personalized medicine, nutrigenomics, metabolic engineering/biotechnology and toxicology [137]. The basis of all these applications has a common aspect; alterations in metabolism due to a functional response of a given condition, results in an alteration in the metabolic profile, leading a characteristic patterns, which could give new insights into the underlying biological state [135].

In summary, metabolomics can help to elucidate different metabolic profiles that will ultimately give information about different pathways in which a specific phenotype or biological system is implicated. Moreover, UPLC-MS based metabolomics is a powerful tool for biomarker discovery in hepatic EVs that, at the end, could allow the development of novel diagnostic methods and therapies.

4. HYPOTHESIS AND OBJECTIVES

It is reported that hepatic EVs contain relevant enzymes involved in drug metabolism such as CES, cytochromes P450 or UGTs. Interestingly, some of these enzymes not only can contribute to drug metabolism but also in DILI development. Furthermore, these families of proteins are target of autoantibodies in several autoimmune diseases, causing immune-mediated liver injury. Based on these data, the possible role of hepatic EVs in DILI is hypothesized. Basing on this hypothesis, hepatic EVs could constitute a powerful tool for DILI biomarker discovery. In this regard, the first objective of this study is to characterize the secretion of hepatic EVs in different DILI *in vitro* models. At the same time, their putative role as liver injury indicators is also evaluated. With this aim, different molecular approaches were employed such as immunostaining, Western Blot Analysis, Cryo-Electron Microscopy (Cryo-EM), particle tracking analysis (NTA) or Raman tweezers microspectroscopy (RTM).

It is known that there are several drug metabolizing enzymes contained in hepatic EVs but, are they active? To address this question, the second objective of this study is to analyze by UPLC-MS technology specific enzymatic reactions. With this aim, an UPLC-MS based enzymatic activity determination and quantification method was developed for each of the studied enzymatic reactions. Moreover, these methods could be used to prevent DILI in a personalized manner by measuring these enzymatic activities in circulating hepatic EVs. In this way, an individual hepatic response could be estimated in order to determine drug optimal dosis.

Finally, the third objective of this study is to elucidate/characterize the metabolic profile of MLP-29 murine cell line derived EVs through UPLC-MS-based metabolomics in order to identify pathways and functions where these vesicles are involved. Moreover, metabolomics as a tool for biomarker discovery on hepatic EVs is evaluated since alterations in metabolism (metabolites downregulation or upregulation) due to a functional response of a given condition such a drug overdose, results in an alteration in the metabolic profile, leading a characteristic pattern that could give new insights into the underlying biological state. In this regard, the screening of biomarkers candidates contained in hepatic EVs would enable the simultaneous profile of a large number of metabolic signatures in a given condition.

In summary, the main objectives of this thesis are:

1. To characterize the secretion of hepatic EVs in different DILI *in vitro* models and evaluate their role as putative low-invasive liver injury indicators.

2. To demonstrate through UPLC-MS that hepatic EVs carry active enzymes.

3. To characterize the metabolic profile of EVs-derived from MLP-29 murine hepatic cell line by using UPLC-MS based metabolomics in order to investigate the pathways in which these vesicles are involved and evaluate metabolomics as a tool for biomarker discovery in hepatic EVs.

5. EXPERIMENTAL PROCEDURES

5.1. REAGENTS AND CELL CULTURE

All chemical reagents were HPLC grade and suppliers are indicated in the specific description of each procedure.

Next are listed antibodies employed in this doctoral thesis:

- Mouse monoclonal antibodies were purchased from the indicated vendors: anti-Rab8 (clone 4/Rab 4), anti-Hsp90 (clone 68), anti-flotillin-1 (clone 18), anti-CD63 (clone H5C6) and anti-BiP/Grp78 from BD Biosciences; anti-TSG101 (4A10) from Santa Cruz Biotech and anti-CD81 (Eat2) from AbD Serotec.
- Rabbit polyclonal antibodies were acquired from the indicated vendors: anti-LIMP II (ab16522) and Cyp 2d1 (ab22590) from Abcam; anti-COX IV (3E11) from cell signaling and anti- MAT1A was developed in-house.
- Goat polyclonal antibodies were acquired from the indicated vendors: anti-CES (M-14) from Santa Cruz Biotech and anti-COMT (ab51984) from Abcam.
- Horseradish peroxidase (HRP)-conjugated secondary antibodies anti-mouse, rabbit, goat, were purchased from GE Healthcare.
- Cy3-conjugated secondary antibodies anti-mouse (715-165-150) and anti-goat (705-165-147) were purchased from Jackson Immuno Reseach.
- Alexa 488-conjugated secondary antibodies anti-mouse (A21202) and anti-rabbit (A21206) were purchased from Molecular Probes.
- Fluorescein isothiocyanate (FITC)-conjugated Phalloidin (P5282) employed to bind F-actin was purchased from Sigma-Aldrich.

Cell tissue cultures employed in this work were primary rat hepatocytes and MLP29 liver-derived murine cell line. Primary hepatocytes were obtained by perfusion of rat liver (see procedure below). MLP29 was provided by Dr. E. Medico [144]. Suppliers of cell culture reagents are indicated in the specific description of the procedures.

5.2. ANIMAL EXPERIMENTATION

Fourteen weeks old male Wistar rats (body weight 300-400 g), were maintained in an environmentally controlled room at 22°C on 12 h light/dark cycle and provided with standard diet (Rodent Maintenance Diet, Harlan Teklad Global Diet 2014) and water *ad libitum*. All surgery required for primary hepatocytes preparation was performed under anaesthetic gas Isoflurane (IsoFLO, Abbott Laboratories), and all efforts were made to minimize suffering.

For *in vivo* model of liver damage in RNA assay/analysis, rats received an intraperitoneal injection of 1 g/kg/5 ml of D(+)-galactosamine hydrochloride (GalN, Sigma-Aldrich). A control group of animals received the same volume of saline solution. Blood samples from each animal were drawn 18 h after the injection, and the sera were transferred to fresh Eppendorf tubes and stored at -80°C.

All animal experimentation was conducted in accordance with the Spanish Guide for the Care and Use of Laboratory Animals, and with International Animal Care and Use Committee Standards. All procedures were approved by the CIC bioGUNE ethical review committee (Permit Number: P-CBG-CBBA-3610) accredited by AAALAC organizations.

5.3. CELL VIABILITY ANALYSIS

Cell viability was measured with a benchtop automated cell counter (Countess^{TM}, Life technologies) that performs cell count and viability (live, dead, and total cells) measurements using trypan blue staining. Briefly, cell sample was mixed 1:1 with trypan blue. A fraction of 10 µL of the sample mixture was then loaded into a Countess™ cell counting chamber slide. The camera of the equipment acquires cell images from the sample on the slide and the image analysis software automatically analyzes acquired cell images, and measures cell count and viability based on trypan blue exclusion method. The measurement provides live and dead cell concentration (per mL), total cell concentration (per mL) and viability (% of live cells).

5.4. IMMUNOFLUORESCENCE STAINING

Primary rat hepatocytes were seed to 50–80% confluence on glass coverslips and after incubation at 37ºC for a period of time under indicated conditions, cells were fixed for 10 min with 2% formaldehyde in Dulbecco’s modified phosphate-buffered saline (DPBS, Gibco) and then washed with DPBS. Successive incubations with primary and fluorophore-conjugated-secondary antibodies diluted in a PBS solution containing 0.1% BSA and 0.1% saponine were carried out for 30 min. After each incubation period, unbound antibodies were removed by washing the coverlips in PBS. Finally, the coverslips were mounted onto glass slides on Fluoromont G (Southern Biotechnology Associates, Birmingham, AL) containing 0.7 g/ml 4',6-diamidino-2-phenylindole (DAPI) to stain DNA (nucleus). All procedure was carried out at room temperature. All immunostainings were analyzed in a Leica Confocal microscope (Leica) and images were taken using a Leica confocal software.

5.5. WESTERN BLOT ANALYSIS

Cell pellets of 1×10^6 cells were lysed during 15 min on ice in the presence of 150 µl of lysis buffer (1% Triton X-100, 300 mM NaCl, 50 mM Tris-HCl, pH 7.4) before centrifugation at

14,000 × *g* for 5 min for clarification of the sample. The supernatant was transferred to a fresh eppendorf tube. The protein concentration of the preparations was determined by means of a Bradford protein assay (Bio-RadLaboratories, Inc) using bovine serum albumin (BSA) as standard [145]. NuPAGE® LDS Sample Buffer (Life Technologies, Inc) was added to the protein extract and incubated for 5 min at 37, 65 and 95ºC in order to prepare protein samples for denaturing gel electrophoresis. After cooling and clarification by centrifugation, samples were loaded and separated on 4-12% pre-casted polyacrylamide gel electrophoresis (NuPAGE® Bis-Tris gel, Life Technologies, Inc). Once the electrophoresis was finished, proteins were transferred to Polyvinylidene difluoride (PVDF) membrane and blocked for 1 h (5% non-fat dry milk and 0.2% Tween-20 in DPBS). PVDF membranes were incubated 1 h with primary antibody followed by DPBS washes and subsequently 30 min incubation with horseradish peroxidase (HRP)-conjugated secondary antibody. Chemioluminiscence detection of bands was performed using ECL Plus chemiluminiscent substrate (GE Healthcare, Buckinghamshire, UK). All proteins were detected under non-reducing conditions.

Protein concentration was determined by Bradford assay (Cat. Num. 5000006, Bio-Rad Laboratories, Inc) using bovine serum albumin as standard.

5.6. CRYO- ELECTRON MICROSCOPY (Cryo-EM)

For Cryo-EM, EVs preparations were directly adsorbed onto glow-discharged holey carbon grids (QUANTIFOIL, Germany). Grids were blotted at 95% humidity and rapidly plunged into liquid ethane with the aid of VITROBOT (Maastricht Instruments BV, The Netherlands). Vitrified samples were imaged at liquid nitrogen temperature using a JEM-2200FS/CR transmission cryo-electron microscope (JEOL, Japan) equipped with a field emission gun and operated at an acceleration voltage of 200 kV. In cryo-EM sessions, digital images were taken using low-dose technique by means of an ULTRASCAN 4000SP (4096 × 4096) cooled slow-scan CCD camera (GATAN). An in-column energy filter (Omega Filter) was used to improve the signal-to-noise ratio of these images by zero-loss filtering.

5.7. RAMAN TWEEZERS MICROSPECTROSCOPY (RTM)

These experiments were carried out at Pierre *et* Marie Curie University in Paris (France) in collaboration with Sergei G. Kruglik and his group.

Raman spectra were recorded using a nearinfrared (NIR) Raman tweezers setup. In the setup, laser excitation light at 780 nm is provided by continuous-wave Ti:Sapphire laser (Spectra Physics, model 3900S) pumped by argon-ion laser (Spectra Physics Stabilite 2017). The focal waist of intense laser radiation has an average power of 100 mW. The same objective is used to collect the Raman signal in a backscattering geometry and to deliver it onto the spectrograph (Acton SpectraPro 2500i).

Raman light is focused onto the spectrograph's entrance slit (semi-confocal configuration, slit width 30-40 µm) by an achromatic lens with f=75 mm. The Raman signal is separated from laser stray light by 2 Semrock RazorEdge long-pass filters (grade ''U''). One filter, with λlaser=780 nm, is placed normally to the optical beam just before the focusing lens; another one, with λlaser= 830 nm, is used as a dichroic beam splitter at an angle of incidence 458: it reflects laser light at 780 nm and transmits all the wavelengths longer 785 nm. Spectral resolution in all Raman experiments was about 5 cm-^{1}. A frequency calibration was performed using Raman lines of toluene with 92 cm^{-1} absolute accuracy and relative frequency position accuracy better than 91 cm^{-1}. Raman spectra were acquired using WinSpec software; further data treatment was performed using Igor Pro for Windows software.

Raman spectra were acquired every 3 seconds during a sequence of 20 consecutive measurements: this constitutes one ''experimental set''. Measurements were kept going until the event of optical trapping of at least several vesicles in the focus of the microscope objective (so-called ''vesicle set''). After this event, a few more experimental sets are sequentially acquired for a better signal averaging. The transition from one vesicle set to another is accomplished by blocking the laser beam for 10 seconds, the trapped particles in the measurable volume being then exchanged by Brownian motion. The process of data treatment consists of the following successive steps:

a) All of the recorded raw Raman spectra are visually inspected and properly selected, to eliminate the spectra without (or with very minor) vesicles contribution, with high background and poor quality.
b) The selected raw Raman spectra are averaged and normalized on the water-bending band around1, 640 cm–^{1}.
c) The contribution from PBS is subtracted.
d) The resulting spectra are smoothed by 2 adjacent pixels, to minimize the etaloning effect in back illuminated NIR-CCD detector.

5.8. RNA ISOLATION AND QUANTITATIVE REAL-TIME PCR (qPCR)

Selected RNAs found in EVs [70] were analyzed by quantitative polymerase chain reaction (qPCR) in EVs of untreated or drug-treated cells. With this purpose, EVs were isolated from tissue culture media using Exoquick as described in 5.11. Afterwards, RNA was isolated from Exoquick-precipitated material using RNeasy Mini Kit columns (Quiagen, Inc) following the manufacturer´s indications. RNA was eluted in 30 µl of RNase free water. The tube containing eluted RNA, was subsequently centrifuged at 13000 rpm during 15 seconds. RNA concentration was measured by means of Nanodrop spectrophotometer (Thermo scientific, Inc). Subsequently, cDNA was synthesized from 10 µl of eluted RNA using the Quanta cDNA SuperMix (Quanta bioscience, Inc). Briefly, reaction reagents (qScript cDNA SuperMix 5X, RNA template and RNase/DNase-free water) are combined and placed into 0.2 mL microtube. After mixing by vortex, the sample was centrifuged briefly to collect components at the bottom of the reaction tube. Then, it was subsequently incubated during 5, 30 and 5 min at 25 ºC, 42ºC and 85ºC respectively and holded at 4ºC. Samples were stored at -20ºC if not use immediately. 1/5th to 1/10th of the cDNA synthesized was employed for PCR amplification using Taq polymerase (Biotools B&M Labs) according to the manufacturer's protocol and an iCycler thermocycler (Bio-Rad Laboratories Inc).

Next, for relative quantification of genes, qPCR was performed in duplicates using SYBR Green PCR Master Mix (Bio-Rad Laboratories Inc) in an iCycler thermocycler. First, reaction master mix for all qPCR reactions was prepared which contains; SYBR Green Master Mix, forward and reverse primers and nuclease-free water. Then, equal aliquots of the master mix were dispensed into each PCR tube. cDNA templates were then added to the qPCR tubes which already contain reaction set up and mixed. Then, formed air bubbles were removed from the reaction mixture and the thermal cycling protocol was programmed in iCycler thermocycler according to manufacturer´s protocol. qPCR tubes were loaded and the qPCR run.

Primers used for cDNA amplification were designed using Primer3 [146] and the selected sequences are listed in the **Table 2.**

Table 2. List of primers used for DNA amplification

Gene	Species	Forward	Reverse
Alb	**Rat**	**AGCAGCCTGCCTGACACCGA**	**CAGGTCGCCGTGACAGCACT**
Gnb2l	**Rat**	**CCACTCCGCAGTTCCCGGAC**	**TCGTCTCGTGGTAGTGCCCGT**
Rbp4	**Rat**	**GCGCTACAGCCAAGGGACGA**	**CCATCCAGATTCTGCAGGCGGC**

The efficiency of each set of primers was determined by serial dilution of the template cDNA. The theoretical value obtained with the iCycler software was 100±5% (Efficiency (%) = 100X [10(-1/slope) –1]; Bio-Rad Laboratories Inc).

Fold changes respect to untreated cells were calculated using the formula 2-δCt, where δCt = Ct treated - Ct untreated.

5.9. RAT LIVER EXTRACT PREPARATION

Liver extract preparation was carried out following protocol described in Van-Liempd *et al* 2013 [147]. Liver tissue aliquots of approximately 50 mg from WT rat were lysed with a Precellys$^{®}$24 tissue homogenizer (Thermo Fisher Scientific Inc. MA, USA) using 500mg of soft tissue homogenizing beads (CK14,Thermo scientific) in standard 2mL tubes (Precellys,Thermo scientific). Each sample was lysed in 2 x 20 second cycles at 6000 rpm in 500 µL of 50 mM HEPES/150 mM KCl pH 8 in case of measurement of MAT activity, and 50 mM sodium phosphate buffer pH 7.4 in the case of measurement of COMT activity. All the buffers contained 10% Glycerol. Subsequently, 400-450 µL of the resulting homogenate was transferred to a fresh Eppendorf® tube and centrifuged at 15,000 × *g* during 15 min at 4°C. Supernatant was transferred to a fresh tube and place at -80 °C for 20 min. The chilled supernatant was stored at LN2 if not used immediately.

Protein concentration was determined by Bradford assay, using bovine serum albumin as standard.

5.10. RAT MICROSOMES PREPARATION

For microsomes preparation, fresh or cultured rat hepatocytes were collected and centrifuged at 800 rpm 5 min at 4°C. The obtained pellet was resuspended in 50 mM HEPES/150 mM KCl pH 8 in the case of measurement for MAT activity and in 100 mM Tris-HCl buffer pH 7.4 in the case of measurement for COMT activity. All the buffers contained 10% Glycerol. The suspension was transferred to a standard 2mL tube containing 500 mg of soft tissue homogenizing beads. The solution was lysed with a Precellys®24 tissue homogenizer in 2 x 20 second cycles at 6000 rpm. The resulting homogenate (400-450µL aprox) was transferred to Eppendorf® tubes and centrifuged at 15,000 × *g* during 15 min at 4°C. Supernatant was then ultracentrifuged at 100,000 x *g* during 60 min at 4°C. Resulting microsomal pellet was solubilized in the corresponding buffer for measurements of each enzyme (MAT and COMT) and stored at LN2 if not used immediately.

Protein concentration was determined by Bradford assay, using bovine serum albumin as standard.

5.11. PRODUCTION AND ISOLATION OF EVs SECRETED BY PRIMARY HEPATOCYTES

Rat hepatocytes (purity >95%) obtained from livers of 14 week old healthy Wistar male rats were purified by two-step collagenase perfusion technique which involves sequential perfusion of the liver with ethylenediaminetetraacetic acid (Sigma-Aldrich, St. Louis, MO, USA) and collagenaseType I (Worthington Biochemical Corp, Lakewood, NJ) [148]. Rat hepatocyte suspension was centrifuged at 400 rpm 3 min and plated in 24 collagen-coated dishes (150 mm) with collagen type I from rat tail (BD Biosciences, San Jose, CA) at 20 million cells per dish. Cells were cultured in complete Dulbecco's modified eagle medium (DMEM, Gibco, Life technologies, Heidelberg, Germany) supplemented with 10% (v/v) fetal bovine serum (Gibco), streptomycin (0.1 mg/L, Lonza, Walkersville, MD, USA), penicillin (100 u/mL, Lonza) and amphotericin-B (0,25 µg/mL, Lonza) for 4 h at 37°C and 5% CO_2. Then, cells were washed twice with DPBS and incubated for 36h in complete DMEM containing 25 mM HEPES and previously depleted from contaminating vesicles by overnight centrifugation at 100,000 × *g*, 4°C. For drug treatments the 24 collagen-coated dishes were divided in 4 groups (6 dishes each group) and incubated individually with no additives, diclofenac Sodium (400 µM, Sigma-Aldrich), acetaminophen (10mM, Sigma-Aldrich), or D-galactosamine (10mM, Sigma-Aldrich). After 36h incubation, media was collected and EVs isolated. In all cases, the 36 h-conditioned medium was centrifuged at 500 × *g* during 10 min and the resultant supernatant was filtrated through a 0.22 µm pore size filter system (Corning, NY USA) to remove large debris while keeping small membranes (under 220 µm) for further purification by ultracentrifugation. This step ensures a high enrichment of the preparation on small EVs. Filtrated supernatant was transferred to 50 mL centrifuge polycarbonate tubes (Beckman Coulter Inc, Brea, California) and ultracentrifuged 30 min at 10,000 × *g* 4°C to remove remaining cell debris. The resultant supernatant was transferred to a fresh tube and centrifuged at 100,000 × *g* 4°C during 75 min to pellet EVs. To eliminate contaminating proteins, the supernatant was completely removed, pellets resuspended in 1 mL of DPBS and pooled in a single centrifuge tube. More DPBS is added to fill 50 mL and ultracentrifuged at 100,000 × *g* 4°C during 75 min. Supernatants were removed and pelleted EVs resuspended in 50 mM sodium phosphate buffer pH 7.4 in the case of measurements of COMT activity, in 50 mM HEPES/150 mM KCl pH 8 in the case of measurements of MAT or PBS for any other use. In the case of EVs destined to enzymatic measurements buffers contained 10% glycerol. Finally, EVs suspensions were split in aliquots to avoid repeated cycles of freezing and thawing. If not used immediately aliquots were frozen at -80ºC or liquid nitrogen in the case of preparations destined to enzymatic measurements.

For the analysis of RNAs present in hepatic EVs, the vesicles were isolated using Exoquick (SBI System Biosciences). After the filtration (0.22 µm) step of the conditioned media, 1 mL aliquots were collected and centrifuge at 3,000 × *g* for 30 min. Supernatant was then transferred to a sterile tube and Exoquick reagent was mixed 1:1 with the media. Subsequently, the mixture solution was incubated at 4°C overnight and centrifuged at 1,500 x *g* for 30 min. After centrifugation, supernatant was aspirated and residual ExoQuick solution spined down by centrifugation at 1500 × *g* for 5 min. Finally, the pellets containing EVs were resuspended in 1/10 of original volume using PBS.

5.12. PRODUCTION AND ISOLATION OF EVs SECRETED BY MLP-29 MURINE CELL LINE

MLP-29 cells were seeded at 15-30 million cells per dish into 150 mm dishes. Cells were cultured with complete DMEM [10% (v/v) Fetal Bovine Serum, Streptomycin (0.1 mg/L), Penicillin (100 u/mL) and Amphotericin-B (0,25 µg/mL)] for 24 h at 37°C and 5% CO_2. Cells were then washed twice with DPBS and incubated in complete DMEM medium containing 25 mM HEPES previously depleted from contaminating vesicles by overnight centrifugation at 100,000 × *g*, 4°C. After 72h incubation, media was collected, and EVs isolated by differential ultracentrifugation as described previously for primary hepatocytes [149]. EVs were suspended in DPBS to between 1/700th and 1/2,000th the original volume of media, aliquoted, and stored at -80°C if not used immediately.

As controls for the experiments destined to the metabolic profiling of hepatic EVs, the same number of dishes of 150 mm of diameter without cells but containing the same medium (complete DMEM-25mM HEPES exosome-depleted) were incubated in same conditions (incubation time, CO2 and 37ºC) than the dishes containing cells. After the incubation period, the media was collected and processed as previously described for the EVs preparation containing cells.

5.13. FRACTIONATION OF EVs ONA CONTINUOUS SUCROSE DENSITY GRADIENT

For some experiments, EVs were obtained from rat hepatocytes treated with hepatotoxic drugs (10mM APAP, 10mM GalN and 400µM DCF) and fractionated in a sucrose density gradient [149]. Briefly, in a tube suitable for ultracentrifugation (Beckman centrifuge tube tube, Cat. No. 344059, SW40 Ti rotor), 6 ml of 0.25 M sucrose solution (20mM HEPES, 0.25 M protease-free sucrose, pH 7.4) were poured on top of 6 ml of a 2 M sucrose solution (20mM HEPES, 2 M protease-free sucrose, pH 7.4). Subsequently, a continuous 0.25-2 M sucrose gradient was slowly performed by means of a gradient maker device (Gradient Master, Biocomp Instruments, Inc). Once the gradient was pre-formed, EVs prepared by differential ultracentrifugation (see section 5.11) was poured carefully on top of the gradient and ultracentrifuged overnight (16 h) at 210,000 × *g*, 4°C, in a SW40 Ti swinging bucket rotor. Then 1 mL fractions were collected from top to bottom by using autodensity-flow gradient fractionator (Labconco, Kansas City, MO, USA). Subsequently, each fraction was diluted in 2 mL of 20 mM HEPES (pH 7.4), placed into a polycarbonate thick wall tube (Cat No 362305, Beckman Counter) and ultracentrifuged during 1 h at 110 000 × *g*, 4°C, in a TLA-110 rotor. Finally, supernatants were aspirated and the pellets were resuspended in 25 µL of PBS and frozen at −80°C if not use immediately. Additionally, 10 µL of each fraction were used for measurement of the refractive index by means of a refractometer (Abbe 2WAJ, PCE Americas, Inc) to obtain the density value.

5.14. NANOPARTICLES TRACKING ANALYSIS (NTA)

Size distribution and concentration within EVs preparations were analyzed using a NanoSight LM10 system (NanoSight, Amesbury, U.K.), which is equipped with a fast video capture and particle-tracking software. In this system, vesicles are visualized by light scattering using a light microscope NTA software tracks the brownian motion of individual vesicles and calculates their size and total concentration.

NTA postacquisition settings were kept constant for all samples, and each video was analyzed to give the median vesicle size, and an estimate of the concentration [150].

5.15. DETERMINATION OF CES ACTIVITY BY USING A FLUOTOMETRIC ASSAY

Fluorometric assay was performed using the protocol followed by Stacey L *et al*, 2006 [151]. Fluorescein formation was measured using a spectrofluorometer (SPECTRAmax Gemini plate reader; Molecular Devices Corp, Sunnyvale, CA) at excitation and emission set at 490 and 520 nM, respectively. Experiment was conducted in 96-well flat bottom plates in a final volume of 200 µl, containing 198 µl of potassium phosphate buffer (0.1 M, pH 7.4) and 1 µl of EVs sample. The plates were preincubated at 37°C in a fluorometer for 3 min. Reaction was initiated by adding 1 µl of the fluorogenic substrate (fluorescein diacetate) at a final concentration of 100 µM . The reaction product (fluorescein) was measured for 10 min at 60 second intervals.

5.16. MEASUREMENTS OF MAT AND COMT ACTIVITIES BY UPLC-MS

5.16.1. INCUBATION CONDITIONS

Previous to COMT and MAT enzymatic activity evaluation, incubation conditions of the enzymatic reaction had to be optimised. This involves the use of cofactors as well as the adjustment of different parameters such as pH, temperature or incubation time of the reaction mixture. It also has to be taken into consideration other factors such as the stability of the compounds that take part in the reaction.

The enzymatic reactions were studied in samples from different origin **(Figure 7)**: Frozen rat liver extract, microsomes coming from non-cultured rat hepatocytes (*Microsomes t0*), microsomes coming from untreated rat hepatocytes cultured for 36 h (*Microsomes t36*) and rat hepatocytes cultured for 36 h treated with 400 µM diclofenac in the case of COMT activity and also treated with 10 mM acetaminophen and 10 mM galactosamine in the case of MAT activity.

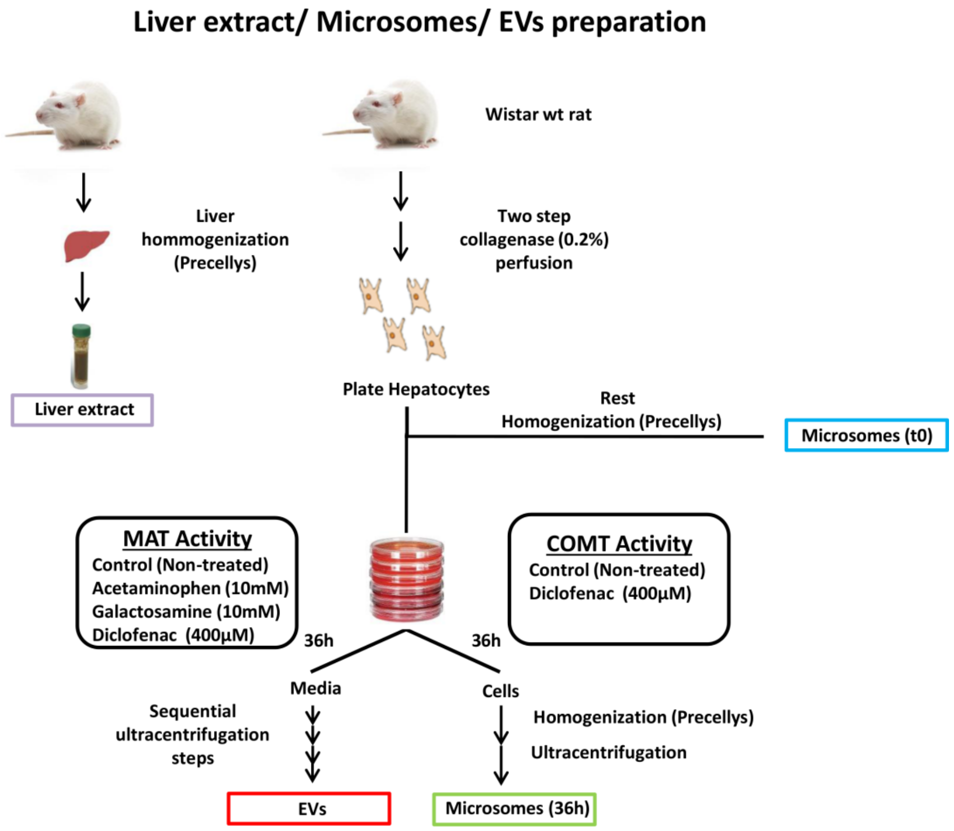
Liver extract/ Microsomes/ EVs preparation
Wistar wt rat
Liver hommogenization (Precellys)
Two step collagenase (0.2%) perfusion
Liver extract
Plate Hepatocytes
Rest
Homogenization (Precellys)
Microsomes (t0)
MAT Activity
Control (Non-treated)
Acetaminophen (10mM)
Galactosamine (10mM)
Diclofenac (400µM)
COMT Activity
Control (Non-treated)
Diclofenac (400µM)
36h
36h
Media
Cells
Sequential ultracentrifugation steps
Homogenization (Precellys)
Ultracentrifugation
EVs
Microsomes (36h)

Figure 7. Experimental design to perform the stydy of the enzymatic activities. This figure shown liver extract, microsomes and EVs obtention procedures carried out to study the enzymatic activities carboxylesterase (CES), methyl-adenosyl-transferase (MAT) of cathecol-O-methyl transferase (COMT).

Incubation conditions for MAT activity

Enzymatic assays after optimization was carried out in a final volume of 250 µL of 50 mM HEPES/ 150 mM KCl pH 8 incubation buffer containing; enzyme provider (liver extract, microsomes or EVs), 5 mM L-Methionine, 10 mM $MgCl_2$, 5 mM DTT, 5 mM ATP and protease inhibitor. The reaction mixture was incubated for 2 h in a water bath at 37°C. Standard stock solutions of L-Methionine (10 mM), ATP (25 mM), protease inhibitor (1x10000) and Dithiothreitol (DTT, 1M) were prepared in incubation buffer and $MgCl_2$ (1000 mM) in water.

Controls-. Not incubated samples were prepared in parallel

Incubation conditions for COMT activity

Enzymatic assay after optimization was carried out in final volume of 300 µL of 50 mM sodium phosphate buffer pH 7.4, 2 mM $MgCl_2$ and 200 µM SAMe (Abbott S.r.l, Campoverde, Italy) without or with 2 mM DA (Sigma-Aldrich) or 0.1 mM NE (Sigma-Aldrich). Reaction mixture was incubated for 1 h at 37°C in a water bath. Standard stock solutions of DA and NE (10 mM) were prepared in incubation buffer and $MgCl_2$ (1000 mM) in water.

Controls-. Three different types of controls were run with each experiment: (a) DA (2 mM) or NE (0.1 mM) in 50 mM sodium phosphate buffer pH 7.4, (b) Rat liver extract/ Microsomes/ EVs incubated in 50 mM sodium phosphate buffer pH 7.4,and (c) Rat liver extract/ Microsomes/ EVs incubated with DA (2 mM) or NE (0.1 mM) in absence of SAMe and $MgCl_2$.

COMT and MAT enzymatic reactions were then stopped by the addition of 1 mL of MeCN/ Water (75/25; v/v%). Then, samples were vortex-mixed for 30 min (4°C) and centrifuged at 15,000 × *g* for 30 min (4°C) to precipitate the proteins. Subsequently, the supernatant (1.1 mL) was reduced to dryness with a speedvac (miVac concentrator, Genevac SP Scientific, USA) and samples reconstituted in 1 mL of ammonium phosphate 10 mM in the case of COMT activity, and in 1 mL of ammonium sulphate 0.01M in the case of MAT activity. Finally they were transferred to solid-phase extraction (SPE) cartridges to clean the samples before injected in the UPLC-MS system. Given the different chemical nature of the analyzed compounds, different SPE method was employed for each activity assay. As described below, a SPE Oasis weak cation exchange (WCX) cartridges in the case of COMT activity and Bond Elute cartridges containing 100 mg of Phenylboronic acid (PBA) in the case of MAT activity were employed.

5.16.2. SOLID-PHASE EXTRACTION (SPE)

SPE was used to process the samples prior to UPLC–MS analysis. The presence of interferences in the original sample matrix can result in instrument downtime due to a buildup of contamination with each injection [152]. In addition, when a saline solution is injected, the formation of the analyte ion could be suppressed by interferences in the sample matrix and the signal strength could be greatly diminished. If the interferences are removed as part of the sample preparation, then the analytes of interest could be analyzed with a more robust method. In this regard, protein precipitation is the most widely employed preparation technique in enzymatic assays, coupled to UPLC-MS. However, it was not enough since deposit of salts were found in the ion source and cone of the mass spectrometer that was translated in decreased sensitivity. Therefore, it was necessary to perform an “extra-clean” step of the samples prior to their injection into UPLC-MS system using SPE in addition to PPT method.

SPE is a sample preparation technology that uses solid particles and chromatographic packing material contained in a cartridge to chromatographically separate the different components of a sample [152]. The first step to develop a SPE method is based on the analytes chemical characteristics. Then, chromatography and SPE strategy can be chosen.

The general SPE procedure has to provide sample extracts not only free of interfering matrix components but also concentrated enough for analytes detection. The protocol consisted of 5-step including conditioning, equilibration, sample loading, washing and eluting the compound of interest [153]. A vacuum manifold system (20 pos, 13x75 mm tubes, Waters Corp., Manchester, UK) was used to house the cartridges.

Analyte Recovery-. The recovery (or extraction efficiency of SPE method) was determined by measuring the response of blank matrix (rat liver extract) spiking analytes before SPE (pre-spiked samples) **(Figure 8B)** and after SPE (post-spiked samples) **(Figure 8C)**. Non-spiked samples were also prepared (rat liver extract in buffer). The recovery was calculated as follows:

$$\text{Recovery (\%)} = \frac{\text{Rat liver extract spiked with the analyte of interest before SPE (Pre-spiked sample)}}{\text{Rat liver extract spiked before UPLC-MS (Post-spiked sample)}}$$

The recovery value must be > 50% to be in acceptable range for routine UPLC-MS analysis [154].

Bond Elut cartridges containing 100 mg phenylboronic acid (PBA) bonded silica from Agilent Technologies (Santa Clara, CA, USA) and Oasis WCX Solid-Phase Extraction from Waters Corporation (Milford, USA) was used for MAT and COMT enzymatic assays respectively.

After incubation period, resulting supernatants were reduced to dryness with a speedvac and reconstituted in appropriate solution depending on the SPE procedure employed for each enzymatic assay. Samples were then transferred to the corresponding SPE cartridges and run through them. The cartridges were then subsequently washed and analytes eluted and evaporated using a speedvac centrifuge. Finally, residues were reconstituted in mobile phase and transferred to an autosampler vial for injection in the UPLC-MS system. A total volume of 2 µL was injected into the UPLC-MS system.

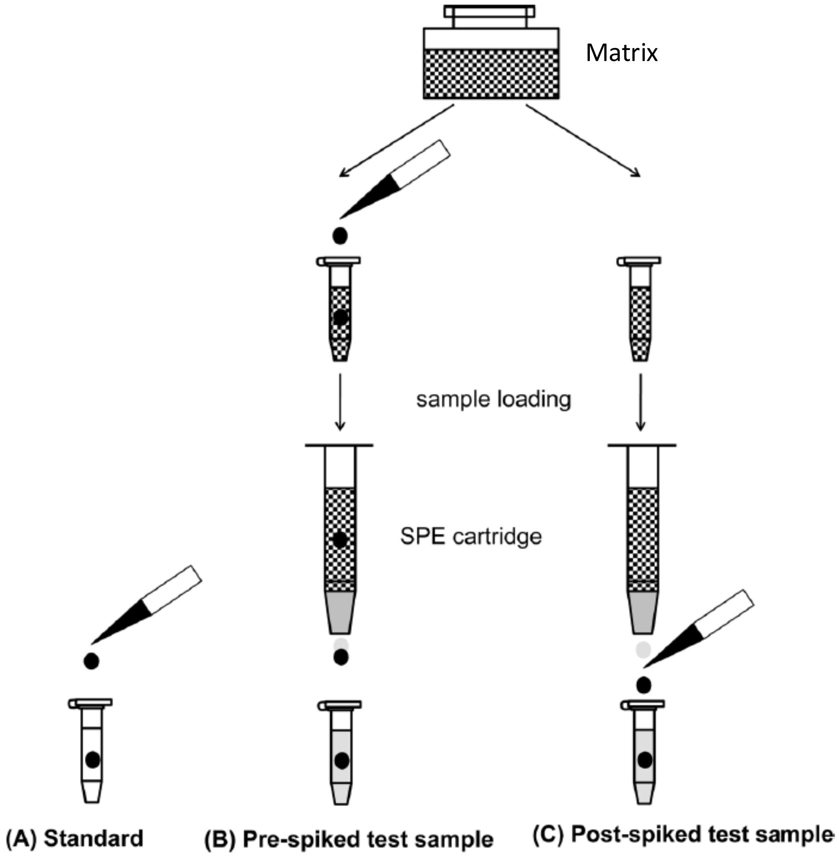

Figure 8. Preparation of standard and test samples for evaluation of Solid phase extraction method recovery. (A) Analytes in solution (B) Analytes spiked in matrix before SPE and (C) Analytes spiked in matrix after SPE

5.16.3. CALIBRATION CURVE AND QUALITY CONTROLS

For quantification of products related with the enzymatic reactions, a matrix-spiked calibration curves were obtained for each assay.

In the case of MAT enzymatic assay, standard stock solutions of the enzymatic components, 10 mM SAMe (Abbort S.r.l, Campoverde, Italy) and 10 mM SAH (Abbort S.r.l, Campoverde, Italy), were prepared in formic acid 0.1 % and 10 mM MTA (Sigma-Aldrich; St. Louis, MO, USA) in MeCN/Water/Formic Acid (75/23.8/1.2; v/v/v%). Working solutions were prepared by appropriate dilution in mobile phase (Acetonitrile (ACN)/ Water/ Formic acid (60/39.9/0.1; v/v/v %)). For the calibration curve different concentrations of these compounds were used: 0.005, 0.01, 0.05, 0.1, 0.25, 0.5, 1, 2.5, 5, 10, 25 and 100 µM. Three non-spiked samples were used to calculate a baseline signal for the analytes. For quality controls (QCs) two concentrations were used, 1 and 10 µM. Calibration samples (non-spiked and spiked samples) were individually prepared in 50 mM HEPES/150 mM KCl buffer pH 8 containing 5 mM ATP, 5 mM Met, 5 mM $MgCl_2$, protease inhibitor and 0.25 mg of protein (rat liver extract). After adding 1 mL of MeCN/Water/Formic Acid (75/23.8/1.2; v/v/v%) to stop the reaction, samples were vortex-mixed for 30 min (4°C) and centrifuged at 15,000 × *g* for 30 min (4°C) to precipitate the protein. To evaporate the organic solvent, the supernatant (1.1

mL) was reduced to dryness with a speedvac centrifuge. Then, the residues were reconstituted in 1 ml of $(NH_4)_2SO_4$ 0.01 M at pH 7.5 and transferred to SPE-PBA cartridges.

In the case of COMT enzymatic assay, standard stock solutions of the enzymatic products (10 mM 3-MT and 10 mM NMN) were prepared in Acetonitrile (MeCN)/ Water/ Formic acid (60/39.9/0.1; v/v/v %). For the calibration curve different concentrations were used: 0.005, 0.01, 0.05, 0.1, 0.25, 0.5, 1, 2.5, 5, 10 and 25 µM. Two non-spiked samples were used to calculate a baseline signal for the analytes. For Quality Controls (QCs), two concentrations were used, 1 and 10 µM. Calibration samples (non-spiked and spiked samples) were prepared individually in 300 µL 50 mM sodium phosphate buffer pH 7.4 containing 0.25 mg of protein (from rat liver extract) and 2 mM $MgCl_2$. Subsequently, 1 mL of MeCN/Water (75/25; v/v%) was added to the mixture reaction and then vortex-mixed for 30 min (4°C) and centrifuged at 15,000 × *g* for 30 min (4°C) to precipitate the protein. To evaporate the organic solvent, the supernatant (1.1 mL) was reduced to dryness with a Speedvac centrifuge). Then, the residues were reconstituted in 1 mL of 1% ammonium phosphate 10 mM (aprox. pH 7.4) and transferred to SPE cartridges.

5.16.4. LIQUID CHROMATOGRAPHY AND MASS SPECTROMETRY (UPLC-MS) CONDITIONS

UPLC conditions

The substrates and products of the reactions were measured and chromatographically separated with an ACQUITY UPLC system (Waters Corp, Milford, USA). The system was equipped with two binary solvent pumps, a cooled autosampler (4°C) with a 10 µL injection loop and a column oven (40°C). An Acquity UPLC BEH AMIDE column, 1.7 µm (Waters Corp.) was used for separation of the analytes. Samples were injected (V_{load} 2 µL; partial loop fill mode) from deactivated total vials (Waters Corp.). A gradient was used to separate the analytes; solvent A consisted of 99.5% water, 0.5% formic acid and 20 mM ammonium formate while solvent B consisted of 29.5% water, 70% MeCN, 0.5% formic acid and 1 mM ammonium formate. The gradient was as follows: from 5% A to 50% A in 2.4 min in curved gradient #8, from 50% A to 99.9% A in 0.2 min, constant at 99.9% A for 1.6 min, back to 05% A in 0.3 min and constant at 5% A for 0.5 min. The flow rate was 0.25 mL/min.

MS conditions

A SYNAPT HDMS G2 Time of Flight (ToF) mass spectrometer (Waters Corp.) was used for the detection of the analytes. The ToF was operated in positive electrospray ionization mode (ESI+). The following source parameters were used for the analysis: capillary voltage 25 V, sample cone voltage 25 V, extraction cone voltage 5 V, desolvation temperature 450°C, source temperature 120°C, cone gas flow 5 L/h and desolvation gas flow 600 L/h. Ion optics were tuned to a resolution of 22.000 (FWHM) for *m/z* 556. In order to guarantee mass accuracy, leucine-enkefaline solution (2 µg/mL in MeCN/Water (50/50; v/v %) and 0.1%

formic acid) was infused into the source via a second ESI probe at 10 µL/min and used as a lock mass. Every 30s a lock mass was recorded for 0.5 s. Analyte spectra were automatically corrected for fluctuations in the lock mass.

Initially, to develop the UPLC-MS method ToF (in the MS), it was operated in Full Scan Mode (50-1200 Da) with a 0.2 s scan time. Then, in order to reach an optimized lower Limit of Detection (LLOD) for 3-MT/NMN and SAH/MTA in the case of COMT and MAT enzymatic activities respectively, the ToF was operated in Enhanced Duty Cycle (EDC) mode. In EDC mode, the expulsion of ion bunches from the transfer T-Wave^{TM} collision cell and the pusher of the ToF analyzer were synchronized so that the duty cycle is optimal for a given *m/z*. 3-MT, NMN, SAH and MTA were measured in a scan function optimized for *m/z* 151, *m/z* 166, *m/z* 385 and *m/z* 298 respectively. The scan rate for these scan functions was 0.2 s.

5.16.5. ANALYTICAL METHOD

After sample cleaning and prior to data analysis, several parameters of the method were determined to establish the sensitivity and specificity of the developed enzymatic activities.

Specificity

This parameter measures the ability of the method to detect potential interferences and differentiate and quantitate the analyte in the presence of other endogenous constituents in the sample. If any inspecificity is present, it will interfere in the detection and quantification of the analyte of interest.

The specificity of the method was determined by the retention time, accurate mass (3 decimal places) and isotope patterns of the analytes. The latter two are indicative of the elemental composition of the analyte. Theoretical values for both, accurate mass and isotope pattern, were calculated with MassLynx software. In order to obtain the proper retention times, blank matrix was spiked with analytes. The retention times of those intensities that increased in the mass window of the theoretical mass were taken as the retention times of the analytes. After comparing theoretical masses and measured masses, the mass error was around 1 mDa that provides the necessary specificity.

Linearity of calibration curves and Lower Limit of Quantification (LLOQ)

As the majority of instrumental methods of analysis, chromatography is not an absolute, but a relative technique. The response for a sample component must be compared with the response of a suitable reference (for example with a substance that closely resembles the sample) and with a known amount of the analyte. Usually, the comparison is based on a calibration curve extending over a concentration range corresponding to the variation of the analyte content in the samples. Once the calibration curve has been constructed, the concentration of an unknown sample can easily be extrapolated [155].

To calculate the absolute amount of formed product, the average of the baseline signals was subtracted from the signals of the serially diluted calibration samples. The calibration curve was obtained over the concentration of a variable range specific of each enzyme.

Power-fit function was used to determine the relation between the signal (peak area) and sample concentration. [signal] = a*[concentration]^b) where a and b are determined by linear regression of the log-transformed values of the concentrations and their associated signals. It gives the least deviation from the theoretical values, especially at low concentrations. Once the sample concentrations were calculated they were converted to amount of product (nmol) obtained per mg of protein employed in 1 h incubation.

The sensitivity expressed as LLOQ was defined as the lowest quantifiable concentration on the calibration curve with an acceptable accuracy (±15%) and a precision below 15% [156]. The deviation from theoretical curve concentration for the LLOQ level should not be more than 20%.

Precision and Accuracy

These parameters are indispensable criteria in the assessment of an analytical method. Monitoring QC during sample analysis is essential to ensure the validity of reported results. The accuracy and precision of the method were assessed by determining QC samples at two concentration levels.

Precision was assessed by the relative standard deviation of the analytes (%CV) for either high or low QC samples;

$$\%CV=100*SD/average$$

Accuracy was calculated by determining the %deviation of the theoretical values at the QC levels:

$$\%dev=100*((\text{calculated concentration})-(\text{theoretical concentration}))/(\text{theoretical concentration}))$$

5.16.6. DATA ANALYSIS OF UPLC-MS RESULTS PROVIDED BY MAT AND COMT ACTIVITY ASSAYS

After samples injection in UPLC-MS system, MAT and COMT activities were determined as follows.

Extracted ion traces were obtained for 3-MT (*m/z* 151.0759), NMN (*m/z* 166.0868), SAH (*m/z* 385.1294) and MTA (*m/z* 298.0974) with a 20 mDa window and subsequently smoothed (2 points, 2 iterations) and integrated with QuanLynx software (Waters Corp.).

Then, to calculate the absolute amount of the products, the average of the baseline signals was subtracted from the signals of the serially diluted calibration samples. Subsequently, Power-fit function ($[\text{Signal}] = a \times [\text{concentration}]^b$) where a and b are the fitted constants) was used to determine the relation between the signal (peak area) and sample concentration. Once the sample concentrations were calculated they were converted to amount (nmol) of product formed per mg of protein employed in 1 h incubation. The amount of products detected in the controls was subtracted from the total amount of product obtained in incubated samples.

5.17. METABOLIC PROFILING OF HEPATIC EVs BY UPLC-MS METABOLOMICS

5.17.1. SELECTION OF METABOLITES EXTRACTION METHOD

Due to the limiting amount of EVs samples, the experiments to select an optimal metabolites extraction method were performed only with cell extracts. Three extraction methods were tested. Each pellet of cells was suspended in a final volume of 500 µl of a variable solvent that depends on the selected extraction method:

- 500 µl MeOH/H_2O (50% v/v)
- 250 µl MeOH/H_2O (50% v/v) + 250 µl Chloroform (“Biphasic method”)
- 500 µl Isopropanol

Twelve cell pellets were mixed and split again into three groups (4 aliquots x 3 extraction methods). Mixtures were vortex for 10 seconds and subsequently sonicated during 15 min on ice. The resulting homogenate was then agitated at 1400 rpm for 30 min, 4°C and subsequently centrifuged at 13,000 rpm for 15 min, 4°C. After centrifugation, 400 µl of the supernatant was collected and placed at -80 °C for 20 min. In the case of MeOH/H_2O/Chroroform (50:50:50, v/v/v) extraction method, two phases were formed (of 200 µl each) which were collected to independent Eppendorf tubes and placed at -80 °C for 20 min. Organic solvent was then evaporated by centrifugation in a speedvac 2 h at 4ºC. Finally, the obtained pellet was solubilized in 200 µl of mobile phase (ACN)/ Water/ Formic acid (60/39.9/0.1; v/v/v %)). A total volume of 2 µl was injected into the UPLC-MS system.

5.17.2. BIPHASIC METABOLIC EXTRACTION OF CELLS AND EVs

Five preparations of 100 µl each containing EVs (140 µg) were prepared from MLP29 cells and used to obtain the metabolome of hepatic EVs. In parallel, three cells suspension of 100 µl each of them, containing 1 million of cells were employed for the characterization of the metabolic profile of the cells.

In addition, control samples obtained from tissue culture media incubated in the absence of cells under same conditions and subjected to same EV isolation procedure, were employed to remove contaminant metabolic signals rising for the media [157].

The extraction method employed for metabolites extraction was MeOH/H_2O/Chloroform (50:50:50, v/v/v) as indicated above. Briefly, 400 µl of MeOH/H_2O (50:50) was added to each aliquot to reach a final volume of 500 µl. Then, 500 µL of Chloroform was added and the resultant mixture was vortex for 10 seconds and sonicated during 15 min on ice. The resulting homogenate was then agitated at 1,400 rpm for 30 min, 4°C and subsequently centrifuged at 13,000 rpm for 15 min at 4°C. After centrifugation, supernatant was collected and the two layers formed (aqueous and organic layer) were collected in independent Eppendorf tubes and placed at -80 °C for 20 min. Organic solvent was then evaporated by centrifugation under vacuum conditions by 2 h at 4ºC. Finally, the obtained pellet was suspended in 100 µl of mobile phase (ACN/ Water/ Formic acid (60/39.9/0.1; v/v/v %)) and injected into the UPLC-MS system.

5.17.3. ULTRA PERFORMANCE LIQUID CHROMATOGRAPHY – MASS SPECTROMETRY CONDITIONS

UPLC conditions

Extracted metabolites were measured with a UPLC system (Acquity, Waters, Manchester) coupled to a Time of Flight mass spectrometer (ToF- MS, SYNAPT G2, Waters Corp.). Two different types of chromatography were used to separate different classes of metabolites.

First the samples were injected on an AMIDE column in order to separate polar metabolites and subsequently on a C18 to separate apolar metabolites. A 2.1 mm x 100 mm, 1.7 µm BEH AMIDE column (Waters), thermostated at 40 °C, was used to separate the analytes. Solvent A (aqueous phase) consisted of 99.5% water, 0.5% formic acid and 20 mM ammonium formate while solvent B (organic phase) consisted of 99% acetonitrile, 0.5% water and 0.5% formic acid. The gradient was as follows: from 0.1% A to 50% A in 8 min in convex gradient (#8), from 50 %A to 99.9 %A in a linear gradient (#6) of 0.2 min, constant at 99 %A for 1.20 min and back to 0.1 %A in 0.2 min to equilibrate. The flow rate was 250 µL/min and the injection volume was 5 µL.

The samples were also separated on a 1 mm x 100 mm, 1.7 µm BEH C18 UPLC column, thermostated at 40 °C. Solvent A (aqueous phase) consisted of 99.9% water, 0.1% formic acid while solvent B (organic phase) consisted of 99.8 % ACN, 0.1% water and 0.1% formic acid. The gradient was as follows: from 95 %A to 1 %A in 8 min in a linear gradient (#6), constant at 1 %A for 1.4 min and back to 95 %A in 0.2 min to equilibrate. The flow rate was 140 µL/ min and the injection volume was 5 µL.

Injection sequences consisted of test mixes, extraction controls, initialization runs, randomized sample sequences and QCs. First, the UPLC and MS performance was evaluated by injecting a test mix of known composition. Then, the extraction control samples were injected. Next, the column was equilibrated by injecting liver extract samples. After equilibration, the randomized sample sets were injected. After each 5 samples a QC sample was injected in order to check the stability of the system.

MS conditions

The mass spectrometer was operated in both ESI+ and ESI- modes with capillary voltages of respectively 250 V and 500 V for both types of chromatography. Thus, two consecutive runs (positive and negative polarity) had to be performed on both columns (amide and C18). The settings described next, were the same for all polarities and chromatographies. The extraction cone voltage was 5 V and sampling cone voltage was 25 V. Source temperature was 120 ºC while capillary temperature was 450 ºC. Two scan functions were used; one for low collision energy (4 V) and one for high collision energy (30 V). Samples were measured in full scan mode from 50 to 1,200 Da. Polar and apolar sets were first measured in ESI+ mode and subsequently in ESI- mode.

5.17.4. DATA PROCESSING, MULTIVARIATE ANALYSIS AND METABOLITE IDENTIFICATION

All data was processed using the MarkerLynx application manager for MassLynx 4.1 software (Waters Corp., Milford, USA), which is a post-adquisition processing package that can be applied to MS data files. A list of chromatographic peak areas for the metabolites detected in each sample injection was generated. Both polarities and chromatographies were separately analyzed. The UPLC-MS data were peak-detected and noise reduced such that only true analytical peaks were further processed by the software. A list of intensities (chromatographic peak areas) of the peaks detected was then generated, using the RT-mz (retention time and *m/z*) data pairs as identifiers in a mass window of 0.02 Da and a RT window of 0.05 min.

After data processing, the RT-mz signals were subjected to Principal components analysis (PCA) to determine metabolic profile differences between cells and EVs. In the PCA, the first two principal components (t[1] and t[2]) are plotted, representing the most important metabolic variation in the samples captured by the analysis. The final dataset was mean centered and log-transformed during multivariate data analysis. Selected peaks were tentatively identified by using the corresponding exact molecular mass and MS data for searching in the databases Metlin (https://metlin.scripps.edu/index.php) and HMDB (http://www.hmdb.ca).

6. RESULTS AND DISCUSSION

6.1 RAT HEPATOCYTES IN MODELS OF DILI

Different hepatotoxic agents are frequently used as model substances to induce liver injury in animals. Nevertheless, due to scientific, ethical and also economical reasons, there is a high tendency to replace animal models by appropriate alternative methods. Isolated primary hepatocytes fulfill these requirements and they could be useful *in vitro* DILI model [158]. This model allows evaluating the injury induced by different hepatotoxicants, such as acetaminophen (APAP), galactosamine (GalN) or diclofenac (DCF) using different molecular and biochemical approaches [20]. Hepatocytes cultured on collagen-coated dishes de-differentiate within 72h period [159][160]. Taking this into consideration, the incubation period of the primary hepatocytes was established in 36 h in order to have enough hepatic secreted EVs for their detection and analysis. Based on published works, the concentrations of drugs employed in this study were 10mM for APAP and GalN [161] [21] and 400µM in the case of DCF [162]. Using these conditions, several cellular parameters were evaluated.

6.1.1. CELL VIABILITY

Cell viability after treatment with APAP, GalN and DCF hepatotoxicants was determined by trypan-blue exclusion method. Then, the obtained values were normalized to the control (untreated), that corresponds with 100% of viability. A slightly decrease in the cell viability in all treatments was observed. After treatments, cell viability ranged from 84 to 95% **(Figure 9)**, being this effect consistent in the 10 independent experiments examined **(Figure 10)**. This small reduction in the viability, indicates that no dramatic cell death was observed under conditions used for this study.

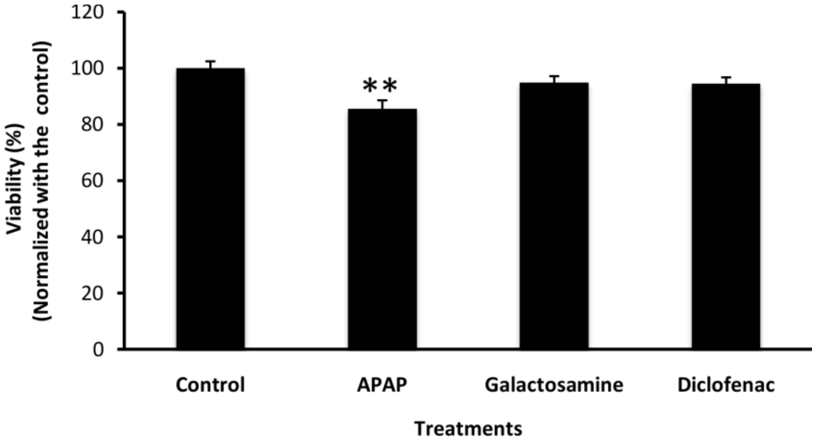

Figure 9. **Cellular viability analysis of rat hepatocytes exposed to liver-damaging drugs**. Cell viability of primary rat hepatocyte was evaluated by trypan-blue exclusion method after cultured during 36h in the presence of APAP (10 mM), GalN (10 mM) or DCF (400µM). Error bars represent standard error (n = 10), ** denotes p<0.01 with respect to the control.

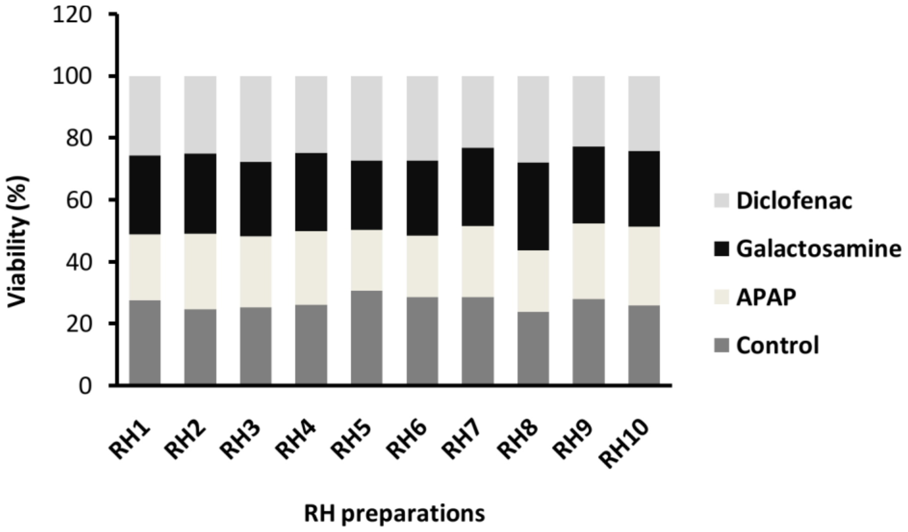

Figure 10. **Reproducibility analysis of cellular viability in independent rat hepatocytes preparations**. . Primary rat hepatocytes (RH) were incubated during 36 hours in the presence of the hepatotoxic compounds and cell viability was determined by trypan-blue exclusion method. Note the reproducibility in terms of cell viability among all preparations.

6.1.2. CELL MORPHOLOGY

In agreement with the low effect on cell viability under assayed conditions, the number of attached cells remains very similar in all APAP, GalN and DCF treatments as can be observed in the inmunofluorecence analysis (Figure 11). The effect of the different treatments on the hepatocyte morphology was studied by examining sub-cellular localization of different proteins by confocal microscopy **(Figure 11).**

To evaluate the effect on the morphology of the cells it was firstly studied the cytoskeleton by staining F-actin with fluorescently labelled phalloidin. As it can be observed, there were no significant morphological alterations in cells treated with the different hepatotoxicants compared to untreated hepatocytes. In particular, a slightly increase in the fluorescence intensity was observed in DCF-treated hepatocytes, indicating changes in the amount of F-actin **(Figure 11, Panel A).**

It was also evaluated the effect on the intracellular distribution of enzymes that have been described to be present in hepatic EVs [69], such as *Ces1d*, P450 2d1, MAT and COMT. In the case of the drug-metabolizing enzyme *Ces1d*, there was no significant alteration neither in their abundance or intracellular cytosolic localization **(Figure 11, Panel B)**.

Which regards to cytochrome P450 2d1 (rat ortholog of human P450 2D6), which takes part in the metabolism of APAP [163], GalN [95] and DCF [164], the cellular staining was mostly associated to plasma membrane. In this case, as occur with *Ces1d*, there was no significant alteration neither in localization or intracellular abundance after treatment with the hepatotoxicants **(Figure 11, Panel C)**.

COMT, which is involved in the elimination of biologically active or toxic catechols and some other hydroxylated metabolites, presents a marked membrane distribution in both, untreated and treated hepatocytes. In this case, an increase in the intracellular content of this enzyme was observed in APAP and GalN-treated hepatocytes respect to the control **(Figure 11, Panel D)**.

Finally, MAT enzyme is involved in the regulation of the central metabolite S-adenosylmethionine (SAMe). Its distribution was mostly cytoplasmic although a marked membrane localization in APAP-treated hepatocytes was clearly observed **(Figure 11, Panel E)**.

Next, the effect of the different treatments on intracellular localization of proteins that are considered markers of EVs such as Cd81 and LIMP II proteins was evaluated. In the case of Cd81, untreated cells showed both, plasma membrane and intracellular vesicular localization. However, in cells treated with APAP and GalN, Cd81 was localized mostly in the plasma membrane losing its intracellular vesicular pattern **(Figure 11, Panel F)**. On the other hand, LIMP II was preferentially localized in intracellular vesicles in all the cases, although the distribution of the vesicles was more perinuclear in untreated cells than in the treated hepatocytes. In this case, it was also possible to appreciate that the abundance of the protein in APAP and GalN-treated hepatocytes was reduced compared to untreated or DCF-treated cells **(Figure 11, Panel G)**.

All these results show that liver-damaging compounds have different effects on the abundance and/or in the intracellular distribution of different proteins. This indicates that different responses are carried out in hepatocytes depending on the induced liver damage.

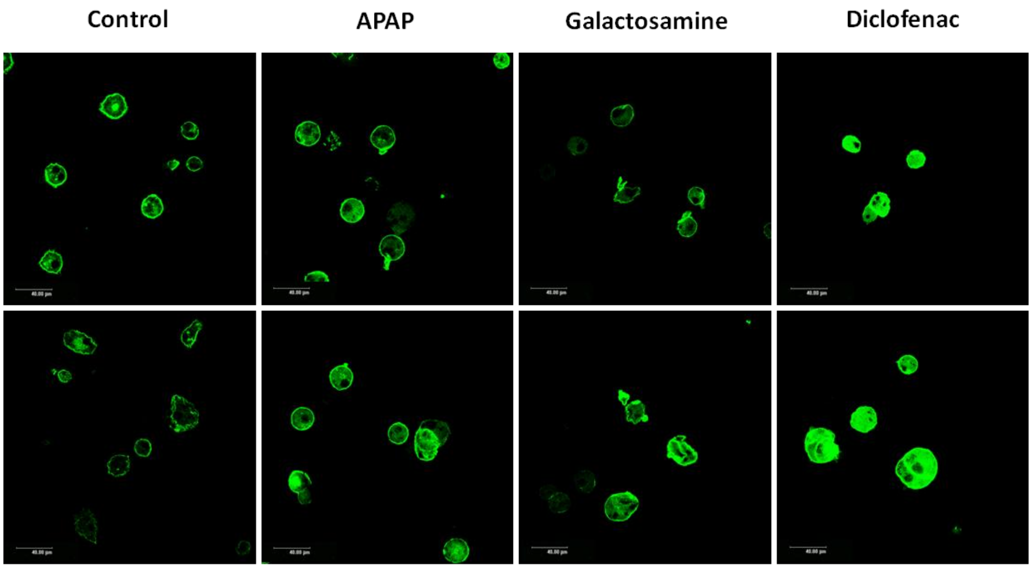

Panel A: F-Actin

Figure 11. **Confocal analysis of primary rat hepatocytes in DILI conditions**. Untreated- or cells-treated with the hepatotoxins during 36 hours were formaldehyde-fixed and processed to analyze indicate markers. The images were captured by confocal microscopy under similar conditions. Scale bar: 40µm.

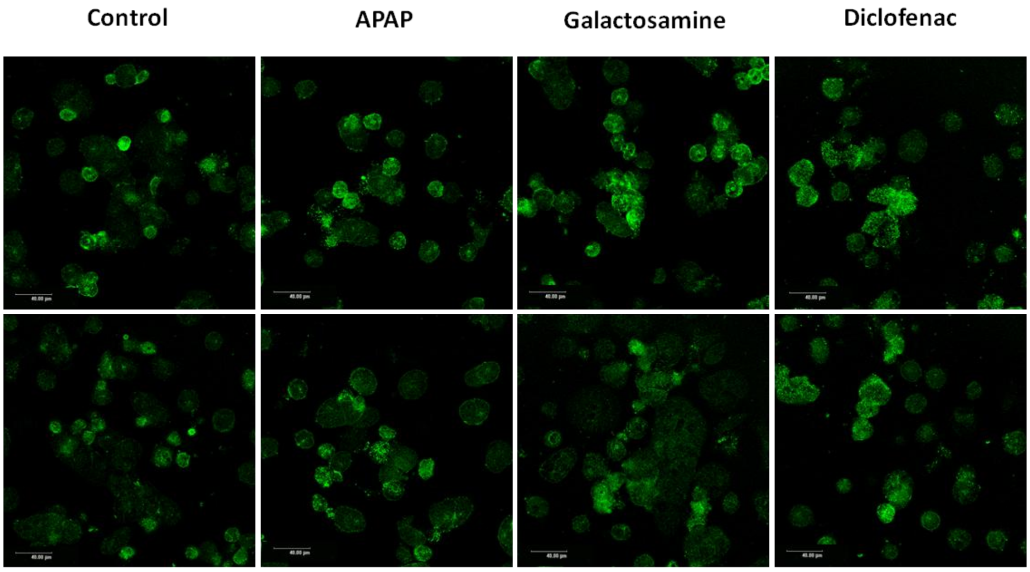
Control
APAP
Galactosamine
Diclofenac

Panel B: CES3

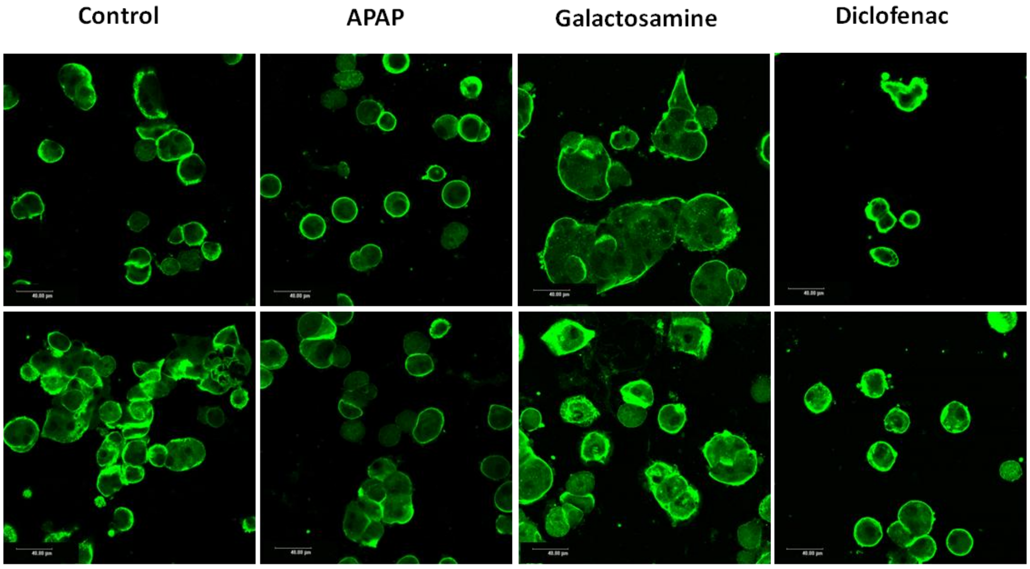
Control
APAP
Galactosamine
Diclofenac

Panel C: Cyp 2d1

Figure 11 (continuation)

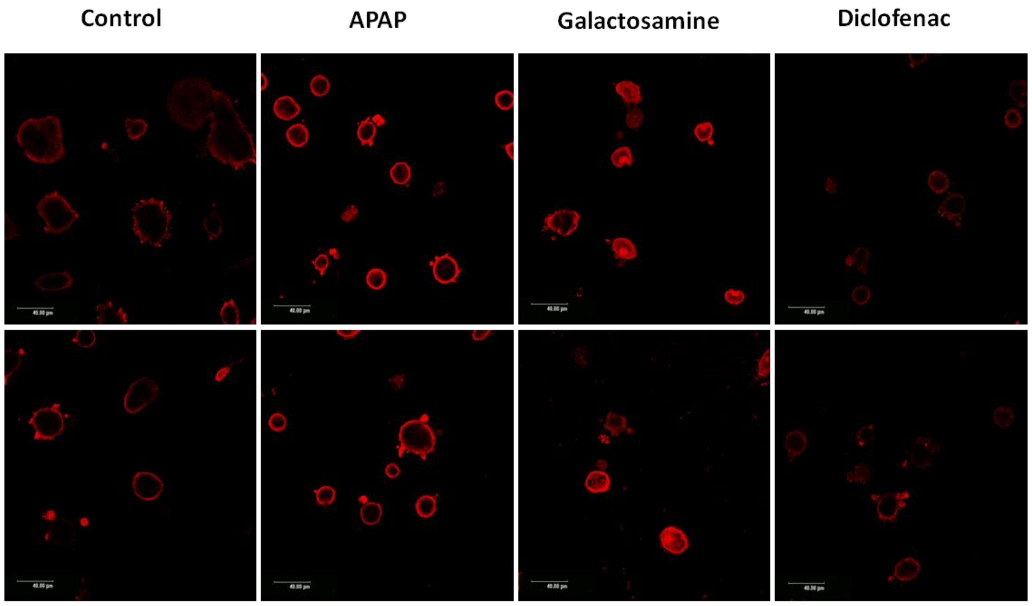
Control
APAP
Galactosamine
Diclofenac

Panel D: COMT

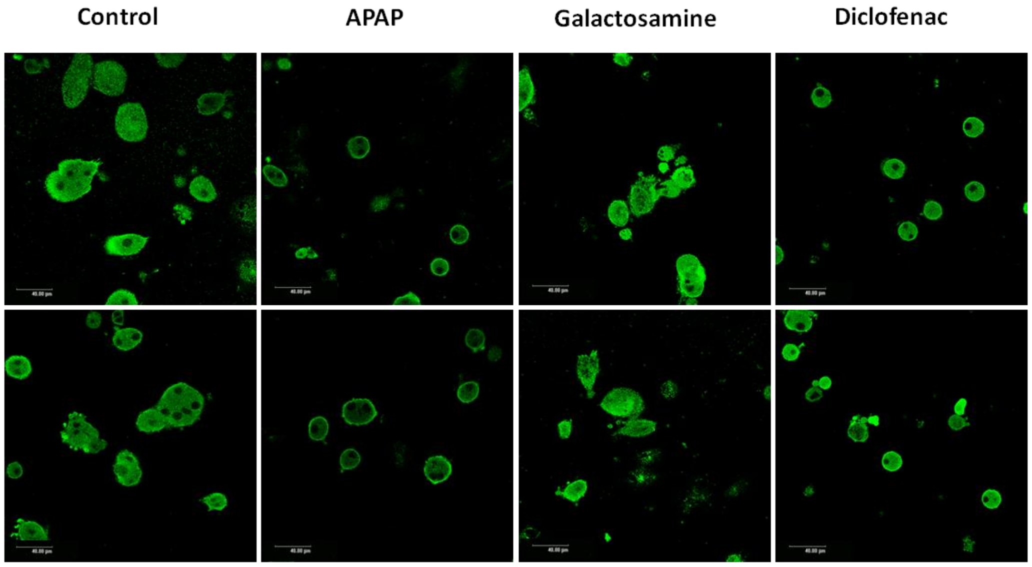
Control
APAP
Galactosamine
Diclofenac

Panel E: MAT1A

Figure 11 (continuation)

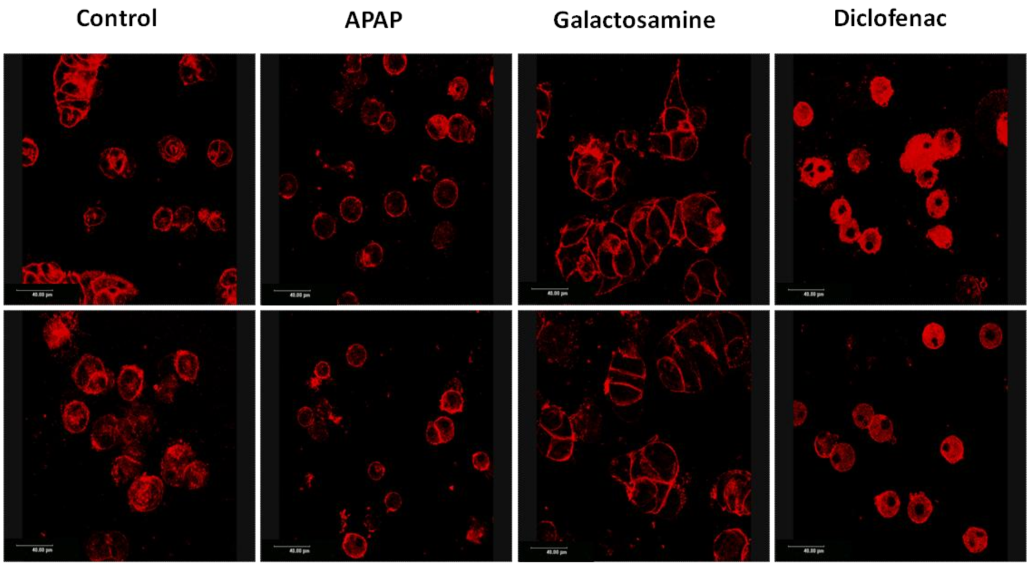
Control
APAP
Galactosamine
Diclofenac

Panel F: Cd81

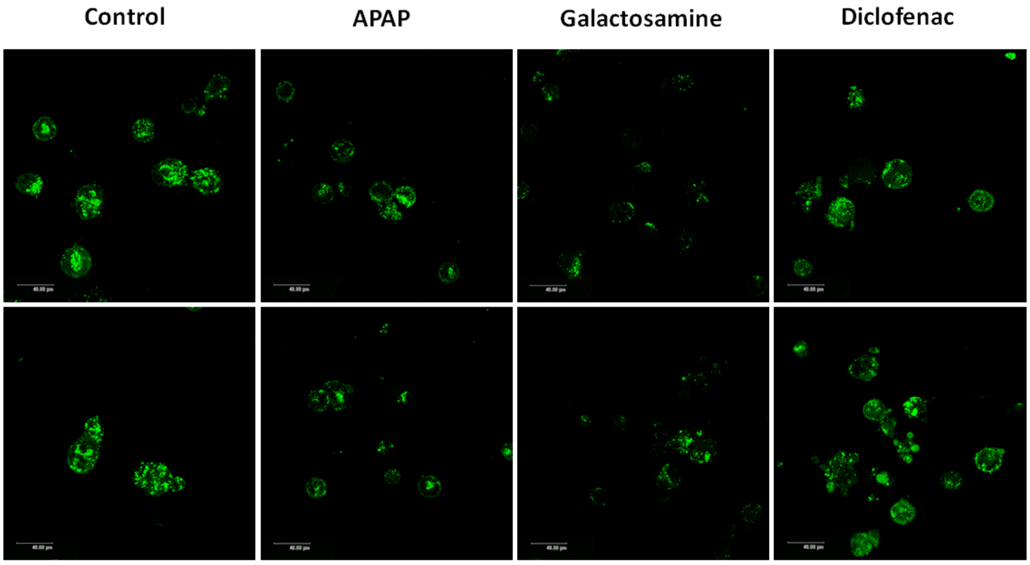
Control
APAP
Galactosamine
Diclofenac

Panel G: LIMP II

Figure 11 (continuation)

6.1.3. WESTERN BLOT ANALYSIS

The effect of the APAP, GalN and DCF drugs on the intracellular content of hepatocytes was also evaluated by Western-blotting, focusing the study on protein markers of EVs (LIMP II, Hsp70, Hsp90, Rab8, Flotillin-1 and Cd63) and on an intracellular compartment as the mitochondria (Cox IV). Several enzymes that were previously detected in hepatocyte-derived EVs (*Ces1d*, MAT, COMT) were also analyzed [69].

Consistent with the results obtained in the confocal microscopy analysis, similar differences were found in the behaviour of the proteins analyzed by Western-blotting, suggesting again different responses of the hepatocytes to the tested drugs. While cellular levels of Cd63 and Hsp70 decreased in all treatments, the levels of *Ces1d* increased in GalN- and DCF-treatments and the levels of Flotillin-1 and COMT increased only in GalN-treated hepatocytes **(Figure 12)**. It is also important to highlight that APAP-treatment caused a drastic reduction in the cellular levels of most of the assayed proteins, suggesting that this drug, under these conditions, provokes the most severe effects. This is in agreement with the cell viability results **(Figure 9)**, where APAP caused the highest drop in cell viability. Interestingly, the only protein that increased in the cells exposed to APAP was the mitochondria marker Cox IV **(Figure 12)**, in accordance with the proposed mechanism of APAP toxicity that implies mitochondria dysfunction [24] [25].

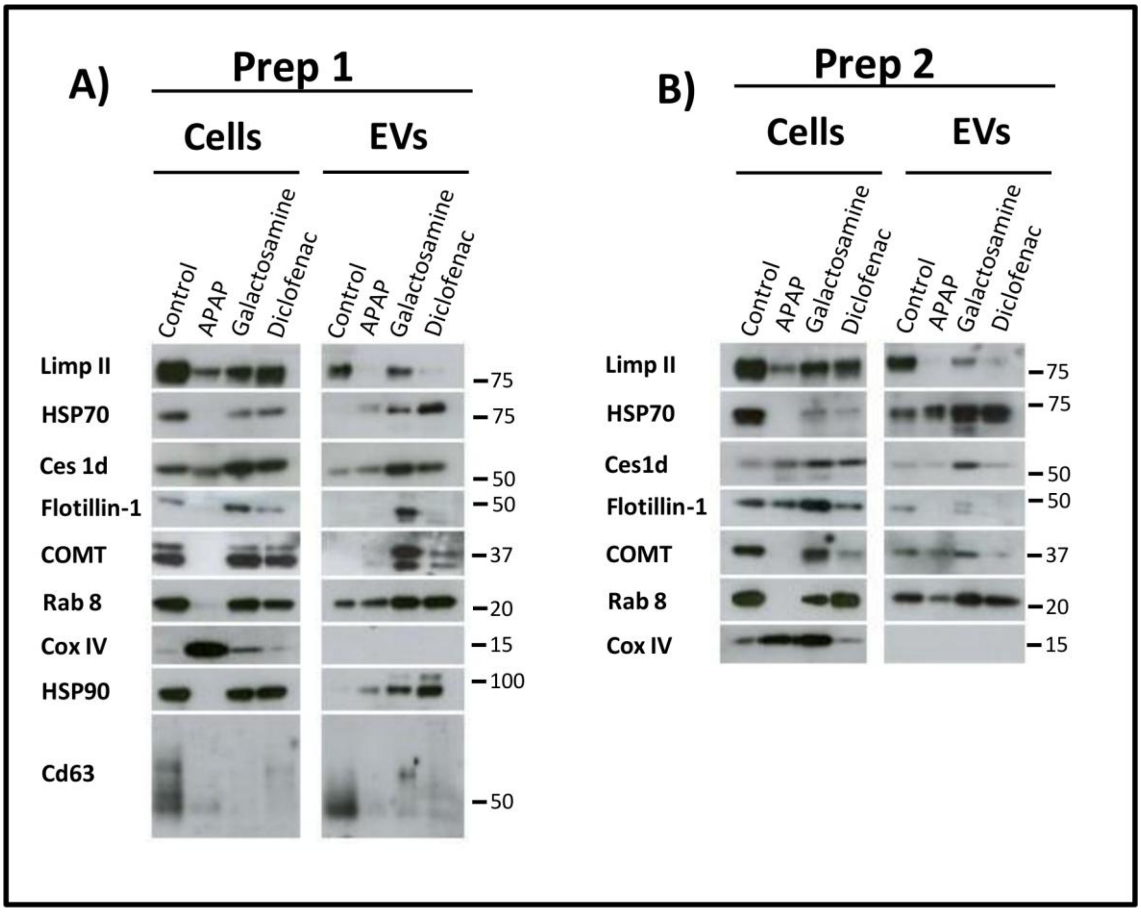
A)
Prep 1
Cells
EVs
Control
APAP
Galactosamine
Diclofenac
Limp II
HSP70
Ces 1d
Flotillin-1
COMT
Rab 8
Cox IV
HSP90
Cd63
75
75
50
50
37
20
15
100
50
B)
Prep 2
Cells
EVs
Control
APAP
Galactosamine
Diclofenac
Limp II
HSP70
Ces1d
Flotillin-1
COMT
Rab 8
Cox IV
75
75
50
50
37
20
15

Figure 12. Western-blot analysis of primary rat hepatocytes and their corresponding secreted EVs. Protein extracts (10ug) prepared from rat hepatocytes and secreted EVs were analyzed by Western-blotting after the exposure of indicated drugs, using antibodies against the following proteins: LIMP II, Hsp 70, CES3, Flotillin-1, COMT, Rab8, COX IV, Hsp90 and CD63. Two representative preparations are shown and molecular weights are indicated in KDa.

6.2. EVs SECRETED BY PRIMARY RAT HEPATOCYTES IN MODELS OF DILI

MOLECULAR CHARACTERIZATION

EVs derived of rat hepatocytes after exposure to APAP, GalN and DCF hepatotoxic drugs were isolated by differential ultracentrifugation and analyzed by NTA, Cryo-EM, Western-blotting and RTM. The use of these complementary techniques allows a rapid characterization of EVs using small amount of material. NTA is valuable for studying the size distribution and concentration, Cryo-EM for morphological characterization (vesicle heterogeneity) [165], while Western-blotting and RTM provides information about the protein and global chemical composition, respectively [166].

6.2.1. EVs SIZE, MORPHOLOGY AND CONCENTRATION ANALYSIS

Nanoparticle Tracking Analysis (NTA) is a simple and rapid method to determine nanoparticles size distribution and concentration [150].

The NTA analysis of EVs from untreated hepatocytes showed two main vesicles populations with 70% of the vesicles ranged on average size of 110 and 180 nm. Regarding EVs released by hepatocytes after exposure to different hepatotoxic drugs, a modification in the size distribution of the vesicles could be observed. In the case of GalN and DCF treatments, 50% of the vesicles maintain these two main vesicle populations, although they are not so pronounced as in untreated cells. Nevertheless, in the case of APAP treatment there is a clear main population on average size of 130 nm consisting of 50% of vesicles **(Figure 13B)**. This result indicates that under these experimental conditions, the hepatotoxins provoke changes in the populations of secreted-vesicles.

In all treatments, Cryo-EM images revealed a membrane vesicles limited by a lipid bilayer **(Figure 13A)**. In the case of DCF-treated hepatocytes, in addition to rounded vesicles, there was amorphous non-vesicular material in the EVs purifications in comparison with the rest of the conditions **(Fig. 13A, DCF-treatment**). It is important to highlight the high heterogeneity of vesicles observed in all the preparations in terms of size and shape. Also in many cases it was possible to observe vesicles inside the vesicles **(Fig. 13A, APAP and GalN-treatment)**.

In summary, these analyses together revealed heterogeneous EVs populations in terms of size and morphology and suggest that the hepatotoxic treatments alter the size distribution of EVs.

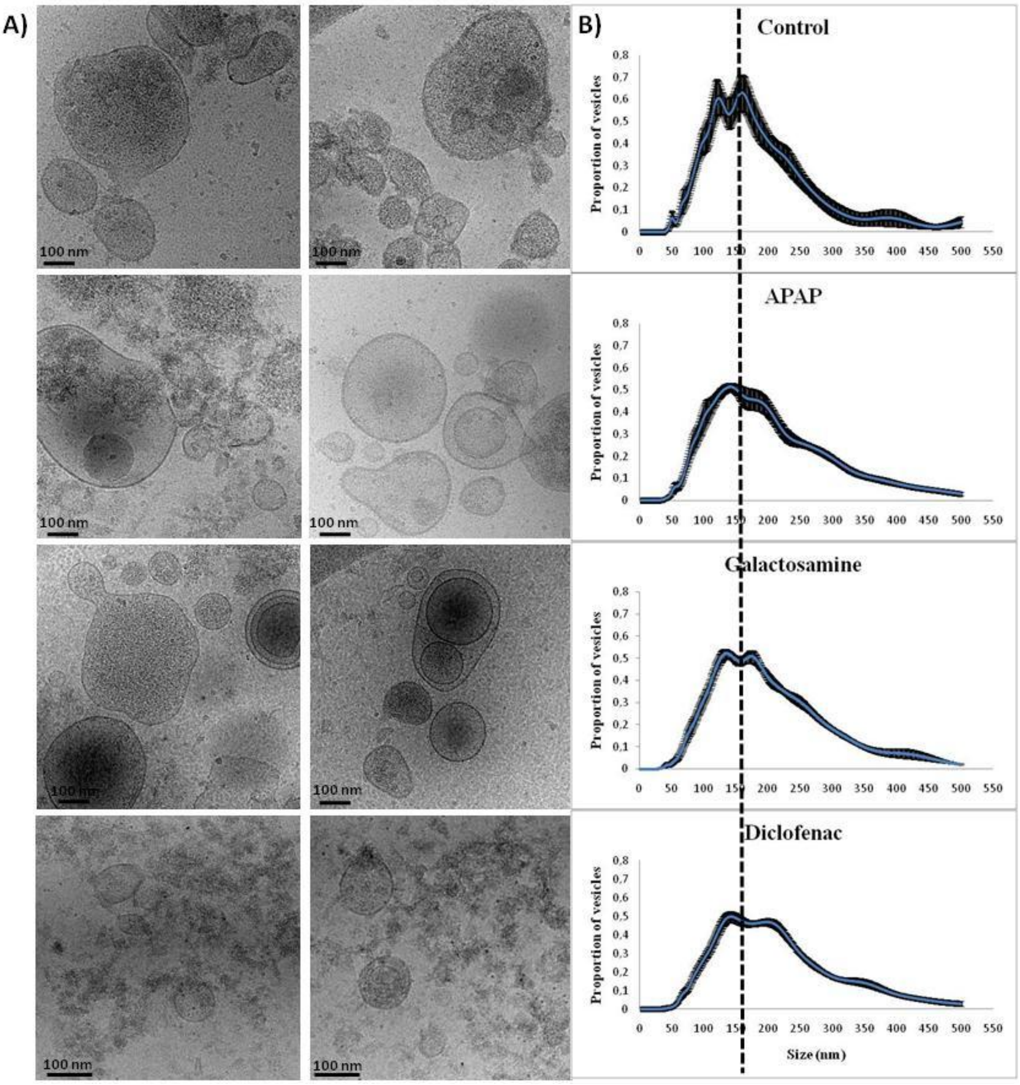
A)
B)
100 nm
Control
APAP
Galactosamine
Diclofenac
Proportion of vesicles
0
0,1
0,2
0,3
0,4
0,5
0,6
0,7
0,8
0
50
100
150
200
250
300
350
400
450
500
550
Size (nm)

Figure 13. Ultrastructural characterization of EVs in DILI models. Comparison of cryo-electron microscopy and Nanosight Tracking Analysis of hepatic EVs after treatment with different hepatotoxic drugs. **(A)** EVs were analyzed by Cryo-EM. Images show electron micrographs of membrane vesicles of different sizes and morphology. Scale bar: 100 nm. **(B)** NTA analysis showing vesicles size distribution (n=10).

NTA also allows the quantification of the number of vesicles present in the preparations. As can be observed in the **Figure 14**, the amount of secreted vesicles increased significantly in treated hepatocytes; 4.5, 3.8 and 3.5 fold in APAP-, GalN- and DCF-treated hepatocytes respectively compared to the level of secretion observed in untreated cells.

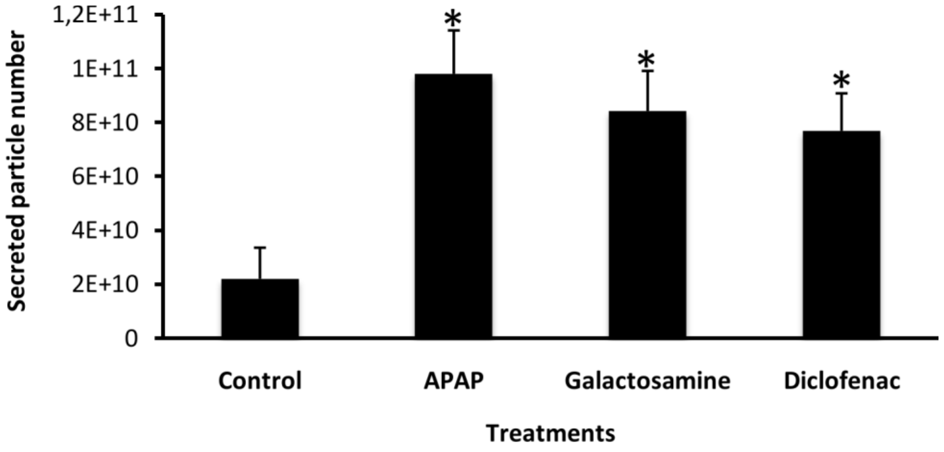

Figure 14. Total number of particles secreted in DILI models. The total number of secreted vesicles contained in each rat hepatocytes preparation after EVs isolation was estimated by means of Nanosight Tracking analysis. The mean number of secreted vesicles from untreated, APAP, GalN and DCF-treated hepatocytes was $2.19 \cdot 10^{10}$, $9.79 \cdot 10^{10}$, $8.41 \cdot 10^{10}$ and $7.68 \cdot 10^{10}$ vesicles respectively. Error bars represent SE (n = 10), * denotes $p<0.01$.

The total number of secreted vesicles estimated by NTA was then compared with the total protein amount of EVs estimated by means of Bradford assay. As shown in **Figure 15**, the total protein amount of hepatic EVs obtained after each treatment correlates with the number of secreted vesicles **(see Figure 14)**. APAP was the treatment with highest values for number of secreted vesicles and amount of protein, followed by DCF, GalN and control in decreasing order.

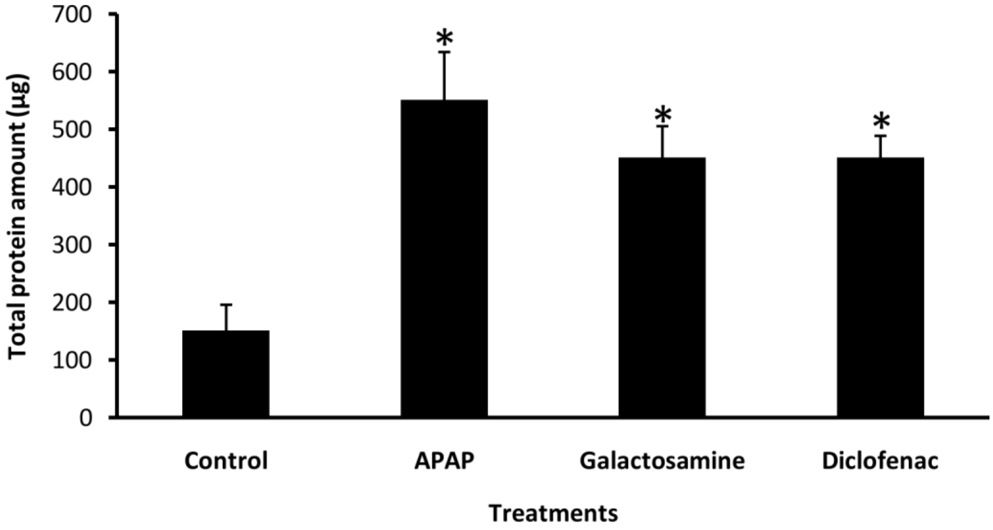

Figure 15. Total protein amount of EVs secreted in DILI models. The total protein amount contained in EVs preparation was determined by means of Bradford assay. The mean protein amount of hepatic EVs control and after treatment with APAP, GalN and DCF was 150, 550, 451 and 450µg respectively. Error bars represent SE (n = 10), * denotes $p<0.01$.

In order to estimate the purity of each preparation of vesicles, it was used the method described by Webber J and Clayton A, 2013 [167]. In this study is hypothesized that vesicle preparations that are more pure exhibit a relatively high ratio of particles to protein (NTA/Bradford). Thus, the presence of contaminating proteins in the samples would decrease this ratio. The ratio (NTA/Bradford) of EVs isolated from untreated and treated hepatocytes were 0.22 and 0.03 respectively. Thus, the ratio is more than 7-fold higher in EVs control than in EVs coming from treated cells. This result suggests that although there is an effect in the number of secreted vesicles under DILI conditions, there is even a higher effect in the release of protein aggregates.

6.2.2. WESTERN BLOT ANALYSIS

Until now, several proteins have been identified as EVs markers, including Cd63, Hsp70, Hsp90, Rab8, Flotillin-1 and LIMP II among others. In this work, the expression of these proteins was analyzed by Western blot in both untreated and treated hepatocytes as well as in their derived EVs **(Figure 12)**.

In the case of Hsp70 and Hsp 90, there is a decreased expression of these proteins in the treated cells that is accompanied by an increase in the corresponding EVs. Regarding Rab 8, there is a significant protein expression decrease in APAP-treatment in both cells and EVs. In contrast, for GalN- and DCF-treatments, there is an increase in the levels of this protein in EVs.

In the case of Flotillin-1, its expression is significantly reduced in both, cells and EVs in APAP- and DCF-treatments. In contrast, in the case of GalN-treatment such expression is increased. Which regards Cd63, there is a significant decrease in protein expression in treated hepatocytes for both, cells and EVs. LIMP II protein expression levels decreased notably in EVs in APAP- and DCF-treatments and, at less extent, in GalN-treatment.

In the case of *Ces1d*, there are increased protein expression levels in GalN- and DCF-treated hepatocytes derived EVs. Finally, COMT protein expression levels were clearly increased in EVs from GalN-treated hepatocytes.

In summary, the different levels of proteins observed in the different treatments suggest that different regulation processes are carried out in response to APAP, GalN and DCF induced liver damage.

6.2.3. EVs OVERALL COMPOSITION ANALYSIS

Once analyzed vesicles size, amount and morphology, it was wanted to fulfill hepatic EVs characterization analyzing their general composition.

Western blotting, as seen previously, allows analyzing the expression of determined proteins but it does not give information about the overall composition including proteins, lipids and nucleic acids. Yet, this analysis is possible using RTM [166]. Thus, changes in EVs global chemical composition in our DILI models were analyzed by RTM technology in collaboration with Sergei G. Kruglik and his group in Pierre *et* Marie Curie University in Paris (France).

RTM is the technique of choice for global chemical study in a time scale of few seconds of trapped EVs. It monitors variations in vesicular composition. In this case, EVs preparations were analyzed in duplicate. As can be observed in **Figure 16**, there is not significant shift variation when comparing each point of the curve of the duplicates, indicating the high reproducibility of the technique.

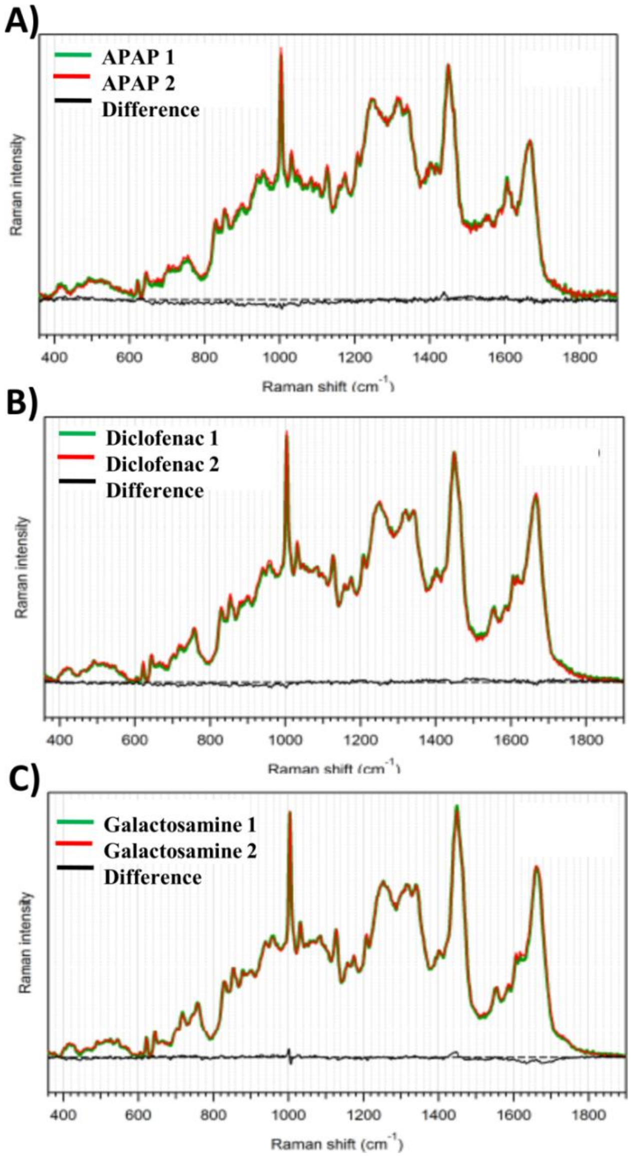

Figure 16. Raman tweezers microspectroscopy technique applied to study EVs global composition in DILI models. Raman spectrum represents the average signal corresponding to the total number of vesicles trapped in the focus of the microscope. All spectra were corrected for the PBS contribution. Shift is given in terms of spectral resolution (cm^{-1}).

Figure 17 shows the proposed interpretation of Raman spectrum originated from the EVs released by untreated rat hepatocytes. It appears that vesicles composition is heterogeneous, with different proportions of the chemical compounds. The main Raman signatures of lipids, proteins and nucleic acids are identified (arrows).

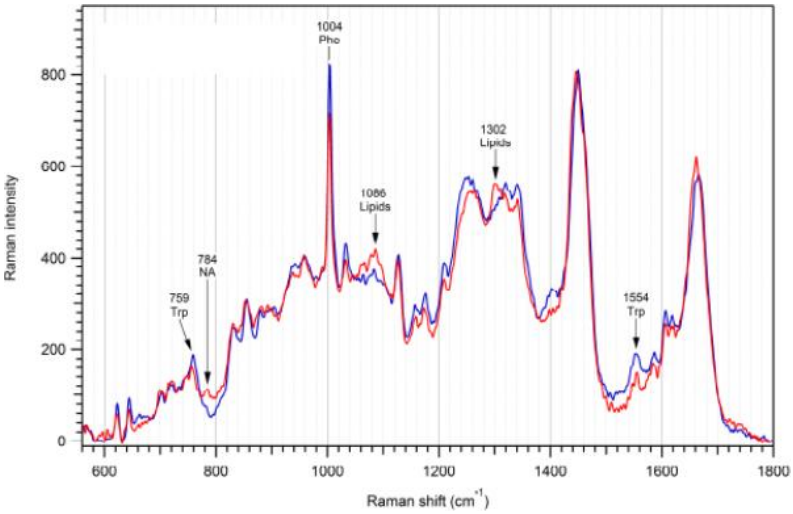

Figure 17. Average Raman spectra interpretation for rat hepatocytes derived EVs. Position, frequencies and bands interpretation for the major spectral differences are indicated by arrows. Raman spectrum represents the average signal corresponding to the total number of the vesicles trapped (n=2) Background was subtracted from both spectra to facilitate the comparison. Shift is given in terms of spectral resolution (cm^{-1}).

In **Figure 18,** the Raman spectrum corresponding to each treatment is represented. On these data, it is possible to characterize differences in composition between treatments. The higher RTM shift differences (black line), the bigger the alteration in EVs composition. In this regard, APAP-treated hepatocytes derived EVs have the major change in composition relative to untreated cells, showing more prominent lipids signatures than the control. Moreover, the amino acid tryptophan has also higher contribution in APAP-treatment **(Figure 18A).** Interestingly, in the Western blot analysis, APAP has a detrimental effect in the expression of the majority of the analyzed proteins **(see Figure 12)**. On the other hand, in GalN- and DCF-treated hepatocytes derived EVs there is a decrease in general lipid contribution with respect to the control, although at less extent compared to APAP-treatment. Finally, regarding nucleic acid composition, there are not significant changes in the treatments with respect to control.

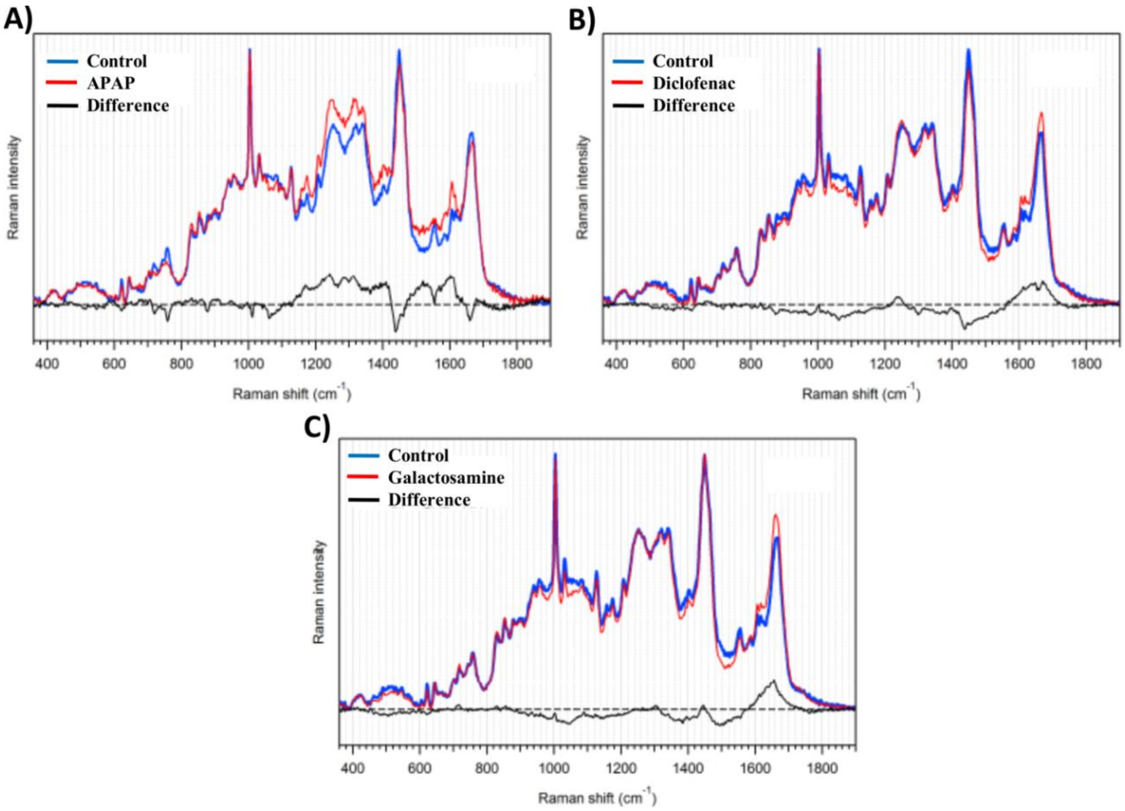

Figure 18. Analsyis of overall composition of hepatocytes-secreted EVs in DILI models. Comparison of the similarity/ variability of RAMAN spectra between untreated and treated hepatocytes is shown. **(A)** Control vs APAP, **(B)** control vs DCF and **(C)** control vs GalN is compared. Shift or composition differences between different treatments is given in terms of spectral resolution (cm^{-1}). Raman spectrum represents the average signal corresponding to the total number of the vesicles trapped. All spectra were corrected for the PBS contribution.

These results also suggest that different regulatory processes are carried out in response to APAP, GalN and DCF induced damage. Indeed, the general composition, amount and cargo of EVs has been observed to vary according to induced liver damage reflecting in this way the physiological condition of the liver [33]. In this regard, APAP is the treatment with the highest number of secreted vesicles, the most detrimental effect in the expression of most of the analyzed proteins and also with the highest alteration in overall composition, suggesting a severe liver damage.

Overall, it seems plausible to discriminate between different DILI treatments basing on EVs general composition analysis, strongly supporting the application of EVs as a source of non-invasive DILI biomarkers.

Finally, it is important to remark that the approach of a rapid characterization of EVs could be proposed by the joint use of the three complementary methods, NTA, Cryo-EM and RTM, with easy sample preparation and without the use of any added label.

6.2.4. EVs RNA CONTENT ANALYSIS

Since the demonstration that EVs cargo apart from protein and lipids also contain nucleic acids including both, DNA and RNA, numerous groups have analyzed the presence of genetic material in EVs. In this regard, it has been showed that EVs released by rat hepatocytes also carry RNA [70]. Remarkably, some of those RNAs were enriched in EVs respect to intracellular content. In particular, Albumin (Alb), retinol binding protein 4 (RBP4) and beta polypeptide 2-like 1 (GNB2L1) gene transcripts were analyzed due to their relevance in the biological context of the liver function. Briefly, albumin is synthesized in the liver and secreted into the serum in order to mobilize different molecules. GNB2L1 acts as an anchor or adaptor protein providing a platform for protein-protein interactions involved in cell-signaling pathways [168]. Finally, vitamin A (retinol) is absorbed in the small intestine, stored in liver, and secreted into circulation bound to RBP4 [169].

With the aim of characterizing the effects of hepatotoxic drugs in the RNA cargo of hepatic EVs, EVs derived from hepatocytes exposed to GalN, APAP or DCF were isolated and RNA contained in them was extracted for further analysis.

As it is shown in **Figure 19A**, remarkable differences between the RNA cargos of EVs released after the different liver-damaging treatments were found. All the treatments clearly increased the levels of analyzed RNAs (Alb, GNB2Ll and RBP4) secreted to the culture media. In fact, the amounts of Alb transcript increased from 2 to more than 15-fold in comparison with untreated hepatocytes. In the same way, the levels of transcripts coding for GNB2Ll and RBP4 proteins only increased significantly after GalN and DCF treatments, being more pronounced in the case of DCF. In particular, the levels of GNB2Ll increased 5- and 20-fold after GalN and DCF treatments respectively, whereas APAP treatment had no effect on the expression levels of this transcript. Overall, the levels of the three transcripts increased with GalN and DCF treatments, whereas when treating with APAP only the levels of albumin transcript is increased.

These results were further validated in the *in vivo* model. For this purpose, EVs from serum of rats treated with GalN (controls treated with saline solution) were purified using Exoquick reagent. As shown in **Figure 19B**, the amplification of RNAs associated with EVs, such as Alb, GNB2Ll and RBP4 was observed in GalN-injured animals, which was in agreement with the *in vitro* results.

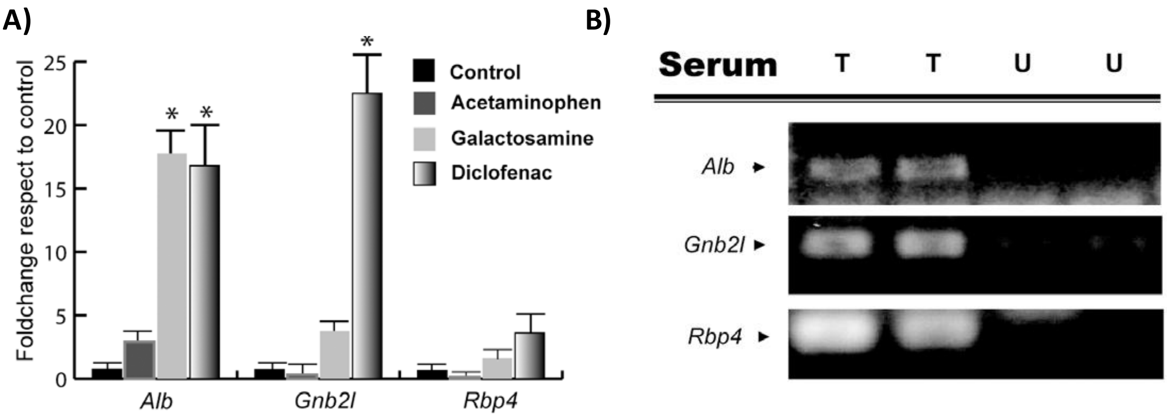

Figure 19. RNA cargo of hepatic EVs in DILI models. (A) qPCR analysis of three RNA transcripts (Albumine (Alb), Retinol binding protein 4 (Rbp4) and beta polypeptide 2-like 1 (Gnb2l)) released by hepatic EVs after exposure to indicated drugs is shown (error bars represent SD of 3 independent experiments (n = 2), * denotes $p<0.05$ with respect to the control **(B)** qPCR analysis of RNA cargo of EVs isolated from serum of untreated (U) rats and rats treated (T) with galactosamine (inducing acute liver injury).

Overall, *in vitro* and *in vivo* evidences suggest that DILI, in addition to modifying protein content, it also modifies the RNA content of hepatocytes-secreted EVs. Therefore, these results suggest that RNA cargo of hepatocyte-derived EVs, such as albumin, Gnb2l or Rbp4, could serve as a suitable non-invasive candidate marker for liver toxicity.

FUNCTIONAL CHARACTERIZATION (ENZYMATIC ACTIVITY ANALYSIS)

In the previous section, focused on the molecular characterization of the hepatocytes-derived EVs, it was showed the presence of many metabolic enzymes including *Ces1d*, MAT and COMT that play important role in endogenous and xenobiotics metabolism. However, the presence of the protein does not mean that is active. Thus, the next objective was to demonstrate that these enzymes were active in hepatocytes-derived EVs. To determine the activity of *Ces1d*, a fluorometric assay was used. However, to determine MAT and COMT activities, it was required to develop in-house methods.

6.2.5. CES ACTIVITY ANALYSIS

Firstly, it was tested if carboxylesterase (*Ces1d*) activity is present in hepatic EVs. To measure this activity, a fluorometric assay was performed using the protocol followed by Stacey L *et al*, 2006 [151]. EVs preparations were incubated at 37ºC in the presence of fluorescein diacetate and the formation of fluorescein by the action of *Ces1d* was measured in a fluorometer. As carboxylesterase activity was detected in control EVs, then, it was determined if DILI affected it in accordance to the Western blot results **(see Figure 12)**.

6.2.5.1. Esterase Activity analysis

Figure 20 shows the esterase activity detected in two independent preparations of EVs secreted by rat hepatocytes. In both preparations, EVs isolated from untreated hepatocytes showed esterase activity almost 2 times higher than the mock (absence of EVs). In addition, both independent preparations of EVs follow a similar trend.

When analyzed the effect of DILI in EVs associated carboxilesterase activity, the lowest activity was detected in EVs coming from untreated hepatocytes, while in EVs from hepatocytes exposed to liver damaging drugs was increased 2, 3 and 5-fold in APAP, DCF and GalN-treatments respectively compared to control **(Figure 20)**. These results strongly suggest that hepatic EVs carry active enzymes. Moreover, esterase activity is discriminative between different hepatotoxic treatments.

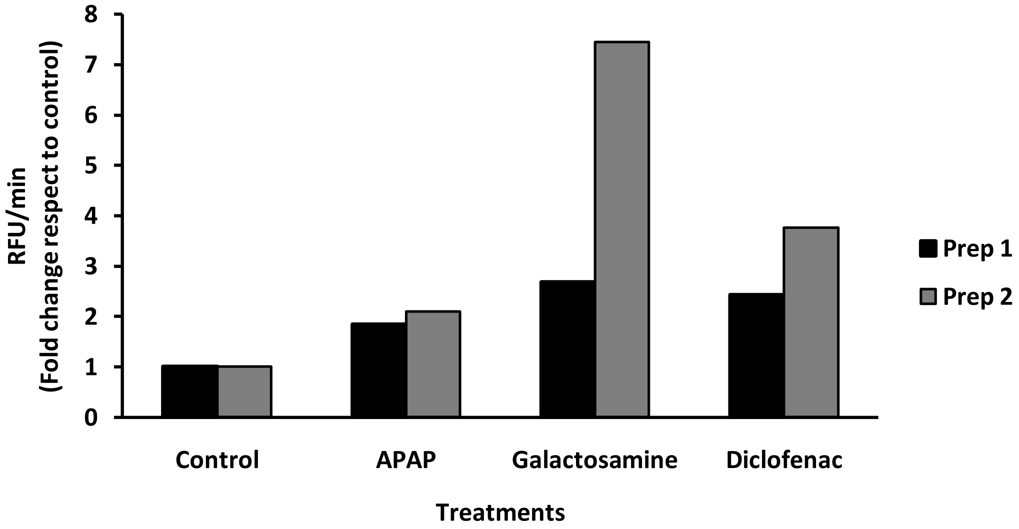

Figure 20. Carboxylesterase activity in EVs from DILI models. CES activity contained in EVs is increased after the exposure of indicated drugs. The activity is expressed in relative fluorescent unit per minute (RFU/min) and expressed as fold change respect to the control. Results from two independent preparations are shown.

6.2.5.2. Continuous density gradient analysis

In order to ensure that detected carboxilesterase activity comes from hepatic EVs, an extra purification step involving a continuous sucrose density gradient was performed to obtain highly pure EVs preparation. This step eliminates additional contaminants, such as proteins non specifically associated with EVs and large protein aggregates that could also be precipitated by ultracentrifugation but do not float on a density gradient [149]. To do that, equal amount (Bradford quantified) of EVs obtained from the control and the DILI models were subfractioned in sucrose density gradient. Then, all the fractions were analyzed by Western blotting and also assayed for CES activity. In all the cases, the carboxilesterase activity appears enriched in a fraction having a density of 1.21 g/ml (F9) **(Figure 21B)**. This was in complete agreement with the detection of the protein in the same fraction of the gradients by Western-blotting **(Figure 21A).** The activity was 2 and 5-fold higher in APAP and GalN-treatments with respect to control.

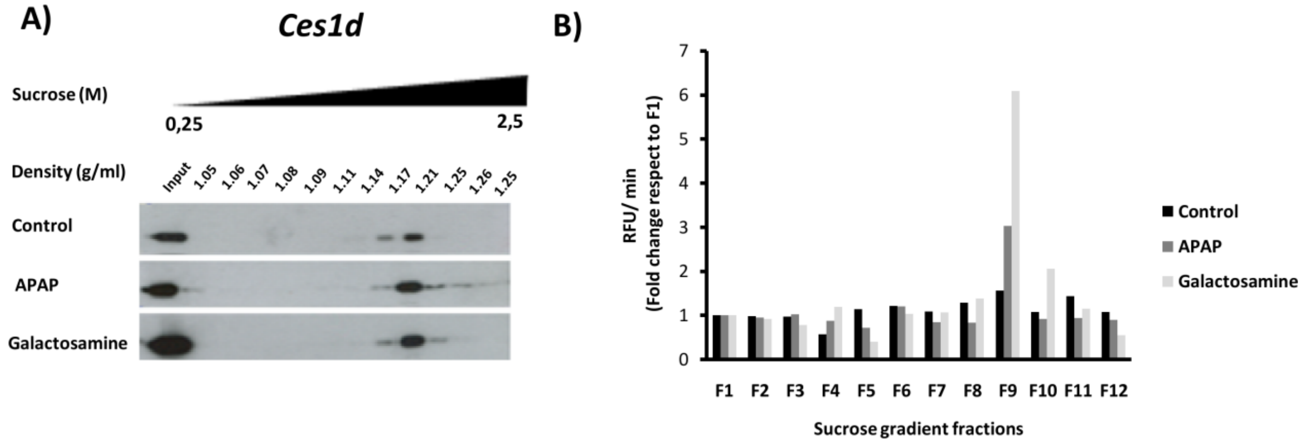

Figure 21. Density fractionation and CES activity analysis of hepatic EVs in DILI models. (A) Fractions obtained from sucrose density gradient were analyzed by Western-blotting. 5 µl of EVs sample were loaded in the input (13µg Control, 22.9µg APAP and 26.65µg in GalN) and 10µg of each fraction. The most abundant band was found in the fraction corresponding to EVs density. Treated EVs show more diversity, with vesicle populations fractionating at different densities than untreated. **(B)** EVs were sub-fractioned in a continuous sucrose density gradient and the esterase activity determined in each fraction. Esterase activity is expressed in relative fluorescent unit per minute (RFU/min), given in fold change respect to fraction 1 (F1).

It is important to highlight that the density of the EVs where *Ces1d* was localized was not significantly modified by DILI treatments, indicating that not dramatic changes in global composition of the vesicles were provoked.

In summary, these results correlate throughout the different assays. Both, protein expression levels (Western blotting) and enzymatic activity (Esterase activity measurement) increase with APAP, DCF and GalN-treatments in increasing order with respects to control. Therefore, CES activity varies depending on the induced liver damage, being able to discriminate between different liver injuries.

ANALYTICAL METHOD DEVELOPMENT OF MAT AND COMT ACTIVITIES

It is known the presence of COMT and MAT1A enzymes in hepatic EVs showed by proteomics and Western-blotting [69], but nothing about their activities in this localization has been reported so far. In order to address this question properly, a method to measure the activity of each of these enzymes using UPLC-MS technology was developed, which provides high specificity and sensitivity. Following section, describes the optimization of several parameters of the procedure that were required before the analysis of hepatic EVs.

6.2.6. MAT ACTIVITY ANALYSIS

6.2.6.1. Analytical method development

6.2.6.1.1. Optimization of the incubation condition for the enzymatic reaction to assay MAT activity

Although several studies have reported kinetic data of MAT activity in liver, the enzymatic reaction conditions are not well established yet. Initially, MAT activity was studied in rat liver extract following the protocol reported by Kim *et al.* 2008. Under these conditions, not reproducible results were obtained, being necessary to optimize several parameters of the enzymatic reaction including pH, ATP, salts, methionine and incubation time.

During the optimization process, the standard conditions of the assay were performed in a final volume of 250 µl containing 100 mM Tris-HCl buffer pH 8.7: enzyme provider (250µg of rat liver extract), 5 mM ATP, 5 mM L-methionine, 150 mM KCl, 10 mM $MgCl_2$, protease inhibitor (1 x 1,000) and 5 mM DTT. A reducing agent (DTT) is necessary since the oxidation of the enzyme produces an internal disulfide that could cause the inhibition of the enzyme [170]. The parameters to be optimized were modified as indicated for the specific experiments.

pH optimization

To determine optimal pH, Tris-HCl buffer 100 mM ranging from pH 7.4 to 9.2 was assayed under standard conditions (mentioned above) **(Figure 22)**. Under these conditions, the enzyme reached its major activity at pHs between 8.0 and 9.2 and shown optimal activity at pH 8.7 **(Figure 22A)**, which was in agreement with the value reported by Suma *et al.* 1986. The activity of the enzyme decreased above pH 9.2, suggesting that highly alkaline conditions may have a detrimental effect on enzyme and compounds stability. During the incubation period, the amount of consumed methionine was also measured **(Figure 22B**) at pH 8.7. In this way, reaction specificity was also confirmed.

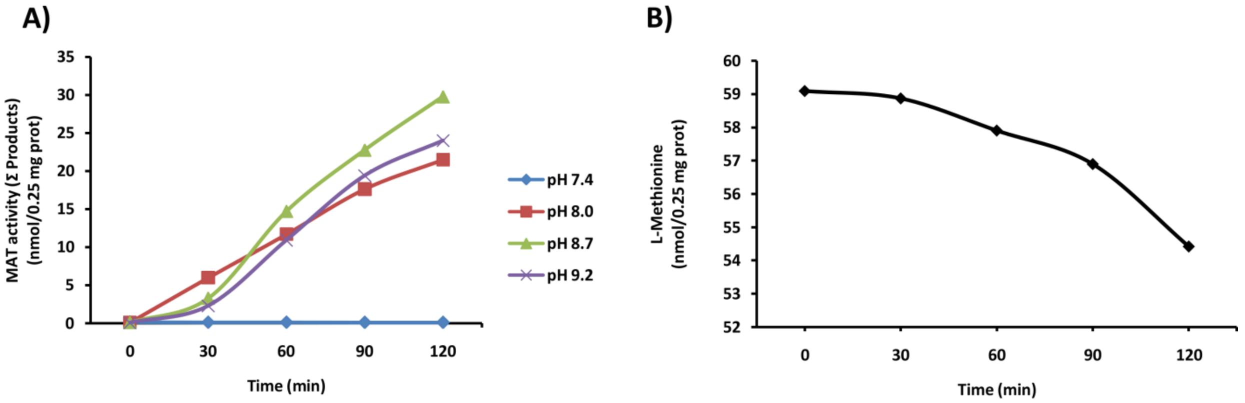

Figure 22. Optimization of pH for MAT enzymatic activity.**(A)** The enzymatic assay was performed at 37°C in 100mM Tris-HCl buffer at different pHs (7.4, 8.0, 8.7 and 9.2) and time points (0, 30, 60, 90 and 120min). **(B)** The amount of consumed L-Methionine during the reaction was measured at pH 8.7 and different time points (0, 30, 60, 90 and 120min). The reaction mixture contained the following components in a final volume of 250 µl: 250 µg of protein (rat liver extract), 5 mM ATP, 0.1 mM methionine, $MgCl_2$ 5 mM, KCl 50 mM, 5 mM DTT and protease inhibitor (1x1,000). MAT activity is expressed as Σ products (SAMe and SAH) in nmol/0.25mg protein.

Optimization of temperature of incubation for the reaction

Once fixed the pH, the optimal temperature of the enzymatic activity was determined under standard assay conditions, incubating the reaction mixture at increasing temperatures ranging from 27°C to 52°C. The highest MAT activity at pH 8.7, was obtained at 37°C **(Figure 23A)**. Rat liver basal temperature is 39.3°C [171], which is found in the range of MAT enzymatic activity optimum temperature (37°C-42°C). MAT denaturation studies on recombinant rat liver MAT activity, showed its irreversibility at temperatures between 47–51°C [172], which is in agreement with obtained results. In addition, SAMe is thermolabile, which could be translated in a partial decay of SAMe during prolonged incubation periods at high temperatures. In this regard, SAMe would be cleaved into MTA and homoserine by a nucleophilic attack of the carboxylate group which, at the end, would complicate the analytical study of SAMe [173]. During the incubation period, the amount of consumed methionine was also measured at 37°C **(Figure 23B)**. In this way, reaction specificity could also be confirmed.

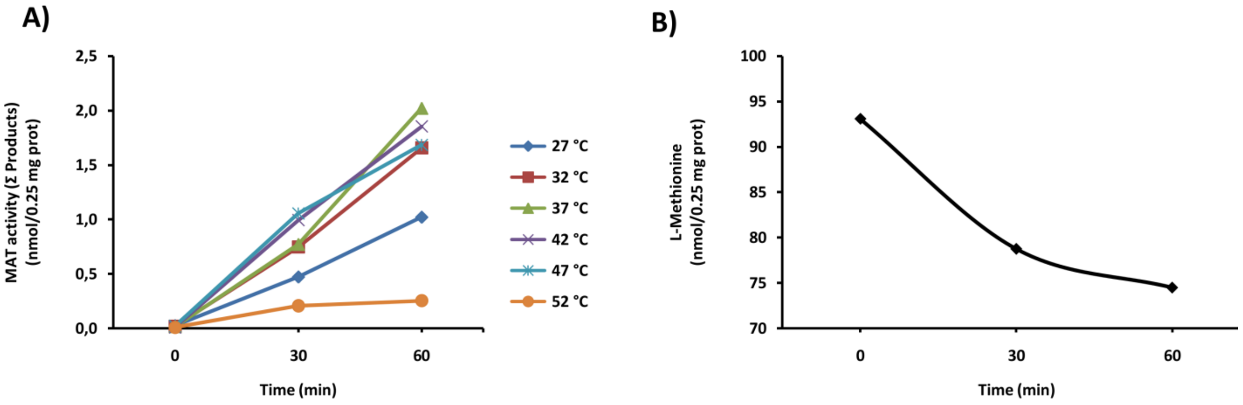

Figure 23. Optimization of temperature reaction for MAT activity. (A) The enzymatic assay was performed at 37°C in 100mM Tris-HCl buffer at pH 8.7 at different temperatures (27, 32, 27, 42, 47 and 52°C) and timepoints (0, 30 and 60 min). **(B)** The amount of consumed L-Methionine during the reaction was measured (nmol/0.25mg prot) at 37°C and different timepoints (0, 30 and 60 min) The reaction mixture was incubated under standard assay conditions; 250 µg of protein (rat liver extract), 5 mM ATP, 0.1 mM methionine, $MgCl_2$ 5 mM, 50 mMKCl, 5 mM DTT and protease inhibitor. MAT activity is expressed as Σ products (SAMe and SAH) in nmol/0.25mg protein.

Optimization of divalent (Mg^{2+}) and monovalent (K^+) cations content in the reaction.

MAT activity requires both Mg^{2+} and K^+ cations for maximal activity [101], [174] given that the mechanism of hydrolysis of the ATP requires these cations. When these cations are in high concentrations, MAT activity could be inhibited due to the effect of high ionic strength [175]. The **Figure 24** shows the effect of combined concentrations of Mg^{2+} and K^+ cations in MAT activity. The optimal salts concentrations were established at 10 mM $MgCl_2$ and 150 mM KCl.

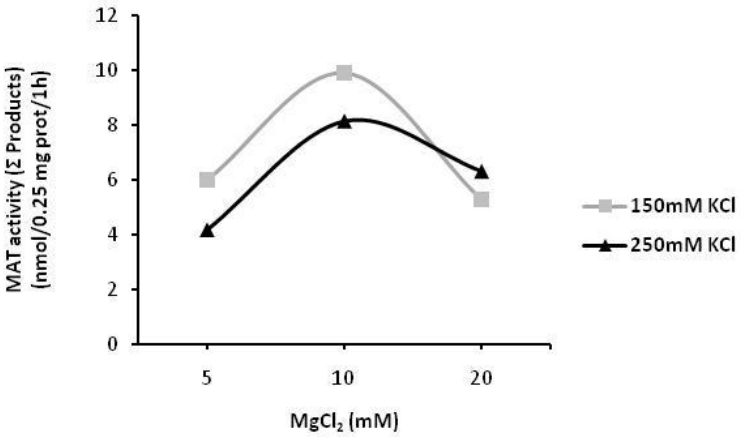

Figure 24. Optimization of divalent (Mg^{2+}) and monovalent (K^+) cations content in the reaction. Effect of Mg^{2+} and K^+ on enzyme activity of MAT was evaluated in Tris-HCl buffer (100 mM, pH 8.7) at 37°C for 60 min. The reaction mixture was incubated under standard assay conditions (250 µg of protein from rat liver extract, 5 mM ATP, 0.1 mM methionine, 5 mM DTT and protease inhibitor), using different concentrations of $MgCl_2$ (5, 10 and 20 mM) and KCl (150 and 250 mM) in a final volume of 250µl. MAT activity is expressed as Σ products (SAMe and SAH) in nmol/0.25mg protein/1h.

Optimization of L-methionine concentration in the reaction assay

Optimal L-methionine concentration for MAT enzymatic activity was determined under standard assay conditions, incubating L-methionine at increasing concentrations ranging from 0.1 to 10 mM. As can be observed in the **Figure 25,** the highest MAT activity efficiency was reached when incubating rat liver extract with 5 mM L-methionine.

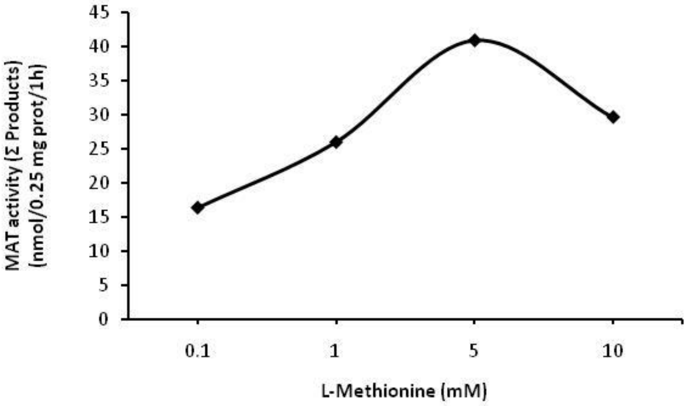

Figure 25. **Optimization of L-methionine concentration for MAT activity.** The enzymatic assay was performed in Tris-HCl buffer (100 mM, pH 8.7) at 37°C for 60 min. The reaction mixture was incubated under standard assay conditions; 250 µg of rat liver extract, 5 mM ATP, 10 mM $MgCl_2$, 150 mM KCl, 5 mM DTT and protease inhibitor in a final volume of 250 µl, using different concentrations of L-methionine (from 0.1 to 10 mM.). MAT activity is expressed as Σ products (SAMe and SAH) in nmol/0.25mg protein/1h.

Optimization of ATP concentration

Optimal ATP concentration for MAT enzymatic activity was determined under standard assay conditions (fixing L-methionine at 5mM), in increasing concentrations that ranging from 0.1 to 10 mM. The highest MAT activity efficiency was reached when incubating rat liver extract with 5 mM ATP **(Figure 26).**

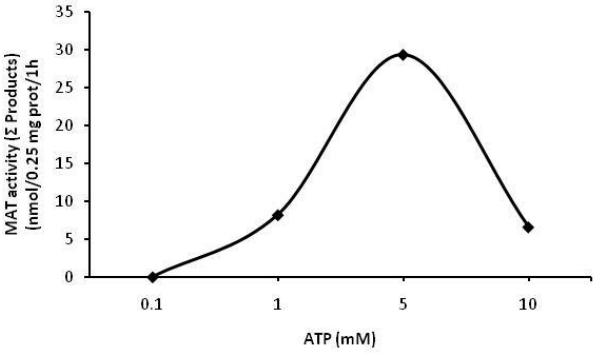

Figure 26. **Optimization of ATP concentration for MAT activity.** The enzymatic assay was performed in Tris-HCl buffer (100 mM, pH 8.7) at 37°C for 60 min. The reaction mixture was incubated under standard assay conditions 250 µg of rat liver extract, 10 mM $MgCl_2$, 150 mM KCl, 5 mM DTT, 5mM L-Methionine and protease inhibitor in a final volume of 250 µl using different ATP concentrations (from 0.1 to 10 mM.). MAT activity is expressed as Σ products (SAMe and SAH) in nmol/0.25mg protein/1h.

Optimization of reaction incubation time

The incubation time was also evaluated from 0 to 3 hours; aliquots were collected every 30 min. As can be observed in the **Figure 27**, during the whole tested time the reaction didn´t reached a maximum for MAT activity even after 3 hours incubation. Given that incubation times longer than two hours are not recommended because of SAMe instability in long incubation periods, 2-hours period was chosen as optimal to evaluated the MAT activity.

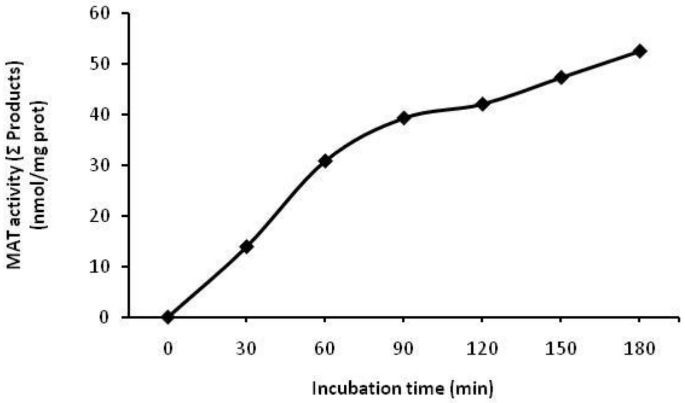

Figure 27. **Optimization of incubation reaction time for MAT activity.** The enzymatic assay was performed in Tris-HCl buffer (100 mM, pH 8.7) at 45°C. The reaction mixture was incubated under standard assay conditions;250 µg of rat liver extract, 10mM $MgCl_2$, 150 mM KCl, 5 mM DTT, 5mM ATP, 5mM L-Methionine and protease inhibitor (1x1,000) in a final volume of 250µl. Different incubation periods were assayed (30, 60, 90, 120, 150 and 180min). MAT activity is expressed as Σ products (SAMe and SAH) in nmol/0.25mg protein.

As results of the optimization process, different parameters of the enzymatic reaction were adjusted in order to obtain the optimal enzymatic activity efficiency. The established conditions were 2-hours of incubation at 37ºC in a final volume of 250 µL containing 100mM Tris-HCl buffer pH 8.7, 5 mM ATP, 5 mM L-methionine, 150 mM KCl, 10 mM $MgCl_2$, protease inhibitor and 5 mM DTT.

6.2.6.1.2. Ultra performance Liquid Chromatography-Mass Spectrometry optimization

Once the samples were incubated in the reaction mixture, it was necessary to optimize next steps prior to data process; UPLC-MS conditions, SPE and analytical method.

Hydrophilic Interaction Chromatography (HILIC) was used to quantify SAMe and SAH. HILIC is an alternative to reserved-phase chromatography (or hidrophobic chromatography) and uses hidrophilic stationary phase for applications involving polar compounds such as these [176]. HILIC can offer a tenfold increase in sensitivity over reversed-phase chromatography when used with electrospray-ionization mass spectrometry detection mode

[177]. In addition, HILIC is ideal for very polar compounds that are difficult to retain in reversed-phase chromatography. The main products that take part in the reaction, SAMe and SAH, were scanned in ESI+ mode and analyzed in matrix solution (in this case, rat liver extract). As can be observed in the **Figure 28**, both compounds appear completely separated in the chromatogram. The spectra of SAMe and SAH were dominated by protonated molecules $[M+H]^+$ and no significant adducts or fragments ions were observed. SAMe was detected at a *m/z* of 399.145 and a retention time of 2.99 min, and SAH at a *m/z* of 385.129 and a retention time of 2.35 min **(Table 3)**.

Table 3. MAT activity derived metabolites structure and properties. In this table is shown SAMe and SAH m/z ratio, the retention time in matrix (rat liver extract) and molecular formula and structure of each compound.

Compound	Structure and formula	$[M+H]^+$	t_r (min)
S-Adenosyl methionine (SAMe)	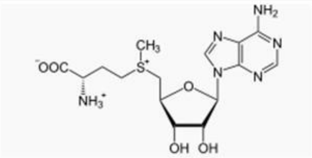 NH2 CH3 N N ⁻OOC S⁺ O N N NH3⁺ OH OH $C_{15}H_{22}N_6O_5S$	**399.145**	**2.99**
S-Adenosyl homocysteine (SAH)	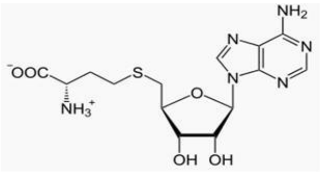 $C_{14}H_{20}N_6O_5S$	**385.129**	**2.35**

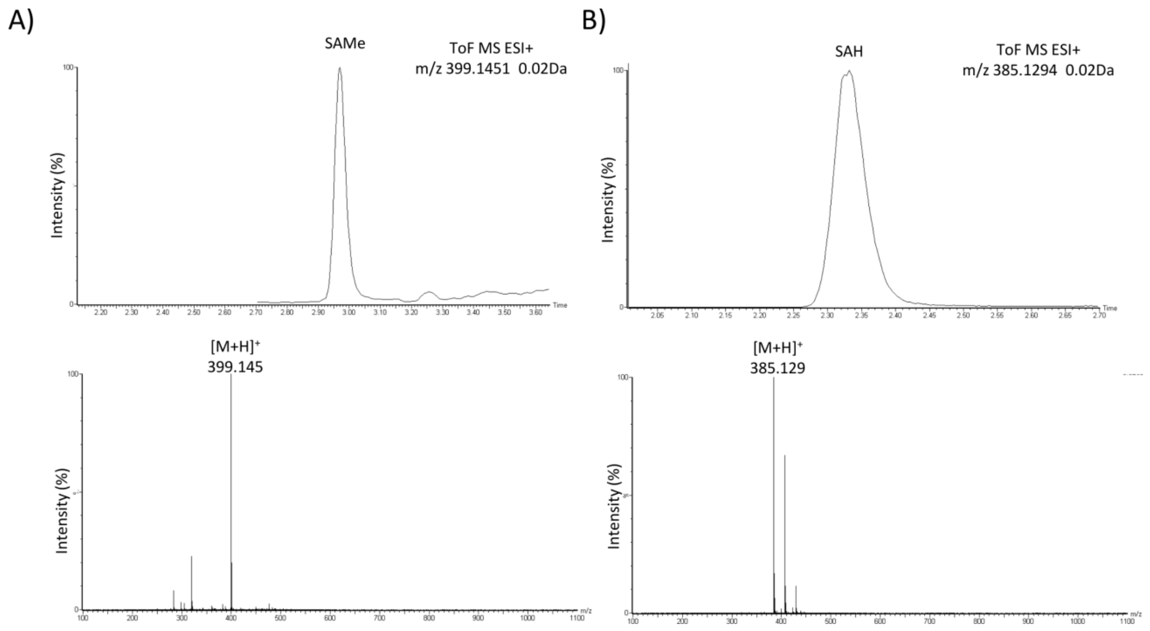

Figure 28. Representative chromatograms (top) and mass spectra (bottom) obtained from rat liver extract spiked with SAMe (A) and SAH (B)

6.2.6.1.3. Solid-Phase Extraction (SPE) method development

In order to clean the samples before injecting them in the mass spectrometry, SPE was optimized to remove mostly the elevated levels of salts required to perform the enzymatic reaction. This step is required since high concentration of salts could interfere in analytes ionization and detection, in addition to shorten the lifespan of the column.

SPE method selection

Different protocols were combined to optimize the SPE for SAMe, SAH and MTA (see references Delabar *et al.*1999 [178], Gellekink *et al.* 2005 [179], Cataldi *et al.* 2009 [179]), trying different cartridge conditioning and sample pre-treatments. SPE methods based on non-polar (Van der Waals forces), polar or ionic interactions are relatively non-specific. In contrast, covalent bond, is based on a specific union between a functional group of the analyte with the cartridge sorbent surface, which results in an increased specificity of the extraction method. In this regard, extraction of SAMe, SAH and MTA was performed using Bond Elute cartridges containing 100 mg phenilboric acid (PBA) bonded silica [180][181]. The choice of the PBA cartridge was based on the affinity of boronate for the cis-hydroxyl group of a ribose moiety, which is present in SAMe, SAH and MTA.

The mechanism of boronate binding is illustrated in **Figure 29**. The immobilized PBA is first equilibrated with an alkaline solution to obtain the reactive boronate form, $RB(OH)_3^-$ **(Figure 29A).** The sample is then applied and the covalent bond will be specifically formed with those compounds containing cis-hydroxyl group **(Figure 29B).** Once the compounds of interest are retained (SAMe, SAH and MTA in this case), contaminants will be selectively washed from the bonded phase. As long as the pH of the aqueous component of the wash solvent remains alkaline, the covalent complex will remain intact. Finally, the compounds of interest will be elute by acidification of the boronate complex, which releases the diol-containing compound and renders the immobilized phenylboronic acid neutral ($RB(OH)_2$) **(Figure 29C).**

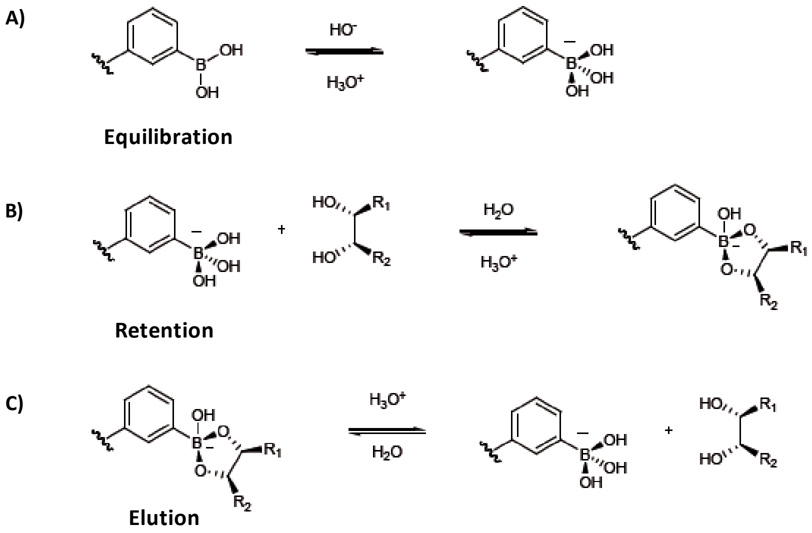

Figure 29. Phenilboric acid (PBA) based solid phase extraction mechanism. The three step process of borate binding includes equilibration, retention and elution; the sample is loaded at pH 7.5 and the analytes (SAMe, SAH and MTA) are bound to reactive boronate form ($RB(OH)_3^-$). Then the chromatographic column is washed subsequently in order to elute contaminants present in the sample. Finally, the compounds of interest are eluted adding an acidic solution that disrupts analyte and sorbent binding.

Buffer selection

Apart from the SPE method selection, it is necessary to choose the appropriate buffer for PBA-based SPE. To ensure good extraction efficiency, the first requirement is the use of an alkaline pH for column conditioning and subsequent sample application. The use of buffers that are themselves capable of forming covalent adducts with the PBA, such as Tris-HCl buffer, is clearly not recommended since this will avoid the formation of the covalent bond between boronate (chromatographic column reactive group) and the analyte. In this regard, to study MAT activity, initially, as mentioned before, the protocol reported by Kim *et al* 2008 [182] was followed, whom studied MAT activity using Tris-HCl buffer. Later on, due to the elevated contaminants (mostly salts) existing in the reaction assay, it was needed to perform an extra-cleaning step using PBA-based SPE, which was incompatible with Tris-HCl buffer. Therefore, it was decided to change Tris-HCl to HEPES buffer taking as a reference the study reported by Shapiro *et al.* 2011 [183]. They carried out a comparative study between Tris-HCl and HEPES-NaOH buffers at different pHs. This buffer was tested at two different pHs (7.5

and 9.5). To choose the optimal pH, matrix effect, process efficiency and recovery was evaluated **(see Figure 8)**. The matrix effect is an important issue to be addressed in method development, validation, and routine use of UPLC-MS. It is the alteration of ionization efficiency by the presence of coeluting substances in the sample of interest, having deleterious impact on method accuracy and sensitivity [184][185]. The presence of ion suppression was determined from the ratio C/A **(**The compound of interest added to the matrix after extraction/The same amount of compound injected directly in mobile phase). The data for the compound in mobile phase (A) provide a relative 100% response value whereas the data for the same amount of compound added to extracted samples (C) show the effect of sample matrix on MS response (ion suppression) [186]. In the **Figure 30** is shown the matrix effect for SAMe, SAH and MTA at different pHs (7.5 and 9.5). The negative values indicate ion suppression. For SAMe, there is not matrix effect at pH 7.5 (0.82 %) whereas at pH 9.5 increased notably (-8.77%) **(Figure 30).** Regarding SAH, there is ion suppression at both pHs, being higher at pH 9.5 (-5.92 at pH 7.5 and -10.48 at pH 9.5). Finally, the matrix effect on MTA is almost the same at both pHs (-36.96 and -36.36 for pH 7.5 and 9.5 respectively). Overall, there is not an important ion suppression for SAMe and SAH.

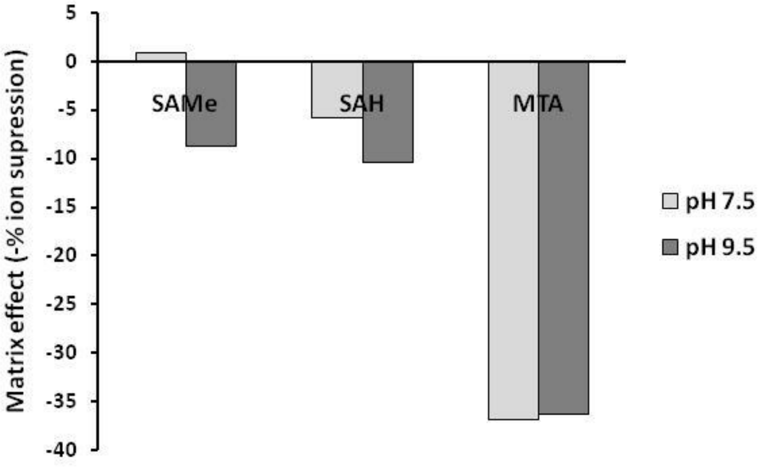

Figure 30. UPLC-MS analysis of matrix effects for SAMe, SAH and MTA. Matrix effect for SAMe, SAH and MTA at pH 7.5 and pH 9.5 are shown. The negative % values indicate ion suppression.

The efficacy of the SPE method was determined from the ratio of test solutions B/A, being B the mass spectrometric signal obtained before SPE extraction and A, the same amount of compound injected directly in mobile phase **(see Figure 8)**. This parameter (process efficiency) shows the loss of signal (if present) attributable to the extraction process expressed in percentage (%) [186]. For SAMe, SPE efficiency was slightly higher at pH 7.5 (58.34%) than at pH 9.5 (53.97%). In the case of SAH, it was notably higher at pH 7.5 (53.95) than at pH 9.5 (36.75%). Finally, in the case of MTA, SPE efficiency was practically the same at both pHs (28.64% at pH 7.5 and 28.09% at pH 9.5) **(Figure 31)**.

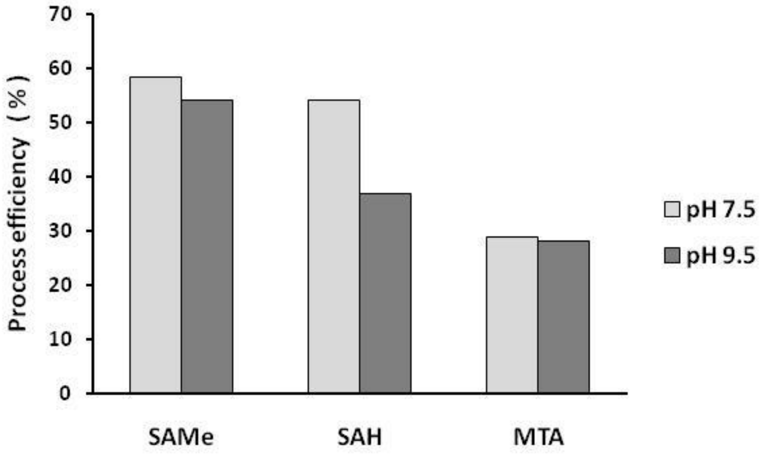

Figure 31. SPE process efficiency for for SAMe, SAH and MTA. Solid-phase extraction (SPE) efficiency for SAMe, SAH and MTA is shown. The efficiencies obtained for SAMe, SAH and MTA were in decreasing order.

Recovery Analysis

With respect to recoveries, they were determined from the ratio of test solutions B/C, being B the signal obtained when the compound of interest is added to the matrix before extraction, and C the signal obtained when same amount of compound is added to the matrix after the extraction procedure **(see Figure 8)**.

$$\text{Recovery (\%)} = \frac{\text{Rat liver extract spiked with SAMe/SAH/MTA before SPE (Pre-spiked sample)}}{\text{Rat liver extract spiked before UPLC-MS (Post-spiked sample)}}$$

The recovery of SAMe and SAH determined at 5 µM was 58%. This value was in the acceptable range for UPLC-MS analysis [187]. Nevertheless, the recovery obtained for MTA was 45%, under acceptable range. Low recovery efficiency together with the high matrix effect obtained in MTA make this method to be restricted to SAMe and SAH analysis. Indeed, the majority of the reported studies evaluate MAT activity quantifying simultaneously SAMe and SAH.

The recovery for SAMe was very similar at pH 7.5 (57.86%) and at pH 9.5 (59.16%) **(Figure 32).** Which regards to SAH, the recovery increases notably at pH 7.5 (57.35%), being under acceptable range at pH 9.5 (41.03%).Therefore, without taking MTA into consideration, the PBA-based SPE with the highest recoveries and lowest matrix effect were obtained at pH 7.5.

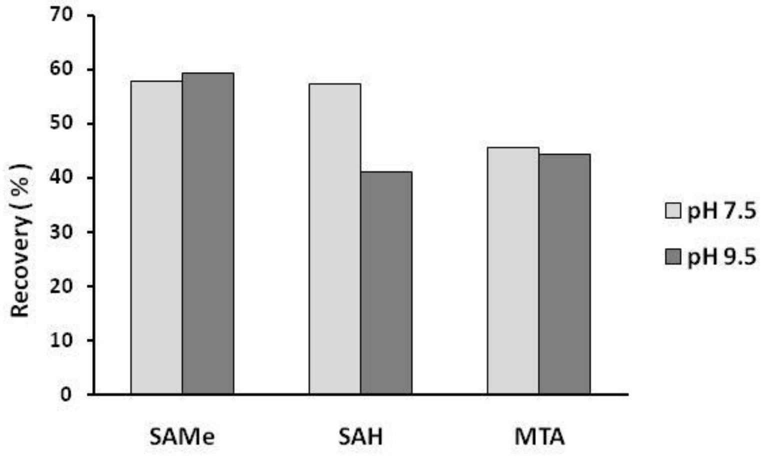

Figure 32. Recovery analysis for SAMe, SAH and MTA in the PBA-SPE method. Obtained recoveries for SAMe, SAH and MTA are shown. Except for MTA, obtained recoveries were in acceptable range of analysis.

Overall, prior to UPLC-MS analysis, an extra-cleaning step (PBA-SPE) was applied to already incubated samples.

6.2.6.2. Analytical method optimization

In order to quantify the amount of the product formed in the enzymatic reaction, it was required to consider the following parameters to obtain sensitive and specific determination of the enzymatic activity.

6.2.6.2.1. Specificity of the enzymatic assay

It is reported that SAMe is stable at acid pH. Therefore, it was injected into UPLC-MS system in acidic conditions [188].

Moreover, SAMe is formed from the union of methionine and ATP. Thus, the new SAMe formed after incubation can only come from enzymatic reaction.

6.2.6.2.2. Linearity of Calibration Curves and Lower Limits of Quantification (LLOQ)

To calculate the absolute amount of obtained products (SAMe and SAH), the average of baseline signals were subtracted from the signals of the serially diluted calibration samples. The calibration curve was obtained over the concentration range of 0.025-100 µM for SAMe and 0.025-25 µM for SAH.

Power fit equation was employed to determine the relation between the signal (peak area) and sample concentration:

SAMe: $[\text{Signal}] = 987.73 \times [\text{concentration}]^{1,0962}$ ($R^2 > 0.99$)
SAH: $[\text{Signal}] = 1776.6 \times [\text{concentration}]^{1,0774}$ ($R^2 > 0.99$)

Once the sample concentrations were calculated, they were converted to amount (nmol) of product formed (Σ products: SAMe and SAH) per mg of protein in 1 h incubation. The amount of SAMe and SAH detected in the controls (not incubated) was considered background and subtracted from the samples. The activity of MAT was estimated by quantifying jointly SAMe and SAH production. The present UPLC–MS method offered a LLOQ of 0.025 µM for SAMe and SAH.

6.2.6.2.3. Precision and Accuracy of the enzymatic assay

Accuracy and precision were deemed to be acceptable (<15%) for SAMe, SAH and MTA.

6.2.7. COMT ACTIVITY ANALYTICAL METHOD

6.2.7.1. Analytical method development

6.2.7.1.1. Optimization of the incubation condition for the enzymatic reaction to assay COMT activity

Similar to MAT activity, an optimization of different parameters was required before COMT [189], [190] enzymatic activity evaluation. Incubation conditions of the enzymatic reaction had to be optimised in order to obtain the optimal enzymatic activity efficiency. This involves the use of cofactors as well as different parameters adjustments such as pH. Moreover, the stability of the compounds that take part in the reaction has to be taken also into consideration.

In COMT enzymatic reaction Mg^{2+} ions are required since they are coordinated to three amino acid residues (Asp, Asn and Glu) in the catalytic site of COMT [191]. Therefore, Mg^{2+} ions are routinely added to reaction mixture (2 mM $MgCl_2$).

COMT assays are normally performed under physiological conditions (pH around 7.4 and temperature 37°C). The enzyme has two-isoforms one associated to membrane (MB-COMT) and other soluble (S-COMT). For the measurement of MB-COMT and S-COMT activity, different approaches have been performed. These include the separation of the two isoforms by differential ultracentrifugation and the use of two different substrates such as Dopamine (DA) or Norepinephrine (NE) at different concentrations and pHs (7.4 for MB-COMT and 7.8 for S-COMT) [128] (Data not shown).

In order to simplify the assay and try to detect COMT activity in EVs, this study was focused on MB-COMT activity, which has higher affinity (but lower O-methylation capacity) for the catecholamines (DA and NE) than S-COMT [191].

6.2.7.1.2. Ultra Performance Liquid Chromatography-Mass Spectrometry optimization

Once the samples were incubated in the reaction mixture, it was necessary to optimize next steps prior to data process; UPLC-MS conditions, SPE and analytical method. As same as in the case of MAT, with COMT, HILIC was also used to analyze DA/3-MT and NE/NMN. In this regard, HILIC column conditions were optimized in order to achieve the best chromatographic separation of the compounds of interest. Considering the strong relation between chromatographic conditions and mobile phase, different concentrations of ammonium formate were tested to see their effect on the analytes retention (Data not shown). In the absence of ammonium formate, the peak shapes were broad and irregular. Regular peak shape and identical retention time were achieved for each analyte when the salt concentration reached 20 mM. The pH of the buffer may also have significant influence on the analytes chromatographic behavior. 0.5% formic acid was used to separate the analytes. In these conditions, analytes of interest were positively charge and completely separated **(Table 4).**

Table 4. COMT activity derived metabolites structure and properties. In this table is shown m/z ratio, retention time in matrix (rat liver extract) and molecular formula and structure of dopamine (DA), 3-Methoxytyramine (3-MT), norepinephrine (NE) and normetanephrine (NMN).

Compound	Structure and formula	$[M+H]^+$	Base peak (*m/z*)	t_r (min)
Dopamine (DA)	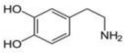 $C_{11}H_8NO_2$	154.086	137.063* $[M+H-NH_3]^+$	1.33
3- Methoxytyramine (3-MT)	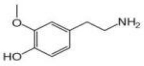 $C_9H_{13}NO_2$	168.102	151.075* $[M+H-NH_3]^+$	1.15
Norepinephrine (NE)	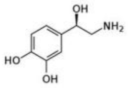 $C_8H_{11}NO_3$	170.081	151.075* $[M+H-H_2O]^+$	1.54
Normetanephrine (NMN)	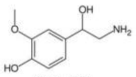 $C_9H_{13}NO_3$	184.097	166.086* $[M+H-H_2O]^+$	1.30

* Fragmentation in the source

Once the analytes were properly separated, the corresponding chromatograms and mass spectra were obtained. The **Figure 33** and **Figure 34** show the mass spectra and the chromatograms of DA/3-MT and NE/NMN, respectively. In the spectra of DA and 3-MT, a loss of one molecule of ammonia was observed, forming the predominant ion $[M+H-NH_3]^+$, whereas in the case of NE and NMN, a loss of one molecule of water was observed, forming the predominant ion $[M+H-H_2O]^+$ represented as base peak in the spectra [190], [192].

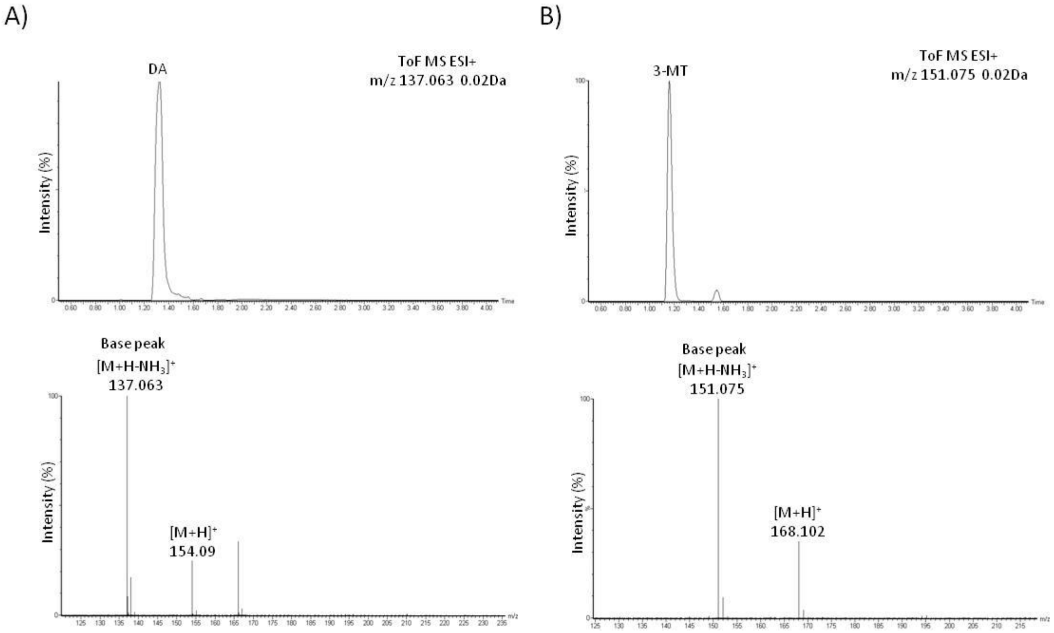

Figure 33. Representative chromatograms (up) and mass spectra (down) obtained from rat liver extract spiked with Dopamine (A) and 3-Methoxytyramine (B)

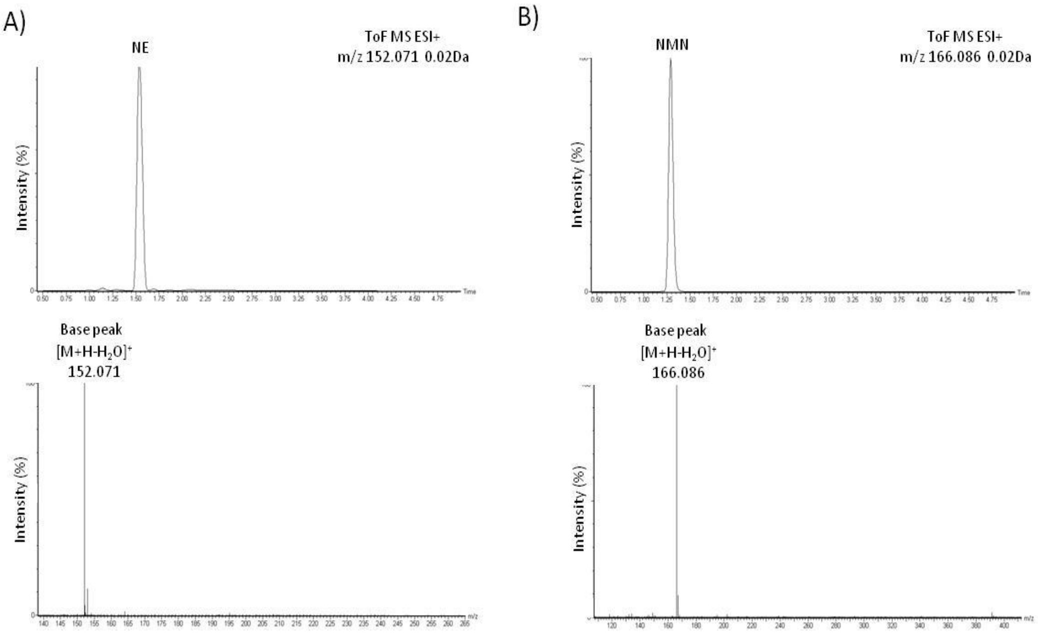

Figure 34. Representative chromatograms (up) and mass spectra (down) obtained from rat liver extract spiked with Norepinephrine (A) and Normetanephrine (B).

In all cases, after UPLC-MS optimization process, good chromatographic separation of the analytes was achieved as well as excellent mass spectrometric response.

6.2.7.1.3. Solid-Phase Extraction (SPE) Method development

SPE method selection

In this case, given the nature of the products of the COMT activity reaction, it was chosen ion exchange SPE to clean the samples before UPLC-MS analysis. Thus, cationic compounds were isolated by using WCX bonded silica cartridges. The retention mechanism is a mix of ion exchange and reversed phase, which improves retention of basic analytes, having especial selectivity and sensitivity for strong bases. The retention is based mainly on the electrostatic attraction of the charged functional group on the compound to the charged group that is bonded to the silica surface [193] **(Figure 35).**

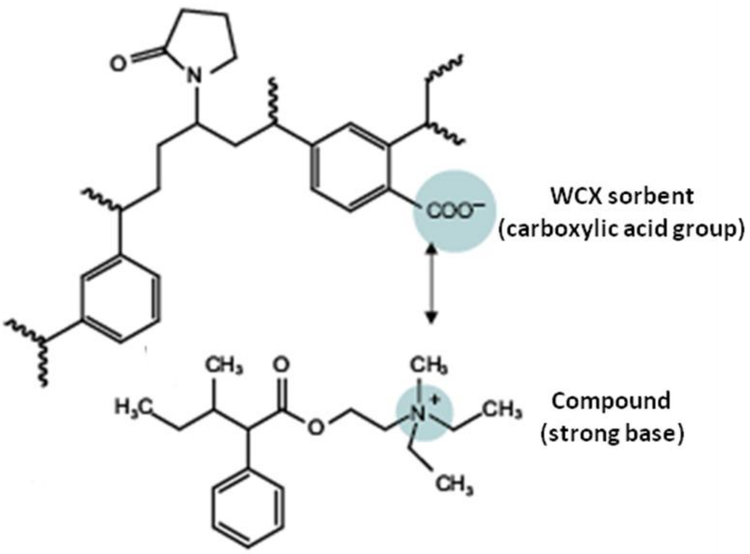

Figure 35. Oasis WCX retention mechanism for strong bases. The retention is based mainly on the electrostatic attraction of the charged functional group on the compound to the charged group that is bonded to the silica surface.

The WCX SPE material contains an aliphatic carboxylic acid group that is bonded to the silica surface. The carboxylic acid group is a weak anion and will isolate cations, as 3-MT and NMN, when both are charged. A solution having a pH that neutralizes either, the compound's functional group (3-MT or NMN) and the functional group on the sorbent surface, is used to elute the compounds of interest. Highly selective retention enables much stronger washes, resulting in very clear extracts. When one of these functional groups is neutralized, the electrostatic force that binds the two together is disrupted and the compound is eluted. An acidic solution was used to elute the analytes of interest. At low pH, the sorbent is un-ionized, which shuts off the ion-exchange mechanism [152].

Recovery Analysis

With respect to recoveries, they were determined from the ratio of test solutions B/C, being B the compound of interest added to the matrix before extraction and C the same amount of compound added to the matrix after the extraction **(see Figure 8)**.

The Recovery was calculated as follows:

$$\text{Recovery (\%)} = \frac{\text{Rat liver extract spiked with 3-MT/NMN before SPE (Pre-spiked sample)}}{\text{Rat liver extract spiked before UPLC-MS (Post-spiked sample)}}$$

The recoveries determined at 2.5µM were 82% (for 3-MT) and 75% (for NMN). These recoveries were in the acceptable range for routine UPLC-MS analysis [187].

6.2.7.2. Analytical Method optimization

In order to quantify the amount of the product formed in the enzymatic reaction, it was required to consider the following parameters to obtain sensitive and specific determination of the enzymatic activity.

6.2.7.2.1. Specificity of the enzymatic assay

To evaluate the specificity and selectivity of the method, different controls were carried out as follows. In the case of 3-MT, rat liver extract was incubated in buffer **(Figure 36A)** where no product was detected indicating that no endogenous compound was present in the sample. Rat liver extract was also incubated with DA in absence of SAMe and $MgCl_2$ cofactors which are necessary for the reaction to happen. In this case, 3-MT was detected, indicating DA degradation during the incubation period **(Figure 36B)**. In order to calculate the amount of 3-MT obtained during the reaction, the amount of 3-MT detected in this control was subtracted from the total amount of product obtained. Finally 3-MT was incubated in buffer **(Figure 36C)**.

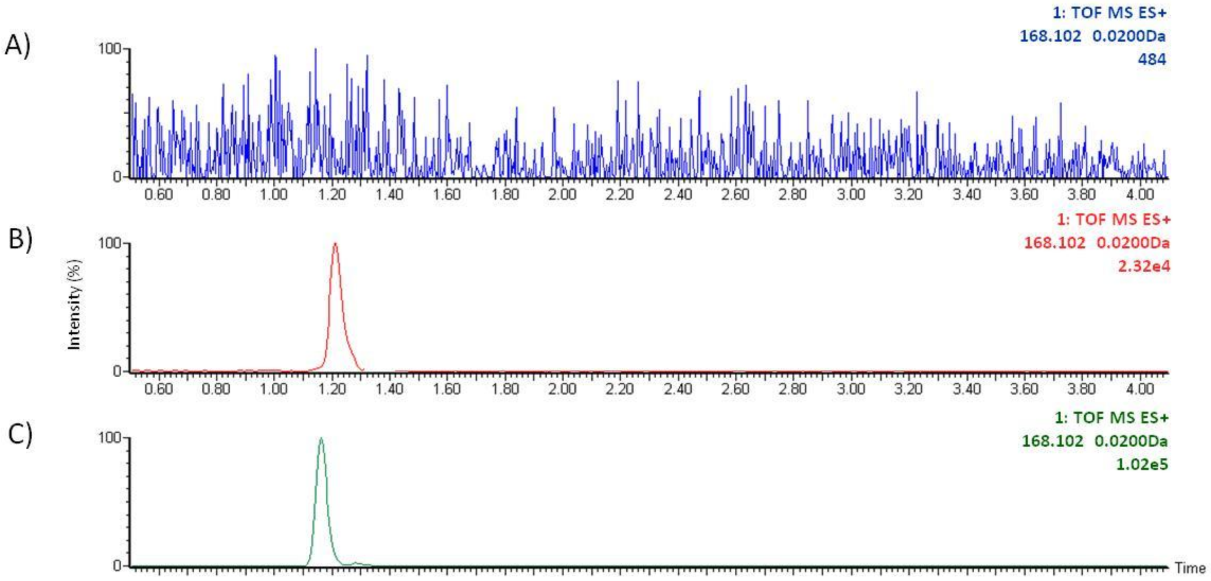

Figure 36. Chromatograms obtained for 3-Methoxytyramine (*m/z* 151.075, t_r 1.15) derived from: **(A)** Rat liver extract incubated in 50mM sodium phosphate buffer without adding DA, **(B)** rat liver extract incubated with Dopamine in absence of SAMe and $MgCl_2$, **(C)** 3-Methoxytyramine in 50mM sodium phosphate buffer.

Regarding NMN, the same controls as in the case of 3-MT, were performed. No endogenous product **(Figure 37, blue)** either NE degradation was detected **(Figure 37, red)**. Thus, no subtractions were needed from the controls. Rat liver spiked with NMN is also shown **(Figure 37, green).**

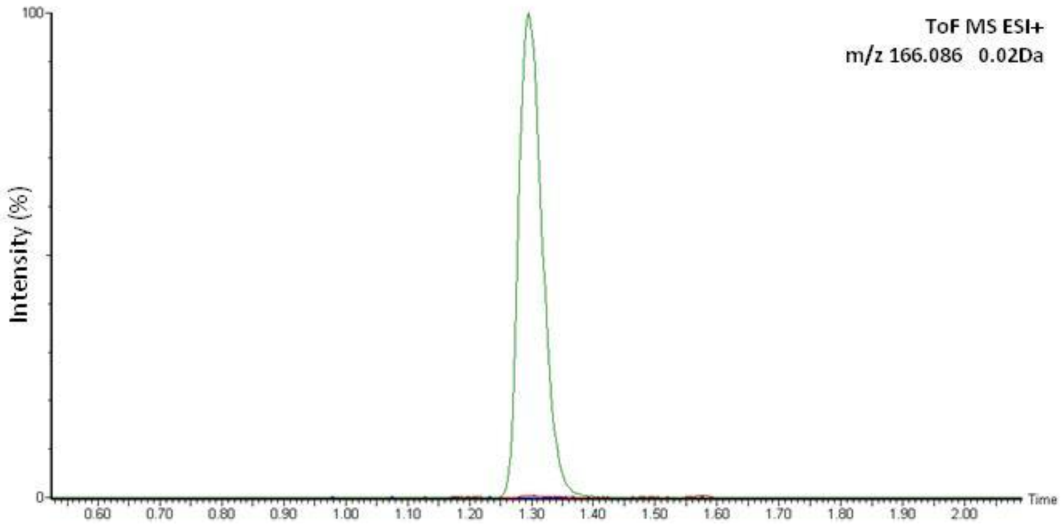

Figure 37. Superimposed chromatogram obtained for Normetanephrine (*m/z* 166.086, t_r 1.30) derived from: Rat liver extract incubated in 50mM sodium phosphate buffer (blue), rat liver extract incubated with Norepinephrine in absence of SAMe and $MgCl_2$ (red) and rat liver extract spiked with Normetanephrine (green). Note that the product NMN is detected only in the condition where the compound is spiked into the sample indicating that no endogenous and no degradation of the substrate is observed under assay conditions.

6.2.7.2.2. Linearity of Calibration Curves and Lower Limits of Quantification (LLOQ)

To calculate the absolute amount of 3-MT generated by COMT activity, the average of the two baseline signals was subtracted from the signals of the serially diluted calibration samples. In the case of NMN, this subtraction was not necessary since not endogenous product either NE degradation was detected. The calibration curves were obtained over the concentration ranges of 0.01-25 µM (for 3-MT) and 0.005-25 µM (for NMN).
Power fitting equation was used to determine the relation between the signal (peak area) and sample concentration:

3- MT: $[\text{Signal}] = 10411 \times [\text{concentration}]^{0{,}9238}$ ($R^2 > 0.99$)
NMN: $[\text{Signal}] = 1177 \times [\text{concentration}]^{0{,}8336}$ ($R^2 > 0.99$)

Once the sample concentrations were calculated, they were converted to amount (nmol) of 3-MT or NMN produced per mg of protein obtained in 1 h.

The developed UPLC-MS methods developed offered a LLOQ of 0.01 µM for 3-MT and 0.005 µM for NMN.

6.2.7.2.3. Precision and Accuracy of the enzymatic assay

Precision and accuracy were deemed to be acceptable (<15%).

Overall, after this comprehensive optimization of the parameters for incubation conditions, SPE and UPLC-MS analysis, sensitive and specific methods were successfully established for measuring COMT and MAT enzymatic activities. The final conditions established for the determination of the activities were:

For MAT activity: Enzymatic assays after optimization was carried out in a final volume of 250 µL of 50 mM HEPES/ 150mM KCl pH 8 incubation buffer containing; enzyme provider (liver extract, microsomes or EVs), 5 mM L-Methionine, 10 mM $MgCl_2$, 5 mM DTT, 5mM ATP and protease inhibitor. The reaction mixture was incubated for 2 hours in a water bath at 37°C. After incubation, samples were transferred to PBA bonded silica cartridges to clean them. Finally, samples were injected into UPLC-MS system; products of the reactions were chromatographically separated with an Acquity UPLC BEH AMIDE column and detected with a SYNAPT HDMS G2 Time of Flight (ToF) mass spectrometer operated in ESI+.

For COMT activity: Enzymatic assay after optimization was carried out in final volume of 300 µL of 50 mM sodium phosphate buffer pH 7.4 incubation buffer containing: enzyme provider (liver extract, microsomes or EVs), 2 mM $MgCl_2$, 200 µM SAMe and 2 mM DA or 0.1 mM NE. The reaction mixture was incubated for 1 hour in a water bath at 37°C. After incubation, samples were transferred to WCX bonded silica cartridges to clean them. Finally, samples were injected into UPLC-MS system; products of the reactions were chromatographically separated with an Acquity UPLC BEH AMIDE column and detected with a SYNAPT HDMS G2 Time of Flight (ToF) mass spectrometer operated in ESI+.

MAT AND COMT ENZYMATIC ACTIVITIES ANALYSIS IN HEPATIC EVs

The UPLC-MS based methods established above were used to analyze COMT and MAT activities in hepatic EVs in different DILI models. Moreover, it was also employed to compare hepatic EVs activities with the activities produced by microsomal (intracellular) preparations and liver extracts. In order to be able of correlating abundance of enzyme and measured activity, protein extracts of each type of sample was analyzed by Western-blotting **(Figure 38).** As can be observed, EVs markers (LIMP II, Hsp90) were detected in preparations. On the contrary, endoplasmic reticulum (Grp78) and mitochondria (COXIV) markers were not detected in EVs preparations supporting that they were not produced by undesired cellular lysis. Finally, we also detect the presence of the studied enzymes (CES, COMT and MAT) in the EVs preparations **(Figure 38).**

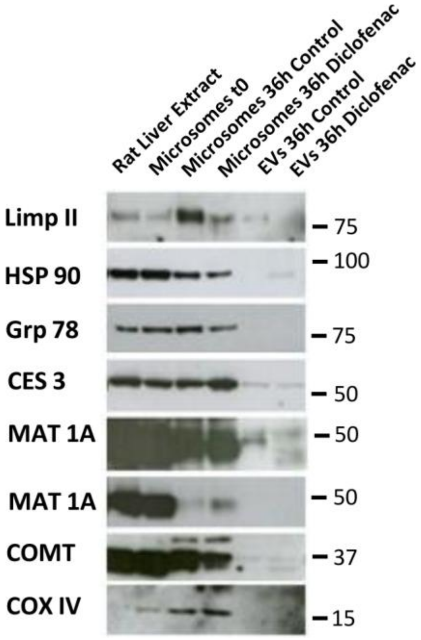

Figure 38. Western-blot analysis of samples employed for measuring MAT and COMT enzymatic activity. Liver extract, microsomes and EVs released by non-treated and DFC-treated rat hepatocytes were analyzed by Western blotting using antibodies against the indicated proteins. The amount of protein was determined by Bradford assay and same amount of protein was loaded in all cases (10 µg)

6.2.8. MAT ENZYMATIC ACTIVITY ANALYSIS IN HEPATIC EVs

MAT activity was measured by UPLC-MS in rat liver extract, microsomes obtained from hepatocytes previous to seed into collagen-coated dishes (t0) or after 36 hours cultivated in the dishes (t36) and finally in hepatic EVs. Obtained results are shown in **Table 5.**

Table 5. MAT activity in liver extract, microsomes and EVs from primary hepatocytes. Microsomes obtained from hepatocytes just after the liver perfusion (t0) and after 36h of incubation on collagen coated dishes (t36) were assayed. The amount of product obtained is expressed in nmol per mg of protein and per hour. Total MAT activity was estimated as Σ Products (SAM and SAH). ND; Not detected.

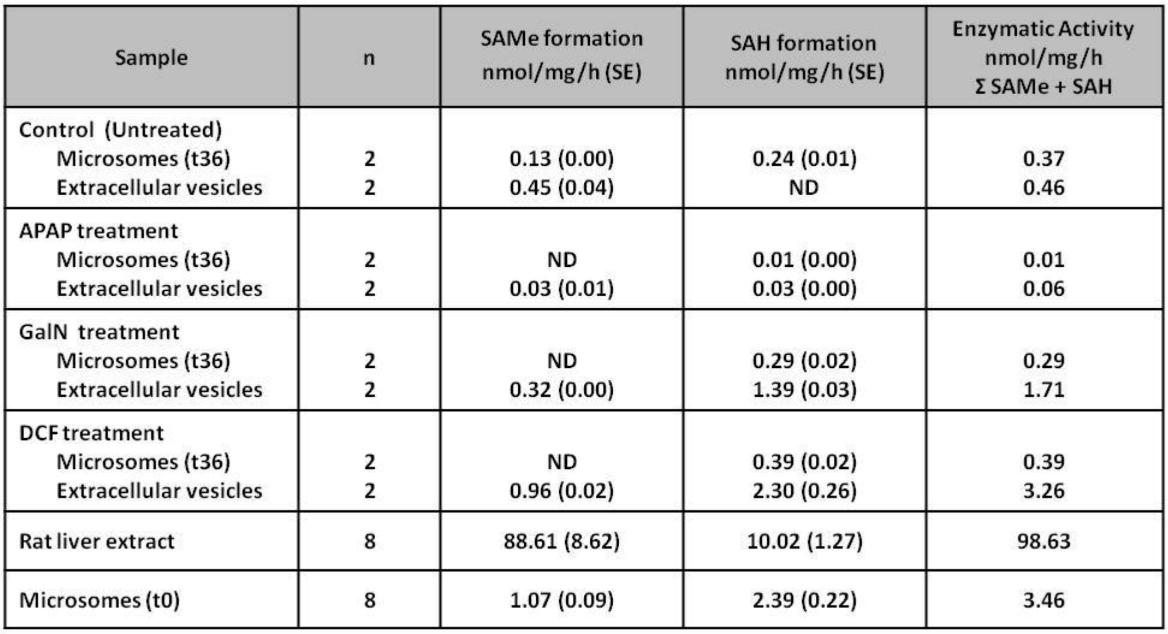

Sample	n	SAMe formation nmol/mg/h (SE)	SAH formation nmol/mg/h (SE)	Enzymatic Activity nmol/mg/h Σ SAMe + SAH
Control (Untreated)				
Microsomes (t36)	2	0.13 (0.00)	0.24 (0.01)	0.37
Extracellular vesicles	2	0.45 (0.04)	ND	0.46
APAP treatment				
Microsomes (t36)	2	ND	0.01 (0.00)	0.01
Extracellular vesicles	2	0.03 (0.01)	0.03 (0.00)	0.06
GalN treatment				
Microsomes (t36)	2	ND	0.29 (0.02)	0.29
Extracellular vesicles	2	0.32 (0.00)	1.39 (0.03)	1.71
DCF treatment				
Microsomes (t36)	2	ND	0.39 (0.02)	0.39
Extracellular vesicles	2	0.96 (0.02)	2.30 (0.26)	3.26
Rat liver extract	8	88.61 (8.62)	10.02 (1.27)	98.63
Microsomes (t0)	8	1.07 (0.09)	2.39 (0.22)	3.46

First, it was analyzed MAT activity in liver extracts **(Table 5, Figure 39)** comparing the amount of SAMe and SAH detected when the reaction was incubated for 2 h at 37ºC **(Figure 39, in red)** and without incubation **(Figure 39, in green).** As can be observed under enzymatic conditions employed in the study, there was very low amount of endogenous SAMe and SAH indicating that most of the detected products were newly formed by MAT enzymatic activity present in liver extract. Indeed, the products increased more than 44 (SAMe) and 156-fold (SAH) due to this activity **(Figure 39).**

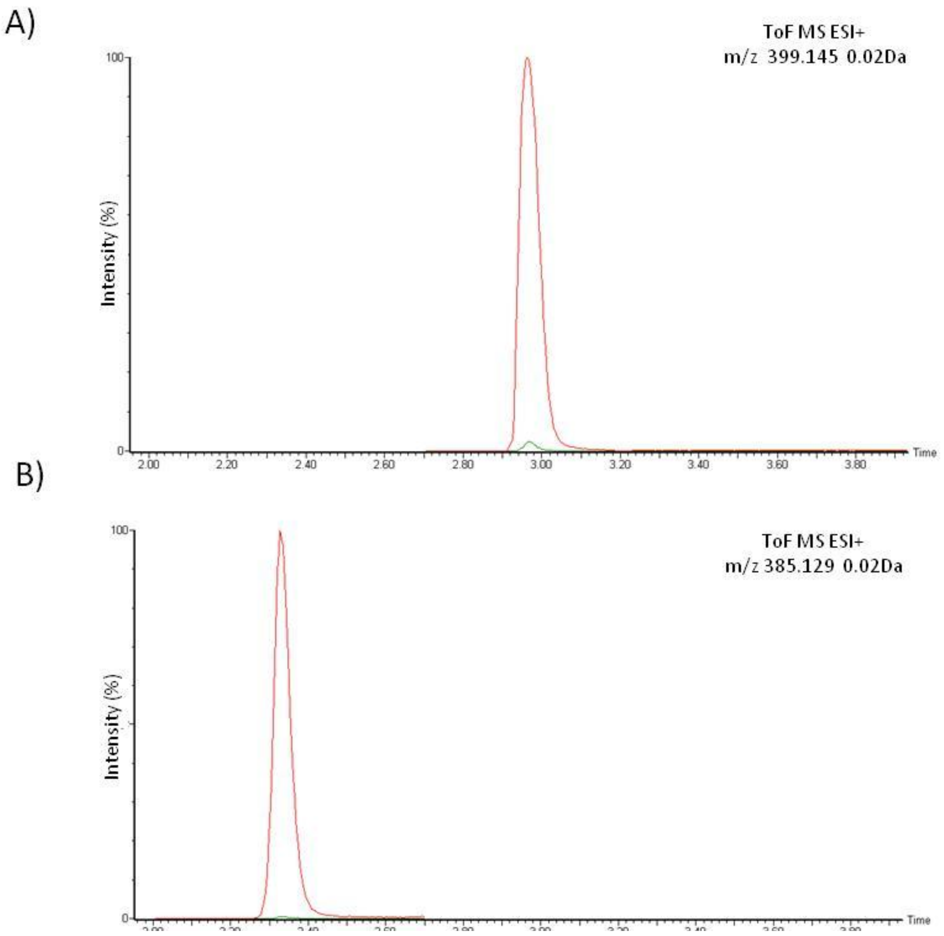

Figure 39. Chromatograms of SAMe and SAH generated by MAT enzymatic activity in liver extract. (A) SAMe coming from enzymatic reaction (87.78 µM, in red) and endogenous SAMe (2.85 µM, in green). **(B)** SAH coming from enzymatic reaction (12.51µM, in red) and endogenous SAH (0.08 µM, in green). The concentrations of SAMe and SAH were determined based on calibration curve.

MAT activity was also detected in microsomes prepared from hepatocytes **(Figure 40, Table 5)**. The comparison of liver extract and *microsomes t0*, revealed that MAT activity decreased notably in the later, however, protein expression levels remain very similar **(Figure 38).** This result suggests that during perfusion of the liver there is some inactivation of MAT activity by an unknown mechanism at this time. Furthermore, there was also a decrease in MAT activity in microsomes prepared from hepatocytes cultivated for 36 hours in comparison with MAT activity detected in microsomes prepared from hepatocytes just obtained after perfusion, *microsomes t0* **(Table 5).** This activity decrease correlates with a decrease in protein expression level observed by Western (**see Figure 38**).

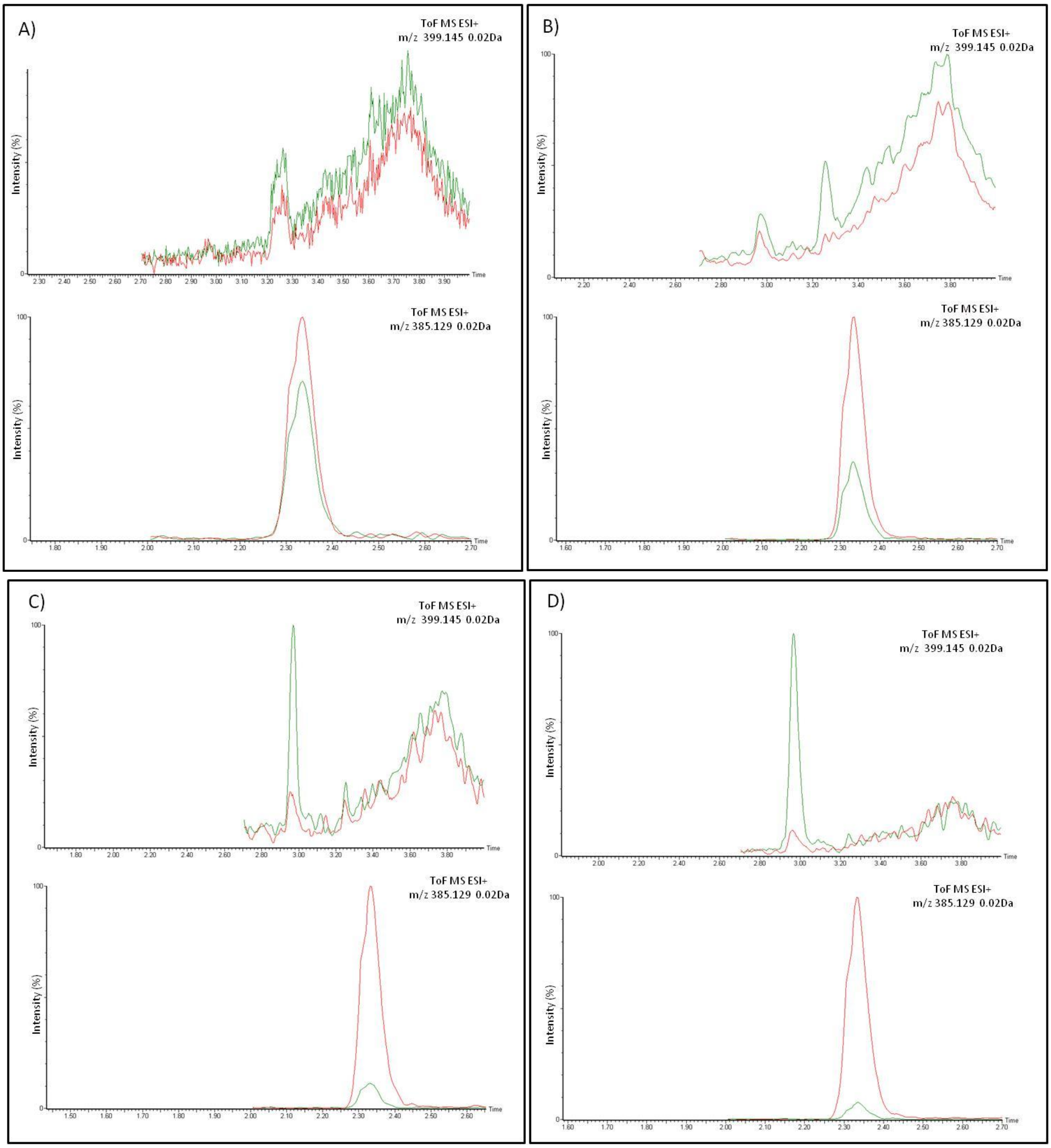

Figure 40. MAT activity in microsomes prepared from untreated and drug-treated primary hepatocytes. Superimposed chromatograms showing the amount of products obtained (SAMe in the top and SAH in the bottom) with (in red) or without incubation (in green) in microsomes prepared from: **(A)** untreated hepatocytes (signal corresponding to 0.01 µM for SAMe and 0.02 µM for SAH), **(B)** APAP-treated hepatocytes (signals under limit of quantitation for both products), **(C)** GalN-treated hepatocytes (signal under limit of quantitation for SAMe, and corresponding to 0.164 µM for SAH) and **(D)** DCF-treated hepatocytes (signal under limit of quantitation for SAMe and corresponding to 0.308 µM for SAH).

In the case of EVs, MAT activity was clearly detected in EVs preparations obtained from DCF and GalN-treated hepatocytes, whereas a minimal activity was quantified in the case of untreated and APAP-treated hepatocytes **(Figure 41, Table 5**). In order to confirm if the amount of detected products came from the enzymatic reaction or were already present in the EVs preparation (endogenous), chromatograms after samples incubation **(Figure 41, in red)** or without incubating **(Figure 41, green)** were obtained**.** As can be observed in the case of EVs secreted by DCF and GalN-treated hepatocytes, the product is newly formed by the enzymatic reaction **(Figure 41C and Figure 41D)**. In the case of DCF, the products SAMe and SAH increases 28 and 30-fold, respectively. In the case of GalN treatment, the products SAMe and SAH increases 67 and 17-fold, respectively **(Table 5).** In the EVs obtained from untreated hepatocytes **(Figure 41A)** it was also possible to determine MAT activity although barely quantified (0.45 nmol/mg/h) due mostly to the low yield of EVs production in untreated conditions. EVs secreted by APAP-treated hepatocytes also showed low MAT activity (0.06 nmol/mg/h) **(Figure 41B, Table 5)**. However, in this case, the amount of EVs employed to test the enzymatic assay was not a limitation. Thus, the result suggests that APAP treatment reduce MAT activity in hepatocyte-secreted EVs in agreement with previous reports showing a decrease in intracellular MAT activity caused by APAP overdose [194].

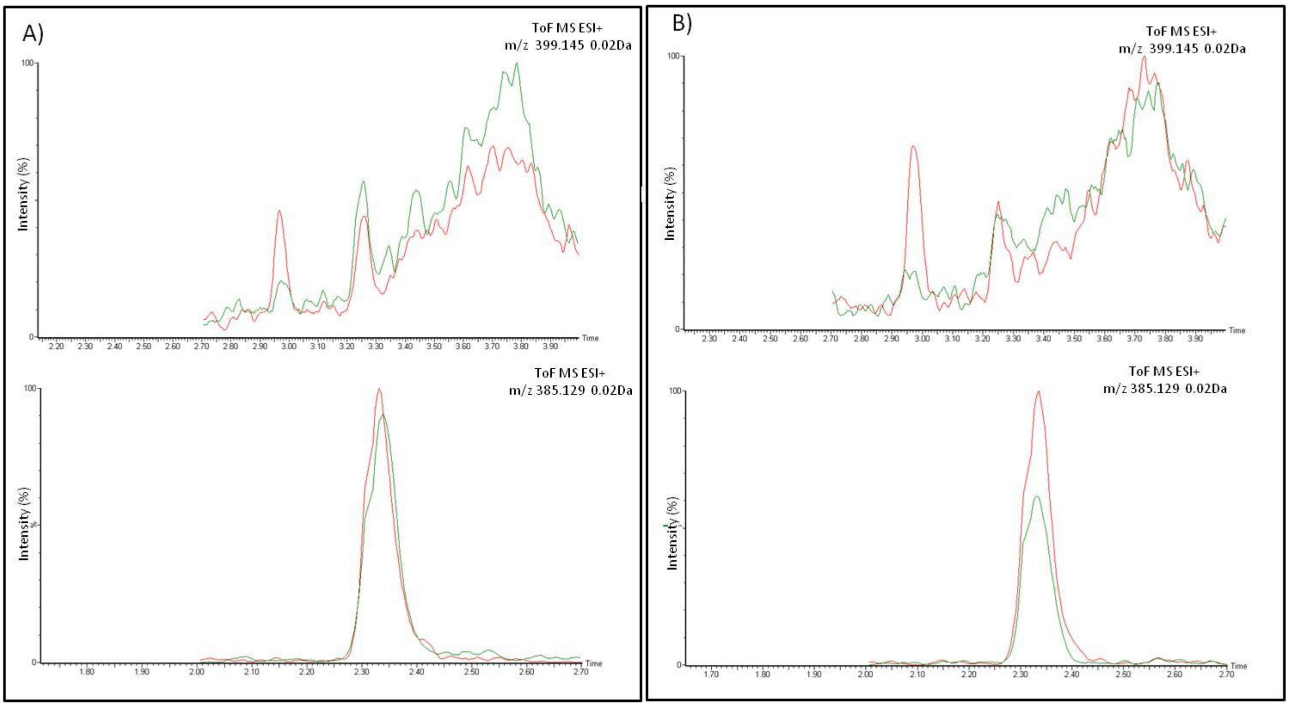

Figure 41. SAMe and SAH formed in EVs released by rat hepatocytes treated with different liver-damaging drugs. Superimposed chromatograms showing SAMe (top) and SAH (bottom) formed (in red) in EVs released by: (A) Non-treated hepatocytes (SAMe 0.039µM, SAH ND), (B) Acetaminophen-treated hepatocytes (SAMe 0.032µM, SAH 0.030µM), (C) Galactosamine-treated hepatocytes (SAMe 0.203µM, SAH 0.87µM) and (D) Diclofenac -treated hepatocytes (SAMe 0.770µM, SAH 1.84µM). Not incubated samples were used as endogenous controls (in green): (A) Non-treated hepatocytes (SAMe ND, SAH 0.06µM), (B) Acetaminophen-treated hepatocytes (SAMe 0.005µM, SAH 0.05µM), (C) Galactosamine-treated hepatocytes (SAMe 0.003µM, SAH 0.05µM) and (D) Diclofenac -treated hepatocytes (SAMe 0.027µM, SAH 0.06µM). Not incubated samples were used as endogenous control.

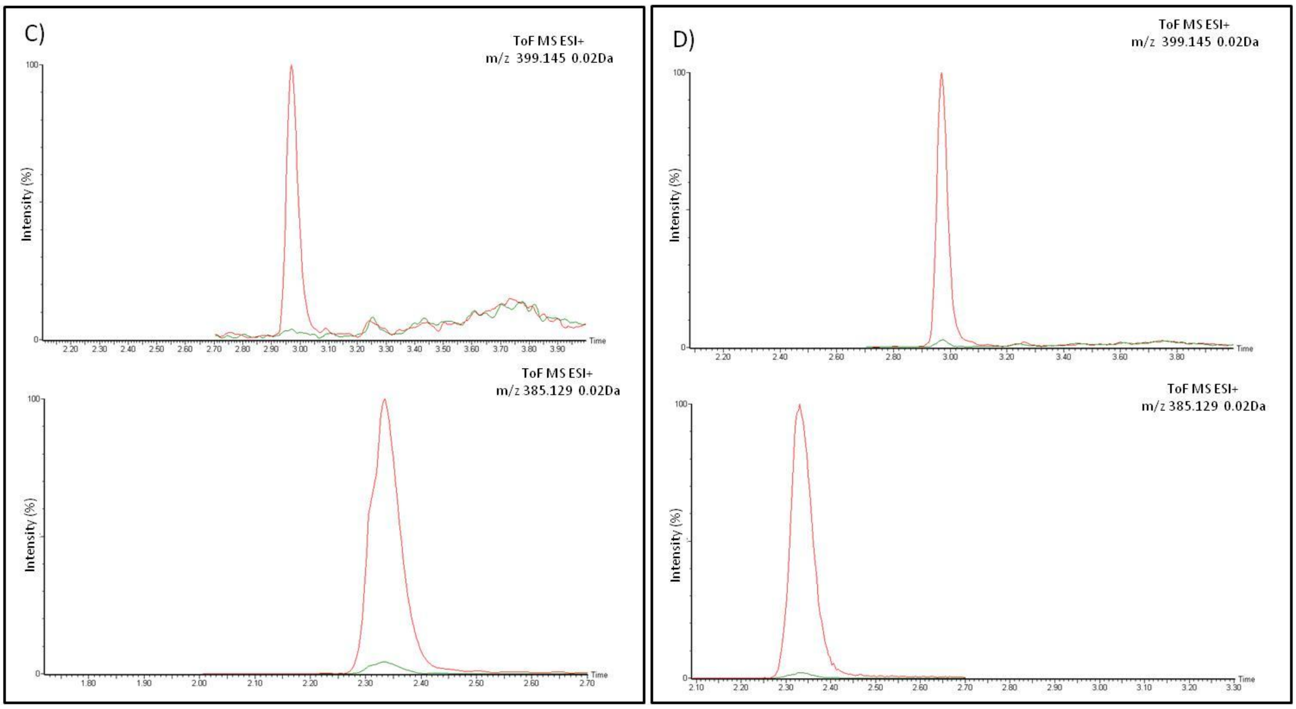

Figure 41 (continuation)

In summary, MAT activity was measured by UPLC-MS in rat liver extract, microsomes t0, microsomes t36 and hepatic EVs. As expected by the amount of protein observed in the Western-blot analysis **(Figure 38),** the highest activities were obtained in liver extract and microsomes t0 **(Table 5)**. MAT activity was significantly reduced in hepatocytes after 36h incubation in all the cases (microsomes t36, **Table 5**) suggesting that during the culture the hepatocytes get out of this enzymatic activity. Remarkably, MAT enzymatic activity was detected in hepatic EVs from untreated and drug-treated hepatocytes **(Table 5)** being significantly higher in GalN and DCF treatments. The comparison between enzymatic activity in microsomes t36 and EVs in the different treatments aroses different response to the treatments. Thus, in untreated conditions the activity was quite similar in microsomes (intracellular) and EVs whereas in GalN and DCF conditions MAT activity was much higher in EVs. Finally the activity obtained in APAP conditions was not significant neither in EVs nor in microsomes t36. These results indicated that intracellular retention or secretion of MAT activity is regulated depending on the mechanism of damage.

In conclusion, these results showed that MAT enzyme associated to hepatic EVs is active and this could have important implications in methionine metabolism.

6.2.9. COMT ENZYMATIC ACTIVITY ANALYSIS IN HEPATIC EVs

COMT activity was measured by UPLC-MS in rat liver extract, microsomes obtained from hepatocytes previous to seed into collagen-coated dishes (t0) or after 36 hours cultivated in the dishes (t36) and finally in hepatic EVs. Obtained results are shown in **Table 6.**

Table 6. COMT enzymatic activity in rat liver extract, microsomes and EVs. Amount of products obtained (3-MT and NMN) per mg of incubated protein in 1 hour incubation. ND; Not detected.

Sample	n	Enzymatic activity nmol/mg/hour (SE)	
		3-MT	NMN
Rat liver extract (Frozen)	3	119.42 (20.13)	106.03 (19.26)
Microsomes (t0)	3	78.80 (4.04)	109.98 (17.96)
Microsomes (t36) Control Microsomes (t36) Diclofenac	3 3	24.70 (0.36) 13.80 (0.03)	29.47 (0.58) 13.53 (1.01)
EVs(t36) Control EVs (t36) Diclofenac	3 (3-MT/ 1NMN) 4	0.27 (0.02) 0.32 (0.03)	0.05 1.12 (0.00)

COMT activity was measured by UPLC-MS in rat liver extract, microsomes t0, microsomes t36 and hepatic EVs. COMT activity was clearly detected in liver extract (**Figure 42,** in red). As can be observed, the activity was abrogated by the lack of two cofactors in the reaction, SAMe and $MgCl_2$ (**Figure 42,** green line) further supporting that detected activity was specific of COMT enzyme.

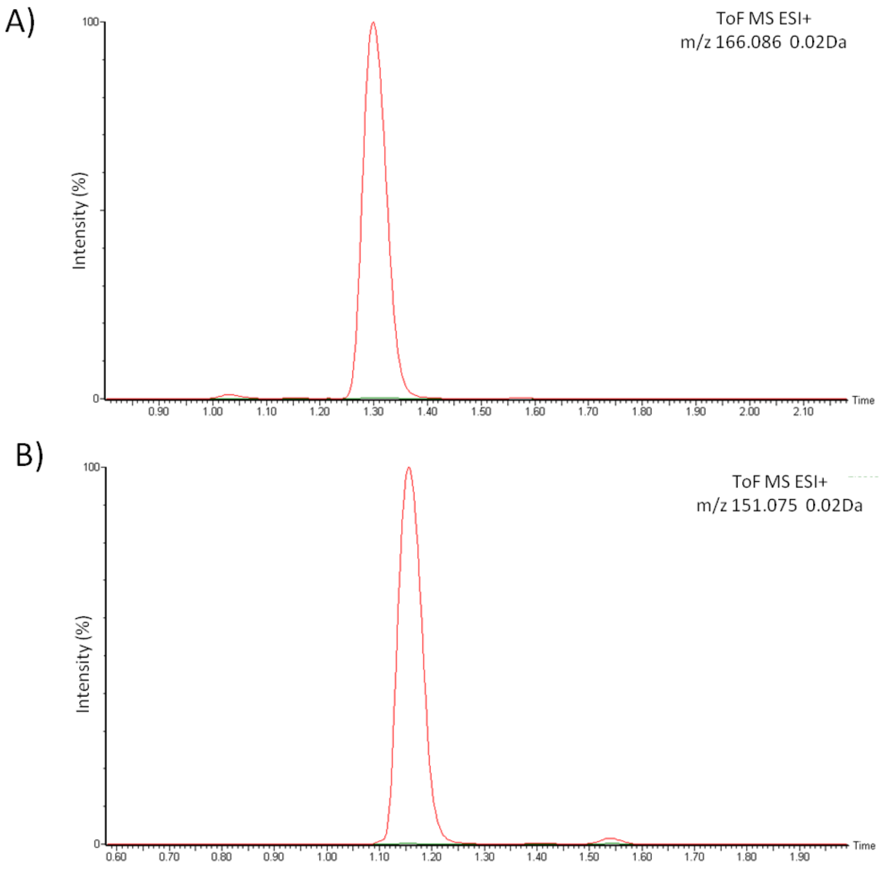

Figure 42. Chromatograms of the products, NMN or 3-MT of COMT activity in liver extract. Liver extract were incubated with (in red) or without (in green) SAMe and $MgCl_2$. **(A)** NMN product was detected with a signal corresponding to 13.03 µM in the mixture reaction containing all components, and to 0.01 µM in the mixture reaction lacking SAMe and $MgCl_2$. **(B)** 3-MT product was detected with a signal corresponding to 16.02 µM in the mixture reaction containing all components, and to 0.01 µM in the mixture reaction lacking SAMe and $MgCl_2$.

Hepatic microsomes also showed detectable levels of COMT activity. Significant differences were observed between microsomes prepared from untreated and treated hepatocytes **(Figure 43, Table 6)** showing lower activity in microsomes from DCF conditions. These results were in concordance with the immunostaining **(see Figure 11)** that showed a decrease in COMT protein expression in DCF-treated hepatocytes with respect to untreated cells indicating that hepatic COMT activity is altered in DILI. Furthermore, there was significant difference in COMT activity between microsomes t0 and microsomes t36 **(Figure 44, Table 6).** In this regard, a comparison of the activity measured in microsomes t0 and microsomes t36 showed a clear COMT activity decrease within time for both products NMN (**Figure 44A)** and 3-MT **(Figure 44B).** This result also correlates with a decrease in COMT protein expression observed by Western blotting **(see Figure 38).**

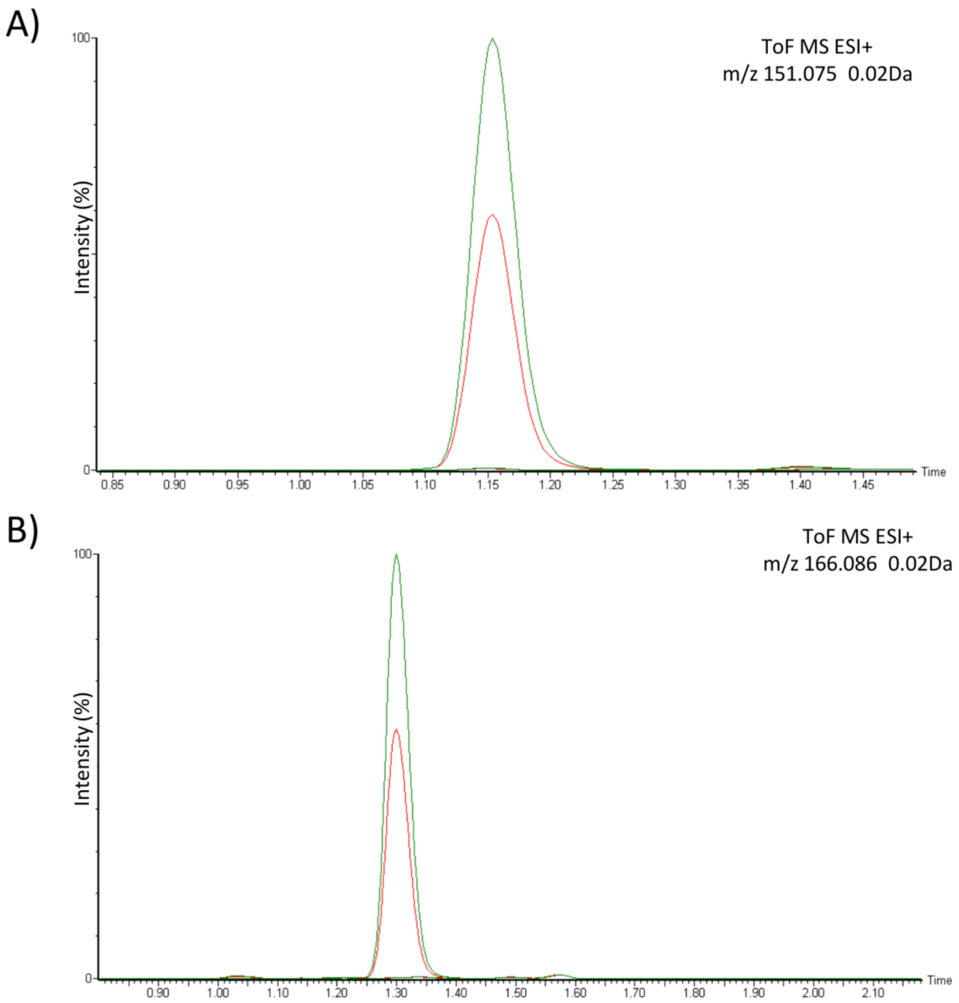

Figure 43. COMT enzymatic activity in hepatic microsomes from untreated and DCF-treated hepatocytes. (A) Superimposed chromatograms showing the amount of 3-MT formed in microsomes. Amount of 3-MT obtained in the presence of *Microsomes Control t36* (the observed signal correspond to 2.81µM, green) and in the presence of *Microsomes Diclofenac t36* (1.60µM, red). The amount of 3-MT resulting from dopamine degradation was under LLOQ (slightly visible at the bottom of the chromatogram). **(B) Superimposed chromatograms showing the amount of NMN formed in microsomes**: *Microsomes Control t36* (3.07µM, green) and *Microsomes Diclofenac t36* (1.42µM, red). The amount of obtained product coming from Norepinephrine (substrate) degradation was under LLOQ (At the bottom of the chromatogram).

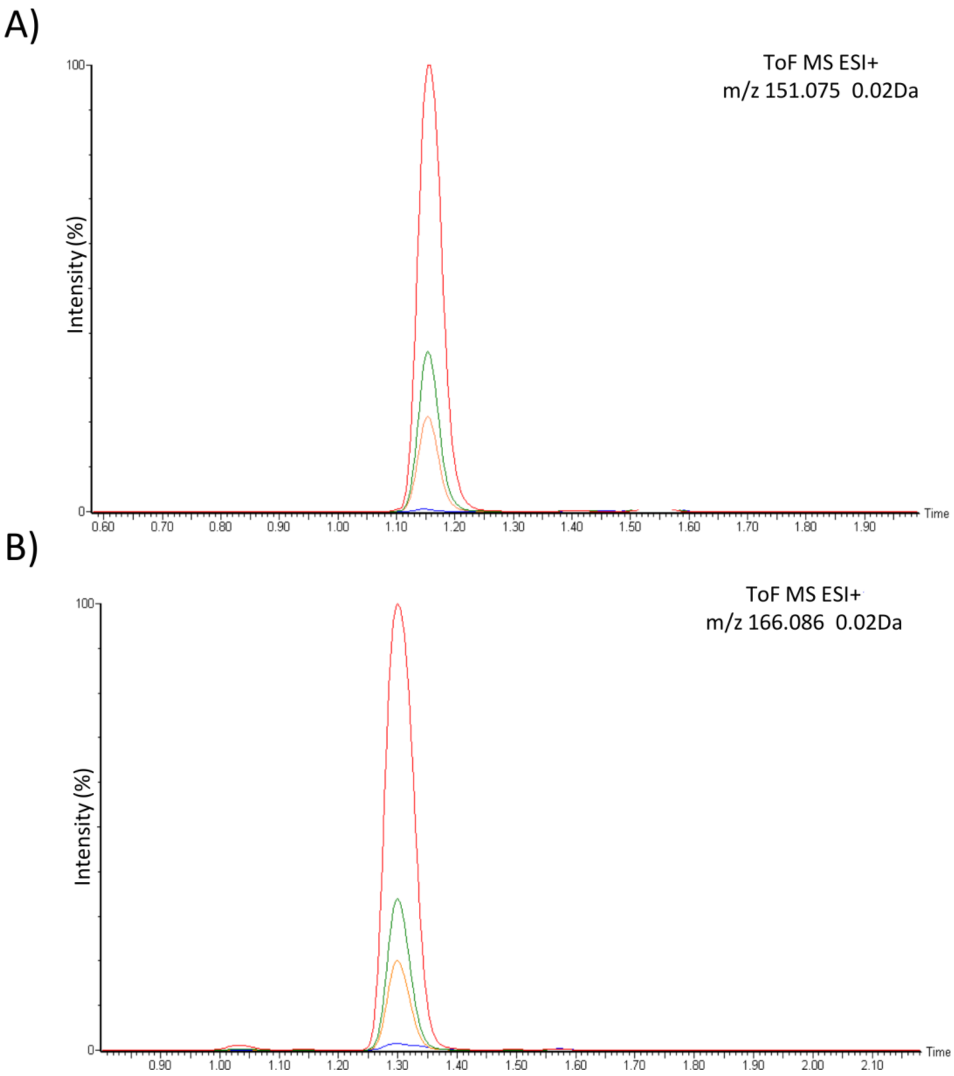

Figure 44. COMT enzymatic activity in hepatic microsomes and EVs (A) Superimposed chromatograms showing the amount of 3-MT formed in: *Microsomes t0* (9.41µM, red), *Microsomes Control t36* (2.81 µM, green), *Microsomes Diclofenac t36* (1.60 µM, yellow) and *EVs Diclofenac* (0.03 µM, blue). **(B) Superimposed chromatograms showing the amount of NMN formed** in: *Microsomes t0* (13.30 µM, red), *Microsomes Control t36* (3.07 µM, green), *Microsomes Diclofenac t36* (1.42µM, yellow) and EVs Diclofenac (0.07 µM, blue).

Remarkably, hepatic EVs also showed COMT enzymatic activity. On this regard, as can be observed in the **Figure 45**, specific activity in *EVs* secreted from untreated hepatocytes using DA **(Figure 45A)** and NE **(Figure 45B)** as substrates was detected although it was quite low (0.27 and 0.05 nmol/mg/h respectively) **(Table 6).** Conversely to microsomes, in the case of EVs, the activity was higher in EVs secreted by DCF-treated hepatocytes compared to EVs secreted by untreated cells **(Table 6)**.

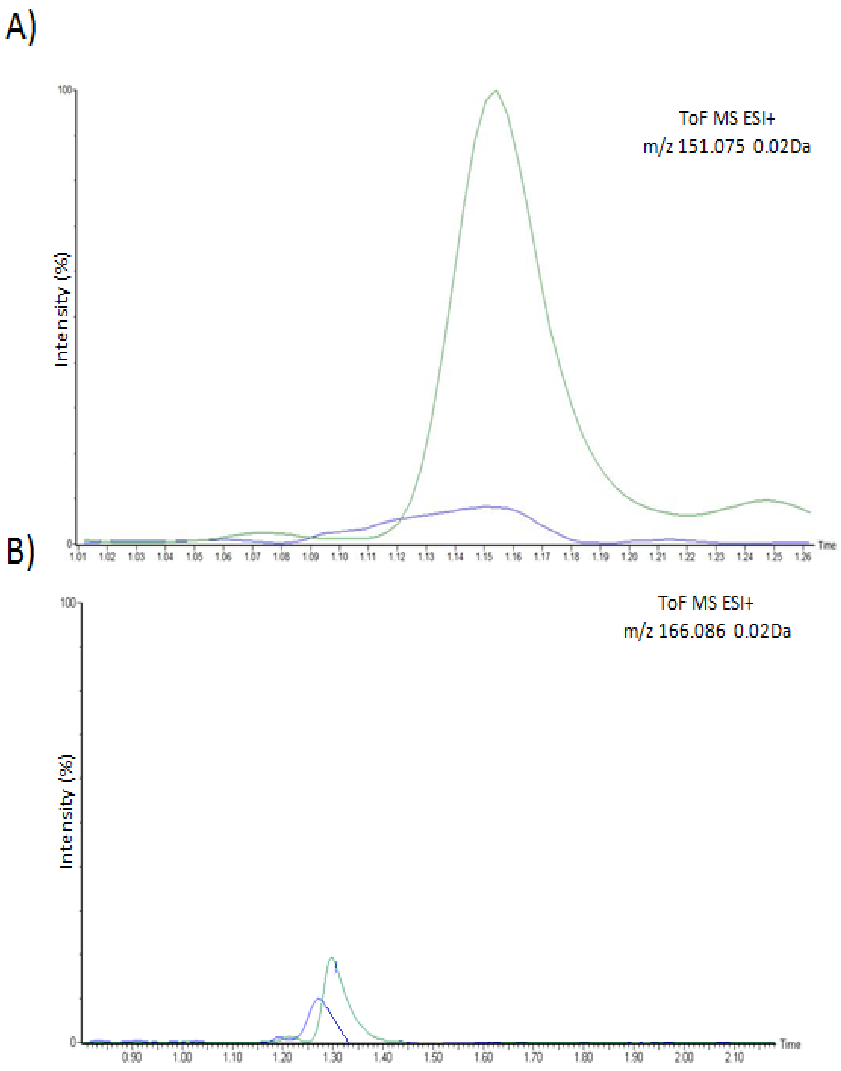

Figure 45. COMT enzymatic activity in hepatic EVs. (A) Superimposed chromatograms showing the amount of 3-MT formed in EVs released by non-treated rat hepatocytes cultured for 36h. Incubating: 30µg of EVs in the reaction mixture (0.02 µM, green) or 30µg of EVs in buffer (Not detectable, blue). **(B) Superimposed chromatograms showing the amount of NMN formed in EVs released by non-treated rat hepatocytes cultured for 36h.** Incubating: 30µg of EVs in the reaction mixture (0.0031, green) or 30 µg of EVs in buffer (Not detectable, blue).

As showed in **Figure 46,** there was dose-dependence COMT activity for both compounds DA **(Figure 46A)** and NE **(Figure 46B).** Thus, when the amount of protein employed in the reaction was doubled from 50 to 100 µg, 5.6 (3-MT) and 6.6 (NMN) fold more products were obtained from DA and NE, respectively.

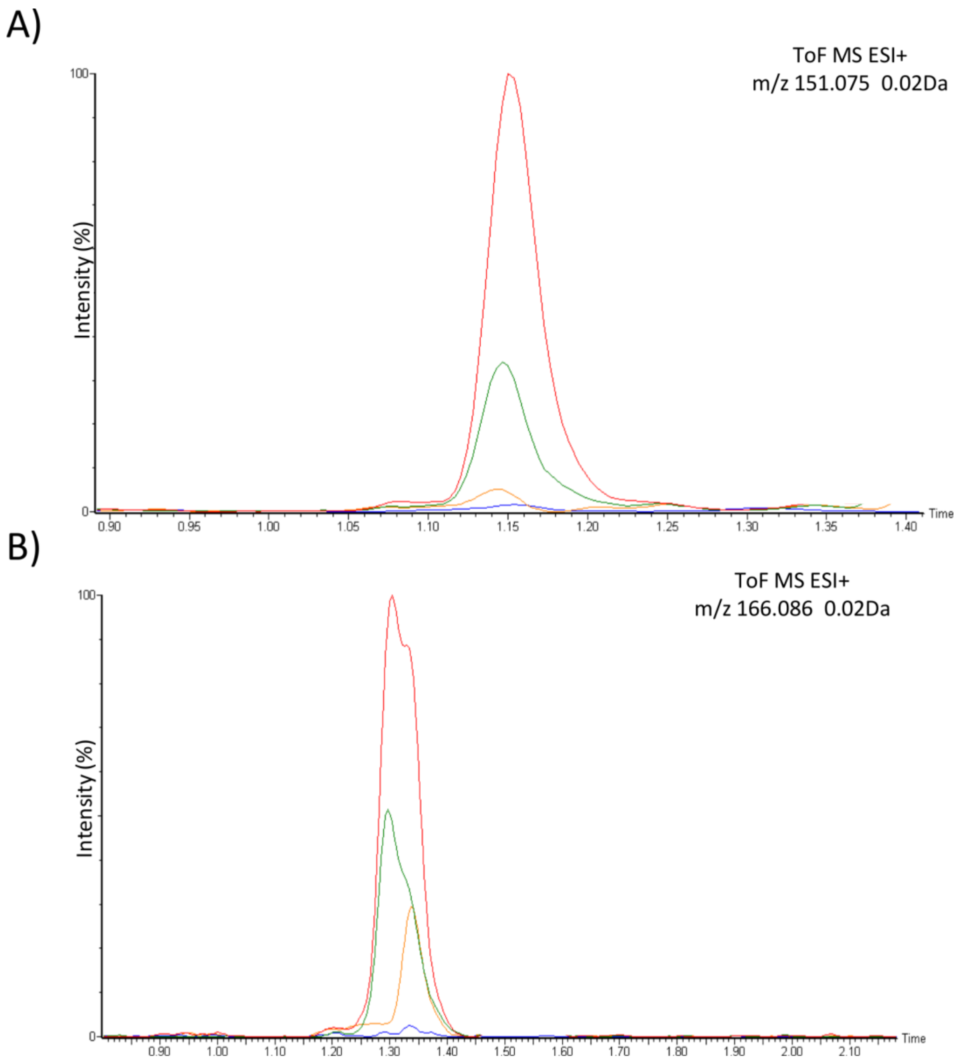

Figure 46. COMT enzymatic activity in hepatic EVs incubating different amounts of protein. (A) Superimposed chromatograms showing the amount of 3-MT formed in EVs secreted by primary hepatocytes cultured for 36h in the presence of DCF. Each peak represent different incubation reactions as follows: 100 µg (in red) or 50 µg (in green) of EVs in the reaction mixture, 50 µg of EVs with DA in absence of SAM and $MgCl_2$ (3-MT resulting from dopamine chemical degradation, under LLOQ, yellow) and 50 µg of EVs in buffer (endogenous 3-MT, under LLOQ, blue). **(B) Superimposed chromatograms showing the amount of NMN formed in EVs** secreted by rat hepatocytes cultured for 36h in the presence of DCF. Each peak represent different incubation reaction as follows, incubating: 100 µg (in red) or 50 µg (in green) of EVs in the reaction mixture, 50 µg of EVs with NE in absence of SAM and $MgCl_2$ (NE degradation, in yellow) and 50 µg of EVs in buffer (Endogenous NMN, under LLOQ, blue)

In summary, in all cases, COMT activity was detected **(Table 6)**. These results support the presence of active COMT enzyme in hepatic EVs, increasing its activity in DILI conditions.

Overall, employing fluorometric assay or UPLC-MS based metabolomics, significant changes in the activities of the studied enzymes, CES, MAT and COMT contained in hepatic EVs in DILI models were detected. These results also support the development of diagnosis methods based on these activities for DILI detection in a low-invasive manner.

6.3. METABOLIC PROFILING OF HEPATIC EVs

As shown in the previous sections, hepatic EVs are complex in composition containing several active metabolic enzymes supporting an important role in metabolism regulation in the extracellular space. Following this aim of elucidating the function of these hepatic EVs, UPLC-MS metabolomics was applied. It constitutes a powerful unbiased tool to identify metabolites associated with a determined biological system. The detection of these metabolites would identify additional metabolic pathways and functions where hepatic EVs could play a physiological role.

Metabolomics experiments must be carefully designed to ensure the reproducibility of the results. Thus, they must combine the appropriate use of analytical tools to allow the maximum coverage of the metabolome. In addition, due to the high heterogeneity of the metabolites (chemical structure, physicochemical properties and concentration), the process always has a certain degree of bias which is dependent on the metabolite selection and will occur from the metabolite extraction until its detection [136][195]. Thus, metabolomic approaches must apply adequate sample collection, handling, extraction, preparation and storage procedures to reduce these effects [196]. In the same way, the application of adequate tools to acquire, store, normalize, analyze and evaluate the data will be necessary in order to draw accurate conclusions. Recent advances in both, analytical and computational approaches, as well as the optimization of sample preparation protocols, have led to a wide coverage of the metabolome [137]. Since there are not studies reported on metabolomics applied to EVs, it was necessary to establish the conditions to apply this technology. Thus, for this section, we chose hepatic EVs released by MLP-29 murine cell line was choosen since they offer more flexibility and homogeneity that primary culture of hepatocytes. The metabolic profile of EVs secreted by this cell line is described using UPLC-MS based metabolomics in order to elucidate pathways and functions where these vesicles could be involved. Moreover, in this doctoral thesis it was also carried out a systematic characterization of metabolic signals detected and in some cases enriched in EVs when compared to the cellular content.

6.3.1. METABOLITES EXTRACTION METHOD SELECTION

Successful metabolome research requires effective metabolic extraction. Extraction is the process by which compounds, in this case metabolites, are selectively separated from other compounds, often undesired, such as proteins in this study [197].

For metabolic studies, it is important to perform an appropriate extraction method selection to choose that one that will extract the maximum number of metabolites in their original state. Given the metabolome complexity (metabolites of different chemical nature), there is not one unique extraction procedure for metabolome analysis that will cover all metabolites so different extraction protocols must be tested. In metabolome studies, metabolites are usually extracted with organic solvents, being frequent the use of more than one solvent in the extraction procedure [198]. In this study, due to the limiting amount of EVs sample, extraction method evaluation was only performed in cells. The following metabolites extraction protocols were tested for UPLC-MS based untargeted metabolic analysis:

- *MeOH/Water (50:50, v/v):* Methanol and water are miscible within each other and able to dissolve polar compounds. Methanol is usually used as aqueous phase co-solvent to enhance solubility of less polar metabolites.
- *MeOH/Water/Chloroform (25:25:50, v/v/v)*: Aqueous phase (methanol/water) is often paired with organic phase (chloroform) which are immiscible between them, forming a two phase system that allows the separation of polar (in the aqueous phase) and non-polar (in the organic phase) metabolites for subsequent chromatographic separation and analysis.
- *Isopropanol*: Same as Methanol, Isopropanol is also used as aqueous phase co-solvent to improve the solubility of less polar metabolites.

After cell lysis by sonication, the three extraction methods listed above were tested in triplicate. After metabolic extraction, the solvents were removed by centrifugation under vacuum condition and then solubilized in mobile phase and injected into UPLC-MS system to obtain the metabolic profile of each method.

In the **Figure 47** is shown the multivariate analysis (PCA) of the metabolic profiles corresponding to the different extraction methods analyzed in a C18 chromatographic column. A clear group clustering is observed due to the different metabolic profiles obtained for each extraction method. There are three clusters clearly separated: one related to metabolites extracted with Methanol/Water and Isopropanol methods. Both are very close in the PCA, given that they extract metabolites with very similar chemical nature (polar metabolites). Regarding MeOH/Water/Chloroform extraction method, two differentiated clusters are shown: one group correspond to the metabolites extracted in the organic phase (chloroform) and the other to metabolites extracted in the aqueous phase (MeOH/Water). Thus, apolar and polar metabolites are separated respectively.

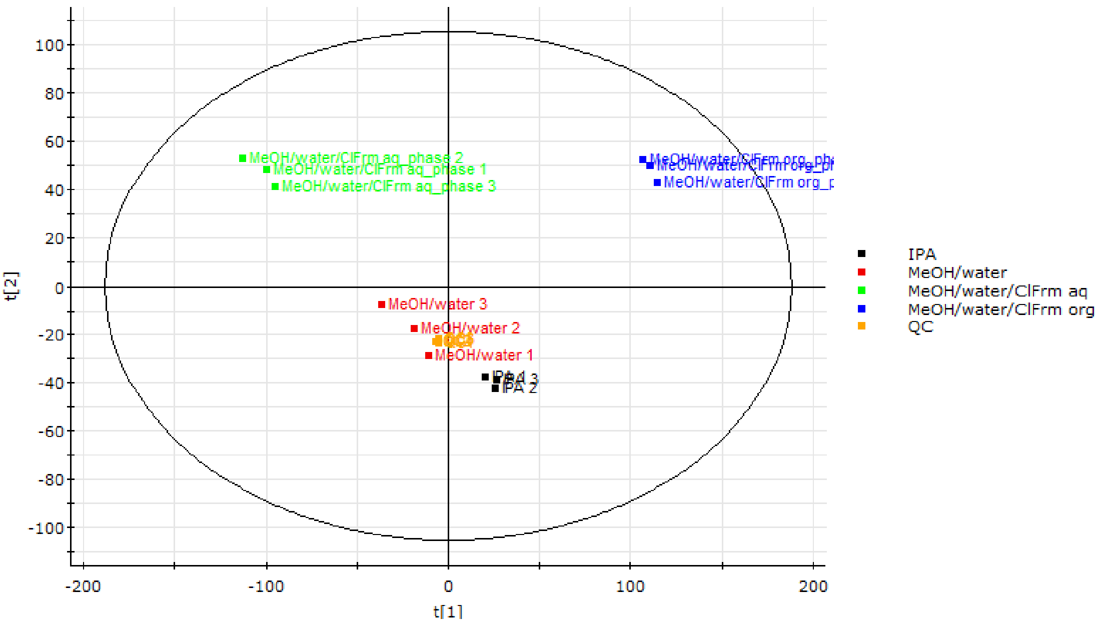

Figure 47. Principal Component Analysis (PCA) of the metabolic profiles obtained using different extraction methods. Three extraction methods were tested each of them in triplicated.: Methanol/Water (red), Isopropanol (IPA, black) and Methanol/Water/Chloroform (organic phase in blue and aqueous phase in green). Quality controls are also included (QCs, yellow). *t[1]* denotes sample type and *t[2])* intraclass variation.

Once metabolites were extracted, they were chromatographically separated using two different retention columns in order to cover the maximum number of metabolites: C18 enables the chromatographic separation of both polar and non-polar compounds and amide retains very polar compounds. In the **Table 7** is shown the number of metabolic signals detected using the different extraction methods combined with C18 or amide chromatographic columns. As can be deduced by the sum of the number of metabolites extracted in the aqueous phase (2459 signals in the amide column) and in the organic phase (1569 signals in the C18 column), Methanol/Water/Chloroform was clearly the most efficient extraction method.

Table 7. Number of metabolic signals in C18 and amide columns using different metabolites extraction methods. Note: methanol/Water/Chloroform extraction method obtains the highest number of extracted metabolites.

Extraction method	C18	Amide
Isopropanol (IPA)	**1734**	**2955**
Methanol/Water	**1848**	**2947**
Methanol/Water/Chloroform: Aquous Phase	**1654**	**2459**
Methanol/Water/Chloroform: Organic Phase	**1569**	**2530**

In conclusion, MeOH/Water/Chloroform showed to be the most effective extraction method, for both polar and non-polar compounds providing the highest number of metabolic signals.

6.3.2. ULTRA PERFORMANCE LIQUID CHROMATOGRAPHY – MASS SPECTROMETRY ANALYSIS

Because the metabolome is highly complex there is not a single detection/separation technique that covers the entire metabolome. The combined application of several different techniques is needed in order to enable a broad coverage of the metabolome (polar and non-polar metabolites). In this regard, in this study two separated chromatographic techniques coupled with MS were used to perform optimal metabolic separation. First, reversed-phase liquid chromatography-MS (RP-UPLC/MS) was employed using C18 column that results in the separation and detection of both polar and non-polar compounds [199]. As the capability of RP columns to retain ionic or highly-polar compounds is limited [200][201], an amide column was also used in the study which enables the chromatographic separation of very polar compounds.

The conditions of each chromatographic technique are detailed in section 5.17.3 of “Experimental procedures”.

6.3.3. DATA PROCESSING

In contrast to targeted approaches (such as used in the previous section regarding enzymatic assays), untargeted UPLC-MS-based metabolomics provides an enormous volume of data that cannot be manually analyzed, and is complicated even more due to experimental drifts in the instrumentation [135], [200]. Thus, before data analysis, MS spectra must be corrected for all variation caused by experimental variables adjusting different parameters. This is a critical part in data mining as it can drastically interfere with the next step, multivariate data analysis [202]. To overcome these issues, specific software that offers the possibility to adjust all these parameters are employed.

After metabolites extraction and injection in the UPLC-MS system, the generated data was processed using MassLynx 4.1 software that is a post-acquisition processing package that can be applied to MS data files. Both chromatographies (C18 and amide) and their corresponding mass spectrometry polarities (ESI+ and ESI- modes) were analyzed separately. The UPLC/MS data were peak-detected and noise reduced such that only true analytical peaks were further processed by the software. By doing this process, the metabolic background introduced during isolation and extraction processes were removed from the data in order to identify the metabolome truly associated with the samples of interest. A list of intensities (chromatographic peak areas) of the peaks detected was then generated, using the *Rt-m/z* (retention time and *m/z*) data pairs as identifiers (in a mass window of 0.02 Da and a RT window of 0.05 min).

In the **Table 8** is shown the total number of detected signals (cells and EVs) and also those ones present in EVs.

Table 8. Metabolic signals detected by UPLC-MS in MLP29 cells and their secreted EVs. Detected signals using two chromatographic columns (Amide and C18) and running the samples in positive and negative ion mode. Total number of detected signals (cells and EVs) as well as those ones present in EVs are indicated.

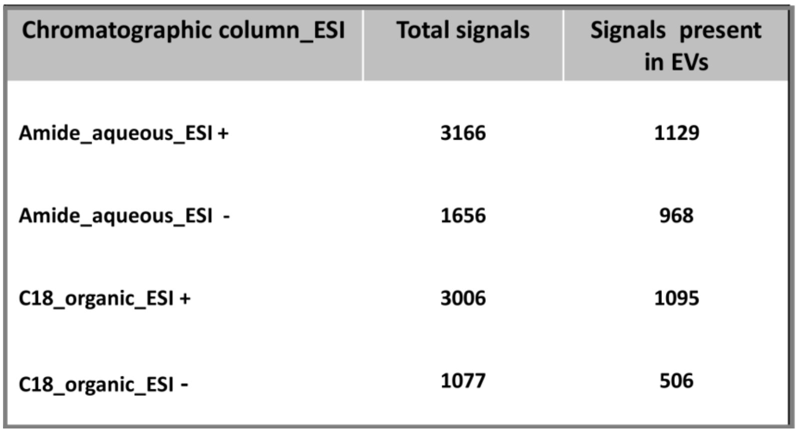

Chromatographic column_ESI	Total signals	Signals present in EVs
Amide_aqueous_ESI +	**3166**	**1129**
Amide_aqueous_ESI -	**1656**	**968**
C18_organic_ESI +	**3006**	**1095**
C18_organic_ESI -	**1077**	**506**

6.3.4. MULTIVARIATE DATA ANALYSIS: PRINCIPAL COMPONENT ANALYSIS (PCA)

The UPLC-MS data obtained by peak extraction and background reduction using MassLynx is now suitable for mathematical and statistical analyses in order to identify significant difference between sample groups. In this regard, multivariate data analysis is a statistical approach that facilitates the identification of differences or similarities between groups comparing the samples by statistical methods [203]. Its principal objective is to reduce the dimensionality of the complex data set to enable easy visualization of any metabolic clustering of the different groups of samples [137], in this case cells and EVs. This is achieved by PCA where the discrimination between samples is done based on their metabolic profiling without prior knowledge of sample classes. Basically, the data matrix is reduced to a series of principal components (PCs), each a linear combination of the original *Rt-m/z* pair peak areas [204].

After data processing, base peak chromatograms extracted in the organic (apolar dataset) and aqueous (polar dataset) phase, in ESI+ and ESI- mode, were obtained. In the **Figure 48** is observed the different chromatographic profiles obtained for cells and EVs, suggesting a variable metabolic content. In base peak chromatograms, is clearly observed the enrichment of some metabolic signals in EVs (in green) with respect to cells (in red) given the clear differences in peaks intensities between two sample groups.

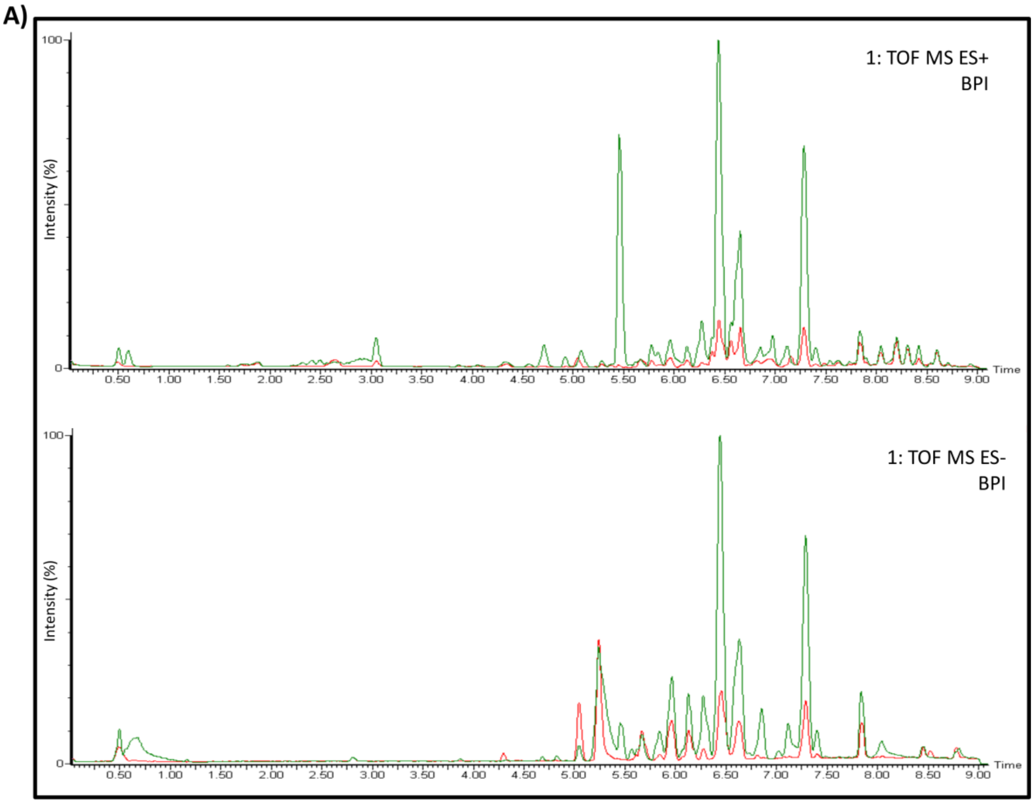

Figure 48. **Representative base peak chromatograms of UPLC-MS analysis of MLP29 cells and corresponding secreted EVs.** Base peak chromatograms of MLP29 cell line (in red) and secreted EVs (in green), extracted in organic (C18 column) **(A)** and aqueous (amide column) **(B)** phase and run in ESI+ (top) and ESI- (bottom) mode.

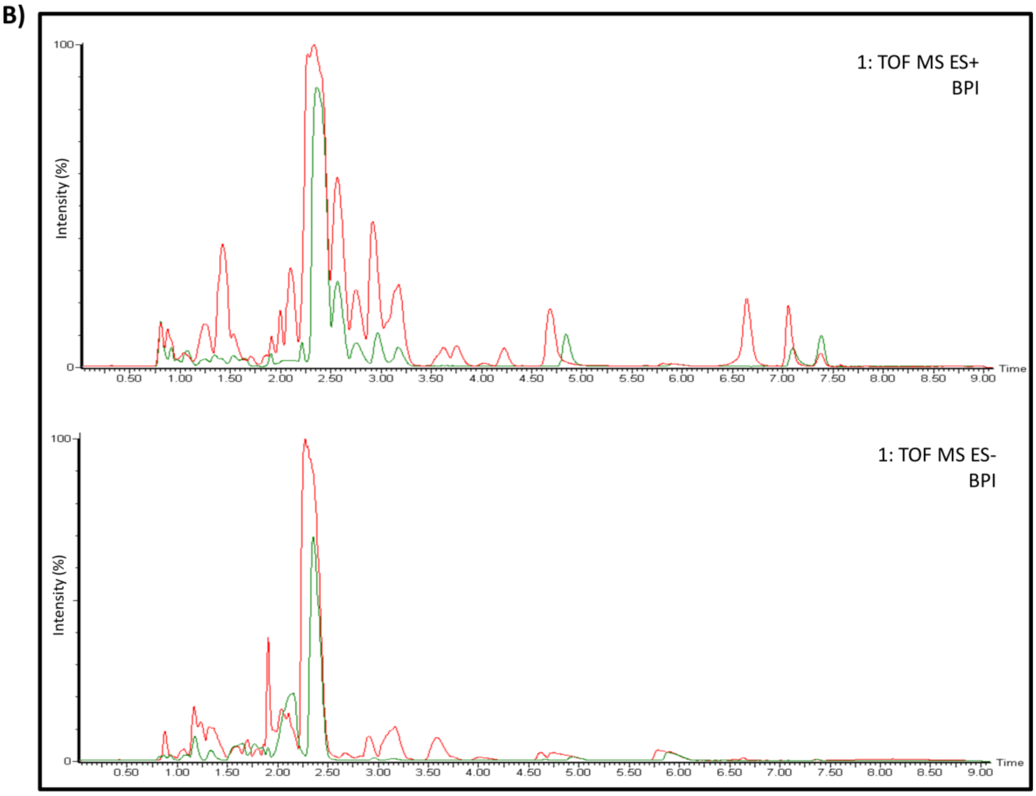

Figure 48 (continuation)

Moreover, apart from the base peak chromatograms, the *Rt*-mz signals were subjected to PCA to determine metabolic profile differences between cells and EVs. **Figure 49** shows the PCAs corresponding to MLP29 cells and their corresponding EVs samples for polar and apolar datasets run in ESI+ or ESI- ion mode. Polar dataset correspond to those metabolites extracted in the aqueous phase and apolar dataset to those ones extracted in the organic phase. The final dataset was mean centered and log-transformed during multivariate data analysis. As can be observed in the **Figure 49**, this analysis showed clear metabolic clustering that reveals metabolic profile differences between cells and EVs, which is in concordance with previously shown base peak chromatograms **(see Figure 48).** Metabolic profile differences are due to sample type which is given by the first principal component (*t[1]).* Second principal component (*t[2])*denotes intraclass variation which is very small in both cases, indicating good reproducibility.

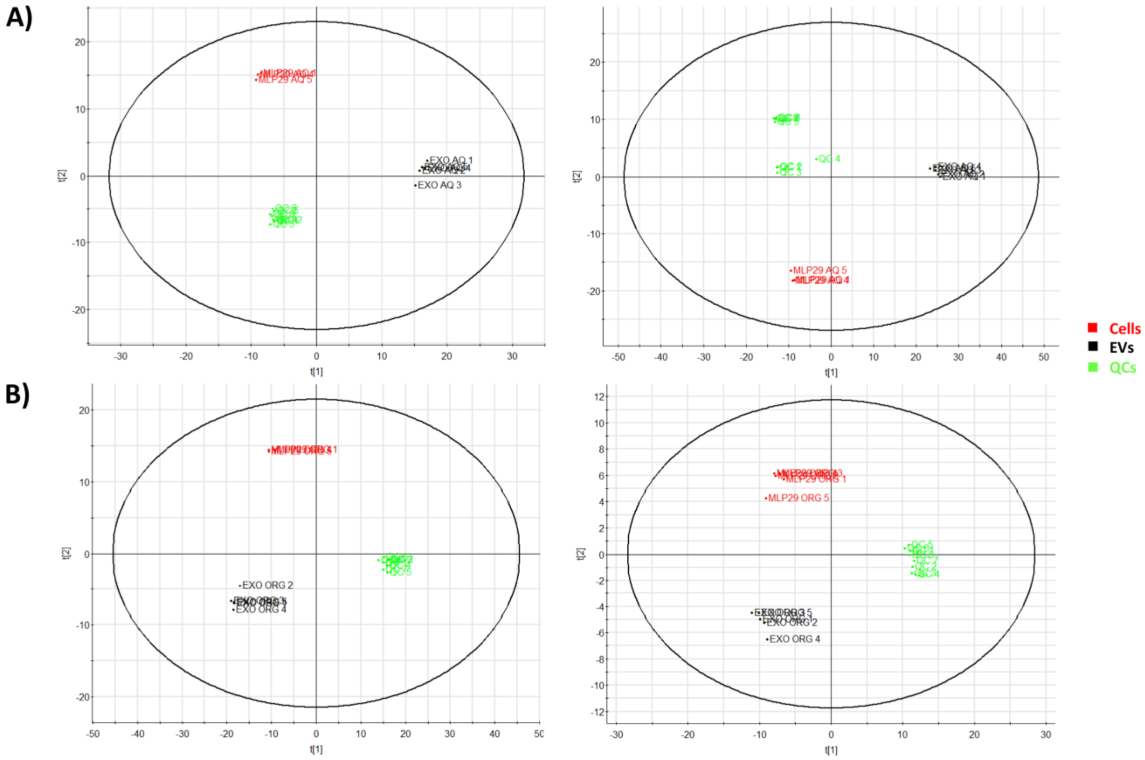

Figure 49. Principal component analysis of UPLC-MS data obtained from MLP29 cells and their corresponding secreted EVs. PCA of polar (A) and apolar (B) datasets run in positive (left) and negative (right) ion mode reveals metabolic profile differences between cells and EVs. The first two principal components (t[1] and t[2]), represent the most important metabolic variation in the samples captured by the analysis. t[1] denotes the contribution of a particular marker to the group differences and t[2] intraclass variation. A clear metabolic clustering between cells and EVs is shown which is translated in significant metabolic profile differences. Note that Quality Controls (QCs) are not in the center because they were made only with cells.

6.3.5. EVs METABOLIC PROFILING, METABOLIC SIGNAL SELECTION AND METABOLITE IDENTIFICATION

After multivariate analysis, next step was to detect on one side metabolic signals that are present in hepatic EVs (metabolome of EVs) and on the other side to detect metabolic signals that could be enriched in hepatic EVs. For this second aim, scatter plots representation obtained from the PCAs, what allows distinguishing the signals that discriminate the two sample groups, were used as a statistical tool. Finally, once obtained the list of metabolic signals forming EVs metabolome or the signals enriched in them, some metabolic signals were pre-selected for further identification. This latter step implicates elemental composition calculation together with database search (METLIN/HMDB) [205].

A robust metabolic profile (metabolome) of hepatic EVs was established among all the metabolic signals detected after noise reduction and removing the metabolic signals coming from tissue culture media [157] **(Figure 50)**. The applied selection criteria was as follows: all the metabolic signals must be present in all analyzed EVs samples (n=5) and their coefficient of variation (CV) must be < 20%. Overall, the number of metabolic signals detected in the EVs samples in amide (ESI+), C18 (ESI+) and C18 (ESI-) were 3166, 3006 and 1077, respectively. By applying the selection criteria, the number of metabolic signals was reduced to 224 (amide ESI+), 81 (C18 ESI+) and 37 (C18 ESI-) **(Table 9).** The metabolic signals extracted in aqueous phase analysed in negative ion mode were not considered given that CV was higher than 20% in all the cases. It is important to highlight that a metabolite can originate multiple metabolic signals. Thus, the number of metabolites represented in this metabolome (formed by 342 metabolic signals) is overestimated, until further identification of the signals is achieved.

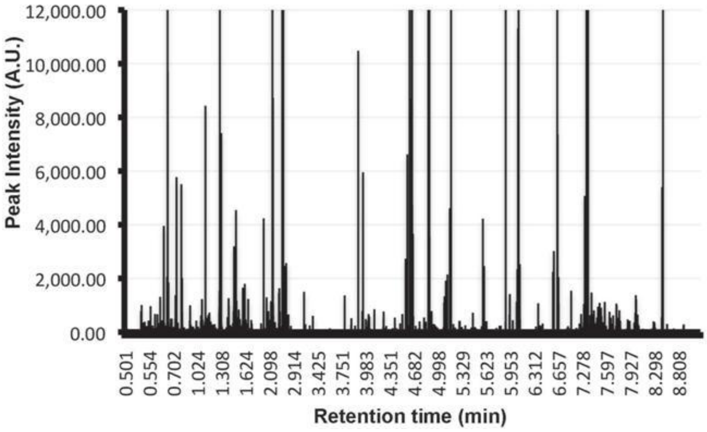

Figure 50. Metabolic background introduced by tissue culture media in EVs analysis. Metabolites were extracted using Chloroform:methanol from the pellet obtained by applying the conventional ultracentrifugation-based exosomal purification procedure to 300 ml of EVs-depleted complete media incubated at 37°C during 72h in absence of cells. Extracted metabolites were analyzed by UPLC-MS using a C18 chromatographic column. Retention time of the metabolites along with their peak intensities are indicated in the plots. Note the elevated number of metabolites of different chemical nature that are isolated using the EVs purification procedure and that need to be removed in order to determine the metabolome that is truly associated to EVs.

Table 9. The metabolome of EVs secreted by MLP-29 hepatic cell line. In this table are listed all the metabolic signals present in EVs once subtracted background noise and contaminants coming from culture media. The signals are ordered in increasing retention time (RT) and with their respective *m/z* value. All these metabolic signals are present in all EVs samples (n=5) and have a coefficient of variation (CV) < 20%.

Metabolic signals present in hepatic EVs				
Amide_ESI +	**Amide_ESI +**	**Amide_ESI +**	**C18_ESI +**	**C18_ESI -**
0.88_425.1392	1.45_451.2660	3.02_303.1779	0.58_277.1069	0.49_446.9074
0.92_468.3084	1.45_564.2747	3.03_184.0735	1.76_300.2040	0.49_604.8720
0.92_494.3240	1.46_129.0687	3.06_261.1634	2.09_282.1929	2.88_187.0975
0.92_892.4553	1.47_229.1190	3.08_416.2979	4.32_540.3351	5.04_239.1296
0.93_592.3338	1.47_291.0705	3.08_521.3194	4.56_522.3237	5.24_692.3842
0.93_756.3907	1.49_307.0444	3.09_129.1029	5.10_355.1115	5.26_497.2933
0.94_245.1860	1.50_158.8439	3.10_374.2144	5.25_383.3315	5.68_194.0823
0.94_279.1714	1.53_112.0533	3.10_408.2523	5.72_367.2471	5.82_450.2620
0.94_710.8664	1.55_248.0905	3.12_213.0988	5.84_266.6424	5.84_194.0827
0.96_232.1548	1.61_1089.4787	3.12_261.0898	5.94_367.2467	5.98_297.1534
1.00_516.3019	1.62_1173.4403	3.12_275.1724	6.27_267.6490	6.07_194.0821
1.01_297.1547	1.62_294.8445	3.12_290.1465	6.29_107.0724	6.16_194.0822
1.01_472.2759	1.63_248.0904	3.12_333.1873	6.31_308.2814	6.24_452.3133
1.02_275.1113	1.67_448.7408	3.14_257.1245	6.37_504.3079	6.25_443.3486
1.03_184.9807	1.67_532.7013	3.24_289.1622	6.40_246.6258	6.40_452.2785
1.07_202.1086	1.67_700.6267	3.31_168.0771	6.40_454.2933	6.40_520.2650
1.10_215.1396	1.67_702.6244	3.32_303.1777	6.40_476.2757	6.42_421.2803
1.15_335.1061	1.67_786.5878	3.33_584.3580	6.41_494.2903	6.44_1035.6603
1.16_296.1582	1.68_196.8574	3.37_116.0712	6.42_434.3391	6.44_608.3187
1.17_430.2658	1.81_122.0719	3.37_133.0977	6.42_949.6222	6.60_478.2935
1.17_452.2474	1.82_163.0982	3.45_239.1065	6.43_400.3432	6.60_546.2791
1.17_468.2076	1.87_214.0070	3.50_517.2859	6.44_1003.1501	6.63_634.3339
1.18_352.1838	1.88_606.7881	3.59_348.0712	6.44_1011.1448	6.65_526.3508
1.19_261.1452	2.18_275.1356	3.61_215.6495	6.44_1013.6511	6.66_301.1664
1.20_357.2134	2.19_102.0563	3.63_118.0871	6.44_276.6343	6.66_522.2827
1.22_326.1701	2.19_120.0664	3.75_211.0852	6.44_297.1491	6.83_466.2954
1.22_375.2245	2.19_402.2457	3.78_118.0871	6.44_478.3301	6.86_554.3457
1.22_397.2044	2.20_242.6425	3.84_402.2824	6.44_515.3137	7.08_480.3436
1.22_495.2536	2.21_175.1197	3.85_206.1030	6.44_524.2980	7.09_480.3101
1.23_213.1242	2.21_188.1762	3.97_304.0168	6.44_534.2951	7.25_480.3087
1.23_438.2318	2.21_364.2079	4.20_328.2844	6.46_425.3750	7.25_548.2962
1.24_260.1598	2.22_249.1087	4.22_484.1184	6.48_447.3563	7.29_585.3521
1.24_282.1434	2.23_361.2188	4.26_164.9290	6.53_373.2964	7.32_325.1839
1.25_423.2210	2.25_257.1246	4.28_399.1450	6.60_259.6340	7.34_449.3109
1.25_509.2688	2.25_375.2341	4.28_452.2429	6.60_462.2966	8.16_367.2638
1.26_253.1196	2.25_427.1763	4.33_328.2851	6.60_480.3083	8.45_311.2009
1.26_312.1541	2.25_502.8259	4.34_282.2795	6.63_280.6563	8.52_381.1748

Table 9. (continuation)

(Continuation)	Metabolic signals present in hepatic EVs		
Amide_ESI +	**Amide_ESI +**	**Amide_ESI +**	**C18_ESI +**
1.26_339.1639	2.26_476.2730	4.36_164.9309	6.63_541.3288
1.26_353.1790	2.26_562.7655	4.63_427.0952	6.64_438.2985
1.26_566.2939	2.28_414.7210	4.64_449.0773	6.65_504.3418
1.27_575.1305	2.29_742.4016	4.65_471.0594	6.66_422.3388
1.27_813.4551	2.30_374.2385	4.66_635.1414	6.67_496.3399
1.29_219.1347	2.30_806.4510	4.67_613.1603	6.78_466.3310
1.29_325.0545	2.45_360.2243	4.67_657.1240	6.80_464.3138
1.29_401.2400	2.48_484.2550	4.81_112.1125	7.08_436.3549
1.30_303.0718	2.49_473.2830	4.81_129.1391	7.08_482.3234
1.30_480.2475	2.50_189.1352	4.81_146.1658	7.09_315.1755
1.30_854.3631	2.50_317.1933	4.90_110.0095	7.11_546.3527
1.30_945.0115	2.55_400.0519	4.90_151.0358	7.23_395.2773
1.31_407.2643	2.55_502.8258	4.90_223.9896	7.25_260.6406
1.31_458.2610	2.55_520.0116	5.15_146.1657	7.25_464.3138
1.32_629.3980	2.56_515.2131	5.20_129.1392	7.25_482.3245
1.34_247.1316	2.63_375.1982	5.39_146.1658	7.25_504.3092
1.35_260.1612	2.64_189.1352	5.75_146.1659	7.25_963.6367
1.35_387.2244	2.66_612.3472	5.90_146.1658	7.27_1027.6648
1.36_612.3358	2.69_124.0866	6.03_146.1658	7.27_517.3721
1.38_137.0463	2.69_868.9383	6.14_146.1661	7.29_1069.7114
1.39_444.3186	2.70_893.4486	6.25_146.1658	7.29_552.3305
1.40_783.4347	2.71_375.1980	6.40_146.1656	7.29_805.0245
1.41_254.1602	2.72_822.4104	6.47_308.2186	7.29_808.0329
1.41_805.4183	2.74_326.0147	6.56_146.1657	7.30_151.0978
1.42_310.1404	2.75_228.0372	6.58_614.3002	7.31_562.3252
1.42_470.2612	2.75_367.1396	6.70_146.1659	7.35_149.0248
1.42_854.4720	2.75_382.8651	6.83_350.2666	7.37_508.3400
1.43_276.1453	2.75_86.0972	6.84_343.1451	7.39_379.2854
1.43_325.1482	2.76_402.6980	6.88_393.5685	7.40_294.6718
1.43_332.1219	2.78_347.2019	6.88_589.8485	7.43_429.2607
1.43_369.1733	2.83_232.1406	6.94_350.2670	7.48_526.3136
1.43_493.2381	2.83_238.0463	7.08_305.1487	7.49_468.3449
1.44_123.0450	2.83_427.1939	7.09_301.1138	7.52_510.3920
1.44_147.0447	2.86_130.1591	7.09_303.1108	7.54_470.3501
1.44_430.3012	2.88_222.6569	7.19_625.2798	7.56_508.3758
1.44_862.4368	2.90_429.2453	7.20_466.2747	7.60_695.4128
1.44_876.4544	2.93_157.1091	7.74_203.2236	8.14_413.3239
1.45_282.2791	2.96_413.2181	7.84_203.2233	8.14_552.4017
1.45_359.2653	2.99_257.1781		8.14_574.3864
			8.21_303.2906
			8.21_325.2716
			8.21_369.2985
			8.21_480.4254
			8.21_578.4174

Once selected metabolic signals belonging to hepatic EVs metabolome, some of them that belong to the analysis done in aqueous phase (amide) started to be identified by elemental composition calculation and database search**. Table 10** summarizes some of the origins of the metabolic signal together with their corresponding implications. Roughly, the characterization of EVs metabolome reveals a very diverse metabolic content that covers a wide range of functions and implications in different pathways. Among others, it has been detected polypeptides involved in nitric oxide cycle, tissue regeneration or redox reactions. Amino acids and related compounds involved in methionine cycle. Lipids involved in lipid metabolism, biological membrane integrity, antigen presentation or signal transduction. Nucleotides involved in DNA/RNA or glycogen metabolism. Polyamines involved in DNA stabilization and proliferation **(Table 10)**.

In addition to this general characterization of EVs metabolome, in this part of the work a targeted metabolomics approach was also employed to look for metabolites that were routinely analyzed in the metabolomics platform of CIC-bioGUNE corresponding to the methionine cycle [147]. As can be observed in the **Table 11,** it was possible to detect significant levels of SAMe, SAH, MTA, Spermine, Spermidine and GSSG. The detection of these metabolites in hepatic EV indicates that these EVs could have a role in the methionine metabolism in the extracellular environment. This is also supported by the detection of MAT activity in hepatic EVs showed in the previous section of enzymatic activities. Another metabolite present in hepatic EVs was the oxidized form of glutathione (GSSG). Interestingly, while GSSG was clearly present in all EVs samples, reduced form (GSH) was not detected in any of the sample, suggesting that EVs could provide a selective transport of GSSG outside the cell.

Table 10. Hepatic EVs metabolome characterization. Metabolic signals extracted in the aqueous phase started to be characterized. In this table are summarized some of these metabolic signals origins together with their corresponding implications. Abbreviations: IDs; Identifications, PUFAs; Poliunsaturated Fatty Acid.

	Metabolic signals	
Origin	**Implications**	**Possibles IDs**
Polypeptides (Di-, Tri-, Tetra-peptides)	Protein catabolism	Aspartyl-Arginine
	Nitric Oxyde cycle	L-NMMA (N^G-monomethyl-L-arginine)
	Urea cycle	Ornithine
	Collagen synthesis (Regeneration)	L-Proline
		4-Amino-2-methylenebutanoic acid
	Redox reactions (Prevent damage caused by ROS)	GSH (Glutatione)/ GSSG (Gluthathione disulfide)
		Cysteineglutathione disulfide
Amino Acids and related compounds	Methylation (Methionine cycle)	Methionine
		S-adenosyl methionine (SAMe)
		S-adenosyl homocysteine (SAH)
Lipids		
Short chain lipids	Steroids degradation	2-Oxo-4E-hexenoic acid
		7-beta-D-Glucopyranosyloxybutylidenephthalide
Phospholipids	Lipids metabolism	Glycerylphosphorylethanolamine
		Phosphocholine
		sn-glycero-3-phosphoethanolamine
	Biological membranes integrity, Antigen presentation	Phosphatidylcholine (O-12:0/O-1:0) (PC)
		Phosphatidylethanolamine(O-16:0/0:0) (PE)
	Protein targeting	PIP2(20:1(11Z)/18:1(9Z))
Glycosphingolipids	Signal transduction	Gangliosides
	Muscle and nerve cell membrane integrity	Cerebrosides
PUFAs	Membrane structure and function	Docosahexaenoyl Acid (DHA)
	Fatty acids oxidation	5,8-tetradecadienoic acid
		Palmitoyl-L-carnitine
Nucleotides	DNA/ RNA metabolism, glycogen metabolism	Adenosine monophosphate (AMP)
		Deoxyguanosine 5'-monophosphate (dGMP)
		7-alpha-D-Ribosyladenine 5'-phosphate
Aromatic compounds	Purine metabolism	Tetrahydroxypteridine (Pteridine)
		Xanthine-8-carboxylate
	Folic acid metabolism	Tetrahydrofolate
Polyamines	DNA stabilization, cell division, cell differentiation	N8-Acetylspermidine
		N1-Acetylspermidine
		Spermine
Dicarboxylic acids	Polyamines and poliesters synthesis	Undecanedioic acid
	Krebs cycle intermediary	Disodium succinate
Steroid Hormones	Androgenic activity	Testosterone sulfate
Salts	Chemical synthesis	Zinc acetate

Table 11. Metabolites implied in different pathways are contained in hepatic EVs. The intensity of detected compounds is indicated. All of them were detected in cells (data not shown) and EVs except GSH which was only detected in cells. Both, cells and EVs, n=5. Abbreviations: SAMe; **S**-Adenosyl Methionine, SAH; S-Adenosyl Homocysteine, MTA; 5'-methylthioadenosine, GSH; Glutathione, GSSG; Glutathione disulfide, N.D; Not detected. Controls: EVs isolation, Metabolites derived from the culture media; Extraction, Metabolites derived from the extraction procedure.

		Metabolites						
		SAMe	**SAH**	**MTA**	**Spermine**	**Spermidine**	**GSH**	**GSSG**
Controls	EVs isolation	N.D	N.D	N.D	677,167	138,066	N.D	N.D
	Extraction	N.D	N.D	N.D	N.D	N.D	N.D	N.D
Samples	EVs_1	316,213	13,102	47,784	5286,412	11065,136	N.D	339,27
	EVs_2	237,822	7,612	51,379	3916,716	9433,967	N.D	302,309
	EVs_3	267,865	9,378	57,418	5083,345	9673,424	N.D	320,599
	EVs_4	311,038	13,55	48,913	5787,432	10134,849	N.D	359,135
	EVs_5	391,789	5,856	53,814	5369,561	11116,04	N.D	378,672

A second aim in the UPLC-MS metabolomics analysis of hepatic EVs, was to detect metabolic signals that are enriched in EVs having into account the abundance of this metabolic signal in the cells. With this aim, the scatter plots of extracted metabolic signals were obtained from the PCAs. In the **Figure 51** are represented the scatter plots corresponding to polar and apolar datasets run in positive and negative ion mode. Each dot represents an individual EMRT (exact mass-retention time pair). Above the straight line that crosses the intercept, are plotted those metabolic signals detected preferentially in EVs, whereas the metabolic signals enriched in cells are represented behind the line. The signals located in the intercept are supposed to be present in both sample groups at similar levels. EVs samples (n=5) and their coefficient of variation (CV) must be < 20% (**Table 12).**

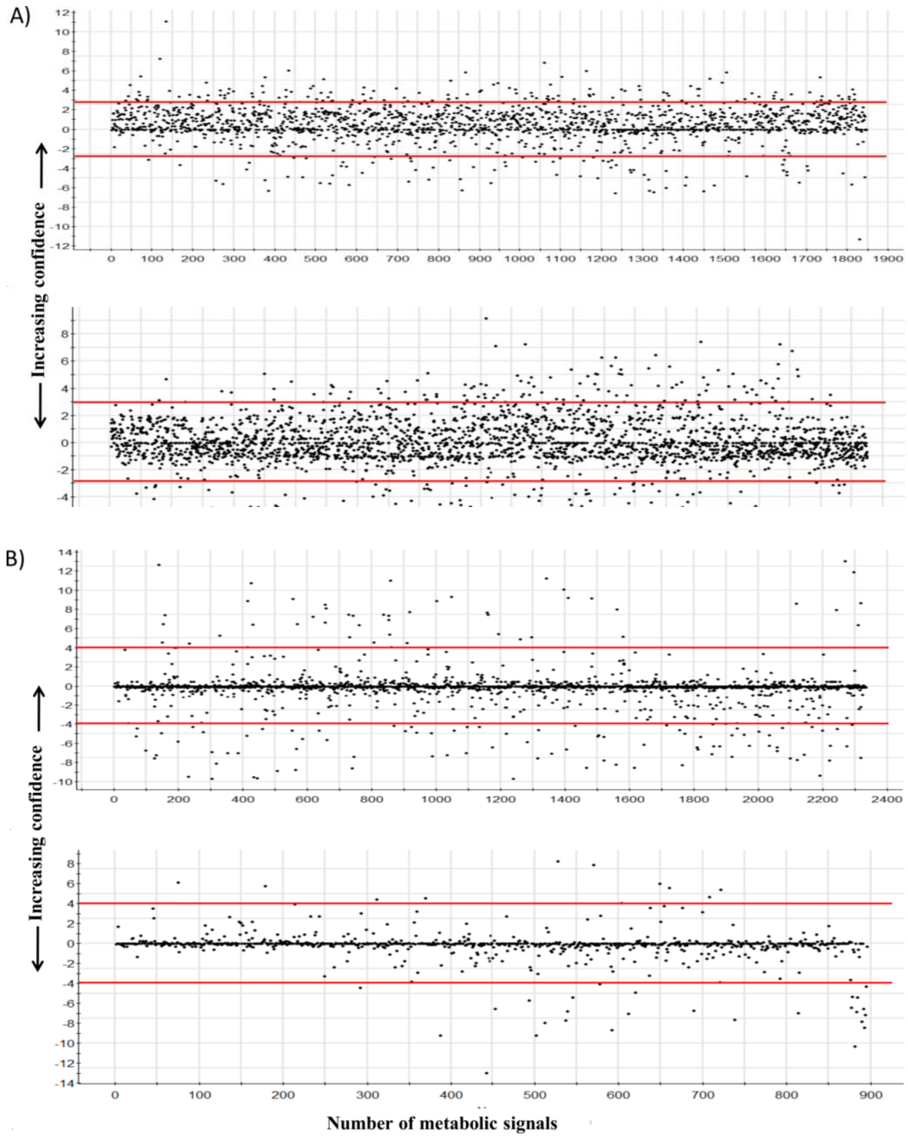

Figure 51. Scatter plots of polar (A) and apolar (B) dataset, run in ESI+ (top) and ESI- (bottom) mode for MLP-29 cells and secreted EVs. Each dot represents a single data point. The *x* axis represents the number of metabolic signals and *y* axis denotes the confidence of a signal contribution to the group differences. Above the straight line that crosses the intercept, are plotted those metabolic signals corresponding to EVs, whereas the metabolic signals related to cells are those represented behind the line. The signals situated in the intercept are supposed to be present in both sample groups. The cut-off (red line) delimits the metabolites that are considered to be present in one of the two sample groups. The closer the data points come to 0, the higher the similarity between the two sample group and vice versa.

Thus, in order to obtain metabolic signals enriched in hepatic EVs a cut-off (red line) in the *scatter plot* was arbitrary established in order to delimit the metabolic signals considered to be enriched in one of the two sample groups (**Figure 51**). The metabolic signals enriched in EVs (above de cut-off) were selected and listed in the **Table 12** indicating their *Rt_m/z* value.

Table 12. Metabolic signals enriched in hepatic EVs secreted by MLP-29 cell line. Metabolic signals are ordered in increasing retention time (RT) which their respective *m/z* value. The ion mode is also specified. Its color represent a unique metabolite which different structural conformation

Metabolic signatures enriched in hepatic EVs		
RT	*m/z*	ESI
0,9083	482,3253	+
0,9123	480,3086	+
0,9202	454,2928	+
0,9262	1133,6344	+
0,9324	734,4066	+
0,9332	685,354	+
0,9983	516,3019	+
1,0281	813,4538	+
1,1618	296,1582	+
1,2171	495,2536	+
1,2194	397,2044	+
1,2381	282,1434	+
1,251	509,2688	+
1,2523	381,211	+
1,258	353,179	+
1,2631	813,9544	+
1,2728	575,1305	+
1,2732	813,4551	+
1,2732	359,2288	+
1,3066	407,2643	+
1,4306	332,1219	+
1,4426	862,4368	+
1,4495	359,2653	+
2,1996	242,6425	+
2,2744	403,7301	+
2,4983	317,1933	+
2,5388	663,2362	+
2,5472	400,0519	+
2,5479	520,0116	+
2,7143	375,198	+
2,743	326,0147	+
2,7779	347,2019	+
2,8832	222,6569	+
3,0824	416,2979	+
3,1154	290,1465	+
3,1183	333,1873	+
3,6076	215,6495	+
3,9671	304,0168	+
4,8098	129,1391	+
7,1926	625,2798	+
0,8941	568,3602	-
0,9304	661,3566	-
2,1214	472,2772	+
2,2332	521,2569	+
2,2357	516,3034	+
2,325	560,3275	+
2,4068	609,3104	+
2,4166	604,3542	+
2,4932	327,1725	+
2,4935	316,1809	+
2,4941	648,3805	+
2,5669	338,195	+
2,5672	692,4065	+
2,569	346,7079	+
2,6328	736,4312	+
2,6348	377,2329	+
2,6352	360,2077	+
2,6358	368,7207	+
2,6666	348,7243	+
2,6986	382,2211	+
2,6989	399,2465	+
2,6991	390,734	+
2,7289	509,8041	+
2,7337	518,3172	+

Metabolic signatures enriched in hepatic EVs		
RT	*m/z*	ESI
2,7589	404,2329	+
2,762	412,7474	+
2,763	421,2597	+
2,7737	540,3304	+
2,7769	531,816	+
2,8086	443,2729	+
2,8105	434,7593	+
2,8147	553,8292	+
2,8154	562,3425	+
2,8563	584,356	+
2,8573	465,2868	+
2,892	597,8554	+
2,894	606,37	+
2,9284	628,383	+
2,964	650,3964	+
2,994	672,4093	+
3,0241	694,422	+
3,096	498,3096	+
3,1115	512,9849	+
3,1404	527,6607	+
6,2511	421,3407	+
6,2652	554,2876	+
6,3989	246,6258	+
6,4354	762,9791	+
6,4578	425,375	+
6,6265	1065,6788	+
7,1097	546,3527	+
7,2485	260,6406	+
7,2938	808,0329	+
7,3647	365,3208	+
8,1255	383,3314	+
8,2124	303,2906	+
5,2407	692,3842	-
5,2559	565,2795	-
5,259	497,2933	-
5,401	367,0765	-
5,5667	498,2625	-
5,8404	606,3017	-
5,9465	568,2667	-
6,0489	524,2775	-
6,0769	476,2769	-
6,0793	500,2774	-
6,2419	526,2937	-
6,4182	947,6074	-
6,4228	421,2803	-
6,4388	1035,6603	-
6,4637	1061,6769	-
6,5942	957,5947	-
6,595	546,2791	-
6,5962	578,2182	-
6,611	999,6387	-
6,6299	1087,6941	-
6,6595	522,2827	-
6,725	554,3438	-
6,7985	462,2981	-
6,8584	554,3457	-
7,2495	961,6268	-
7,2677	1003,671	-
7,2888	1091,7223	-
7,3513	417,2858	-
7,4822	443,3009	-
7,7673	623,4178	-
7,0826	482,3234	+
7,0884	480,3101	-

Some of the metabolic signals enriched in EVs were pre-selected for further identification. Thus, those signals that showed a clear difference in peak intensity (peak area) between cells and EVs were selected. With this aim, the extracted ion chromatogram (XIC) and *trendplot* were obtained for the EVs-enriched metabolic signals. XIC represents the selected peak after each extraction from the entire chromatogram and the *trendplot* displays a plot of intensities of the selected metabolite throughout the replicates (n=5) and sample types. Two representative examples of EV-enriched metabolic signals are showed in **Figures 52** and **Figure 53**. In the chromatogram (A) is clearly observed how, in both cases, the intensity of the peak is much higher in EVs (in green) than in cells (in red). Moreover, this intensity remains more or less similar across all samples (n=5) as revealed by the *trendplot* (B), supporting the reproducibility of the analysis.

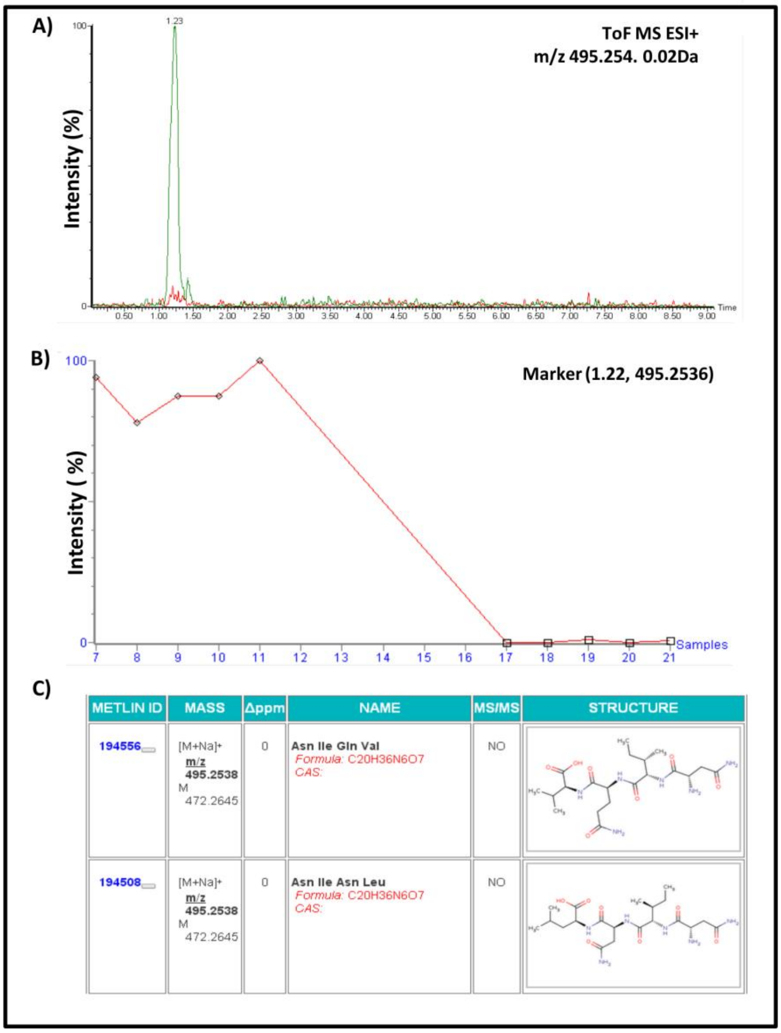

METLIN ID	MASS	Δppm	NAME	MS/MS	STRUCTURE
194556	[M+Na]+ m/z 495.2538 M 472.2645	0	Asn Ile Gln Val *Formula:* C20H36N6O7 *CAS:*	NO	
194508	[M+Na]+ m/z 495.2538 M 472.2645	0	Asn Ile Asn Leu *Formula:* C20H36N6O7 *CAS:*	NO	

Figure 52. Example of the identification of a metabolite enriched in EVs in the aqueous phase. **(A)** Extracted Ion Chromatogram: *y* axys denotes the intensity of the peak in percentage. *X* axys indicate the retention time of the metabolite. The peak that corresponds to EVs is represented in green and cells in red. **(B)** Trendplot: *y* axys denotes the intensity of the peak in percentage and X axys analyzed sample in the trendplot. Samples 7-11 correspond to EVs and 17-21 to cells. **(C)** Possible identifications of the metabolite after a database search.

For organic phase some polipeptides and abundant lipids were detected. In **Figure 54** are shown some examples of metabolites enriched in EVs extracted in organic phase.

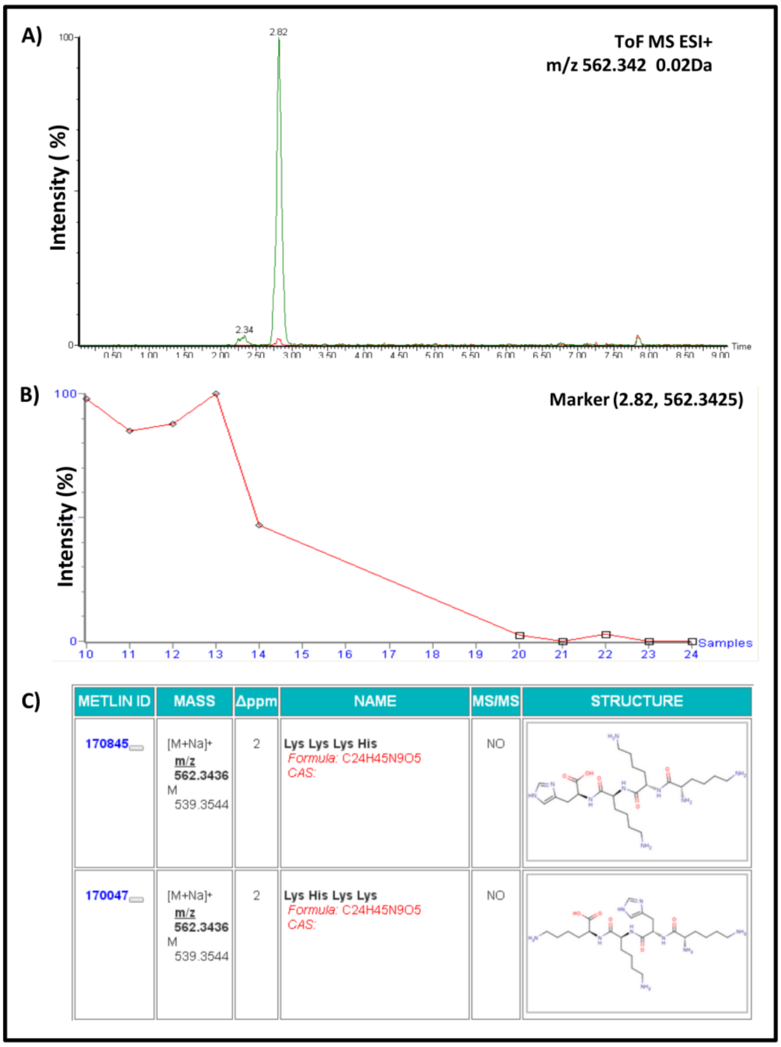

METLIN ID	MASS	Δppm	NAME	MS/MS	STRUCTURE
170845	[M+Na]+ **m/z** **562.3436** M 539.3544	2	**Lys Lys Lys His** *Formula:* C24H45N9O5 *CAS:*	NO	
170047	[M+Na]+ **m/z** **562.3436** M 539.3544	2	**Lys His Lys Lys** *Formula:* C24H45N9O5 *CAS:*	NO	

Figure 53. Example of the identification of a metabolite enriched in EVs in the organic phase. **(A)** Extracted Ion Chromatogram: *y* axys denotes the intensity of the peak in percentage. *X* axys indicate the retention time of the metabolite. The peak that corresponds to EVs is represented in green and cells in red. **(B)** Trendplot: *y* axys denotes the intensity of the peak in percentage and X axys analyzed sample in the trendplot. Samples 10-14 correspond to EVs and 20-24 to cells. **(C)** Possible identifications of the metabolite after a database search.

In summary, metabolomics applied to the functional study of hepatic EVs offer a powerful tool to identify the different pathways in which hepatic EVs are implied. Moreover, several potential metabolic signatures discovered through untargeted metabolomics have been reported over the past year in several diseases. Therefore, the recognition of the potential of EVs as a source of biomarkers discovery could open novel perspectives in the prediction, diagnosis, prognosis, and therapy of hepatic diseases and liver injury.

7. GENERAL DISCUSSION

This work is focused on the study of the functional role that hepatic EVs could play in the endogenous and xenobiotics metabolism in the organism. The results obtained by using different cellular models of DILI in combination with cellular and biochemical techniques as well as UPLC-MS-based metabolomics technology have provided strong indications that hepatic EVs carry active enzymes and metabolites that can influence significantly the extracellular environment. In addition, the study has also provided several molecules and enzymatic activities that could be useful to develop low-invasive diagnosis methods for DILI.

A key interest in clinical diagnosis and pharmaceutical industry is to have a repertoire of non-invasive biomarkers to be able to predict the degree of liver injury caused by a pathological condition or a drug. The first part of this thesis shows that compounds and drugs-causing acute liver injury, such as GalN, APAP and DCF, modified the intracellular distribution and in some cases the abundance of RNAs, proteins and metabolic enzymes that can be detected in hepatic EVs. In addition, modified-molecules play important role in different cellular pathways, supporting that modified-EVs would impact biological processes by several mechanisms. Thus, a chaperone protein induced under stress conditions [206] as Hsp70 is increased in hepatic-EVs secreted in GalN and DCF treatments, which is, at the same time, accompanied with a decrease in cells. This suggests a selective transport of this protein outside the cell under acute liver injury, maybe to avoid the damage of extracellular proteins. On the other side, the expression of Rab8 protein was significantly reduced by the APAP treatment in both, cells and EVs, whereas in GalN and DCF treatments the protein is increased in the secreted EVs. This result points that the cellular response to GalN and DCF could implicate vesicular trafficking that depends on Rab 8 protein. This differential impact of the drugs on the intracellular trafficking is also supported by the alteration in the levels of LIMP II, that plays a role in the regulation of endosome and lysosome biogenesis [207]. Another protein affected by the drugs is the tetraspanin Cd63, an endosomal and exosomal marker implicated in immune response [80]. These results, apart from supporting the effect of the drugs on intracellular trafficking also implicates the secreted EVs in the regulation of the immune response under DILI conditions.

The protein levels and also the activity in hepatic EVs of metabolic enzymes such as CES, COMT and MAT are differentially altered in DILI cellular models. This supports the existence of different mechanisms of action ejected by the cells to overcome a toxic challenge and importantly, supports hepatic EVs as the vehicles to perform a response to overcome the damage. In this context, COMT enzyme expression levels decreased significantly in EVs in APAP and DCF treatments, subsequently affecting the catechols methylation carried out by COMT activity. In this regard, it is reported that the inactivation of catecholamines by COMT in the brain have an effect on blood pressure regulation [208]. The data provided in this doctoral thesis indicates that modifications in the EVs-associated COMT-activity could regulate blood pressure in the liver under DILI conditions. In agreement with this hypothesis, it has been shown that the methylation ability of catecholamines by COMT is attenuated in liver and kidney of spontaneously hypertensive rats [128]. Yet, not only the protein cargo is affected by DILI conditions, also the RNA cargo of EVs was differentially altered under DILI conditions tested in this study. This effect on the RNA suggests that EVs carry the information to respond to a determined stress in a time depending manner. Thus, a first quick wave of response mediated by direct protein interaction and enzymatic activities, and then a time-delay response ejected by the regulation of the translation of determined RNAs in the recipient cells. Thus, the mixture composition of the vesicles highlights the complex mechanisms implicated in the DILI. It is also important to highlight that all DILI models used in this study increased significantly the amount of EVs secreted by the hepatocytes. Together, all these data strongly support that hepatocytes under liver-damaging conditions employ the secretion of EVs to respond to liver insults loading them with specific cargos depending on the mechanism of action required to overcome the challenge.

Furthermore, the data also supports the study of EVs under controlled conditions as an approach to identify low-invasive candidate markers for early detection of disease conditions.

The use of EVs as a source to identify DILI biomarkers has several advantages [209]. First, it may be possible to identify highly specific DILI biomarkers in circulating EVs. This is important as currently used DILI biomarkers lack organ specificity [210]. Second, EVs components are protected from degradation [49] and thus have a longer survival time, providing a wider time window for injury detection. Third, efforts to directly use serum and plasma to discover new DILI biomarkers are often hindered by highly abundant blood constituents. The true signal may escape detection among those very strong and irrelevant background signals. Using isolated EVs may avoid this problem. Finally, one additional benefit of using EVs in DILI is that not only changes in their sizes, but also patterns of their association with specific molecules maybe is indicative of the etiology of liver injury [211]. Over the past years, several potential metabolic signatures discovered through untargeted metabolomics have been reported in several diseases such as hepatocarcinoma in patients with cirrhosis [212], Parkinson’s disease diagnosis and progression [213], depression ,schizophrenia, diabetes and also cardiovascular and coronary artery disease [137]. The recognition of the potential of EVs will open novel perspectives in the prediction, diagnosis, prognosis, and therapy of hepatic diseases and liver injury in general.

In addition to the molecular characterization of EVs, a second aim of the work was the study of the role that these vesicles could play in the development and progression of DILI. The proteomics analysis of hepatocyte-derived EVs revealed the presence of metabolic enzymes involved in the central regulation of hepatocyte metabolism (MAT enzyme) as well as specifically in the xenobiotics and endogenous compounds metabolism (CES, COMT enzymes). In this work, alterations on the protein level of these enzymes were found under tested DILI models. Furthermore, these three enzymes activities were detected in hepatic EVs extending the intracellular effects described for them in relation with DILI to the extracellular space.

CES activity efficiently catalyzes the hydrolysis of a variety of ester- and amide-bonds contained in chemicals and drugs to their respective free acids. In this way, CES activity is involved in detoxification of various drugs, environmental toxicants and carcinogens. Apart from metabolizing drugs to their corresponding inactive form, it also is responsible of other drugs metabolic activation that may cause a toxicological effect through direct hepatotoxicity allowing, in this way, the development of DILI. A clear example is 7-ethyl-10-[4-(1-piperidino)-1-piperidino] carbonyloxy-camptothecin (CPT-11) which is a drug currently used for the treatment of different types of cancers such as colon or rectum [214]. CPT-11 requires the CES activity mediated biotransformation to convert to its active metabolite 7-ethyl-10 hydroxycamptothecin (SN-38), which is approximately 100-1000 fold more cytotoxic than the parent drug [215].

MAT enzyme is responsible for the biosynthesis of SAMe, the principal biological donor of methyl groups [100] and a master regulator of hepatocyte metabolism [216]. Abnormal activity of this enzyme is linked to many diseases outside (e.g. depression and osteoarthritis [216]) and inside (e.g. steatohepatitis, cirrhosis, HCC [100]) the liver. With regards its possible implication in DILI, it has been observed an increase in MAT1A protein expression levels, one of the subunits forming the enzyme, in EVs released by primary cultures of rat hepatocytes exposed to GalN and in serum-isolated EVs from GalN treated rats [95]. In this sense, ethionine is an amino acid structurally related to methionine with an ethyl group instead of a methyl group [217] and it is also a substrate for MAT. *In vivo*, ethionine causes hepatic SAMe and ATP depletion leading to DILI [218]. Indeed, this toxin induces steatosis, impaired methylation reactions and hepatic glucose and glycogen depletion among others [219]. Another example that connects MAT with DILI is cycloleucine, an inhibitor of MAT activity [217]. This non metabolizable analog of methionine, induces SAMe and GSH depletion and potentiates drug-induced cytochrome P-450 2E1 (CYP2E1)-mediated cytotoxicity in hepatocytes [220].

In the case of COMT activity, its general function is the elimination of biologically active or toxic catechols and some other hydroxylated metabolites. COMT protein has been recently reported as a biomarker of liver injury in APAP induced toxicity model. Indeed, in the early stages, even before the current standard liver biomarker ALT and histopathology indicated liver injury, COMT protein levels changed significantly in both liver tissue and plasma [126]. Moreover, COMT has several substrates related to DILI. 17-beta estradiol is a cathecol drug converted to its toxically active form by the activity of the COMT enzyme [112][113]. Is an essential estrogen hormone for females that has important effects in the liver. For example, it can lead to cholestasis by inducing a reversible inhibition of bile flow. Another cathecholic drug is Salvianoic acid A (SAA). COMT is responsible of methylated transformation of this phenolic acid metabolically unstable. Metabolites derived from O-methylation of SAA, display high antioxidant potency against liver lipid peroxidation [114]. Moreover, considerable evidence has also demonstrated the potent protective effects of SAA against ischemia-induced injury [115][116].

As conclusion of this part of the work, the presence of these activities in hepatic EVs suggest a possible contribution of these secreted vesicles to the metabolism of drugs what should be taken into consideration in further studies to avoid undesired secondary effects.

In the case of MAT and COMT activities, it was necessary to develop in-house methods using UPLC-MS technology. As a result, sensitive and specific methods for determination of MAT and COMT activities were developed, being now available for the scientific community for future laboratory and clinical research.

Finally, it is important to remark that these EVs-associated activities are differentially expressed depending on the treatment, offering a way to discriminate among different type of liver injuries. In this regard, the introduction of novel detection methods that enable the identification of EV signatures in patients with liver injury and also in-depth characterization of EVs derived from liver would help to identify DILI low-invasive markers and novel therapeutics targets.

The characterization of EVs metabolome was further achieved to unravel metabolic pathways and functions that hepatic EVs could be performing in the organism. Our study reveals a very diverse metabolic content that covers a wide range of putative functions and suggest the implication of hepatic EVs in different cellular pathways. In this regard, an elevated number of metabolic signals were clearly associated to these vesicles and comparing with chemical standards, some of them were identified. The presence of several intermediaries of methionine cycle including SAMe, SAH and MTA was confirmed in hepatic EVs. The presence of these metabolites joined to the fact that hepatic EVs also carry MAT enzymatic activity strongly suggest that hepatic EVs could have an important role in the methionine cycle regulation in the extracellular environment or in adjacent or far-away-localized recipient cells. The polyamines, spermine and spermidine, were also detected in hepatic EVs, supporting the hypothesis of these vesicles as vehicles sending metabolic signals influencing DNA synthesis and stabilization, gene expression regulation or cell proliferation among others functions that are controlled by these metabolites [221]. In this sense, it has been reported that EVs released by adult stem cells residing in the liver have the capacity to repair damage tissue by inducing liver regeneration [222]. Moreover, it is known that polyamines are also involved in carcinogenesis, prompting intensive research into polyamine metabolism as a target in cancer therapy. Furthermore, the implication of hepatic EVs in polyamine metabolism it is also supported by the fact that SAMe takes part also in the polyamine biosynthesis [100]. Another metabolite detected in hepatic EVs is the oxidized form of glutathione (GSSG). Interestingly, while GSSG was clearly detected, the reduced form GSH was not, suggesting that hepatic EVs could constitute a selective transport of GSSG outside the cell. GSH is an important antioxidant that prevents damage caused by reactive oxygen species such as free radicals or peroxides. In redox reactions, GSH is converted to GSSG. An increased GSSG-to-GSH ratio is considered indicative of oxidative stress [223]. Hence, the elevated presence of GSSG in EVs could be considered an indication of oxidative stress in the cell from where it came from. Moreover, SAMe is an important precursor of GSH since SAMe is the precursor of SAH, which is then hydrolysed to homocysteine which finally forms GSH in the transsulfuration pathway. Here again, it is observed certain correlation between the metabolites contained in hepatic EVs, suggesting an organized functionality inside the EVs.

In conclusion, several metabolites detected in these vesicles, indicate the implication of hepatic EVs in methylation, polyamine and DNA synthesis (amynopropylation) and oxidative stress (transsulfuration) response.

Other metabolic signals from the hepatic EV metabolome were tentatively identified using mass accuracy and database search. Among this group of metabolites, tetrahydroxypteridine and tetrahydrofolate were detected, both implicated in the synthesis of purines and DNA. The presence of these two metabolites along with the polyamines above mentioned, indicate that one of the mechanism of action of hepatic EVs could implicate the regulation of these processes. In agreement with this, it has been also reported that EVs derived from endometrial epithelial cells have a potential role in purine metabolism [224]. Another metabolic signals tentatively identified was adenosine monophosphate (AMP), that has an important role in glycogen metabolism in the liver, suggesting that hepatic EVs could be implicated in regulation of the energetic metabolism. N^G-monomethyl-L-arginine (L-NMMA), an inhibitor of nitric oxide synthase, was also among the possible metabolites contained in hepatic EVs, suggesting a possible role of these vesicles in controlling the vasodilatation and vasoconstriction of blood vessels. This effect could be connected with the COMT enzymatic activity found in hepatic EVs.

Another group of metabolic signals of hepatic EVs with tentative IDs belong to the lipids. In agreement with the membrane-base of these vesicles, two structural membrane lipids such as phosphatidylcholine and phosphatidylethanolamine were in this group. Lipids involved in the sorting of molecules into vesicles including docosahexaenoic acid (DHA) and phosphatidylinositol-(4,5)-bisphosphate (PIP2) phospholipids were also in the lipid group [225] [226], indicating that they could be involved in sorting to hepatic EVs. An intermediary of the unsaturated fatty acid oxidation, 5,8-tetradecadienoic acid [140], was also identified as a possible metabolite contained in hepatic EVs, as well as the glyceryl phosphorylethanolamine, which is a membrane breakdown product that acts as a growth stimulating factor for hepatocytes [227].

In conclusion, all these data clearly support the complexity of the cellular processes in which hepatic vesicles could be involved, being required additional experimentation to elucidate in more detail. In the **Figure 54** is represented a schematic view of the main results obtained in this doctoral thesis.

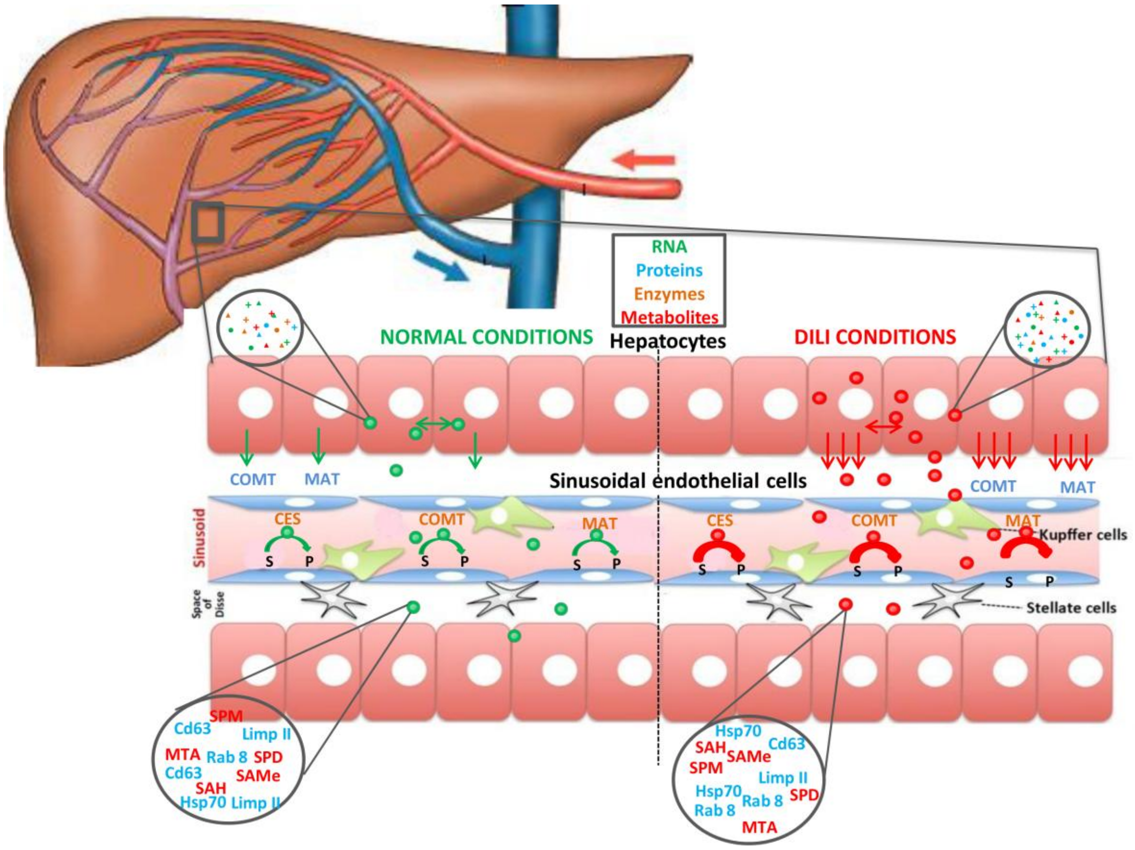
RNA
Proteins
Enzymes
Metabolites
NORMAL CONDITIONS
Hepatocytes
DILI CONDITIONS
COMT
MAT
Sinusoidal endothelial cells
COMT
MAT
Sinusoid
CES
COMT
MAT
S
P
CES
COMT
MAT
Kupffer cells
Space of Disse
Stellate cells
SPM
Cd63
Limp II
MTA
Rab 8
SPD
Cd63
SAMe
SAH
Hsp70
Limp II
Hsp70
Cd63
SAH
SAMe
SPM
Limp II
Hsp70
Rab 8
SPD
Rab 8
MTA

Figure 54. Overview of the main results obtained in this doctoral thesis. In normal (*green*) conditions hepatocytes release EVs *(black dots*) containing RNAs, proteins, enzymes and metabolites into the extracellular environment. These vesicles can be captured by neighbor or distant cells modifying their metabolism. Hepatocytes-secreted EVs could also modify the metabolism in the intercellular space as well as in body fluids. Under DILI (*red*) conditions hepatocytes secrete more EVs to the extracellular environment and bloodstream increasing the risk of damage. The composition of these vesicles varies depending on the induced liver damage being possible to discriminate between different injuries (Hsp70 and Rab 8 proteins expression increases in DILI conditions whereas Cd63 and Limp II decrease). Moreover, the activity of some of the enzymes contained in hepatic EVs such as CES, COMT and MAT, increases in liver damaging conditions. Indeed, the activity varies depending on the induced damage. The implication of these enzymes in DILI suggests that hepatic EVs could be involved in the development of DILI. Furthermore, hepatic EVs metabolome contains metabolites that take part in important cellular pathways such as methionine metabolism (SAMe and SAH), redox reactions (GSSG) or purine and DNA biosynthesis (spermine and spermidine).

8. CONCLUSIONS

1. GalN, DCF and APAP have different effects on hepatocytes indicating that different responses are carried out in hepatocytes depending on the induced liver damage.

2. APAP affects more severely to the hepatocytes than GalN and DFC under tested conditions.

3. Hepatocytes secreted more EVs under DILI conditions.

4. Composition of EVs is altered by DILI conditions and different drugs affect differentially to the composition of the EVs.

5. Hepatic EVs display CES, MAT and COMT activities and the activities vary depending on treatments with DCF, GalN or APAP.

6. Hepatic EVs are a suitable biological source to identify markers for detecting and classifying DILI.

7. The implication of CES, MAT and COMT activities in DILI suggests that hepatic EVs could be involved in the development of DILI.

8. UPLC-MS based metabolomics is a good technology to characterize MAT and COMT activities in EVs, and to identify the metabolites that are associated with hepatic EVs.

9. The metabolome of hepatic EVs is constituted by more than 340 metabolic signals.

10. Hepatic EVs carry a complex mix of metabolites belonging to different cellular pathways including methionine metabolism, redox metabolism, purine and DNA biosynthesis.

9. BIBLIOGRAPHY

[1] “Falcon-Perez JM, Lu SC, Mato JM. Sub-proteome approach to the knowledge of liver. Proteomics Clin Appl. 2010; 4, 407–415.”

[2] “Klover PJ, Mooney RA. Hepatocytes: critical for glucose homeostasis. Int J Biochem Cell Biol. 2004; 36(5), 753-8.”

[3] “Charlton MR. Protein metabolism and liver disease. Baillieres Clin Endocrinol Metab.1996; 10(4), 617-35.”

[4] “Nguyen P, Leray V, Diez M, Serisier S, Le Bloc’h J, Siliart B, Dumon H. Liver lipid metabolism. J Anim Physiol Anim Nutr (Berl). 2008; 92(3), 272-83.”

[5] “Sturgill MG, Lambert GH. Xenobiotic-induced hepatotoxicity: mechanisms of liver injury and methods of monitoring hepatic function.Clinical Chemistry. 1997; 43(8), 1512–1526.”

[6] “Royo F, Falcon-Perez JM. Liver extracellular vesicles in health and Disease. Journal of extracellular vesicles. 2012.”

[7] “Seki E, Brenner DA. Toll-like receptors and adaptor molecules in liver disease: update. Hepatology. 2008; 48(1), 322-35.”

[8] “Moreira RK. Hepatic stellate cells and liver fibrosis. Arch Pathol Lab Med. 2007;131(11), 1728-34.”

[9] “Jones AL. Anatomy of the normal liver. In: Zakin D, Boyer TD, eds. Hepatology: a textbook of liver disease, 3rd ed. Philadelphia: WB Saunders. 1996; 3-32.”

[10] “Ostapowicz G, Fontana RJ, Schiodt FV. Results of a prospective study of acute liver failure at 17 tertiary care centers in the United States. Ann Intern Med. 2002; 137, 947-954.”

[11] “Larrey D . Drug-induced liver diseases. J Hepatol. 2000; 32, 77 - 88.”

[12] “Gunawan B , Kaplowitz N . Clinical perspectives on xenobiotic induced hepatotoxicity. Drug Metab Rev. 2004; 36, 301 - 312.”

[13] “Holt MP, Ju C. Mechanisms of Drug-Induced Liver Injury. The AAPS Journal. 2006; 8 (1), 48-54.”

[14] “Li Z, Diehl AM. Innate immunity in the liver. Curr Opin Gastroenterol. 2003; 19, 565 - 571 .”

[15] “Zimmerman HJ . Drug-induced liver disease. In: Zimmerman HJ , ed. Hepatotoxicity: The Adverse Effects of Drugs and Other Chemicals on the Liver. 2nd ed. Philadelphia, PA : Lippincott Williams & Wilkins. 1999; 427- 456.”

[16] “Kaplowitz N. Drug-induced liver disorders: Implications for drug development and regulation. Drug Safety. 2001; 24, 483–490.”

[17] “Ozer J, Ratner M, Shaw M, Bailey W, Schomaker S. The current state of serum biomarkers of hepatotoxicity. Toxicology. 2008; 245, 194–205.”

[18] “Muller PY, Dieterle F. Tissue-specific, non-invasive toxicity biomarkers: Translation from preclinical safety assessment to clinical safety monitoring. Expert Opinion on Drug Metabolism.2009; 5, 1023–1038.”

[19] “Chang CY, Schiano TD. Review article: drug hepatotoxicity. Aliment Pharmacol Ther. 2007; 25(10), 1135-51.”

[20] “Kucera O, Lotková H, Kanďár R, Hézová R, Mužáková V, Červinková Z. The model of d-galactosamine-induced injury of rat hepatocytes in primary culture. Acta Médica (Hradec Kralove) 2006; 49(1), 59–65.”

[21] “Keppler D, Lesch R, Reutter W, Decker K. Experimental hepatitis induced by D-galactosamine. Exp Mol Pathol. 1968; 9, 279–90.”

[22] “Mangeney-Andreani M, Sire O, Montagne-Clavel J, Nordmann R, Nordmann J: Inhibitory effect of D-galactosamine administration on fatty oxidation in rat hepatocytes. FEBS Lett. 1982; 145, 267-270.”

[23] “Mitchell JR, Jollow DJ, Potter WZ, Davis DC, Gillette JR, Brodie BB. Acetaminophen-induced hepatic necrosis. I. Role of drug metabolism. J Pharmacol Exp Ther. 1973; 187(1), 185-94.”

[24] “Donnelly PJ, Walker RM, Racz WJ. Inhibition of mitochondrial respiration in vivo is an early event in acetaminophen-induced hepatotoxicity. Arch Toxicol. 1994; 68(2), 110-8.”

[25] “Meyers LL, Beierschmitt WP, Khairallah EA, Cohen SD. Acetaminophen-induced inhibition of hepatic mitochondrial respiration in mice. Toxicol Appl Pharmacol. 1988; 93(3), 378-87.”

[26] “Boelsterli UA. Diclofenac-induced liver injury: a paradigm of idiosyncratic drug toxicity. Toxicology and Applied Pharmacology; 2003, 192, 307–322.”

[27] “Livertox. Clinical and research information on drug induced liver injury. National library of medicine.”

[28] “Duijvesz D, Luider T, Bangma CH, Jenster G . Exosomes as biomarker treasure chests for prostate cancer. Eur Urol . 2011; 59, 823–831.”

[29] “Chargaff E, West R. The biological significance of the thromboplastic protein of blood. J Biol Chem. 1946; 166(1), 189-97.”

[30] “Wolf P. The nature and significance of platelet products in human plasma. Br J Haematol. 1967;13(3), 269-88.”

[31] “Dalton AJ. Microvesicles and vesicles of multivesicular bodies versus ‘virus-like’ particles. J Natl Cancer Inst. 1975; 54(5), 1137-48.”

[32] “Johnstone RM, Adam M, Hammond JR, Orr L, Turbide C. Vesicle formation during reticulocyte maturation. Association of plasma membrane activities with released vesicles (exosomes). J Biol Chem. 1987; 262(19), 9412-20.”

[33] “Müller G. Microvesicles/exosomes as potential novel biomarkers of metabolic diseases. Diabetes, Metabolic Syndrome and Obesity: Targets and Therapy. 2012; 5, 247–282.”

[34] “Ronquist G, Brody I. The prostasome: its secretion and function in man. Biochim Biophys Acta. 1985; 822(2), 203-18.”

[35] “Park BK, Pirmohamed M, Kitteringham NR.The role of cytochrome P450 enzymes in hepatic and extrahepatic human drug toxicity. Pharmacol Ther. 1995; 68(3):385-424.”

[36] “Caby MP, Lankar D, Vincendeau-Scherrer C, Raposo G, Bonnerot C. Exosomal-like vesicles are present in human blood plasma. Int Immunol. 2005;17(7), 879-87.”

[37] “Huebner AR, Somparn P, Benjachat T, Leelahavanichkul A, Avihingsanon Y, Fenton RA, Pisitkun T. Exosomes in urine biomarker discovery. Adv Exp Med Biol. 2015; 845, 43-58.”

[38] “Ogawa Y, Miura Y, Harazono A, Kanai-Azuma M, Akimoto Y, Kawakami H, Yamaguchi T, Toda T, Endo T, Tsubuki M, Yanoshita R. Proteomic analysis of two types of exosomes in human whole saliva. Biol Pharm Bull. 2011;34(1), 13-23.”

[39] “Admyre C, Johansson SM, Qazi KR, Filén JJ, Lahesmaa R, Norman M, Neve EP, Scheynius A, Gabrielsson S. Exosomes with immune modulatory features are present in human breast milk. J Immunol. 2007;179(3), 1969-78.”

[40] “Asea A, Jean-Pierre C, Kaur P, Rao P, Linhares IM, Skupski D, Witkin SS. Heat shock protein-containing exosomes in mid-trimester amniotic fluids. J Reprod Immunol. 2008; 79(1), 12-7.”

[41] “Andre F, Escudier B, Angevin E, Tursz T, Zitvogel L. Exosomes for cancer immunotherapy. Ann Oncol. 2004; 15(4), 141-144.”

[42] “Vella LJ, Sharples RA, Nisbet RM, Cappai R, Hill AF. The role of exosomes in the processing of proteins associated with neurodegenerative diseases. Eur Biophys J. 2008; 37(3), 323-32.”

[43] “Masyuk AI, Huang BQ, Ward CJ, Gradilone SA, Banales JM, Masyuk TV, Radtke B, Splinter PL, LaRusso NF. Biliary exosomes influence cholangiocyte regulatory mechanisms and proliferation through interaction with primary cilia. Am J Physiol Gastrointest Liver Physiol. 2010; 299(4).”

[44] “Akers JC, Gonda D, Kim R, Carter BS, Chen CC. Biogenesis of extracellular vesicles (EV): exosomes, microvesicles, retrovirus-like vesicles, and apoptotic bodies. J Neurooncol. 2013; 113(1), 1-11.”

[45] “Gyorgy B, SzaboTG, Pasztoi M, Zsuzsanna P, Misjak P, Aradi B, Laszlo V , Pallinger E, Pap E, Kittel AG, Nagy G, Falus A, Buzas E.Membrane vesicles, current state-of-the-art: emerging role of extracellular vesicles. Cell Mol Life Sci. 2011; 68, 2667–2688.”

[46] “Harding C, Heuser J, Stahl P. Receptor-mediated endocytosis of transferrin and recycling of the transferrin receptor in rat reticulocytes. J Cell Biol 1983;97(2):329-339.”

[47] “Raposo G, Nijman HW, Stoorvogel W et al. B lymphocytes secrete antigen-presenting vesicles. J Exp Med 1996;183(3):1161-1172.”

[48] “Pan BT, Teng K, Wu C, Adam M, Johnstone RM. Electron microscopic evidence for externalization of the transferrin receptor in vesicular form in sheep reticulocytes. J Cell Biol 1985;101(3):942-948.”

[49] “Raposo G, Stoorvogel W. Extracellular vesicles: exosomes, microvesicles, and friends. J Cell Biol. 2013; 200(4), 373-83.”

[50] “Kowal J, Tkach M and Thery C. Biogenesis and secretion of exosomes. Current Opinion in Cell Biology 2014; 29; 116–125.”

[51] “Klumperman J, Raposo G. The complex ultrastructure of the endolysosomal system. Cold Spring Harb Perspect Biol. 2014; 6(10).”

[52] “Stoorvogel, Oorschot V and Geuze HJ. A Novel Class of Clathrin-coated Vesicles Budding from Endosomes. The Journal of Cell Biology. 1996; 132 (1 & 2), 21-33.”

[53] “Stoorvogel W, Kleijmeer MJ, Geuze HJ, Raposo G. The biogenesis and functions of exosomes. Traffic. 2002; 3(5), 321-330.”

[54] “Colombo M, Raposo G, Thery C. Biogenesis, Secretion, and Intercellular Interactions of Exosomes and Other Extracellular Vesicles. Annu. Rev. Cell Dev. Biol. 2014; 30, 255–89.”

[55] “Nan Niel GI, Porto-Carreiro S, Raposo G. Exosomes: a common pathway for a specialized function. J Biochem. 2006; 140, 13–21.”

[56] “Hemler, M.E. Tetraspanin proteins mediate cellular penetration, invasion, and fusion events and define a novel type of membrane microdomain. Annu. Rev. Cell Dev Biol. 2003; 19, 397–422.”

[57] “Valadi H, Ekström K, Bossios A, Sjöstrand M, Lee JJ, Lötvall JO. Exosome-mediated transfer of mRNAs and microRNAs is a novel mechanism of genetic exchange between cells. Cell Biol. 2007; 9(6), 654-9.”

[58] “Ratajczak J, Wysoczynski M, Hayek F, Janowska-Wieczorek A, Ratajczak MZ. Membrane-derived microvesicles: important and underappreciated mediators of cell-to-cell communication. Leukemia. 2006; 20(9), 1487-95.”

[59] “Bellingham SA, Coleman BM, Hill AF. Small RNA deep sequencing reveals a distinct miRNA signature released in exosomes from prion-infected neuronal cells. Nucleic Acids Res. 2012; 40, 10937–10949.”

[60] “Nolte-’t Hoen EN, Buermans HP, Waasdorp M, Stoorvogel W, Wauben MH, Hoen PA. Deep sequencing of RNA from immune cell-derived vesicles uncovers the selective incorporation of small non-coding RNA biotypes with potential regulatory functions. Nucleic Acids Res. 2012; 40, 9272–9285.”

[61] “Llorente A, Skotland T, Sylvänne T, Kauhanen D, Róg d T, Orłowski A, Vattulainen I, Ekroos K, Sandvig K. Molecular lipidomics of exosomes released by PC-3 prostate cancer cells. Biochimica et Biophysica Acta 1831. 2013; 1302–1309.”

[62] “Thery C, Regnault A, Garin J, Wolfers J, Zitvogel L, Ricciardi-Castagnoli P, Raposo G, Amigorena S. Molecular characterization of dendritic cell-derived exosomes. Selective accumulation of the heat shock protein hsc73. J Cell Biol. 1999; 147(3), 599-610.”

[63] “Wubbolts R, Leckie RS, Veenhuizen PT, Schwarzmann G, Möbius W, Hoernschemeyer J, Slot JW, Geuze HJ, Stoorvogel W. Proteomic and biochemical analyses of human B cell-derived exosomes. Potential implications for their function and multivesicular body formation. J Biol Chem. 2003; 278, 10963-72.”

[64] “Simpson RJ, Kalra H, Mathivanan S. ExoCarta as a resource for exosomal Research. Journal of Extracellular Vesicle. 2012; 1, 18374.”

[65] “Kalra H, Simpson RJ, Ji H, Aikawa E, Altevogt P, Askenase P, Bond VC, Borras FE, Breakefield X, Budnik V, Buzas E, Camussi G, Clayton A, E Cocucci E, Falcon-Perez JM, Gabrielsson S, Gho YS, Gupta D, Harsha HC, Hendrix A, Hill AF, Inal JM, Jenster G, Krämer-Albers EM, Kiang Lim S, Llorente A, Lötvall J, Marcilla A, Mincheva-Nilsson L, Nazarenko I, Nieuwland R, Nolte-’t Hoen E, Pandey A, Patel T, Piper MG, Pluchino S, Keshava Prasad TS, e Rajendran L, Raposo G, l Record M, Reid GE, Sánchez-Madrid F, Schiffelers RM, Siljander P, Stensballe A, Stoorvogel W, Taylor D, Thery C, Valadi H, . M. van Balkom BW, Vazquez J, Vidal M, Wauben M, Yañez-Mo M, Zoeller M, Mathivanan S. Vesiclepedia: A Compendium for Extracellular Vesicles with Continuous Community Annotation. PLOS Biology. 2012; 10(12), e1001450.” .

[66] “Kim DK, Lee J, Kim SR, Choi DS, Yoon YJ, Kim JH, Go G, Nhung D, Hong K, Jang SC, Kim SH, Park KS, Kim OY, Park HT, Seo JH, Aikawa E, Baj-Krzyworzeka M, van Balkom BW, Belting M, Blanc L, Bond V, Bongiovanni A, Borràs FE, Buée L, Buzás EI, Cheng L, Clayton A, Cocucci E, Dela Cruz CS, Desiderio DM, Di Vizio D, Ekström K, Falcon-Perez JM, Gardiner C, Giebel B, Greening DW, Gross JC, Gupta D, Hendrix A, Hill AF, Hill MM, Nolte-’t Hoen E, Hwang do W, Inal J, Jagannadham MV, Jayachandran M, Jee YK, Jørgensen M, Kim KP, Kim YK, Kislinger T, Lässer C, Lee DS, Lee H, van Leeuwen J, Lener T, Liu ML, Lötvall J, Marcilla A, Mathivanan S, Möller A, Morhayim J, Mullier F, Nazarenko I, Nieuwland R, Nunes DN, Pang K, Park J, Patel T, Pocsfalvi G, Del Portillo H, Putz U, Ramirez MI, Rodrigues ML, Roh TY, Royo F, Sahoo S, Schiffelers R, Sharma S, Siljander P, Simpson RJ, Soekmadji C, Stahl P, Stensballe

A, Stępień E, Tahara H, Trummer A, Valadi H, Vella LJ, Wai SN, Witwer K, Yáñez-Mó M, Youn H, Zeidler R, Gho YS. EVpedia: a community web portal for extracellular vesicles research. Bioinformatics. 2015; 31(6), 933-939."

[67] "Fevrier B, Vilette D, Archer F et al. Cells release prions in association with exosomes. Proc Natl Acad Sci USA. 2004; 101(26), 9683-9688."

[68] "Van der Pol E,. Böing AN, Harrison P, Sturk A, Nieuwland R. Classification, Functions, and Clinical Relevance of Extracellular Vesicles. Pharmacological reviews. 2012; 64(3), 677-700."

[69] "Conde-Vancells J, Rodriguez-Suarez E, Embade N, Gil D, Matthiesen R, Valle M, Elortza F, Lu SC, Mato JM, Falcon-Perez JM. Characterization and comprehensive proteome profiling of exosomes secreted by hepatocytes. J Proteome Res. 2008 Dec; 7(12): 5157-66."

[70] "Royo F, Schlangen K, PalomoL, Gonzalez E, Conde-Vancells J, Berisa A, Aransay AM, Falcon-Perez JM. Transcriptome of Extracellular Vesicles Released by Hepatocytes. Plos ones. 2013; 8(7)."

[71] "Cocucci E, Racchetti G, Meldolesi J. Shedding microvesicles: artefacts no more."

[72] "Simons M, Raposo G. Exosomes _ vesicular carriers for intercellular communication. Curr Opin Cell Biol. 2009; 21, 575-81."

[73] "Wetmore BA, Brees DJ, Singh R, Watkins PB, Andersen ME, Loy J, et al. Quantitative analyses and transcriptomic profiling of circulating messenger RNAs as biomarkers of rat liver injury. Hepatology. 2010; 51, 2127-39."

[74] "Burlone ME, Budkowska A. Hepatitis C virus cell entry: role of lipoproteins and cellular receptors. J Gen Virol. 2009; 90, 1055_70."

[75] "Masciopinto F, Giovani C, Campagnoli S, Galli-Stampino L, Colombatto P, Brunetto M, et al. Association of hepatitis C virus envelope proteins with exosomes. Eur J Immunol. 2004; 34, 2834-42."

[76] "Herrera MB, Fonsato V, Gatti S, Deregibus MC, Sordi A, Cantarella D, et al. Human liver stem cell-derived microvesicles accelerate hepatic regeneration in hepatectomized rats. J Cell Mol Med. 2010; 14, 1605-18."

[77] "Deregibus MC, Cantaluppi V, Calogero R, Lo Iacono M, Tetta C, Biancone L, et al. Endothelial progenitor cell derived microvesicles activate an angiogenic program in endothelial cells by a horizontal transfer of mRNA. Blood. 2007; 110, 2440-8."

[78] "Ratajczak J, Miekus K, Kucia M, Zhang J, Reca R, Dvorak P, Ratajczak MZ. Embryonic stem cell-derived microvesicles reprogram hematopoietic progenitors: evidence for horizontal transfer of mRNA and protein delivery. Leukemia. 2006; 20(5), 847-56."

[79] “Lee SO, Masyuk T, Splinter P, Banales JM, Masyuk A, Stroope A, et al. MicroRNA15a modulates expression of the cell-cycle regulator Cdc25A and affects hepatic cystogenesis in a rat model of polycystic kidney disease. J Clin Invest. 2008; 118, 3714-24.”

[80] “Thery C, Zitvogel L, Amigorena S. Exosomes: composition, biogenesis and function. Nat Rev Immunol. 2002; 2, 569-79.”

[81] “Thery C, Duban L, Segura E, Veron P, Lantz O, Amigorena S. Indirect activation of naive CD4_ T cells by dendritic cellderived exosomes. Nat Immunol. 2002; 3, 1156_6.”

[82] “Sadallah S, Eken C, Schifferli JA. Ectosomes as modulators of inflammation and immunity. Clin Exp Immunol. 2011; 163, 26-32.”

[83] “Croce CM. Causes and consequences of microRNA dysregulation in cancer. Nat Rev Genet. 2009; 10, 704-14.”

[84] “Kogure T, Lin WL, Yan IK, Braconi C, Patel T. Intercellular nanovesicle-mediated microRNA transfer: a mechanism of environmental modulation of hepatocellular cancer cell growth. Hepatology. 2011; 54, 1237-48.”

[85] “Jin M, Drwal G, Bourgeois T, Saltz J, Wu HM. Distinct proteome features of plasma microparticles. Proteomics. 2005; 5(7), 1940–1952.”

[86] “Looze C, Yui D, Leung L, et al. Proteomic profiling of human plasma exosomes identifies PPARgamma as an exosome-associated protein. Biochem Biophys Res Commun. 2009; 378(3), 433–438.”

[87] “Conde-Vancells J, Gonzalez E, Lu S, Mato JM, Falcon-Perez JM. Overview of Extracellular Microvesicles in Drug Metabolism. Expert Opin Drug Metab Toxicol. 2010 May; 6(5): 543–554.”

[88] “Nagar S, Remmel RP. Uridine diphosphoglucuronosyltransferase pharmacogenetics and cancer. Oncogene. 2006; 25, 1659–1672.”

[89] “Strange RC, Spiteri MA, Ramachandran S, Fryer AA. Glutathione-S-transferase family of enzymes. Mutat Res. 2001; 482(1-2), 21-6.”

[90] “Pushparajah DS, Umachandran M, Plant KE, Plant N, Ioannides C. Up-regulation of the glutathione S-transferase system in human liver by polycyclic aromatic hydrocarbons; comparison with rat liver and lung. Mutagenesis. 2008; 23(4), 299-308.”

[91] “Monks TJ, Anders MW, Dekant W, Stevens JL, Lau SS, van Bladeren PJ. Glutathione conjugate mediated toxicities. Toxicol Appl Pharmacol. 1990; 106(1), 1-19.”

[92] “Obermayer-Straub P, Strassburg CP, Manns MP. Target proteins in human autoimmunity: cytochromes P450 and UDP- glucuronosyltransferases. Can J Gastroenterol. 2000; 14(5), 429-39.”

[93] “Evans MJ, von Hahn T, Tscherne DM, Syder AJ, Panis M, Wolk B, et al. Claudin-1 is a hepatitis C virus co-receptor required for a late step in entry. Nature. 2007; 446, 801-5.”

[94] “Royo F, Schlangen K, Palomo L, Gonzalez E, Conde-Vancells J, et al. (2013) Transcriptome of Extracellular Vesicles Released by Hepatocytes. PLoS ONE. 2013; 8(7).”

[95] “Rodríguez-Suárez E, Gonzalez E, Hughes C, Conde-Vancells J, Rudella A, Royo F, Palomo L, Elortza F, Lu SC, Mato JM, Vissers JPC, Falcón-Pérez JM. Quantitative proteomic analysis of hepatocyte-secreted extracellular vesicles reveals candidate markers for liver toxicity. Journal of proteomics. 2014; 103, 227-240.”

[96] “Hosokawa M. Structure and catalytic properties of Carbolxylesterases isoenzymes involved in metabolic activation of prodrugs. Molecules. 2008 Feb; 13: 412-431.”

[97] “Ross M, Borazjani A. Enzimatyc activity of human Carboxylesterases. Current Protocols in toxicology. 2007 Aug; 4.24.1-4.24.14.”

[98] “Holmes RS, Wright MW, Laulederkind SJF, Cox LA, Hosokawa M, Imai T, Ishibashi S, Lehner R, Miyazaki M, Perkins EJ, Potter, PM. Recommended nomenclature for five mammalian carboxylesterase gene families: human, mouse, and rat genes and proteins. Mamm Genome. 2010; 21: 427-441.”

[99] “Sanghani SP, Sanghani PC, Schiel MA, Bosron WF. Human carboxylesterases: an update on CES1, CES2 and CES3. Protein Pept Lett. 2009;16(10), 1207-14.”

[100] “Mato JM, Martínez-Chantar ML; Lu SC. S-adenosylmethionine metabolism and liver disease. Ann Hepatol. 2013 ; 12(2), 183–189.”

[101] “Mato JM, Alvarez L, Ortiz P, M. Pajares A. S-adenosylmethionine synthesis: molecular mechanisms and clinical implications. Pharmacol Ther. 1997; 73(3),265–280.”

[102] “Petrossian TC, Clarke SG. Uncovering the human methyltransferasome. Mol Cell Proteomics. 2011; 10:M110.000976.”

[103] “Mato JM, Corrales FJ, Lu SC, Avila MA. S-Adenosylmethionine: a control switch that regulates liver function. FASEB J. 2002; 16,15-26.”

[104] “Mudd SH, Poole JR. Labile methyl balances for normal humans on various dietary regimens. Metabolism. 1975; 24, 721–35.”

[105] “S. H. Mudd and J. R. Poole. Labile methyl balances for normal humans on various dietary regimens. Metabolism. 1975; 24(6), 721–735.”

[106] “J. D. Finkelstein. Methionine metabolism in mammals. J. Nutr. Biochem. 1990; 1(5), 228–237.”

[107] “Männistö PT, Kaakkola S. Catechol-O-methyltransferase (COMT): Biochemistry, Molecular Biology, Pharmacology, and Clinical Efficacy of the New Selective COMT Inhibitors. Pharmacological Reviews. 1999; 51, 593-628.”

[108] “Pihlavisto P, Reenilä I. Review. Separation for catechol O-methyltransferase activity assay: physiological and pathophysiological relevance. Journal of Chromatography B. 2002; 781, 359–372.”

[109] “Pekka T. Männistö. Catechol-O-Methyltransferase. Encyclopedia of Molecular Pharmacology. 2008; 335-339.”

[110] “Schweigert N, Zehnder A and Eggen R. Chemical properties of catechols and their molecular modes of toxic action in cells, from microorganisms to mammals. Environmental Microbiology. 2001; 3(2), 81-91.”

[111] “Zhu BT. Catechol-O-Methyltransferase (COMT)-mediated methylation metabolism of endogenous bioactive catechols and modulation by endobiotics and xenobiotics: importance in pathophysiology and pathogenesis. Curr Drug Metab. 2002; (3), 321-49.”

[112] “Butterworth M, Lau SS, Monks TJ. 17 beta-estradiol metabolism by hamster hepatic microsomes: comparison of catechol estrogen O-methylation with catechol estrogen oxidation and glutathione conjugation. Chem Res Toxicol. 1996; 9(4), 793-9.”

[113] “Meyers M, Slikker W, Pascoe G, Vore M. Characterization of cholestasis induced by estradiol-17 beta-D-glucuronide in the rat. J Pharmacol Exp Ther. 1980; 214(1), 87-93.”

[114] “Xu H, Li Y, Che X, Tian H, Fan H, Liu K. Metabolism of Salvianolic Acid A and Antioxidant Activities of Its Methylated Metabolites. Drug Metab Dispo. 2014; 42, 274–281.”

[115] “Pan HJ, Li DY, Fang F, Chen D, Qi LL, Zhang RQ, Xu TD, Sun H. Salvianolic acid A demonstrates cardioprotective effects in rat hearts and cardiomyocytes after ischemia/ reperfusion injury. J Cardiovasc Pharmacol. 2011; 58, 535–542.”

[116] “Fan HY, Yang L, Fu FH, Xu H, Meng QG, Zhu HB, Teng LR, Yang MY, Zhang LM, and Zhang ZL, et al. (2012) Cardioprotective effects of salvianolic acid a on myocardial ischemia-reperfusion injury in vivo and in vitro. Evid Based Complement Alternat Med. 2012; 12.” .

[117] “Mansari M, Guiard B, Chernoloz O, Ghanbari R, Katz N, Blie P. Relevance of Norepinephrine-Dopamine Interactions in theTreatment of Major Depressive Disorder. CNS Neuroscience & Therapeutics. 2010 (16).”

[118] “Orth M, Schapira AHV. Mitochondrial involvement in Parkinson’s Disease. 2002; Neurochem Int, 40, 533-541.”

[119] “Männistö PT, Ulmanen I, Lundström K, Taskinen J, Tenhunen J, Tilgmann C, Kaakkola S. Characteristics of catechol O-methyl-transferase (COMT) and properties of selective COMT inhibitors. Prog Drug Res. 1992; 39, 291-350.”

[120] “Poewe W. The role of COMT inhibition in the treatment of Parkinson’s disease. Neurology. 2004; 62, 31–38.”

[121] “Teräväinen H, Rinne U, Gordin A. Catechol-O-methyltransferase inhibitors in Parkinson’s disease. Handbook of Parkinson’s Disease, Fifth Edition. 2001; 311-325.”

[122] “Benabou R, Waters C. Hepatotoxic profile of catechol-O-methyltransferase inhibitors in Parkinson’s disease. Expert Opin Drug Saf. 2003; 2(3), 263-7.”

[123] “Clemmesen JO, Galatius S, Skak C, Dalgaard P, Larsen FS, Ott P. The effect of increasing blood pressure with dopamine on systemic, splanchnic, and lower extremity hemodynamics in patients with acute liver failure. Scand J Gastroenterol. 1999; 34(9), 921-7.”

[124] “Kathleen M. Nicholls, Michael D. Shapiro, Vicki J. Van Putten, Rudiger Kluge, Hsiao-Min Chung, Daniel G. Bichet, and Robert W. Schrier. Elevated Plasma Norepinephrine Concentrations in Decompensated Cirrhosis. Association with Increased Secretion Rates, Normal Clearance Rates, and Suppressibility by Central Blood Volume Expansion. Circulation Research. 1985; 56 (3), 457-461.”

[125] “Myöhänen TT, Schendzielorz N, Männistö PT. Distribution of cathecol-O-methyltransferase (COMT) proteins and enzymatic acticities in wild-type and soluble COMT deficient mice. Journal of neurochemistry. 2010; 113, 1632-1643.”

[126] “Hu Z, Lausted C, Yoo H, Yan X, Brightman A, Chen J, Wang W, Bu X, Hood L. Quantitative liver-specific protein fingerprint in blood: a signature for hepatotoxicity. Theranostics. 2014; 4, 215-228.”

[127] “Tunbridge EM, Harrison PJ, Weinberger DR. Catechol-O-methyltransferase, cognition, and psychosis: Val1 58 Met and beyond. Biological Psychiatry. 2006; 60, 141-151.”

[128] “Tsunoda M, Takezawa K, Masuda M, Imai K. Rat liver and kidney catechol-O methyltransferase activity measured by high-performance liquid chromatography with fluorescence detection. Biomedical Chromatography. 2002; 16, 536-41.”

[129] “Aoyama N, Tsunoda M, Imai K. Improved assay for catechol-O-methyltransferase activity utilizing norepinephrine as an enzymatic substrate and reversed-phase high-performance liquid chromatography with fluorescence detection. Journal of Chromatography A 2005; 1074, 47-51.”

[130] “Masuda M, Tsunoda M, Imai K. Low Catechol-O-methyltransferase Activity in the Brain and Blood Pressure Regulation. Biol Pharm Bull. 2005; 29(2), 202-205.”

[131] “Hirano Y, Tsunoda M, Shimosawa T, Fujita T, Funatsu T. Measurement of catechol-O-methyltransferase activity in the brain of Dahl salt-sensitive rats. Biological and Pharmaceutical Bulletin. 2007; 30, 2178-2180.”

[132] “Reenilä I, Rauhala P. Simultaneous analysis of catechol-O-methyl transferase activity, S- adenosylhomocysteine and adenosine. Biomedical Chromatography. 2010; 24, 294-300.”

[133] “Cijiang He J, Chuang PY, Ma’ayan A and Iyengar R.Systems biology of kidney diseases. Kidney Int. 201; 81(1), 22–39.”

[134] “Boccard J, Veuthey JL and Rudaz S. Knowledge discovery in metabolomics: An overview of MS data handling. JSS. 2010; 33, 290–304.”

[135] “Patti GJ, Yanes O and Siuzdak G. Metabolomics: the apogee of the omic triology. Nat Rev Mol Cell Biol. 2013; 4, 263–269.”

[136] “Griffiths WJ, Koal T, Wang Y, Kohl M, Enot DP, Deigner HP. Targeted metabolomics for biomarker discovery. Angew Chem Int Ed Engl. 2010; 49(32), 5426-45.”

[137] “Monteiro MS, Carvalho M, Bastos ML and Guedes de Pinho P. Metabolomics Analysis for Biomarker Discovery: Advances and Challenges. Current Medicinal Chemistr. 2013; 20, 257-271.”

[138] “Dunn WB, Erban A, Weber RJM, Creek DJ, Brown M, Breitling R, Hankemeier T, Goodacre R, Neumann S, Kopka J and Viant MR. Mass appeal: metabolite identification in mass spectrometry-focused untargeted metabolomics. Metabolomics. 2012; 9, S44–S66.”

[139] “Nicholson JK, Lindon JC, Holmes E. Metabonomics: understanding the metabolic responses of living systems to pathophysiological stimuli via multivariate statistical analysis of biological NMR spectroscopic data. Xenobiotica. 1999; 29(11), 1181-1189.”

[140] “Reddy JK, Rao MS. Lipid Metabolism and Liver Inflammation. II. Fatty liver disease and fatty acid oxidation. Am J Physiol Gastrointest Liver Physiol. 2006; 290, G852–G858.”

[141] “Commisso M, Strazzer P, Toffali K, Stocchero M, and Guzzo F. Untargeted metabolomics: an emerging approach to determine the composition of herbal products. CSBJ.2013; 4 (5).”

[142] “Oldiges M, Lütz S, Pflug S, Schroer K, Stein N, Wiendahl C. Metabolomics: current state and evolving methodologies and tools. Appl Microbiol Biotechnol. 2007; 76(3), 495-511.”

[143] “Roessner U and Bowne J. What is metabolomics all about?. BioTechniques.2009; 46, 363-365.”

[144] “Medico E, Mongiovi AM, Huff J, Jelinek MA, Follenzi A, Gaudino G, Parsons JT, Comoglio PM. The tyrosine kinase receptors Ron and Sea control ‘scattering’ and morphogenesis of liver progenitor cells in vitro. Mol Biol Cell. 1996; 7(4), 495–504.”

[145] “Bradford M M. A rapid and sensitive method for the quantitation of microgram quantities of protein utilizing the principle of protein-dye binding. Analytical Biochemistry 1976; 72, 248–254.”

[146] “Rozen S, Skaletsky H. Primer3 on the WWW for general users and for biologist programmers. Methods Mol Biol. 2000; 132, 365-386.”

[147] "S van Liempd, Cabreda D, Mato JM, Falcon-Pérez JM. A fast method for the quantification of key metabolites of the methionine pathway in liver tissue by high-resolution mass spectrometry and hydrophilic interaction ultra-performance liquid chromatography. Anal Bioanal Chem. 2013; 405, 5301-5310."

[148] "Leffert H.L, Koch K.S, Moran T, Williams M. Liver cells. MethodsEnzymol. 1979; 58:536–544." .

[149] "Thery C, Amigorena S, Raposo G, Clayton A. Isolation and characterization of exosomes from cell culture supernatants and biological fluids. Curr Protoc Cell Biol. 2006; 3 (3.22)."

[150] "Dragovic RA, Gardiner C, Brooks AS, Tannetta DS, Ferguson DJ, et al. Sizing and phenotyping of cellular vesicles using Nanoparticle Tracking Analysis. Nanomedicine. 2011; 7, 780-788."

[151] "Stacey L, Cao H, Lu P, Gibson CR. Effect of cytochromes p450 chemical inhibitors and monoclonal antibodies on human liver microsomal esterase activity. DMD. 2006; 34 (8), 1361-1366."

[152] "Arsenault JC. Beginner's Guide to SPE [Solid-Phase Extraction]. 2012. Waters Corporation."

[153] "Lucci P, Pacetti D, Frega N, Núñez O. Current Trends in Sample Treatment Techniques for Environmental and Food Analysis. Chromatography - The Most Versatile Method of Chemical Analysis. 2012; Chapter 5, 127-164."

[154] "Method validation and quality control procedures for pesticide residues analysis in food and feed. 2012. Document N°SANCO/12495/2011."

[155] "Galan L. Linear calibration curve. Chromedia Analytical Science. 2015."

[156] "FDA. Bioanalytical Method Validation. 2001."

[157] "Palomo L, Casal E, Royo F, Cabrera D, Van-Liempd S, Falcon-Perez JM. Considerations for applying metabolomics to the analysis of extracellular vesicles. Frontiers in Immunology.Inflammation. 2014; 5, 651."

[158] "Godoy P et al. Recent advances in 2D and 3D in vitro systems using primary hepatocytes, alternative hepatocyte sources and non-parenchymal liver cells and their use in investigating mechanisms of hepatotoxicity, cell signaling and ADME. Archiv Toxicol. 2013; 87,1315–1530."

[159] "Tuschl G, Mueller SO. Effects of cell culture conditions on primary rat hepatocytes-cell morphology and differential gene expression. Toxicology. 2006; 218, 205-215."

[160] "Godoy P, Hengstler JG, Ilkavets I, Meyer C, Bachmann A, Múller A, Tuschl G, Mueller SO, Dooley S. Extracellular Matrix Modulates Sensitivity of Hepatocytes to Fibroblastoid Dedifferentiation and Transforming Growth Factor –Induced Apoptosis. Hepatology. 2009; 49(6), 2031-2043."

[161] “Toyoda Y, Tamai M, Kashikura K, Kobayashi S, Fujiyama Y, Soga T, Tagawa Y. Acetaminophen-Induced Hepatotoxicity in a Liver Tissue Model Consisting of Primary Hepatocytes Assembling around an Endothelial Cell Network. Drug metabolism and disposition. 2011; 40(1), 169-177.”

[162] “Bort R, Ponsoda X, Jover R, Gómez-lechón MJ, Castell JV. Diclofenac Toxicity to Hepatocytes: A Role for Drug Metabolism in Cell Toxicity. The Journal of Pharmacology and Experimental Therapeutics. 1998; 288 (1), 65-72.”

[163] “Patten CJ, Thomas PE, Guy RL, Lee M, Gonzalez FJ, Guengerich FP, Yang CS. Cytochrome P450 enzymes involved in acetaminophen activation by rat and human liver microsomes and their kinetics. Chem Res Toxicol. 1993; 6(4), 511-8.”

[164] “Tang W, Stearns RA, Bandiera SM, Zhang Y, Raab C, Braun MP, Dean DC, Pang J, Leung KH, Doss GA, Strauss JR, Kwei GY, Rushmore TH, Chiu SH, Baillie TA. Studies on Cytochrome P-450-mediated bioactivation of diclofenac in rats and in human hepatocytes: identification of glutathione conjugated metabolites. Drug metabolism and disposition. 1999; 27(3), 365-372.”

[165] “Milne JLS, Borgnia MJ, Bartesaghi A, Tran EH, Earl LA, Schauder DM, Lengyel J, Pierson J, Patwardhan A, Subramaniam S. Cryo-electron microscopy: A primer for the non-microscopist. FEBS J. 2013 ; 280 (1), 28–45.”

[166] “Tatischeff I, Larquet E, Falcon-Perez JM, Turpin PY, Kruglik SG. Fast characterisation of cell-derived extracellular vesicles by nanoparticles tracking analysis, cryo-electron microscopy, and Raman tweezers microspectroscopy. Journal of Extracellular Vesicles. 2012; 1, 19179.”

[167] “Webber J, Clayton A. How pure are your vesicles? Journal of Extracellular Vesicles 2013; 2, 19861.”

[168] “Atlas of Genetics and Cytogenetics in Oncology and Haematology. GNB2L1.”

[169] “Alapatt P, Guo F, Komanetsky SM, Wang S, Cai J, Sargsyan A, Rodríguez Díaz E, Bacon BT, Aryal P, Graham TE. Liver retinol transporter and receptor for serum Retinol-binding Protein (RBP4). The Journal of Biological Chemistry. 2013; 288(2), 1250-1265.”

[170] “Pajares M.A., Durane C., Corraslesn F., Pliego M.M., Mato J.M. Modulation of Rat Liver S-Adenosylmethionine Synthetase Activity by Glutathione. The Journal of Biological Chemistry. 1992; 267, 17598–17605.”

[171] “Grayson J mendel D. The distribution and regulation of temperature in the rat. J. physiol. 1956; 133, 334-346.”

[172] “Iloro I., Chehin R., Goni F. M., Pajares M. A., Arrondo J. L. Methionine adenosyltransferase alpha-helix structure unfolds at lower temperatures than beta-sheet: a 2D-IR study. Biophysical Journal 2004; 86, 3951–3958.”

[173] “Porcelli M, Cacciapuoti G, Carteni-FarinaM, Gambacorta A. S-Adenosylmethionine synthetase in the thermophilic archaebacterium Sulfolobus

solfataricus. Purification and characterization of two isoforms. Eur. J. Biochem. 1988; 177, 273-280."

[174] "Markham GD, Pajares MA.Structure-function relationships in methionine Adenosyltransferases. Cell Mol Life Sci. 2009; 66(4), 636–648."

[175] "Geller A.M., Kotb M.Y., Jernigan H.M. Jr, Kredich N.M. Purification and properties of rat lens methionine adenosyltransferase. Experimental Eye Research 1986; 43: 997-1008."

[176] "Olsen Ba. Hydrophilic interaction chromatography using amino and silica columns for the determination of polar pharmaceuticals and impurities. J chromatograf A. 2001; 913(1-2), 113-22."

[177] "Eric S. Hydrophilic Interaction Chromatography Using Silica Columns for the Retention of Polar Analytes and Enhanced ESI-MS Sensitivity. LCGC magazine. 2004; 22(10)."

[178] "Cataldi1 T, Bianco G, Abate S, Mattia D. Analysis of S-adenosylmethionine and related sulfur metabolites in bacterial isolates of Pseudomonas aeruginosa (BAA-47) by liquid chromatography/ electrospray ionization coupled to a hybrid linear quadrupole ion trap and Fourier transform ion cyclotron resonance mass spectrometry. Rapid Commun. Mass Spectrom. 2009; 23, 3465–3477."

[179] "Gellekink H, Oppenraaij-Emmerzaal D, van Rooij A, Struys E, Heijer M, Blom HJ. Stable-Isotope Dilution Liquid Chromatography–Electrospray Injection Tandem Mass Spectrometry Method for Fast, Selective Measurement of S-Adenosylmethionine and S-Adenosylhomocysteine in Plasma. Clinical Chemistry. 2005; 51(8), 1487–1492."

[180] "Wilson I.D., Martin P. Solid-Phase Extraction mediated by covalent bonding: applications of immobilized phenylboronic acid in: Solid-Phase Extraction: Principles, Techniques, and Applications. Edited by Nigel J.K. Simpson. 2000."

[181] "Agilent Bond Elut Plexa and Polymeric SPE Selection Guide (Agilent Technologies)."

[182] "Kim S.J., Know D.Y., Choi K.H., Choi D.W., Kim Y.C. Impaired Metabolomics of Sulfur Containing Substances in Rats Acutely Treated with Carbon Tetrachloride. Toxicology Research 2008; 24, 281–287."

[183] "Shapiro A.B., Gao N., Thresher J., Walkup G.K., Whiteaker J. A High-Throughput Absorbance-Based Assay for Methionine Produced by Methionine Aminopeptidase Using S-Adenosyl-L-Methionine Synthetase. Journal of Biomolecular Screening 2011; 16, 494–505."

[184] "Taylor PJ. Matrix effects: the Achilles heel of quantitative high-performance liquid chromatography-electrospray-tandem mass spectrometry. Clin Biochem. 2005; 38(4), 328-34."

[185] “Trufelli H, Palma P, Famiglini G, Cappiello A. An overview of matrix effects in liquid chromatography-mass spectrometry. Mass Spectrom Rev. 2011; 30(3), 491-509.”

[186] “Annesley TM.Ion Suppression in Mass Spectrometry. Clinical Chemistry. 2003; 49(7), 1041–1044.”

[187] “Method validation and quality control procedures for pesticide residues analysis in food and feed. 2012. Document N°SANCO/12495/2011.”

[188] “Krijt J, Dutá A, Kozich V. Determination of S-Adenosylmethionine and S-Adenosylhomocysteine by LC–MS/MS and evaluation of their stability in mice tissues. Journal of Chromatography B. 2009; 877, 2061–2066.”

[189] “Bonifacio 2003_Purification of mb bound COMT.pdf.”

[190] “Peaston R.T., Graham K.S., Chambers E., van der Molen J.C., Ball S. Performance of plasma free metanephrines measured by liquid chromatography-tandem mass spectrometry in the diagnosis of pheochromocytoma. Clinica Chimica Acta. 2010; 411, 546-52.”

[191] “Pekka T, Annisto O, Seppo Kaakkola. Catechol-O-methyltransferase (COMT): Biochemistry,Molecular Biology, Pharmacology, and Clinical Efficacy of the New Selective COMT Inhibitors. Pharmacological reviews. 1999; 51(4).”

[192] “Zhang X, Rauch A, Lee H, Xiao H, Rainer G, Logothetis NK. Capillary hydrophilic interaction chromatography/mass spectrometry for simultaneous determination of multiple neurotransmitters in primate cerebral cortex. Rapid Communication in Mass Spectrometry. 2007; 21, 3621-3628.”

[193] “Oasis WCX SPE Products for Strongly Basic Compounds. Waters Corporation. 2005.”

[194] “Brown JM, Ball JG, Hogsett A, Williams T, Valentovic M. Temporal Study of Acetaminophen (APAP) and S-Adenosyl-Lmethionine (SAMe) Effects on Subcellular Hepatic SAMe Levels and Methionine Adenosyltransferase (MAT) Expression and Activity. Toxicol Appl Pharmacol. 2010; 247(1), 1–9.”

[195] “Edelstein CL. Biomarkers in kidney disease. Elsevier. 2011.”

[196] “Weckwerth, W. Metabolomics in systems biology. Annu Rev Plant Biol. 2003; 54, 669-89.”

[197] “Sana T and Fischer S. Maximizing metabolite extraction for cohomprensive metabolomics studies of erytrocytes. Agilent technologies. 2007.”

[198] “Silas G, Villas-Boas, Mas S, Akesson M, Smedsgaard J and Nielsen J. Mass spectrometry in metabolome analysis. Mass Spectrometry reviews. 2005; 24, 613-646.”

[199] “Guzzetta A. Reverse Phase HPLC Basics for LC-MS.Tutorial. 2001.” .

[200] “Wang J, Byun J,Pennathur S. Analytical Approaches to Metabolomics and Applications to Systems Biology. Semin Nephrol. 2010; 30(5), 500–511.”

[201] “Yanes O, Tautenhahn R, Patti GJ, Siuzdak G. Expanding Coverage of the Metabolome for Global Metabolite Profiling. Anal Chem.2011; 83(6), 2152–2161.”

[202] “Rasmusse LG, Savorani F, Larsen TM, Dragsted LO, Astrup A, Engelsen SB. Standardization of factors that influence human urine metabolomics.Metabolomics. 2011; 7, 71–83.”

[203] “MarkerLynx XS Training. Waters Corporation.”

[204] “Gonzalez E, Van liempd S, Conde-Vancells J, Gutierrez-de Juan V, Perez-Cormenzana M, Mayo R, Berisa A, Alonso C, Marquez CA, Barr J, Lu SC, Mato JM and Falcon-Perez JM. Serum UPLC-MS/MS metabolic profiling in an experimental model for acute-liver injury reveals potential biomarkers for hepatotoxicity. Metabolomics. 2012; 8(6), 997–1011.”

[205] “MS:Elemental composition calculations and their interpretations. Mass Spectrometry- Essays and Tutorials. 2006.”

[206] “Blake MJ, Udelsmant R, Feulner GJ, Norton DD, Holbrook N. Stress-induced heat shock protein 70 expression in adrenal cortex: An adrenocorticotropic hormone-sensitive, age-dependent response. Proc Nati Acad Sci. 1991; 88, 9873-9877.”

[207] “Zhao Y, Ren J, Padilla-Parra S, Fry EE, Stuart D. Lysosome sorting of b-glucocerebrosidase by LIMP-2 is targeted by the mannose 6-phosphate receptor. Nature Communications. 2014; 14(5).”

[208] “Masuda M, Tsunoda M, Imai K. Low Catechol-O-methyltransferase Activity in the Brain and Blood Pressure Regulation. Biol Pharm Bull. 2006; 29(2,) 202-205.”

[209] “Yang X, Weng Z, Mendrick DL, Shi Q. Circulating extracellular vesicles as a potential source of new biomarkers of drug-induced liver injury. Toxicology Letters. 2014; 225(3).”

[210] “FDA, 2009. Guidance for Industry: Drug-Induced Liver Injury: Premarketing ClinicalEvaluation. 2013.”

[211] “Bala, S., Petrasek, J., Mundkur, S., Catalano, D., Levin, I., Ward, J., Alao, H., Kodys, K.,Szabo, G., 2012. Circulating microRNAs in exosomes indicate hepatocyte injury and inflammation in alcoholic, drug-induced, and inflammatory liver diseases. Hepatology. 2012; 56 (5), 1946–1957.”

[212] “RessomHW, Xiao JF, Tuli L, Varghese RS, Zhou B, Tsai TH, Nezami Ranjbar M, Zhao Y, Wang J, Di Poto C, Cheema AK, Tadesse MG, Goldman R, Shetty K. Utilization of Metabolomics to Identify Serum Biomarkers for Hepatocellular Carcinoma in Patients with Liver Cirrhosis. Anal Chim Acta. 2012; 743C, 90–100.”

[213] “Bogdanov M, Matson WR, Wang L, Matson T, Saunders-Pullman R, Bressman SS, Beal MF. Metabolomic profiling to develop blood biomarkers for Parkinson’s disease. Brain. 2008; 131, 389-396.”

[214] “Potmesil M. Camptothecins: from bench research to hospital wards. Cancer Research. 1994; 54: 1431–1439.”

[215] “Mathijssen RH, Van Alphen RJ, Verweij J, Loos WJ, Nooter K, Stoter G, Sparreboom A. Clinical pharmacokinetics and metabolism of irinotecan (CPT-11). Clin Cancer Res. 2001 Aug; 7: 2182-2194.”

[216] “Lu S.C., Mato J.M. S-adenosylmethionine in liver health, injury and cancer. Physiological Reviews 2012; 92, 1515–1542.”

[217] “Lombardini JB, Chou TC, Talalay P. Regulatory properties of adenosine triphosphate- L-methionine S-adenosyltransferase of rat liver. Biochem. 1973; 135, 43–57.”

[218] “Mato JM, Lu SC. Role of S-Adenosyl-L-Methionine in Liver Health and Injury. Hepatology. 2007; 45(5), 1306-1312.”

[219] “Skordi E, Claus SP, Martin FP, Cloarec O, Lindberg J, Schuppe-Kolstinen I, Holmes E, Nicholson JK. Analysis of time-related metabolic fluctuations induced by ethionine in the rat. J Proteome Res. 2007; 6, 4572–4581.”

[220] “Zhuge J, Cederbaum AI. Depletion of S-adenosyl-L-methionine with cycloleucine potentiates cytochrome P450 2E1 toxicity in primary rat hepatocytes. Arch Biochem Biophys. 2007; 486, 177–185.”

[221] “Ramani D, De Bandt JP, Cynober L. Aliphatic polyamines in physiology and diseases. Clin Nutr. 2014; 33(1), 14-22.”

[222] “Tetta C, Bruno S, Fonsato V, Deregibus CM, Camussi G. The role of microvesicles in tissue repair. Organogenesis. 2011; 7(2), 105-115.”

[223] “Volodymyr I. Lushchak. Glutathione Homeostasis and Functions: Potential Targets for Medical Interventions. Journal of Amino Acids.2011; 2012, 736837-26.”

[224] “Hunt Ng Y, Rome S, Jalabert A, Forterre A, Singh H, Hincks CL, Salamonsen LA. Endometrial Exosomes/Microvesicles in the Uterine Microenvironment: A New Paradigm for Embryo-Endometrial Cross Talk at Implantation. Plos One. 2013; 8(3).”

[225] “Shen B, Wu N, Yang JM, Gould S. Protein targeting to exosomes/microvesicles by plasma membrane anchors. The Journal of Biological Chemistry. 2011; 286, 14383-14395.”

[226] “Stillwell W. The role of polyunsaturated lipids in membrane raft function. Scandinavian Journal of Food and Nutrition. 2006; 50 (S2), 107-113.”

[227] “Human Metabolome Database: Glycerylphosphorylethanolamine (HMDB00114).”

10. SUPPORT

This work was supported by:

- Grants PI060621, PS09/00526 and PI12_01604, cofinanced by the ISCIII Subdirección General de Evaluación and Fondo Europeo de Desarrollo Regional (FEDER).

- Travel grants of European COST Actions BM0901 and BM1202 financed by European Science Foundation (ESF).

- Departamento de Educación Política Lingüística y Cultura del Gobierno Vasco (PI2012-45).

- Departamento de Sanidad del Gobierno Vasco (2012-2015)

- Subprograma Ramón y Cajal RYC2007-00228

- Predoctoral grant from the CIC bioGUNE.